UNIVERSITY OF PERUGIA

UNIVERSITY OF COPENHAGEN
FACULTY OF SCIENCE

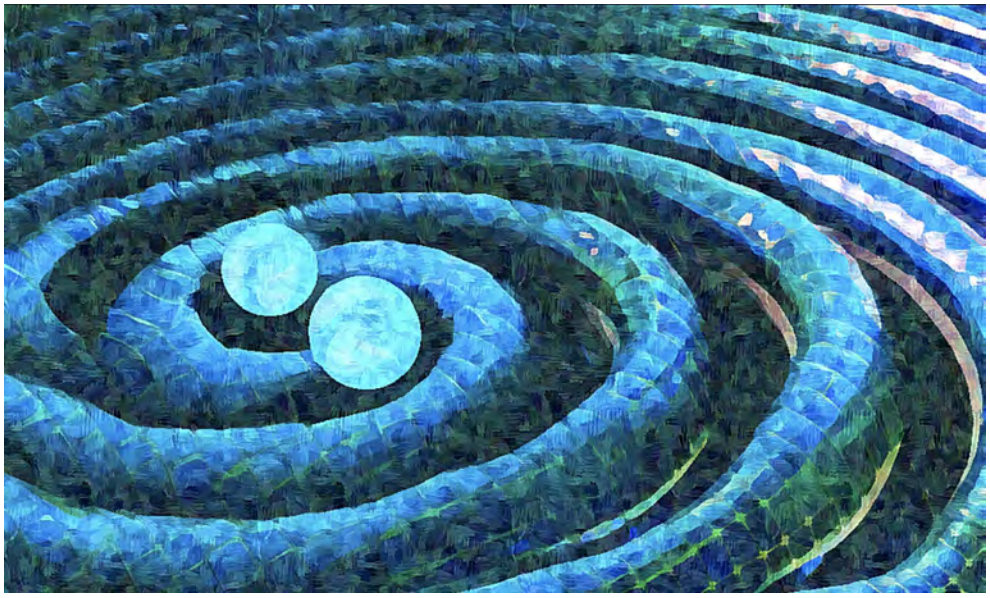

PhD thesis

Gravitational wave modeling for eccentric binaries within the effective one-body approach

Andrea Placidi

Advisors: Gianluca Grignani, Troels Harmark

Submitted: January 30, 2023

This thesis has been submitted to the PhD School of The Faculty of Science, University of Copenhagen and to the PhD school of the University of Perugia

Declaration of Authorship

I, Andrea Placidi, declare that this thesis titled "Gravitational wave modeling for eccentric binaries within the effective one-body approach" is the outcome of my own work and of the scientific collaborations listed below, except where specific reference is made to the work of others. This Thesis is based on the following research papers published either in preprint servers and in peer-reviewed journals and listed in chronological order.

- *Exploiting Newton-factorized, 2PN-accurate waveform multipoles in effective-one-body models for spin-aligned noncircularized binaries.*

  Authors:
  A. Placidi, S. Albanesi, A. Nagar, M. Orselli, S. Bernuzzi, G. Grignani

  Journal:
  Physical Review D, volume 105, article id. 104030 (2022).

  DOI: 10.1103/PhysRevD.105.104030

  URL: https://doi.org/10.1103/PhysRevD.105.104030

  Preprint: https://arxiv.org/abs/2112.05448

  Comments:
  Part of the content of this paper has been adapted in Sec. 3.1, Sec. 3.4 and Sec. 3.6 of this Thesis.

- *Assessment of Effective-One-Body Radiation Reactions for Generic Planar Orbits.*

  Authors:
  S. Albanesi, A. Nagar, S. Bernuzzi, A. Placidi, M. Orselli

  Journal:
  Physical Review D, volume 105, article id. 104031 (2022).

  DOI: 10.1103/PhysRevD.105.104031

  URL: https://doi.org/10.1103/PhysRevD.105.104031

  Preprint: 10.48550/arXiv.2202.10063

  Comments:
  Part of the content of this paper has been adapted in Sec. 3.5.

- *New Avenue for Accurate Analytical Waveforms and Fluxes for Eccentric Compact Binaries.*

  Authors:
  S. Albanesi, A. Placidi, A. Nagar, M. Orselli, S. Bernuzzi

  Journal:
  Physical Review D, volume 105, article id. L121503 (2022).

  DOI: 10.1103/PhysRevD.105.L121503

URL: https://doi.org/10.1103/PhysRevD.105.L121503

Preprint: 10.48550/arXiv.2203.16286

Comments:
Part of the content of this paper has been adapted in Sec. 3.7

The papers listed above are the outcome of my research activity, conducted at the University of Perugia and at the University of Copenhagen between November 2019 and January 2023.

Part of the Thesis has been available through arxiv.org with these references:

- https://doi.org/10.1103/PhysRevD.105.104030,
  PDF available at https://arxiv.org/abs/2112.05448.
- https://doi.org/10.1103/PhysRevD.105.104031,
  pdf available at https://doi.org/10.48550/arXiv.2202.10063.
- https://doi.org/10.1103/PhysRevD.105.L121503.
  pdf available at https://doi.org/10.48550/arXiv.2203.16286.

Contents

Contents i

Introduction 3

1 Gravitational waves from post-Newtonian sources 9
1.1 The field equations of general relativity 10
1.2 Gravitational radiation in linearized gravity 13
1.2.1 Gauge symmetry in linearized theory 14
1.2.2 Leading-order quadrupole formalism 15
1.2.3 General linear solution 19
1.2.4 Linear GWs and the asymptotic region 25
1.3 Beyond the linear order: Blanchet-Damour generation formalism 26
1.3.1 Multipolar post-Minkowskian expansion in the exterior region 29
1.3.2 PN expansion in the near region 37

1.3.3 PN-MPM matching in the overlapping region 39
1.3.4 Non-linear waveform at infinity 42

2 The effective one-body approach to coalescing compact binaries 47
2.1 Conservative dynamics in the EOB approach 49
2.1.1 EOB conservative dynamics at 2PN 49
2.1.2 EOB Hamiltonian at 3PN 58
2.1.3 EOB Hamiltonian at 4PN 62
2.1.4 EOB conservative dynamics beyond the 4PN order . . . 67
2.2 Radiation reaction and inspiral-plunge waveform in the EOB approach 69
2.3 EOB description of merger and ringdown 77

3 Eccentricity effects in EOB waveform models 81
3.1 The eccentric insplunge of `TEOBResumS-DALI` 84
3.2 Factorized 2PN noncircular corrections in the insplunge waveform 87
3.2.1 2PN noncircular waveform in EOB coordinates 88
3.2.2 New noncircular waveform factors at 2PN accuracy ($m \neq 0$) 94
3.2.3 2PN noncircular corrections for the $m = 0$ modes 97
3.3 Waveform validation: test-mass limit 99
3.3.1 Eccentric insplunge in the test-mass limit 99
3.3.2 Resummation of the noncircular tail factor 102
3.3.3 Resummation of the noncircular instantaneous factor . . 104
3.3.4 Resummed noncircular corrections for the subdominant modes 107
3.3.5 Testing the noncircular corrections for the $m = 0$ modes 114
3.3.6 Dynamical captures in the test-mass limit 115
3.4 Waveform validation: the comparable-mass case 117
3.4.1 Phase comparisons in the time domain 117
3.4.2 EOB/NR unfaithfulness 120
3.5 2PN noncircular corrections in $\hat{\mathcal{F}}_\varphi$ 121
3.5.1 2PN-accurate noncircular quadrupolar flux 123
3.5.2 Factorization and resummation 124
3.5.3 Testing the 2PN noncircular correction of $\hat{\mathcal{F}}_\varphi$ 126
3.6 Comparisons with others eccentric EOB models 128
3.7 Alternative prescription for the quadrupolar noncircular instantaneous factor 134
3.7.1 Time-derivative dependent noncircular instantaneous factor 135
3.7.2 Assessment of the new waveform factor 136

Conclusions 143

Appendix **149**

Appendix A Useful mathematical tools **149**
A.1 Symmetric-trace-free projection of a generic tensor 149
A.2 Padé approximants 149

Appendix B `TEOBResumS` for spin-aligned coalescing binaries **151**
B.1 Spin effects in the EOB Hamiltonian 151
B.2 Spin effects in insplunge waveform and radiation reaction force 155

Appendix C Long analytical expressions **157**
C.1 2PN noncircular factors for the subdominant modes ($m \neq 0$) . 157
C.2 2PN-accurate subdominant multipoles of $\hat{\mathcal{F}}_\varphi$ ($m \neq 0$) 163
C.3 2PN noncircular instantaneous factor with time derivatives ($\ell = m = 2$) 164

Bibliography **169**

Introduction

In the past few years, gravitational wave (GW) physics has quickly risen to become one of the most fruitful and promising field of astrophysics, both from an experimental and a theoretical point of view. After the groundbreaking detection of the now iconic GW signal GW150914, announced by the LIGO scientific collaboration and the Virgo collaboration on 11 February 2016 [1], it became clear that GWs could be directly detected and used to gain fundamental insights into otherwise inaccessible aspects of our Universe, ranging from signatures of its birth and evolution [2] to some of the most compelling phenomena that populate it, such as supernovae, pulsars, and binary systems of compact celestial objects. Actually, as of now, the history of the achieved GW detections revolves entirely around binary systems of stellar-mass black holes and neutron stars, which evolve by losing energy and angular momentum through the emission of GWs, with their component objects that get closer and closer until they merge in a single remnant object, typically a Kerr black hole. The ground-based laser interferometers Advanced LIGO [3] and Advanced Virgo [4] have so far successfully detected a total of 90 GW signals [5–7],[1] all produced in the coalescences of stellar-mass compact binaries. The GWs sourced by these phenomena are in fact the loudest in the frequency band [10 Hz, 10 kHz], which roughly represent the one probed by our current array of detectors. These GW observations have already pushed forward our astrophysical knowledge with invaluable results. Just to name a few: the proof of the existence of black holes with mass up to hundreds of solar masses [8, 9]; the discovery of a population of bound systems of black holes and neutron stars, which merged in less than the current age of the Universe; the inference of the properties of such binaries (masses, spins, luminosity distance, sky position), together with insights on their formation mechanisms [7, 10, 11]; the development of a new method to measure the Hubble constant [12–14]; numerous confirmations of general relativity (GR), notably also in the previously unexplored strong gravity regime [15, 16]. Moreover, the first detected GW signal from a binary neutron star merger, GW170817 [17], and the followup observation of the gamma ray burst GRB 170817A in the electromagnetic

[1] We refer in particular to the events that have a probability greater than 0.5 of being of astrophysical origin; with different thresholds their number is subject to change.

(EM) domain [18] have ushered in a new branch of *multi-messenger astronomy*, demonstrating the link between these two phenomena and cementing the interplay between GW and EM searches [19–23].

If the present of GW astronomy is undoubtedly thriving, its future prospects are no less exciting. Over the coming 20 years we will supposedly witness [24]:

- the next observing run (the fourth, O4) of Advanced LIGO and Advanced Virgo, after more than 2 years of upgrades [25, 26] and with the support of the Japanese interferometer KAGRA [27], which will join the detector array at the start of the observing run and then step away for commissioning to return toward the end of the run with enhanced sensibility; the start of O4 is currently scheduled for March 2023 and its planned duration is around a year;

- the enrichment of the ground-based detector network with LIGO-India [28], which should see the light of day in this decade, and with the third generation observatories Einstein Telescope (ET) [29], in Europe, and Cosmic Explorer (CE) [30], in the USA, both planned for the mid 2030s;

- the entry into service of the first space based interferometers, which will search for GW signals in the frequency band [100μHz, 100mHz]; on the European and US side, the Laser Interferometer Space Antenna (LISA) [31–33] is planned to be launched in 2034, whereas the Chinese TianQuin [34] and Taiji [35] are still to be scheduled, even though they are expected to come into operation not long after LISA;

- the realization in space of the Japanese DECI-hertz Interferometer Gravitational wave Observatory (DECIGO) [36], which will aim at detecting primordial GWs, for cosmological purposes; the scientific pathfinder for this project, dubbed B-DECIGO, is planned for launch in the 2030s;

- the first results from the pulsar timing array (PTAs) projects, which are attempting the detections of ultralong GWs (10^{-9} to 10^{-6}Hz) [37] by measuring, with radio telescopes, GW-induced deviations in the arrival time of the pulse from an array of 20-50 millisecond pulsars; the main ongoing PTA projects at the moment are the Australian Parkes PTA [38], the European PTA consortium [39], the US NANOGrav consortium [40] and the Indian PTA [41], all united in the multi-institution concerted program that goes by the name of International PTA (or IPTA) [42]; a first successful PTA detection is expected in the next few years [43].

Regarding the interesting astrophysical data we can expect from this great scientific effort, on the one hand we will have at our fingertips a huge number of GW detections from coalescing binary system of compact objects (thanks in particular to the next generation observatories), spanning a much broader range of masses, spins, and orbital configurations, with the higher sensibility

that will allow for a more accurate inference of their properties; on the other hand, we will hopefully observe unprecedented GW signals from new kind of sources, like isolated neutron stars [44], supernovae [45], or the primordial Universe [46].

Given the pivotal role they play in the present and the expected future of GW astronomy, compact binary coalescences (CBCs) are GW sources of paramount interest. In fact, because of the tremendous energy which characterizes this kind of cataclysmic events, the GW signals they produce are by far the loudest we receive, and hence, in principle, the easiest to measure. Moreover, they have the crucial feature of being *deterministic* and *predictable*, as opposed to stochastic GWs, like those produced during the early stage of the Universe, or deterministic but unpredictable GWs, like those emitted by the supernovae, whose underlying dynamics is way too involved for an appropriate analytical modelization. Therefore, the possibility of an accurate description of how CBCs evolve in time ultimately allows for the manufacture of waveform templates for the GWs they produce. These are then cross-correlated with the noisy output signals of our GW detectors by means of specific CBC search pipelines based on *matched filters* [47, 48], thus boosting their effective GW sensitivity with respect to CBC signals. Secondly, these waveform templates are crucial for the statistical inference techniques that, building on Bayesian statistics [49] (see also Chapter 7 of Ref. [50]), are employed to estimate the relevant properties of CBCs.[2]

Undertaking the task of modeling CBC waveform templates means facing two intertwined problems: (i) the relativistic two-body motion of inspiralling and coalescing binaries; (ii) the emission and propagation to future null infinity of the associated gravitational radiation. On the analytical side, given the challenge posed by the highly non-linear character of general relativity, our only option to address these problems is to resort to approximation schemes. In this respect, a prominent role has been (and still is) played by the *post-Newtonian* (PN) theory. In this perturbation scheme, appeared shortly after the birth of general relativity [52], the Newtonian equations of motion are supplemented with relativistic effects in a weak-gravitational-field and slow-velocity expansion on the dimensionless parameter $v^2/c^2 \sim GM/(rc^2)$, where v is the typical orbital velocity of the binary system, r its typical relative separation, M its total mass, c the speed of light, and G the gravitational constant. The powers of $1/c$ are often used as a counter of the orders in this expansion, with terms of order $\mathcal{O}(1/c^n)$ referred to as $\frac{n}{2}$PN corrections. Over the years, several different approaches have been conceived and developed to come up with a PN description of the two-body motion: the *surface integral method*, introduced by Einstein, Infeld & Hoffman [53] and later pursued by Itoh & Futamase [54–58]; the *PN iteration of Einstein's equations*

[2] See Appendix E of Ref. [51] for an overview of the parameter estimation techniques used in the latest analysis of the LIGO-Virgo-KAGRA collaboration

ushered in by Blanchet, Faye & Ponsot in Ref. [59] and further developed in a series of works, see Refs. [60–68]; the *canonical Hamiltonian formalism* in Arnowitt-Deser-Misner coordinates by Jaranowski, Schäfer & Damour [69–75]; the *effective-field-theory approach* originally proposed by Goldberg & Rothstein [76–78] and extensively used by Foffa & Sturani [79–85] and other authors [86,87];[3] the *Fokker Lagrangian approach* [95] used in Ref. [96]. Focusing on the problem of modeling the associated gravitational radiation, the PN expansion lies at the core of the main analytical frameworks devised to tackle it: the *direct integration of Einstein's equation* by Will, Wiseman & Pati [97–99] and the *PN-matched multipolar post-Minkowskian generation formalism* devised by Blanchet & Damour [100–113]. As the latter construction mechanism is used to derive the PN waveform results upon which each analytical waveform model is built, included the one discussed in the hearth of this Thesis, we will review it in its main aspects in Chapter 1, specifically in Sec. 1.3.

All this being said, one has to bear in mind that, regardless of the specific computational strategy adopted, PN results are naturally faithful only in a portion of the CBC evolution, that is during the early and mid stages of the *inspiral* phase, when the two compact bodies are still far apart in their inspiral motion around each other. In the late inspiral and during the *plunge*, just before merger, we enter a regime where the gravitational field is strong and the typical velocity of the system grows up to around one half of the speed of light. In this regime the PN series shows severe convergence issues, which ultimately spoil the reliability of PN results before merger, both at the level of the binary dynamics and the radiation field; see e.g. Refs. [114–116]. On the one hand, this prompted the development of complementary analytical approaches like *Black hole perturbation theory*, which models compact binaries and their radiation field by expanding perturbatively the field equations in powers of the binary mass-ratio, provided this is sufficiently small.[4]. On the other hand, it gave a strong motivation to pursue the path of *numerical relativity* (NR), in its application to the two-body problem. After a fundamental breakthrough in 2005, by Pretorius & others [133–136], these computational approach allowed for the "exact" (modulo numerical errors) description of the late stages of the CBC evolution, by means of supercomputer simulations; see Refs. [137–139] for some reviews. Although they stand

[3] This approach has also been instrumental to recent developments in the application of the *post-Minkowskian scheme* [88, 89], based on a power series expansion in G with no requirements on the velocity of the system, to study the dynamics of compact binaries; see e.g Refs. [90–94].

[4] After the seminal works of Regge, Wheeler & Zerilli [117, 118] and Teukolsky [119–122] on the GW emission of a test particle moving in the neighborhood of, respectively, a Schwarzschild or a Kerr black hole, a lot of effort has been focused on extending this approach to model extreme-mass-ratio binaries. Moving away from the leading-order test-particle description, the idea is to include perturbatively the alterations that the metric perturbations sourced by the smaller body induce on the motion of the latter around the bigger one, describing them as the effect of a suitably defined *gravitational self-force* [123–132]

at the pinnacle of the accuracy one can reach in dealing with the two-body problem, NR simulations have an extremely high computational cost, with a typical calculation time of the order of several weeks; in addition, they present technical issues in several portions of the CBC parameter space, e.g. when the individual masses of the binary differs sensibly from each other. Analytical methods, therefore, were not rendered obsolete by NR even from a practical point of view, all the more considering the appearance in their ranks of the *effective one-body* (EOB) approach [140–143]. This analytical formalism, introduced in 1998 by Buonanno & Damour [140], takes as input the known conservative PN dynamics of a given compact binary, with component masses m_1 and m_2, and maps it onto the effective non-geodesic dynamics of a single particle of mass $\mu \equiv m_1 m_2/(m_1 + m_2)$, the binary reduced mass, in the effective metric of a Schwarzschild or Kerr black hole (respectively for spinless or spinning binaries) altered by a continuous deformation which is parameterized by the symmetric mass ratio $\nu \equiv \mu/M$, with $M \equiv m_1 + m_2$. Thanks to this surprisingly simple formalism, the EOB approach succeeded in improving drastically the convergence of PN results in strong-field and therefore allowed for a robust description of the motion and radiation of compact binaries in all the stages of the coalescence, from the early inspiral up to the *ringdown* phase, after merger. Accordingly, the EOB approach provided crucial quantitative and qualitative predictions on CBC waveforms, well before the advent of the dedicated NR simulations. Moreover, shortly after the latter appeared, the flexibility of the EOB approach has been exploited to inform EOB models with additional non-perturbative NR information, which improved remarkably their accuracy [144–151]. The fast and accurate waveform models produced in this fashion, usually dubbed EOB[NR] models, have quickly become a stepping stone for the generation of the templates used to sustain GW observations, and over the years have undergone a long process of refinement, with the inclusion of more dynamical/waveform information and extra layers of sophistication in the corresponding prescriptions. This process has ultimately led to the development of two different EOB waveform models, `SEOBNR` [150, 152, 153] and `TEOBResumS` [154–157], the latter being the focus of the waveform modeling activities presented in this Thesis. As part of the ongoing history of endeavors to improve and extend EOB-flavored waveform models, the main scope of this Thesis is in fact to propose, discuss and test an updated version of the generic planar orbit branch of `TEOBResumS`, now known as `TEOBResumS-DALI`, supplemented with additional corrections aimed at better capturing the waveform modulations induced by the eventual noncircularity of the sourcing dynamics.

Coming to the actual structure of the Thesis, it is organized in three Chapters, each made up of several sections and subsections. The first two Chapters are intended as a review of the main concepts upon which the original work presented in the third is based, so to make it as self-consistent as possible and thus accessible also to readers with limited expertise on the subject at hand. In the third Chapter, instead, after a recap on the current state of the

art of `TEOBResumS-DALI`, we present our original contributions to its further development, building on our associated publications [158–160].

More in details:

- Chapter 1 addresses the waveform generation problem, illustrating, first in linearized gravity and then in the full non-linear theory, how the gravitational radiation at infinity can be modeled on the basis of the energy-momentum content of its source, under the necessary simplifications that come with the application of suitable approximation schemes, PN theory in particular.

- Chapter 2 introduces the reader to the effective one-body approach to the motion and radiation of compact binary systems, explaining its take on the binary dynamics and presenting the associated waveform model for the whole CBC process (inspiral-plunge and merger-ringdown). Here we limit the discussion to the native quasi-circular version of EOB models, primarily referring to the one of `TEOBResumS`, which now goes by the name of `TEOBResumS-GIOTTO`.

- In Chapter 3 we finally discuss our contribution to the development of `TEOBResumS-DALI`, the branch of `TEOBResumS` realized for modeling GWs from coalescing binaries in motion on non-circularized orbits. After a brief review of this waveform model, we introduce and thoroughly test our proposal for its extension, mainly revolving around new 2PN-accurate analytical factors specifically designed to be incorporated in the preexisting prescriptions for the pre-merger waveform and radiation-reaction force. As we will see, the result is a new waveform model with improved performance when dealing with noncircular dynamics.

Chapter 1

Gravitational waves from post-Newtonian sources

The overarching theme of this opening Chapter is the theoretical description of the gravitational radiation produced by *post-Newtonian sources* (PN sources). Here we address this topic by offering a personal review which will also lay the groundwork for the rest of the Thesis, from a formal and conceptual point of view. Indeed the content presented in this Chapter is not original, but results from the elaboration of several pieces of literature on the subject, in particular Refs. [104, 108, 112, 161–164].

To begin with, we specify that we dub as "post-Newtonian" every GW source that is both slowly moving and weakly stressed by its self-gravitation. Following Ref. [112], we summarize this with the requirement

$$\epsilon \equiv \max\left\{\left|\frac{T^{0i}}{T^{00}}\right|, \left|\frac{T^{ij}}{T^{00}}\right|^{1/2}, \left|\frac{V_{\rm N}}{c^2}\right|^{1/2}\right\} \ll 1, \tag{1.1}$$

where $T^{\mu\nu}$ is the stress-energy tensor of the matter source and $V_{\rm N}$ its Newtonian gravitational potential.

Coming to the GW sources of our interest, that is CBCs, one may have the legitimate concern that they do not comply to the above definition, as their constituent compact objects present indeed strong gravitational fields. Actually, as long as the two objects are sufficiently far apart, the *effacement principle* of general relativity [165] ensures that a PN description is still applicable for these sources. This can be shown using the surface integral method we quoted in the Introduction, e.g. see Ref. [166] or Sec. 5.5 of Ref. [163]. Of course, as the CBC evolution proceeds and the compact bodies approach each other, considerations of this kind no longer apply. Therefore, the CBC waveform information that is computed using the techniques presented in this Chapter, ultimately given in terms of truncated PN series, is truly physically sound only in the initial inspiral phase of the coalescence, up to several orbital cycles before merger time. Nevertheless, within the EOB formalism,

such waveform information is an essential ingredient in the development of the complete inspiral-plunge-merger-ringdown models that are used in actual data analysis. We defer to the next Chapter the discussion of how the EOB approach makes use of this results, pushing their validity up to merger, and complementing them with a GW model for the ringdown part of the signal.

Another important aspect regarding compact binaries and the effacement principle is that the internal structure of their component bodies has a marginal impact on their dynamics, with the first structure-dependent effects appearing at the 5PN order in the equations of motion. Accordingly, even when the compact objects in question are neutron stars, in first approximation one can model their gravitational radiation as if they were systems of two structureless point particles, fully described by their mass and, eventually, their spin. At the level of the energy-momentum tensor $T^{\mu\nu}$, this amounts to consider

$$T^{\mu\nu}(t,\mathbf{x}) = \sum_{A=1,2} \frac{m_A v_A^\mu v_A^\nu}{\sqrt{-g_{\alpha\beta} v_A^\alpha v_A^\beta / c^2}} \frac{\delta^{(3)}(\mathbf{x}-\mathbf{y}_A(t))}{\sqrt{-g}}, \tag{1.2}$$

where m_A is the mass of the particle A, $\mathbf{y}_A(t)$ is its trajectory, and $v_A^\mu = (c, d\mathbf{y}_A/dt)$. Beyond the 1PN order, the Dirac distributions appearing in Eq. (1.2) give rise to ultra-violet divergences, which need to be regularized. This process is far from trivial and the details of the regularization schemes adopted, the Hadamard and dimensional self-field regularizations, can be found in Sec. 6 of Ref. [112]; for a recent work on the subject, see instead Ref. [167]. In what follows, the GW generation problem will be addressed while assuming a general and smooth (C^∞) energy-momentum tensor with spatial compact support, knowing that the discussion can be specialized anytime to the compact binary case (1.2), with the additional cost of having to include a regularization prescription for the occurring divergences.

More in details, after we lay down in Sec. 1.1 the fundamental equations we want solve, the rest of this Chapter proposes an extensive dive into the theoretical description of GWs, initially limited to the simplistic prescriptions of linearized gravity, in Sec. 1.2, and then extended to the full non-linear theory, in Sec. 1.3.

1.1 The field equations of general relativity

Let us start by stating precisely the problem we want to solve. The theory of GR in presence of matter can be described by the action $S = S_{\rm EH} + S_{\rm M}$, where

$$S_{\rm EH} = \frac{c^3}{16\pi G} \int d^4x \sqrt{-g} R, \tag{1.3}$$

is the renowned Einstein-Hilbert action, containing the Ricci scalar R and the determinant of the metric $g \equiv \det(g_{\mu\nu})$, and $S_{\rm M} = S_{\rm M}[g_{\mu\nu}, \psi_{\rm M}]$ is the action

term of the matter fields $\psi_{\rm M}$. The variation of the action $S_{\rm M}$ under a change of the metric $g_{\mu\nu} \to g_{\mu\nu} + \delta g_{\mu\nu}$ defines the stress-energy tensor of matter

$$T^{\mu\nu} \equiv \frac{2c}{\sqrt{-g}} \frac{\delta S_M}{\delta g_{\mu\nu}}. \tag{1.4}$$

By extremising the action with respect to the metric field $g_{\mu\nu}$, pursuant to the principle of least action, we get Einstein's field equations in the form

$$R_{\mu\nu} - \frac{1}{2} g_{\mu\nu} R = \frac{8\pi G}{c^4} T_{\mu\nu}, \tag{1.5}$$

which relate the metric, and thus the geometrical properties of spacetime, on the left-hand side, to the energy-momentum distribution of matter, on the right-hand side. Here $R_{\mu\nu}$ is the Ricci tensor, defined by the contraction $R_{\mu\nu} \equiv R^{\alpha}{}_{\mu\alpha\nu}$ of the Riemann curvature tensor,[1] and the Ricci scalar $R = R^{\alpha}{}_{\alpha}$ is its trace. Since Eq. (1.5) is written in terms of symmetric tensors of rank 2, it can be actually seen as a set of ten independent equations: four of them determine the evolution of matter, with the contracted Bianchi identities that imply

$$\nabla_\alpha T^{\mu\alpha} = 0, \tag{1.6}$$

the conservation of the matter stress-energy tensor; the other six constrain the ten components of the metric, with four residual unconstrained component that reflect the diffeomorphism invariance of GR and can be fixed by selecting a specific coordinate system. Our variable of reference to study GWs is the metric density

$$h^{\mu\nu} \equiv \sqrt{-g} g^{\mu\nu} - \eta^{\mu\nu}, \tag{1.7}$$

where $g^{\mu\nu}$ is the contravariant metric ($g_{\mu\alpha} g^{\alpha\nu} = \delta^{\nu}_{\mu}$) and $\eta^{\mu\nu} \equiv \mathrm{diag}(-1, 1, 1, 1)$ is a Minkowskian auxiliary metric, which is convenient in the prospects of describing GWs as space-time perturbations that propagate, in first approximation, on a fixed flat background. We now fix the gauge by imposing the *harmonic* (or *De Donder*) *gauge condition*

$$\partial_\alpha h^{\mu\alpha} = 0, \tag{1.8}$$

or equivalently by adopting harmonic coordinates. In this gauge, Einstein's equations (1.5) can be rewritten in the Landau-Lifshitz form[2]

$$\Box h^{\mu\nu} = \frac{16\pi G}{c^4} \tau^{\mu\nu}, \tag{1.9}$$

[1] Adopting Einstein notation, repeated indices are always implicitly summed over all their possible values

[2] These are often called *relaxed Einstein's equations*, because contrary to Eqs. (1.5) they do not imply automatically the conservation of the matter stress-energy tensor. This is instead implied by the harmonic condition (1.8), which in fact is required for the equivalence of Eq. (1.9) with Eqs. (1.5).

a wave-like differential equation characterized by the flat space-time d'Alembertian operator $\Box \equiv \eta^{\alpha\beta}\partial_\alpha\partial_\beta$. The quantity $\tau^{\mu\nu}$ that appears in the source term is the *stress-energy pseudo tensor*

$$\tau^{\mu\nu} \equiv (-g)T^{\mu\nu} + \frac{c^4}{16\pi G}\Lambda^{\mu\nu}, \tag{1.10}$$

which collects the contributions of the matter fields ($T^{\mu\nu}$) and the gravitational field ($\Lambda^{\mu\nu}$). The general expression of the latter in terms of the metric field reads

$$\begin{aligned}\Lambda^{\mu\nu} &= \partial_\alpha h^{\mu\beta}\partial_\beta h^{\nu\alpha} - h^{\alpha\beta}\partial_\alpha\partial_\beta h^{\mu\nu} + g_{\alpha\beta}g^{\rho\sigma}\partial_\rho h^{\mu\alpha}\partial_\sigma h^{\nu\beta} \\ &+ \frac{1}{2}g_{\alpha\beta}g^{\mu\nu}\partial_\rho h^{\alpha\sigma}\partial_\sigma h^{\rho\beta} - g_{\alpha\beta}(g^{\sigma\mu}\partial_\rho h^{\nu\beta} + g^{\sigma\nu}\partial_\rho h^{\mu\beta})\partial_\sigma h^{\rho\alpha} \\ &+ \frac{1}{8}(2g^{\mu\alpha}g^{\nu\beta} - g^{\mu\nu}g^{\alpha\beta})(2g_{\rho\sigma}g_{\lambda\tau} - g_{\sigma\lambda}g_{\rho\tau})\partial_\alpha h^{\rho\tau}\partial_\beta h^{\sigma\lambda}.\end{aligned} \tag{1.11}$$

Indeed, both $g^{\mu\nu}$ and $g_{\mu\nu}$ can be expanded, through Eq. (1.7), in terms of $h^{\mu\nu}$. Once this is done in Eq. (1.11), using $\eta^{\mu\nu}$ to raise and lower indices, $\Lambda^{\mu\nu}$ just depends on $h^{\mu\nu}$ and its spacetime derivatives up to the second. Due to the non-linearity of $g_{\mu\nu}$ as a functional of $h^{\mu\nu}$, this resulting expression has no closed form, as it involves infinite powers of $h^{\mu\nu}$ (and its derivatives), starting from quadratic combinations and going on indefinitely. We have thus the formal structure

$$\Lambda^{\mu\nu} = N^{\mu\nu}[h,h] + M^{\mu\nu}[h,h,h] + L^{\mu\nu}[h,h,h,h] + \mathcal{O}(h^5). \tag{1.12}$$

The quadratic terms, for instance, are given by

$$\begin{aligned}N^{\mu\nu}[h,h] &= -h^{\alpha\beta}\partial_\alpha\partial_\beta h^{\mu\nu} + \frac{1}{2}\partial^\mu h_{\alpha\beta}\partial^\nu h^{\alpha\beta} - \frac{1}{4}\partial^\mu h\partial^\nu h \\ &- \partial^\mu h_{\alpha\beta}\partial^\alpha h^{\beta\nu} - \partial^\nu h_{\alpha\beta}\partial^\alpha h^{\beta\mu} + \partial_\alpha h^{\mu\beta}(\partial^\alpha h^\nu_\beta + \partial_\beta h^{\alpha\nu}) \\ &+ \eta^{\mu\nu}\left(-\frac{1}{4}\partial_\alpha h_{\beta\rho}\partial^\alpha h^{\beta\rho} + \frac{1}{8}\partial_\alpha h\partial^\alpha h + \frac{1}{2}\partial_\alpha h_{\beta\rho}\partial^\beta h^{\alpha\rho}\right),\end{aligned} \tag{1.13}$$

where on the right-hand side we used the notation $h \equiv \eta_{\alpha\beta}h^{\alpha\beta}$. The full (rather long) expressions of the cubic and quartic terms can be found in Eqs. (3.8b)-(3.8c) of Ref. [62].

Let us also mention that the harmonic condition (1.8) implies, through Eq. (1.9), the conservation law $\partial_\alpha\tau^{\alpha\mu} = 0$ for the stress-energy pseudo tensor, and this can be shown to be equivalent to the covariant conservation of energy and momentum, given by Eq. (1.6).

Under the assumption that the gravitational field has been independent of time before some reference finite instant, the so-called *past-stationarity condition*[3], we can write a formal exact solution to Eq. (1.9) as

$$h^{\mu\nu} = \frac{16\pi G}{c^4}\Box^{-1}_{\rm ret}\tau^{\mu\nu}, \tag{1.14}$$

[3]This is a way to impose the no-incoming radiation condition, which states that the source is isolated and does not receive any external radiation.

where we used the retarded inverse d'Alembertian integral operator

$$(\Box^{-1}_{\rm ret} f)(\mathbf{x},t) \equiv -\frac{1}{4\pi}\int \frac{d^3\mathbf{x}'}{|\mathbf{x}-\mathbf{x}'|} f(t-|\mathbf{x}-\mathbf{x}'|/c,\mathbf{x}'), \tag{1.15}$$

such that $\Box^{-1}_{\rm ret}(\Box f) = f$.

Indeed, considering that $\tau^{\mu\nu}$ is a functional of $h^{\mu\nu}$ and its derivatives, Eq. (1.14) is no more than an integro-differential way of rewriting Eq. (1.9); in fact, it cannot be evaluated exactly for realistic astrophysical sources. In the rest of this Chapter we will rather explore how to compute analytically solutions to these field equations using suitable approximation schemes, in particular those that best capture the physics of GWs when they originate from PN sources.

1.2 Gravitational radiation in linearized gravity

We start our dive in the theoretical description of GWs by analyzing the case of *linearized gravity*, a simplified setting where it is assumed that the gravitational field of the source is weak enough that the metric tensor can be decomposed as

$$g_{\mu\nu} = \eta_{\mu\nu} + \tilde{h}_{\mu\nu}, \quad |\tilde{h}_{\mu\nu}| \ll 1, \tag{1.16}$$

namely as the combination of the Minkowskian metric $\eta_{\mu\nu}$, describing a flat background, with a gravitational perturbation $\tilde{h}_{\mu\nu}$ taken to be so small that any contribution more than linear in it can be neglected. For self-gravitating sources, this approximation means that we are describing their dynamics as prescribed by Newtonian gravity. Coming back to our general GW variable $h^{\mu\nu}$, if we use in its definition (1.7) the linear limit relations $\sqrt{-g} \simeq 1 + 1/2\tilde{h}$, where $\tilde{h} = \eta^{\mu\nu}\tilde{h}_{\mu\nu}$, and $g^{\mu\nu} \simeq \eta^{\mu\nu} - h^{\mu\nu}$, we find

$$h^{\mu\nu} \simeq \left(1+\frac{1}{2}\tilde{h}\right)(\eta^{\mu\nu}-\tilde{h}^{\mu\nu}) - \eta^{\mu\nu} \simeq -\left(\tilde{h}^{\mu\nu} - \frac{1}{2}\eta^{\mu\nu}\tilde{h}\right). \tag{1.17}$$

Therefore, the linear approximation of $h^{\mu\nu}$ coincides, modulo an overall sign, to the trace-reversed perturbation $\bar{h}^{\mu\nu} \equiv \tilde{h}^{\mu\nu} - 1/2\,\eta^{\mu\nu}\tilde{h}$, the standard field variable used to study GWs in linearized gravity. Correspondingly, by recasting the general field equations (1.9) in terms of this variable, with $h^{\mu\nu} \simeq -\bar{h}^{\mu\nu}$, and expanding to linear order in $\bar{h}^{\mu\nu}$, we find the linearized field equations

$$\Box\bar{h}_{\mu\nu} = -\frac{16\pi G}{c^4}T_{\mu\nu}, \tag{1.18}$$

which are to be solved with the associated harmonic condition

$$\partial^\alpha \bar{h}_{\alpha\mu} = 0, \tag{1.19}$$

linear limit reduction of Eq. (1.8). Before we start working out a solution to the set of equations (1.18)-(1.19), which fully characterize the GW generation problem in linearized gravity, we have to discuss the specific gauge symmetry of this theory.

1.2.1 Gauge symmetry in linearized theory

Since the linear condition (1.16) is reference-frame dependent, as soon as we enforce the linearized approximation we break the gauge symmetry of GR under arbitrary diffeomorphisms, i.e.

$$x^\mu \to x'^\mu(x) \quad \Longrightarrow \quad g_{\mu\nu}(x) \to g'_{\mu\nu}(x') = \frac{\partial x^\rho}{\partial x'^\mu}\frac{\partial x^\sigma}{\partial x'^\nu} g_{\rho\sigma}(x). \tag{1.20}$$

Nevertheless, in linearized gravity some gauge freedom still remains, and accordingly we are able to select the harmonic gauge (1.19). But there is more: a coordinate change $x^\mu \to x^\mu + \xi^\mu(x)$ on the linear metric (1.16) yields, through Eq. (1.20), the transformation law

$$\tilde{h}_{\mu\nu} \to \tilde{h}_{\mu\nu} - (\partial_\mu \xi_\nu + \partial_\nu \xi_\mu), \tag{1.21}$$

which in terms of $\bar{h}_{\mu\nu}$ becomes

$$\bar{h}_{\mu\nu} \to \bar{h}_{\mu\nu} - (\partial_\mu \xi_\nu + \partial_\nu \xi_\mu - \eta_{\mu\nu}\partial_\alpha \xi^\alpha). \tag{1.22}$$

By applying on the latter a partial derivative, one can easily show that

$$\partial^\nu \bar{h}_{\mu\nu} \to \partial^\nu \bar{h}_{\mu\nu} - \Box \xi_\mu, \tag{1.23}$$

and thus find that the harmonic condition (1.19) does not constrain the coordinate displacement vector ξ^μ, if not for the condition $\Box \xi_\mu = 0$. This manifests the possibility of imposing four additional conditions on $\bar{h}_{\mu\nu}$ through a suitable choice for ξ^μ. A standard choice in this context is to fix ξ^0 so as to enforce $\bar{h} = 0$, and use the remaining spacial components ξ^i to set $\bar{h}^{0i} = 0$, which, via the harmonic condition, also implies $\partial^0 \bar{h}_{00} = 0$. As far as GWs are concerned, which have a non-static character by definition, this last condition means $\bar{h}_{00} = 0$, and we finally have

$$\bar{h}^{0\mu} = 0, \quad \bar{h} = 0, \quad \partial^j \bar{h}_{ij} = 0. \tag{1.24}$$

This is the definition of the *transverse-traceless* (TT) *gauge*, and the corresponding GW variable is denoted as h_{ij}^{TT}. Having completely fixed the gauge, h_{ij}^{TT} only depends on two physical degrees of freedom, i.e the two GW polarizations in the plane transverse to the unit vector $\mathbf{n}$, pointing from the source to the observer. For instance, in a Cartesian coordinate system $\{t, x, y, z\}$ with the z axis oriented along $\mathbf{n}$, we have

$$h_{ij}^{TT} = \begin{pmatrix} h_+ & h_\times & 0 \\ h_\times & -h_+ & 0 \\ 0 & 0 & 0 \end{pmatrix}_{ij}, \tag{1.25}$$

where h_+ and $h_\times$ are respectively the well-known *plus* and *cross* polarizations of a GW, named after the displacement they induce on a ring of test masses

as the GW transversely propagates through it. On more general terms, introducing two orthogonal unit vectors $\mathbf{u}$ and $\mathbf{w}$ in the plane transverse to $\mathbf{n}$, we can define the two physical polarizations of the wave as

$$\begin{aligned} h_+ &\equiv \frac{1}{2}(u_i u_j - w_i w_j) h_{ij}^{TT}, \\ h_\times &\equiv \frac{1}{2}(u_i w_j - w_i u_j) h_{ij}^{TT}. \end{aligned} \tag{1.26}$$

Moreover, defining the vector

$$\mathbf{m} \equiv \frac{1}{\sqrt{2}}(\mathbf{u} + i\mathbf{w}) \tag{1.27}$$

we can also write

$$h_+ - i h_\times = m_a^* m_b^* h_{ab}^{TT}. \tag{1.28}$$

We conclude this discussion by mentioning that, given a GW solution in the harmonic gauge, we can find the associated TT solution by applying the projector

$$\Pi_{ijkl}(\mathbf{n}) \equiv P_{ik}(\mathbf{n}) P_{jl}(\mathbf{n}) - \frac{1}{2} P_{ij}(\mathbf{n}) P_{kl}(\mathbf{n}), \tag{1.29}$$

where $P(\mathbf{n}) \equiv \delta_{ij} - n_i n_j$. Its relevant properties are

$$\Pi_{ijkl}\Pi_{klmn} = \Pi_{ijmn}, \quad n_i \Pi_{ijkl} = n_j \Pi_{ijkl} = ... = 0, \quad \Pi_{iikl} = \Pi_{ijkk} = 0. \tag{1.30}$$

1.2.2 Leading-order quadrupole formalism

We now make the first steps in the resolution of the linearized field equations (1.18). Under the past-stationarity condition, the d'Alembertian operator in Eq. (1.18) can be inverted using a retarded Green's function, as we did in the full non-linear theory to get Eq. (1.14). In this case, the resulting solution reads

$$\bar{h}_{\mu\nu}(t, \mathbf{x}) = \frac{4G}{c^4} \int d^3\mathbf{x}' \, \frac{1}{|\mathbf{x} - \mathbf{x}'|} T_{\mu\nu}\left(t - \frac{|\mathbf{x} - \mathbf{x}'|}{c}, \mathbf{x}'\right), \tag{1.31}$$

where indeed $T_{\mu\nu}$ is the stress-energy tensor of matter. Outside the source, the corresponding TT gauge solution is then given by the TT projector (1.29) as

$$h_{ij}^{TT}(t, \mathbf{x}) = \frac{4G}{c^4} \Pi_{ijkl}(\mathbf{n}) \int d^3\mathbf{x}' \, \frac{1}{|\mathbf{x} - \mathbf{x}'|} T_{kl}\left(t - \frac{|\mathbf{x} - \mathbf{x}'|}{c}, \mathbf{x}'\right), \tag{1.32}$$

where now $\mathbf{n} = \mathbf{x}/|\mathbf{x}|$. Here we can omit the components T_{00} and T_{0k}, since they are related to T_{kl} by the conservation law $\partial^\mu T_{\mu\nu} = 0$, linear-order version of the condition (1.6). Let us denote by d the radius of a time-like world tube enclosing the source and define $r \equiv |\mathbf{x}|$. The integral in Eq. (1.32) has the same

compact support of T_{ij}, i.e. $|\mathbf{x}'| \leq d$. Therefore, if we focus on field points far away from the source, satisfying $r \gg d$, we can expand its integrand according to

$$|\mathbf{x} - \mathbf{x}'| = r - \mathbf{x}' \cdot \mathbf{n} + O\left(\frac{d^2}{r}\right). \tag{1.33}$$

By selecting the leading $\mathcal{O}(1/r)$ component, which is essentially the one we can observe with our detectors, because of the large distance separating them from the typical GW source, we find

$$h_{ij}^{TT}(t, \mathbf{x}) = \frac{1}{r}\frac{4G}{c^4}\Pi_{ijkl}(\mathbf{n}) \int d^3\mathbf{x}'\, T_{kl}\left(t_r + \frac{\mathbf{x}' \cdot \mathbf{n}}{c}, \mathbf{x}'\right), \tag{1.34}$$

where we introduced the retarded time $t_r \equiv t - r/c$. As we already mentioned in the Introduction, for self-gravitating sources like the ones we are interested in, the weak-field condition underlying the linear approximation is paired with the small-velocity condition. The latter, for a source of typical velocity v and internal frequency ω_s, can be written as $v \sim \omega_s d \ll c$. Let us then consider the Fourier transform of the stress-energy tensor

$$T_{kl}\left(t_r + \frac{\mathbf{x}' \cdot \mathbf{n}}{c}, \mathbf{x}'\right) = \int \frac{d^4k}{(2\pi)^4}\, \tilde{T}_{kl}(\omega, \mathbf{k}) e^{-i\omega(t_r + (\mathbf{x}'\cdot\mathbf{n})/c) + i\mathbf{k}\cdot\mathbf{x}'}, \tag{1.35}$$

where $k = (\omega/c, \mathbf{k})$. From the small-velocity condition, the compact support of the integral (1.35), and the fact that $\tilde{T}_{kl}(\omega, \mathbf{k})$ is peaked around a range of frequencies with maximum value ω_s, we infer that the frequencies ω whose contribution to the above Fourier transform is dominant satisfy

$$\frac{\omega}{c}\mathbf{x}' \cdot \mathbf{n} \lesssim \frac{\omega_s d}{c} \ll 1. \tag{1.36}$$

We can thus exploit such condition and perform the expansion

$$e^{-i\omega(t_r + (\mathbf{x}'\cdot\mathbf{n})/c) + i\mathbf{k}\cdot\mathbf{x}'} = e^{-i\omega t_r}\left(1 - i\frac{\omega}{c}x_i' n_i - \frac{1}{2}\frac{\omega^2}{c^2}x_i' x_j' n_i n_j + ...\right). \tag{1.37}$$

When this is inserted in Eq. (1.35), the result is the associated expansion

$$\begin{aligned} T_{kl}\left(t_r + \frac{\mathbf{x}' \cdot \mathbf{n}}{c}, \mathbf{x}'\right) = T_{kl}(t_r, \mathbf{x}') + \frac{x_i' n_i}{c}\dot{T}_{kl}(t_r, \mathbf{x}') \\ + \frac{1}{2c^2}x_i' x_j' n_i n_j \ddot{T}_{kl}(t_r, \mathbf{x}') + ..., \end{aligned} \tag{1.38}$$

where, using a standard notation, each dot represents a derivative with respect to time. In turn, once this is put inside Eq. (1.34), it yields

$$h_{ij}^{TT}(t, \mathbf{x}) = \frac{1}{r}\frac{4G}{c^4}\Pi_{ijkl}(\mathbf{n})\left[S_{kl}(t_r) + \frac{1}{c}n_m \dot{S}_{klm}(t_r) +\right.$$

$$+\frac{1}{2c^2}n_m n_n \ddot{S}_{klmn}(t_r)+...\Bigg] \tag{1.39}$$

where we introduced the stress multipole of T_{ij}, defined as

$$S_{ij}(t) \equiv \int d^3\mathbf{x}\, T_{ij}(t,\mathbf{x}), \qquad \text{[stress monopole]} \tag{1.40}$$

$$S_{ijk}(t) \equiv \int d^3\mathbf{x}\, T_{ij}(t,\mathbf{x}) x_k, \qquad \text{[stress dipole]} \tag{1.41}$$

$$S_{ijkl}(t) \equiv \int d^3\mathbf{x}\, T_{ij}(t,\mathbf{x}) x_k x_l. \qquad \text{[stress quadrupole]} \tag{1.42}$$

Higher orders in Eq. (1.39) involve higher multipoles of T_{ij}, and their definition follows by analogy with the lowest order multipoles listed above. Notice that all these multipoles are separately symmetric in ij and in the set of indices that comes after them.

Given that $\partial_t^n S_{ijk_1...k_n} \sim v^n$, we recognize in Eq. (1.39) the familiar structure in powers of v/c of a PN expansion. Truncating it at leading order gives

$$h_{ij}^{TT}(t,\mathbf{x}) = \frac{1}{r}\frac{4G}{c^4}\Pi_{ijkl}(\mathbf{n})\Big[S_{kl}(t_r)+\mathcal{O}(v^2/c^2)\Big]. \tag{1.43}$$

We want now to rewrite the stress monopole S^{kl} in order to make more explicit its physical meaning. For this purpose we define the multipoles of $\rho \equiv T_{00}/c^2$, the Newtonian mass density, as

$$Q_{i_1...i_n}(t) \equiv \int d^3\mathbf{x}\, \rho(t,\mathbf{x}) x_{i_1}...x_{i_n}, \qquad \text{[mass } 2^n\text{-pole]} \tag{1.44}$$

and the multipoles of the momentum density $\mathcal{P}_i \equiv T_{0i}/c$, as

$$P_{ij_1...j_n}(t) \equiv \int d^3\mathbf{x}\, \mathcal{P}_i(t,\mathbf{x}) x_{j_1}...x_{j_n}. \qquad \text{[momentum } 2^n\text{-pole]} \tag{1.45}$$

From the stress monopole definition S_{ij} we have

$$\begin{aligned} S_{ij} &= \int d^3\mathbf{x}\, T_{ij} = \int d^3\mathbf{x}\, T_{ik}\delta_{kj} = \int d^3\mathbf{x}\, T_{ik}\partial_k x_j = \\ &= -\int d^3\mathbf{x}\, \partial_k T_{ik} x_j. \end{aligned} \tag{1.46}$$

The integration by parts in the last equality is performed considering an integration volume larger than the source, on whose boundaries $T_{\mu\nu} = 0$. Then, the conservation law $\partial_\alpha T^{\alpha\mu} = 0$ tells us

$$\partial_k T_{ki} = -\frac{1}{c}\partial_0 T_{0i}, \tag{1.47}$$

so that, after restoring the original symmetry in ij, we have

$$S_{ij} = \frac{1}{c}\int d^3\mathbf{x}\, \dot{T}_{0(i}x_{j)} = \frac{1}{2}\left(\dot{P}_{ij} + \dot{P}_{ji}\right). \tag{1.48}$$

Here we adopted the notation by which the symmetric part of a tensor with respect of set of its indices is indicated by enclosing such set in the parentheses (). With the same trick we find

$$\begin{aligned} P_{ij} &= \frac{1}{c}\int d^3\mathbf{x}\, T_{0k}\delta_{ki}\, x_j = \frac{1}{c}\int d^3\mathbf{x}\, T_{0k}\big(\partial_k x_i\big)x_j = \\ &= -\frac{1}{c}\int d^3\mathbf{x}\left(\partial_k T_{0k} x_i x_j + T_{0j}x_i\right) = \dot{Q}_{ij} - P_{ji}, \end{aligned} \tag{1.49}$$

and thus

$$S_{ij} = \frac{1}{2}\ddot{Q}_{ij}. \tag{1.50}$$

At this point, we can go back to Eq. (1.43) and plug in it the relation we just found. Since $\Pi_{ijkl}\delta_{kl} = 0$, we do so by trading $Q_{ij}(t)$ with its traceless analogue

$$M_{ij}^{\rm quad}(t) \equiv Q_{ij}(t) - \frac{1}{3}\delta_{kl}Q_{kl}(t) = \int d^3\mathbf{x}\, \rho(t,\mathbf{x})\left(x_i x_j - \frac{1}{3}r^2\delta_{ij}\right), \tag{1.51}$$

finally obtaining

$$h_{ij}^{TT}(t,\mathbf{x}) = \frac{1}{r}\frac{2G}{c^4}\Pi_{ijkl}(\mathbf{n})\left[\ddot{M}_{ij}^{\rm quad}(t_r) + \mathcal{O}(v^2/c^2)\right], \tag{1.52}$$

the famous quadrupole formula originally found by Einstein [168], which shows the leading quadrupolar nature of GWs, a characteristic maintained even in the full non-linear theory. This is in agreement with the field-theoretic take on GR, where the graviton, the carrier of the gravitational interaction, is a massless particle with helicty ± 2, implying that it does not admit a state with total angular momentum $j = 0$ or $j = 1$, as it would be required for a monopolar or dipolar radiation.

We highlight that, in the point-particle case specified by the flat spacetime analogue of the energy-momentum tensor (1.2), the mass quadrupole (1.51) can be conveniently expressed as

$$M_{ij}^{\rm quad}(t) = \mu\left(y_{12}^i(t)y_{12}^j(t) - \frac{1}{3}r_{12}^2(t)\delta_{ij}\right) \tag{1.53}$$

where $\mathbf{y}_{12} \equiv \mathbf{y}_1 - \mathbf{y}_2$ is the relative coordinate of the two particles in the center-of-mass frame, $r_{12} \equiv |\mathbf{y}_{12}|$ their relative separation, and $\mu \equiv m_1 m_2/(m_1+m_2)$ their reduced mass.

Within this leading quadrupole formalism, we can also compute the GW fluxes of energy and angular momentum at infinity, emitted by the source in

all directions. Once we have specified a GW solution at infinity, in the TT gauge, they follow from the general formulas

$$\dot{E} = \frac{r^2 c^3}{32\pi G} \int d\Omega\, \dot{h}^{TT}_{ij} \dot{h}^{TT}_{ij}, \tag{1.54}$$

$$\dot{J}_i, = \frac{r^2 c^3}{32\pi G} \int d\Omega\, \epsilon_{ijk} \big(2\dot{h}^{TT}_{jl} h^{TT}_{kl} - \dot{h}^{TT}_{lm} x_j \partial_k h^{TT}_{lm}\big), \tag{1.55}$$

where Ω is the solid angle and ϵ_{ijk} is the Levi-Civita symbol. Using our leading quadrupole solution (1.52) and performing the integral over Ω with the identity

$$\int d\Omega\, \Pi_{iikl}(\mathbf{n}) = \frac{2\pi}{15}(11\delta_{ik}\delta_{jl} - 4\delta_{ij}\delta_{kl} + \delta_{il}\delta_{jk}), \tag{1.56}$$

we find

$$\dot{E}^{\rm quad} = \frac{G}{5c^5}\left[\dddot{M}^{\rm quad}_{ij}\, \dddot{M}^{\rm quad}_{ij} + \mathcal{O}(v^2/c^2)\right], \tag{1.57}$$

$$\dot{J}^{\rm quad}_{ij} = \frac{2G}{5c^5}\left[\epsilon_{ijk} \ddot{M}^{\rm quad}_{jl}\, \dddot{M}^{\rm quad}_{kl} + \mathcal{O}(v^2/c^2)\right]. \tag{1.58}$$

1.2.3 General linear solution

In the previous section we computed explicitly the leading quadrupolar GW solution in linearized theory and we found in passing that a simple generalization of this solution, with higher order corrections in v/c, can be found in the form a multipole expansion; see Eq. (1.34). Here our intention is to write down, in a convenient and physically meaningful fashion, the most general solution, valid outside the source, to the linearized field equations (1.18). To this end, we will introduce a systematic generalization of the multipole decomposition we encountered previously, which will be also essential for the construction of a GW solution beyond the linear approximation, the central topic of Sec. 1.3. In order to firmly establish the logic of this formalism, we will proceed by first exploring its application to the simpler problems

$$\begin{aligned} &(1) \quad \Delta\phi(\mathbf{x}) = -4\pi S(\mathbf{x}), \\ &(2) \quad \Box\phi(t,\mathbf{x}) = -4\pi S(t,\mathbf{x}), \end{aligned}$$

where ϕ is a scalar field, S its associated source, and $\Delta \equiv \partial_i\partial_i$ the Laplace operator. After that, at the end of this section, we will apply such formalism to the case of linearized gravity, so as to build, accordingly, the sought-for general linear solution.

Multipole decomposition of the Poisson equation

We start our analysis by discussing the static problem

$$\Delta\phi(\mathbf{x}) = -4\pi S(\mathbf{x}), \tag{1.59}$$

for a localized source $S(\mathbf{x})$ whose compact support is enclosed in a sphere of radius d. The associated homogeneous problem, Laplace's equation $\Delta\phi(\mathbf{x}) = 0$, is an elliptic differential equation that admits an analytic solution $\varphi(\mathbf{x})$. We can therefore Taylor-expand the latter around the origin $\mathbf{0}$ of our (here three-dimensional) coordinate system as

$$\varphi(\mathbf{x}) = \varphi(\mathbf{0}) + x_i(\partial_i\varphi)(\mathbf{0}) + \frac{1}{2}x_i x_j(\partial_i\partial_j\varphi)(\mathbf{0}) + ... \quad . \tag{1.60}$$

We introduce a convenient index notation by Blanchet & Damour, according to which any tensor F with ℓ indices, say $(i_1, ..., i_\ell)$, is written in short as $F_L \equiv F_{i_1...i_\ell}$; similarly $x^L \equiv x^{i_1}...x^{i_\ell}$ and $\partial_L \equiv \partial_{i_1}...\partial_{i_\ell}$. In these terms, the above Taylor expansion assumes the compact form

$$\varphi(\mathbf{x}) = \sum_{l=0}^{\infty} x_L F_L, \qquad F_L \equiv \frac{1}{\ell!}(\partial_L\varphi)(\mathbf{0}), \tag{1.61}$$

where we notice that the tensor F_L is indeed symmetric but also *trace-free*, i.e. any possible contraction with the metric returns zero; here the metric is δ_{ij} and, after a contraction with any index of F_L, we have $\partial^k\partial_k\varphi = \Delta\varphi = 0$. We will say that a tensor with such properties is *symmetric-trace-free* (STF). The contraction of a STF tensor with a generic non-STF tensor selects just the STF part of the latter. Therefore, our solution about the origin becomes actually

$$\varphi(\mathbf{x}) = \sum_{\ell=0}^{\infty} \hat{x}_L\hat{F}_L = \sum_{\ell=0}^{\infty} r^\ell\hat{n}_L\hat{F}_L, \tag{1.62}$$

where we use a hat to mark tensors that are STF with respect to all their indices and $\mathbf{x} = r\mathbf{n}$. The formula to compute the STF part of a generic tensor is given in Appendix A.1.

For our discussion we are actually interested in a solution regular at infinity rather than at the origin. Following a similar rationale, it can be shown that this solution can be generally written in the STF language as

$$\varphi(\mathbf{x}) = \sum_{\ell=0}^{\infty} \frac{\hat{n}_L\hat{D}_L}{r^{\ell+1}} = \frac{D_0}{r} + \frac{n_i D_i}{r^2} + \frac{\hat{n}_{ij}\hat{D}_{ij}}{r^3} + ... \quad , \tag{1.63}$$

where $\hat{D}_L$ is a numerical tensor akin to the $\hat{F}_L$ above. We recognize the usual profile of the multipole expansion, now rewritten in closed form thanks to the

STF formalism. Equivalently, if we consider[4]

$$\partial_L \frac{1}{r} = (-)^\ell (2\ell-1)!! \frac{\hat{n}_L}{r^{\ell+1}}, \tag{1.64}$$

and define

$$\hat{C}_L \equiv \frac{\ell!}{(2\ell-1)!!} \hat{D}_L, \tag{1.65}$$

we can rewrite the multipole decomposition (1.63) in the form

$$\varphi(\mathbf{x}) = \sum_{\ell=0}^{\infty} \frac{(-)^\ell}{\ell!} \hat{C}_L \partial_L \frac{1}{r}. \tag{1.66}$$

Let us now come back to our Poisson equation (1.62). The Green's function method readily tells us that, considering

$$\Delta \frac{1}{|\mathbf{x}-\mathbf{y}|} = -4\pi\delta^3(\mathbf{x}-\mathbf{y}), \tag{1.67}$$

its solution is given by the integral

$$\varphi(\mathbf{x}) = \int d^3\mathbf{y}\, \frac{S(\mathbf{y})}{|\mathbf{x}-\mathbf{y}|}. \tag{1.68}$$

Outside the source, where necessarily $r \equiv |\mathbf{x}| > |\mathbf{y}|$, we can expand the denominator as

$$\frac{1}{|\mathbf{x}-\mathbf{y}|} = \sum_{\ell=0}^{\infty} (-)^\ell y_L \partial_L \frac{1}{r} = \sum_{\ell=0}^{\infty} (-)^\ell \hat{y}_L \partial_L \frac{1}{r}, \tag{1.69}$$

where, in the last equality, we used the fact that $\partial_L(1/r)$ is a STF tensor. Therefore, the STF decomposition of the solution (1.68), valid outside the source, is

$$\varphi(\mathbf{x}) = \sum_{\ell=0}^{\infty} \frac{(-)^\ell}{\ell!} \hat{Q}_L \partial_L \frac{1}{r}. \tag{1.70}$$

which has the same structure of Eq. (1.66) but, instead of the numerical tensors $\hat{C}_L$, it features the STF multipole moments of the source

$$\hat{Q}_L \equiv \int d^3\mathbf{y}\, \hat{y}_L S(\mathbf{y}). \tag{1.71}$$

[4]One can easily prove that $\partial_L(1/r)$ is trace-free from $\Delta(1/r) = 0$.

Multipole decomposition of the relativistic wave equation of a scalar field

Now we shift our attention to the wave equation

$$\Box\phi(t,\mathbf{x}) = -4\pi S(t,\mathbf{x}), \tag{1.72}$$

where $S(\mathbf{x})$ is again a source with spacial compact support enclosed in a sphere of radius d. The exact retarded solution of this equation, computed in terms of the retarded inverse operator of the d'Alembertian (1.15), reads

$$\phi(t,\mathbf{x}) = \int d^3\mathbf{y}\,\frac{S(t-|\mathbf{x}-\mathbf{y}|/c,\mathbf{y})}{|\mathbf{x}-\mathbf{y}|}, \tag{1.73}$$

and it is well defined anywhere, even inside the source.

We now want to write down a multipole decomposition for $\phi(t,\mathbf{x})$ valid outside the source, akin to the one in Eq. (1.70). To do so we notice that, for any given function f of the retarded rime $t_r \equiv t - r/c$, we have

$$\Box\left[\frac{f(t_r)}{r}\right] = 0, \tag{1.74}$$

meaning that $f(t_r)/r$ is a solution to Eq. (1.72) in its homogeneous vacuum form, to which it reduces for $r > d$ because of the compact support of $S(\mathbf{x})$. This is still true even after we apply to $f(t_r)/r$ an arbitrary number of partial derivatives ∂_i and we use, in place of f, a multi-index STF tensor. Therefore, the decomposition

$$\phi(t,\mathbf{x}) = \sum_{\ell=0}^{\infty}\frac{(-)^\ell}{\ell!}\partial_L\left[\frac{\hat{F}_L(t_r)}{r}\right], \tag{1.75}$$

written in terms of a set of generic STF tensors $\hat{F}_L$, is ensured to describe a solution to (1.72) in the region outside the source, since each of its terms separately solves the associated vacuum equation. Moreover, Eq. (1.75) actually represents the *most general* solution of this kind. In fact, a STF tensor with ℓ indices, and corresponding $2\ell+1$ independent components, is an *irreducible* representation of weight ℓ and dimension $2\ell+1$ of $SO(3)$, the group of proper rotations. Therefore, the set of STF tensors $\hat{F}_L$, with ℓ ranging from zero to any positive integer value, provides a *complete* set of representations of $SO(3)$.

Having recognized the generality of Eq. (1.75), we still have to relate the STF tensors $\hat{F}_L$ to the source S. As detailed in Appendix B of Ref. [104], this is done by expanding in STF harmonics the integral in Eq. (1.73) and by relating it to Eq. (1.75), in the region outside the source. The result reads

$$\hat{F}_L(t_r) \equiv \int d^3\mathbf{y}\,\hat{y}_L\int_{-1}^{1} dz\,\delta_\ell(z)S(t_r + z|\mathbf{y}|/c,\mathbf{y}), \tag{1.76}$$

where we have a weighted time average in z, with weight function

$$\delta_\ell(z) \equiv \frac{(2\ell+1)!!}{2^{\ell+1}\ell!}(1-z^2)^\ell, \tag{1.77}$$

which satisfies

$$\int dz\, \delta_\ell(z) = 1, \qquad \lim_{\ell\to\infty} \delta_\ell(z) = \delta(z). \tag{1.78}$$

This integral in z can be physically traced back to the time delay between different points within the extended source $S(t,\mathbf{x})$, which becomes irrelevant for large ℓ.

It is important to mention that the integral over z in Eq. (1.76) admits, in the slow-velocity regime, the convenient time-derivative expansion

$$\int_{-1}^{1} dz\, \delta_\ell(z) f(t_r + z|\mathbf{y}|/c, \mathbf{y}) = \sum_{k=0}^{\infty} \frac{(2\ell+1)!!}{2^k k!(2\ell+2k+1)!!}\left(\frac{|\mathbf{y}|}{c}\frac{\partial}{\partial t_r}\right)^{2k} f(t_r), \tag{1.79}$$

which essentially replaces the integral with its formal PN series.

Multipole decomposition in linearized gravity

We are now ready to apply the STF tensor formalism on the linearized field equations, which we recall to be

$$\Box \bar{h}_{\mu\nu}(t,\mathbf{x}) = -\frac{16\pi G}{c^4} T_{\mu\nu}(t,\mathbf{x}), \tag{1.80}$$

with the matter source $T_{\mu\nu}$ assumed to have a spatial compact support. Following the logic we outlined above, while treating each component of $\bar{h}_{\mu\nu}$ as a scalar field, we can write the most general solution, in the exterior region, as

$$\bar{h}_{00}(t,\mathbf{x}) = \frac{4G}{c^4}\sum_{\ell=0}^{\infty}\frac{(-)^\ell}{\ell!}\partial_L\left[\frac{\hat{F}_L(t_r)}{r}\right], \tag{1.81}$$

$$\bar{h}_{0i}(t,\mathbf{x}) = \frac{4G}{c^4}\sum_{\ell=0}^{\infty}\frac{(-)^\ell}{\ell!}\partial_L\left[\frac{G_{i\langle L\rangle}(t_r)}{r}\right], \tag{1.82}$$

$$\bar{h}_{ij}(t,\mathbf{x}) = \frac{4G}{c^4}\sum_{\ell=0}^{\infty}\frac{(-)^\ell}{\ell!}\partial_L\left[\frac{H_{ij\langle L\rangle}(t_r)}{r}\right], \tag{1.83}$$

where we used the usual notation by which the delimiters $\langle\rangle$ enclose subsets of STF indices on tensors that are not completely STF. Among these equations, only Eq. (1.81) can be rightfully said to represent a proper multipole decomposition, as it is given in terms of the STF tensors

$$\hat{F}_L(t_r) = \int d^3\mathbf{y}\, \hat{y}_L \int_{-1}^{1} dz\, \delta_\ell(z) T_{00}(t_r + z|\mathbf{y}|/c, \mathbf{y}), \tag{1.84}$$

irreducible representations of dimension $2\ell+1$ of $SO(3)$, in perfect analogy with the scalar case. All the other components, instead, are written in terms of tensors, $G_{i\langle L\rangle}$ and $H_{ij\langle L\rangle}$, which are STF only in the indices L, and thus actually yield *reducible* representations of $SO(3)$, respectively of the type $D^1\otimes D^\ell$ and $D^1\otimes D^1\otimes D^\ell$. We can however decompose them in a direct sum of irreducible representations, considering $D^1\otimes D^\ell = D^{\ell+1}\oplus D^\ell\oplus D^{|\ell-1|}$. More specifically, in STF terms, we can use the formula [161][5]

$$G_{i\langle L\rangle} = \hat{G}^{(+)}_{iL} + \frac{\ell}{\ell+1}\epsilon_{ai\langle i_\ell}\hat{G}^{(0)}_{L-1\rangle a} + \frac{2\ell-1}{2\ell+1}\delta_{i\langle i_\ell}\hat{G}^{(-)}_{L-1\rangle}, \tag{1.85}$$

where $\hat{G}^{(+)}_{iL}\equiv G_{\langle iL\rangle}$, $\hat{G}^{(0)}_{L}\equiv G_{bc\langle L-1}\epsilon_{i\ell\rangle bc}$, and $\hat{G}^{(-)}_{L-1}\equiv \hat{G}_{bbL-1}$. A repeated application of this formula also yields the decomposition of $H_{ij\langle L\rangle}$ in six irreducible pieces; this is given explicitly in Eqs. (5.7)-(5.8) of Ref. [162].

At the end of this operation, our solution $\bar{h}_{\mu\nu}$ is decomposed in a total of 10 independent sets of STF tensors. We can however relate some of them by specifying our gauge choices: to begin with, the so-decomposed solution does not satisfy automatically the harmonic condition (1.19), and by imposing it we get 4 constraints; then, as described in Sec. 1.2.1, we have the extra gauge symmetry of the linearized theory, which we can use to impose 4 additional constraints. This leads to the possibility of parameterizing our general linear solution in terms of just two residual sets of STF tensors, the so-called *canonical multipole moments* of the source, $\mathcal{M}_L$ and $\mathcal{S}_L$,[6] respectively dubbed of *mass type* and *current type*. For the details of this rather long computation we refer to Ref. [162]. The final result is

$$\bar{h}_{00}(t,\mathbf{x}) = \frac{4G}{c^2}\sum_{\ell=0}^{\infty}\frac{(-)^\ell}{\ell!}\partial_L\left[\frac{\mathcal{M}_L(t_r)}{r}\right], \tag{1.86}$$

$$\bar{h}_{0i}(t,\mathbf{x}) = -\frac{4G}{c^3}\sum_{\ell=1}^{\infty}\frac{(-)^\ell}{\ell!}\left\{\partial_{L-1}\left[\frac{\dot{\mathcal{M}}_{iL-1}(t_r)}{r}\right] + \frac{\ell}{\ell+1}\epsilon_{iab}\partial_{aL-1}\left[\frac{\mathcal{S}_{bL-1}(t_r)}{r}\right]\right\}, \tag{1.87}$$

$$\bar{h}_{ij}(t,\mathbf{x}) = \frac{4G}{c^4}\sum_{\ell=2}^{\infty}\frac{(-)^\ell}{\ell!}\left\{\partial_{L-1}\left[\frac{\ddot{\mathcal{M}}_{ijL-2}(t_r)}{r}\right] + \frac{2\ell}{\ell+1}\partial_{aL-2}\left[\frac{\epsilon_{ab\langle i}\dot{\mathcal{S}}_{j\rangle bL-2}(t_r)}{r}\right]\right\}. \tag{1.88}$$

[5] This is a particular instance of the general rule according to which a generic tensor T_P can be decomposed in a sum over ℓ of terms like $\gamma^L_P\hat{R}_L$, where γ^L_P are tensors made of products of δ_{ij} and ϵ_{ijk}, the invariant tensors of $SO(3)$, and $\hat{R}_L$ are STF tensors built by taking the STF part of the possible contractions of T_p with δ's and ϵ's

[6] In compliance with standard notation, we write these two quantities without the hat, even though they are STF in all their indices. Henceforth, we will do to the same for any other STF multipole moment.

Furthermore, thanks to this formalism, the two sets of canonical multipoles $(\mathcal{M}_L, \mathcal{S}_L)$ can be shown to admit the closed-form expressions [162]

$$\mathcal{M}_L(t_r) = \int d^3\mathbf{y} \int_{-1}^{1} dz \left[\delta_\ell(z)\hat{y}_L \sigma - \frac{4(2\ell+1)}{c^2(\ell+1)(2\ell+3)} \delta_{\ell+1}(z)\hat{y}_{aL}\dot{\sigma}_a \right. \\ \left. + \frac{2(2\ell+1)}{c^4(\ell+1)(\ell+2)(2\ell+5)} \delta_{\ell+2}(z)\hat{y}_{abL}\ddot{\sigma}_{ab} \right] (t_r + z|\mathbf{y}|/c, \mathbf{y}) \tag{1.89}$$

$$\mathcal{S}_L(t_r) = \int d^3\mathbf{y} \int_{-1}^{1} dz\, \epsilon_{ab\langle i_\ell} \left[\delta_\ell(z)\hat{y}_{L-1\rangle a}\sigma_b \right. \\ \left. - \frac{2\ell+1}{c^2(\ell+2)(2\ell+3)} \delta_{\ell+1}(z)\hat{y}_{L-1\rangle ac}\dot{\sigma}_{bc} \right] (t_r + z|\mathbf{y}|/c, \mathbf{y}) \tag{1.90}$$

where, following Ref. [104], we have introduced the source densities $\sigma \equiv c^{-2}(T_{00} + T_{aa})$, $\sigma_i \equiv c^{-1}T_{0i}$, and $\sigma_{ij} \equiv T_{ij}$. Again, if the slow-velocity condition holds, we can replace all the integrals in z with their easier to evaluate PN expansion (1.79).

We finally stress, as it will be useful for later, that if we leave the multipoles $(\mathcal{M}_L, \mathcal{S}_L)$ generic, not specifying their expressions in terms of the source densities, then Eqs. (1.86)-(1.88) also yield the most general solution to the vacuum wave equations $\Box\bar{h}_{\mu\nu} = 0$ in the STF formalism.

1.2.4 Linear GWs and the asymptotic region

Let us now discuss the profile of our generalized linear solution at future null infinity, i.e. in the asymptotic region where GWs can be detected, defined by the limit $r \to \infty$ at constant retarded time t_r. This will also offer the occasion to present the general asymptotic structure of GW solutions, valid regardless of the linear approximation considered here.

In this regard, we have to remark that in the asymptotic limit the harmonic coordinates we used so far are notoriously plagued by the appearance of coordinate-dependent logarithmic terms [169], which are absent when one adopts specially designed coordinate systems, grouped under the name of *radiative coordinates*. We specifically refer to either the Bondi-type coordinates introduced in Refs. [170–172] or their analogue by Newman & Unti [173]. Let us denote such coordinates by $X^\mu = (T, \mathbf{X})$, with $R \equiv |\mathbf{X}|$, retarded time $T_R \equiv T - R/c$, and unit radial vector $\mathbf{N} \equiv \mathbf{X}/R$. It has been proved that, once expressed in radiative coordinates, the asymptotic GW waveform admits, in full generality (notably also in the full non-linear theory), the STF decomposition [174]

$$h_{ij}^{TT}(T_R, \mathbf{N}) = \frac{4G}{c^2 R}\Pi_{ijab}(\mathbf{N}) \sum_{\ell=2}^{\infty} \left[\frac{1}{c^\ell \ell!} U_{abL-2}(T_R)N_{L-2} \right. \\ \left. + \frac{2\ell}{c^{\ell+1}(\ell+1)!} \epsilon_{cd(a}V_{b)dL-2}(T_R) \right]. \tag{1.91}$$

Evidently, we are looking at the leading $1/R$ part of the projection on the TT gauge of a general solution h_{ij}, namely the component of it that we can hope to observe at future null infinity. The two sets of STF tensors $U_L(T_R)$ and $V_L(T_R)$ which parameterize this asymptotic solution are called *radiative multipole moments*, again of mass-type and current-type respectively.

In linearized theory, they can be computed in terms of the canonical multipole moments $(\mathcal{M}_L, \mathcal{S}_L)$ by comparing Eq. (1.91) with the harmonic solution given in Eqs. (1.86)-(1.88), after this is projected in the TT gauge and streamlined down to its leading $1/r$ component with the help of the formula

$$\partial_L f(t_r) = \frac{(-)^\ell}{c^\ell} n_L f^{(\ell)}(t_r), \tag{1.92}$$

where the superscript (ℓ) stands for the ℓth time derivative, here with respect to t_r. In particular, the simplifications that come with the linear approximation also determine that there is no difference between harmonic and radiative coordinates in the linear case. Indeed this is no longer true as we go beyond the linear order, where we anticipate that a proper coordinate transformation is needed.

The results of this computation, which completes our discussion on the GW generation problem in the linearized theory, simply read

$$\big[U_L(T_R)\big]_{\text{linear}} = \mathcal{M}_L^{(\ell)}(T_R), \qquad \big[V_L(T_R)\big]_{\text{linear}} = \mathcal{S}_L^{(\ell)}(T_R). \tag{1.93}$$

If we plug these relations in Eq. (1.91), the first terms in the emerging series turn out to be

$$\Big[h_{ij}^{TT}(T_R, \mathbf{N})\Big]_{\text{linear}} = \frac{2G}{c^4 R}\Pi_{ijab}(\mathbf{N})\bigg\{\ddot{\mathcal{M}}_{ab}(T_R) + \frac{1}{3c}\bigg[\dddot{\mathcal{M}}_{abc}(T_R)N_c + 4\epsilon_{cd(a}\ddot{\mathcal{S}}_{b)dL-2}(T_R)\bigg]\bigg\} + \ldots \quad . \tag{1.94}$$

Considering that $\mathcal{M}_{ij} = M_{ij}^{\text{quad}} + \mathcal{O}(v/c^2)$, we recognize in the leading term the quadrupolar solution derived in Eq. (1.52).

To wrap up, the most general GW solution in linearized gravity can be computed according to the scheme

$$T_{\mu\nu} \to (\mathcal{M}_L, \mathcal{S}_L) \to (U_L, V_L)_{\text{linear}} \to \Big[h_{ij}^{TT}(T_R, \mathbf{N})\Big]_{\text{linear}}, \tag{1.95}$$

through which one connects the energy-momentum tensor $T_{\mu\nu}$ of the GW source under consideration to the observable degrees of freedom of the GW waveform at infinity.

1.3 Beyond the linear order: Blanchet-Damour generation formalism

Up to this point we dealt with the GW generation problem under the approximation that the background spacetime can be assumed to be flat. In this

context we saw how to systematically relate, within an expansion in v/c, the GW waveform at infinity to the energy-momentum content of the source. The additional implicit assumption we made along the way is therefore that the typical velocity of the source and its effect on the background curvature could be treated as they were completely independent. While this may be the case for sources whose internal forces are of non-gravitational nature, the same cannot be said in regard to the post-Newtonian sources we are interested in, which are *by definition* self-gravitating systems. For systems of this kind, in fact, the virial theorem implies the relation[7]

$$\frac{v^2}{c^2} \sim \frac{R_S}{d}, \tag{1.96}$$

where $R_S = 2GM/c^2$ is the Schwarzschild radius associated to the total mass M of the system, and d is its size. The corrections in v/c are then to be consistently paired with extra non-flat contributions to the background curvature, whose magnitude is roughly measured by the ratio R_S/d. In order to properly model GWs radiated by PN sources, in the context of a power series in v/c, one has therefore to go beyond the linear approximation and determine a non-linear generalization of the GW generation scheme of Eq. (1.95). Our goal in this section is precisely to present one of the leading-edge formalism devised to do so. More specifically, what we are going to outline is the Blanchet-Damour GW generation formalism, originally established in Ref. [104].

A first important obstacle we have to face as we go beyond the linear theory is that the PN approximation, by itself, is not anymore adequate to describe GWs far away from their sources. This problem becomes quite manifest if we realize that, in a direct application of the PN expansion, we would attempt to build up, order by order, a retarded gravitational field of the type

$$h_{\mu\nu}(t - r/c) = \frac{1}{r} F_{\mu\nu}(t - r/c), \tag{1.97}$$

from the corresponding expansion for small retardation ($r/c \ll t$)

$$\frac{1}{r} F_{\mu\nu}(t - r/c) = \frac{1}{r} F_{\mu\nu}(t) - \frac{1}{c} \dot{F}_{\mu\nu}(t) + \frac{r}{2c^2} \ddot{F}_{\mu\nu}(t) + O(r^2/c^3). \tag{1.98}$$

We see that this series blows up as $r \to \infty$, in contrast to the asymptotically flat behavior that the gravitational field should have. The PN expansion, in this case, takes on the connotations of a singular perturbation theory, not

[7] In general, for a system of two particle separated by a distance d and interacting with a conservative force of potential of energy $U \sim d^n$, the virial theorem relates the averages over time of its kinetic energy T and the aforementioned U as

$$2\langle T \rangle = n \langle U \rangle.$$

In this sense, Eq. (1.96) is the consequence of taking U to be the gravitational potential of Newtonian mechanics.

uniformly valid in r but limited to a finite region $r < \mathcal{R}$, with the consequential impossibility of imposing the required boundary conditions at infinity, such as the already mentioned no-incoming radiation condition. The radius $\mathcal{R}$ that defines the boundaries of this *near region*, where retardation effects are negligible and the PN expansion is valid, can be determined as the larger radius for which the condition $r \ll \lambda$ holds, where λ is the reduced wavelength of the emitted radiation.

The basic idea of the Blanchet-Damour approach is then the following. Let d be the size of the matter source. In the *exterior region* $r > d$, the energy-momentum tensor $T^{\mu\nu}$ of the compact matter source vanishes and the gravitational field becomes a solution of the vacuum Einstein equations, which is natural to tackle by means of a multipole expansion. Moreover, as far as PN sources are concerned, the gravitational field in the exterior region is sufficiently weak that it can be computed in a *post-Minkowskian* (PM) expansion, treating it as a non-linear metric perturbation of the flat spacetime. Combining the two expansions, the gravitational field in the exterior region is therefore conveniently built in terms of a *multipolar-post-Minkowskian* (MPM) expansion, in which each perturbative order in the PM series entails an underlying expansion in STF multipoles. This description is well defined in the whole spatial domain $d < r < \infty$ and, when recasted in radiative coordinates, has an asymptotic structure at future null infinity that is consistent with the Bondi-Sachs-Penrose paradigm.[8] However, it is completely disconnected from the stress-energy tensor $T^{\mu\nu}$, as it represents instead the most general field solution as seen from the outside of *any* source. On parallel, one has the PN expansion cited above, which determines the inner gravitational field as a functional of $T^{\mu\nu}$, thus connecting it to its specific source, but it is only valid in the near region $r < \mathcal{R}$ around the source. We are at the decisive point of this approach: if the source is post-Newtonian, we can count on the condition $\mathcal{R} \gg d$, which ensures the existence of an *overlapping region* $d < r < \mathcal{R}$ where the PN and MPM expansions are both valid; an illustrative sketch of the different spacetime regions in play is given in Fig. 1.1. Exploiting this overlap, the two perturbative expansions can be matched together with a proper application of the matched asymptotic expansion method. This procedure ultimately specifies, from the starting generality of the MPM solution, the particular and physical exterior field corresponding to the given energy-momentum content of the source, encoded in $T^{\mu\nu}$. It is important to notice that the PN expansion represents the most downstream approximation scheme of the whole generation formalism, and as such it is also the one with respect to which the final waveform results are given.

Before we start illustrating the main aspects of the Blanchet-Damour approach, we wish to point out the existence of another GW generation for-

[8] More specifically Ref. [101] has proved that it is asymptotically simple in the sense of Penrose [172, 175, 176].

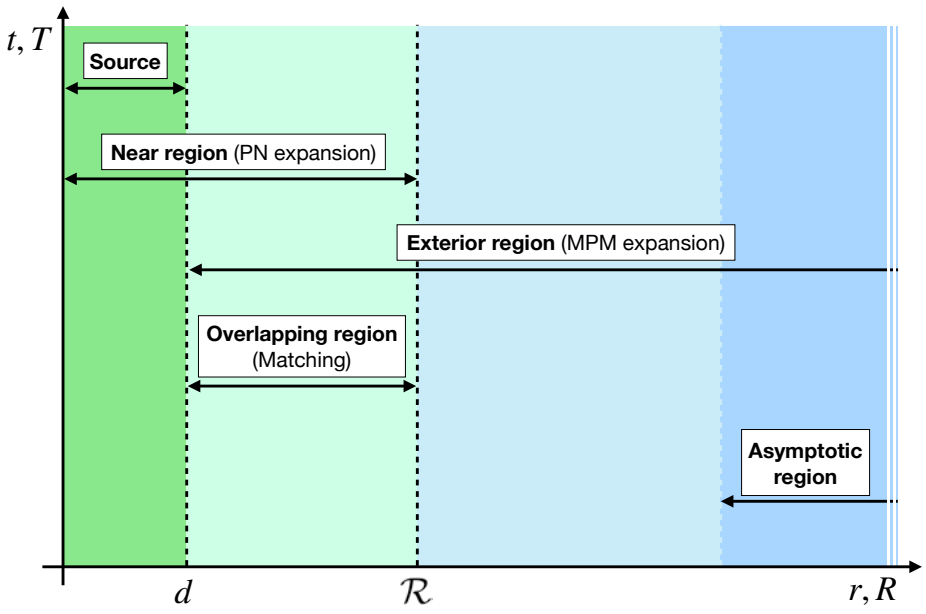

Figure 1.1: Sketch of the spacetime regions considered in the Blanchet-Damour waveform generation formalism. As specified in the text, d and $\mathcal{R}$ respectively enclose the source and its near region. In the exterior region beyond $\mathcal{R}$, we further single out the asymptotic region containing future null infinity, where a proper GW description requires abandoning the harmonic coordinates (t, r) in favor of the radiative coordinates (T, R).

malism, devised by Will, Wiseman & Pati. This is similar in spirit to the one of Blanchet & Damour but, even though the results are the same, it still entails several technical differences; for more details on this formalism see Refs. [97–99].

1.3.1 Multipolar post-Minkowskian expansion in the exterior region

To start our review of the Blanchet-Damour approach, the first aspect we want to explore is its prescription for the general solution to the vacuum Einstein equations, which shape the gravitational field outside the source. We work in harmonic coordinates, using as a reference field variable the metric density $h^{\mu\nu}$ defined in Eq. (1.7), which we can think of as a non-linear metric perturbation

of the flat spacetime. Correspondingly, the field equations we have to solve are obtained from Eq. (1.9) by imposing the vacuum condition $T^{\mu\nu} = 0$ and the harmonic condition. They read

$$\Box h^{\mu\nu} = \Lambda^{\mu\nu}, \qquad \partial_\alpha h^{\alpha\mu} = 0. \tag{1.99}$$

At a distance r from the source, a general weak-field deviation from the Minkowski metric, such as $h^{\mu\nu}$, can be expanded in powers of the dimensionless ratio R_S/r, defining what we call its post-Minkowskian expansion. Since $R_S \sim G$, it is standard to recast this expansion as a power series in G, which on our field variable reads

$$h^{\mu\nu} = \sum_{n=1}^{\infty} G^n h^{\mu\nu}_{(n)}, \tag{1.100}$$

where we identify the coefficient $h^{\mu\nu}_{(n)}$ of G^n as the nPM contribution to $h^{\mu\nu}$. Having the final goal of describing the gravitational field up to a given PN order, we can indeed consider a finite truncation of the series (1.100),[9] but to push the computation to arbitrarily high orders we need to know how to formally determine each coefficient $h^{\mu\nu}_{(n)}$. We will work this out in the form of an iterative algorithm, since inserting Eq. (1.100) in the field equations (1.99) yields the hierarchical system of equations

$$\Box h^{\mu\nu}_{(1)} = 0, \tag{1.101}$$
$$\Box h^{\mu\nu}_{(n)} = \Lambda^{\mu\nu}_{(n)}[h_{(1)}, h_{(2)}, ..., h_{(n-1)}] \quad \text{for } n > 1, \tag{1.102}$$
$$\partial_\alpha h^{\alpha\mu}_{(n)} = 0 \quad \text{for } n \geq 1. \tag{1.103}$$

where the leading order equation is source-less, since $\Lambda^{\mu\nu} = \mathcal{O}(G^2)$, while all the others have a source term with non-compact support defined in terms of the lower-order PM contributions. For instance, recalling the expression of $\Lambda^{\mu\nu}$ as a functional of $h^{\mu\nu}$, shown in Eq. (1.12), at the lowest subleading orders we have

$$\Box h^{\mu\nu}_{(2)} = N^{\mu\nu}[h_{(1)}, h_{(1)}], \tag{1.104}$$
$$\Box h^{\mu\nu}_{(3)} = N^{\mu\nu}[h_{(1)}, h_{(2)}] + N^{\mu\nu}[h_{(2)}, h_{(1)}] + M^{\mu\nu}[h_{(1)}, h_{(1)}, h_{(1)}]. \tag{1.105}$$

The first step is to compute the leading 1PM contribution given by Eq. (1.101) and the associated harmonic condition. This is the same set of equations we encountered while dealing with the linear field in Sec. 1.2.3. Therein we showed that the most general solution can be decomposed in two sets ($\mathcal{M}_L$, $\mathcal{S}_L$) of STF multipoles, see Eqs. (1.86)-(1.88). We recall however that, in the path

[9] The virial theorem relation (1.96) implies that to completely determine the nPN order we need PM contributions up to the $(n-1)$th.

leading to that solution, we had to take advantage of the gauge symmetry (1.22), specific of the linearized theory, and use it to impose four additional constraints. This is no longer possible in the full non-linear theory, for which Eq. (1.22) is *not* a gauge symmetry, implying that the most general solution to Eq. (1.101), in harmonic coordinates, should be given in terms of six, rather than two, sets of STF multipoles. Moreover, such multipoles should be unspecified functions of the harmonic retarded time $t_r \equiv t - r/c$, with no *a priori* connection to the stress-energy tensor of the source, as opposed to the multipoles $\mathcal{M}_L$ and $\mathcal{S}_L$ in the linearized theory, for which we wrote down the closed-form expressions (1.89) and (1.90). We therefore write our multipolar 1PM solution in the form

$$h^{\mu\nu}_{(1)} = k^{\mu\nu}_{(1)} + \partial^\mu \xi^\nu + \partial^\nu \xi^\mu - \eta^{\mu\nu}\partial_\alpha \xi^\alpha. \tag{1.106}$$

Here $k^{\mu\nu}_{(1)}$ is given by

$$k^{00}_{(1)} = -\frac{4}{c^2}\sum_{\ell=0}^{\infty}\frac{(-)^\ell}{\ell!}\partial_L\left[\frac{I_L(t_r)}{r}\right], \tag{1.107}$$

$$k^{0i}_{(1)} = \frac{4}{c^3}\sum_{\ell=1}^{\infty}\frac{(-)^\ell}{\ell!}\left\{\partial_{L-1}\left[\frac{I^{(1)}_{iL-1}(t_r)}{r}\right] + \frac{\ell}{\ell+1}\epsilon_{iab}\partial_{aL-1}\left[\frac{J_{bL-1}(t_r)}{r}\right]\right\}, \tag{1.108}$$

$$k^{ij}_{(1)} = -\frac{4}{c^4}\sum_{\ell=2}^{\infty}\frac{(-)^\ell}{\ell!}\left\{\partial_{L-1}\left[\frac{I^{(2)}_{ijL-2}(t_r)}{r}\right] + \frac{2\ell}{\ell+1}\partial_{aL-2}\left[\frac{\epsilon_{ab\langle i}J^{(1)}_{j\rangle bL-2}(t_r)}{r}\right]\right\}, \tag{1.109}$$

and mirrors the structure of the linear solution (1.86)-(1.88),[10] but replaces the source-rooted multipoles $(\mathcal{M}_L, \mathcal{S}_L)$ with (I_L, J_L), a different set of mass-type and current-type STF multipoles. As we mentioned, at this stage the latter are arbitrary functions of t_r, with the exception of I, $\dot{I}_i$, and J_i which must be constant in time because of the conservation laws for the total mass of the source $M \equiv I$, its total linear momentum $P_i \equiv I^{(1)}_i$, and its total angular momentum J_i. The other three terms in Eq. (1.106) reintroduce, via Eq. (1.22), the four STF multipoles that had been gauged away from the linear solution. In fact, the vector ξ^μ can be decomposed in four general STF multipoles, denoted as (W_L, X_L, Y_L, Z_L) and usually called *gauge moments*,

[10] There are actually two small differences: (i) a factor G is missing in $k^{\mu\nu}_{(1)}$ because it is collected in front of $h^{\mu\nu}_{(1)}$ in its defining relation, Eq. (1.100); (ii) the overall sign is changed due to $[h^{\mu\nu}]_{\rm linear} = -\bar{h}^{\mu\nu}$, as we showed in Eq. (1.17).

according to

$$\xi^0 = \frac{4}{c^3}\sum_{\ell=0}^{\infty}\frac{(-)^\ell}{\ell!}\partial_L\left[\frac{W_L(t_r)}{r}\right], \tag{1.110}$$

$$\xi^i = -\frac{4}{c^4}\sum_{\ell=0}^{\infty}\frac{(-)^\ell}{\ell!}\partial_L\left[\frac{X_L(t_r)}{r}\right] - \frac{4}{c^4}\sum_{\ell=1}^{\infty}\frac{(-)^\ell}{\ell!}\left\{\partial_{L-1}\left[\frac{Y_{iL-1}(t_r)}{r}\right] + \frac{\ell}{\ell+1}\epsilon_{iab}\partial_{aL-1}\left[\frac{Z_{bL-1}(t_r)}{r}\right]\right\}. \tag{1.111}$$

This completely determines the 1PM solution of the exterior field in terms of an expansion in six sets of STF multipole moments, $(I_L, J_L, W_L, X_L, Y_L, Z_L)$. Given that the multipole decomposition has entered the first step of the PM iterative algorithm, we are actually justified in calling the overall procedure a *multipolar-post-Minkowskian* expansion. The multipoles $(I_L, J_L, W_L, X_L, Y_L, Z_L)$ are usually referred to as the *multipole moments of the source*, in anticipation of the fact that they can be related to the source by means of the matching with the PN solution in the overlap region. Despite this remarkable property, using a solution parameterized by six set of multipoles in the iterative algorithm would be quite inconvenient. Besides, we know that GWs have two physical degree of freedom, their two polarization states. Hence, there must exist a reduced set of just two multipoles that is physical equivalent to the one we used above, i.e. that generates the same MPM solution if used to parametrize the leading coefficient $h^{\mu\nu}_{(1)}$ at the basis of the MPM iterative algorithm. Indeed the naif choice $(I_L, J_L, 0, 0, 0, 0)$ is no good, as it is related to $(I_L, J_L, W_L, X_L, Y_L, Z_L)$ by a linear gauge transformation rather than a non-linear diffeomorphism. What we are after must be instead an isometric reduced set $(M_L, S_L, 0, 0, 0, 0)$ where the STF multipoles M_L and S_L, usually called *canonical multipole moments*, are non-linear functionals of the six source multipoles, with the identifications $M_L = I_L$ and $S_L = J_L$ being valid exclusively at a linear level. Of course, decomposing $h^{\mu\nu}_{(1)}$ in canonical moments returns a much simpler expression than its source moment counterpart, with only the $k^{\mu\nu}_{(1)}$ part of $h^{\mu\nu}_{(1)}$ remaining in Eq. (1.106), and therefore it is more easily implemented in the iterative MPM algorithm. However, there is no way of directly connecting these canonical moments to the source even within the matching with the PN expansion. The idea is then to use the canonical moments for the MPM algorithm and later recast the so-constructed solution in terms of the source moments. Evidently, to this end we need the explicit functional relations between canonical and source moments, up to the target PN accuracy of the final waveform results. The procedure to obtain these relations is presented in the recent work [177], where it is formally outlined at every order in the PM expansion and then practically implemented to compute the relations between the mass quadrupoles M_{ij} and I_{ij} up to 4PN. For

instance we have [111, 164]

$$M_{ij} = I_{ij} + \frac{4G}{c^5}\left[I_{ij}W^{(2)} - I^{(1)}_{ij}W^{(1)}\right] + \mathcal{O}\big(1/c^7\big) \tag{1.112}$$

$$S_{ij} = J_{ij} + \frac{2G}{c^5}\left[\epsilon_{ab\langle i}\left(-2I_{j\rangle b}Y^{(2)}_a + I^{(1)}_{j\rangle b}Y^{(1)}_a - I^{(3)}_{j\rangle b}W_a\right) + 3J_{\langle i}Y^{(1)}_{j\rangle} - 2J^{(2)}_{ij}W^{(1)}\right] + \mathcal{O}\big(1/c^6\big). \tag{1.113}$$

Similar relations hold for higher multipoles, with the first correction being always of order $\mathcal{O}(G/c^5)$.

We now investigate by induction how to formally implement the MPM iteration algorithm at every order. The problem at hand is how to compute the nPM coefficient $h^{\mu\nu}_{(n)}$ after the previous $n-1$ have been already determined, starting with the multipolar 1PM solution we just discussed. We have to solve the wave equation (1.102), with the source term $\Lambda^{\mu\nu}_{(n)}$ known by induction hypothesis. A straightforward application of the retarded integral (1.15) is not possible here, because Eq. (1.102) is physically meaningful only outside the source. On the same note, the multipole expansion nested in the source term $\Lambda^{\mu\nu}_{(n)}$ makes the latter manifestly divergent for $r \to 0$, with the divergence order that increases indefinitely as the multipole expansion proceeds towards higher values of ℓ. It is however crucial to remember that the multipole expansion naturally comes with an associated expansion in $1/c$, meaning that if we want to compute the waveform at a given PN order we can neglect any multipole moment beyond a corresponding finite $\ell = \ell_{\max}$. After this truncation, the divergence order of $\Lambda^{\mu\nu}_{(n)}$ becomes actually finite and we have the chance of regularizing the integral $\Box^{-1}_{\rm ret}\Lambda^{\mu\nu}_{(n)}$.

Following Ref. [161], the first step in this direction is to introduce the regularized quantity

$$I^{\mu\nu}_n(B) \equiv \Box^{-1}_{\rm ret}\left[\frac{r^B}{r_0^B}\Lambda^{\mu\nu}_{(n)}\right], \tag{1.114}$$

a function of the complex number B that is defined when $\Re(B)$ is large enough to make $r^B\Lambda^{\mu\nu}_{(n)}$ regular at the origin, where $\Re$ indicates the real part. In particular, if $D_{\max}$ is the maximal divergence order of $\Lambda^{\mu\nu}_{(n)}$, the definition domain of $I^{\mu\nu}_n(B)$ is $\Re(B) > D_{\max} - 3$. The constant length scale r_0 is there with the purpose of making the regularizing factor dimensionless, and it must disappear from the expression of every physical observable. Ref. [161] proved that $I^{\mu\nu}_n(B)$ admits a unique analytic continuation $\tilde{I}^{\mu\nu}_n(B)$ defined for all $B \in \mathbb{C}$ except for some integer values. The function $\tilde{I}^{\mu\nu}_n(B)$ may develop some poles in $B = 0$, but around this point we can always consider the Laurent expansion

$$\tilde{I}^{\mu\nu}_n(B) = \sum_{p=-p_n}^{+\infty} B^p \iota^{\mu\nu}_{n,p}, \tag{1.115}$$

where p_n is the order of these eventual poles, with $p_n = 0$ if there are none. We can then apply the operator $\Box$ to both sides of Eq. (1.115), remembering the definition (1.114). This gives

$$\frac{r^B}{r_0^B}\Lambda^{\mu\nu}_{(n)} = \sum_{p=-p_n}^{+\infty} B^p \Box \iota^{\mu\nu}_{n,p}, \tag{1.116}$$

where, in the left hand side,

$$\frac{r^B}{r_0^B} = e^{B\log(r/r_0)} = \sum_{p=0}^{+\infty} B^p \frac{[\log(r/r_0)]^p}{p!}. \tag{1.117}$$

Equating the different powers of B yields the infinite set of equations

$$\Box \iota^{\mu\nu}_{n,p} = 0 \qquad \text{for} \quad -p_n \leq p \leq 1, \tag{1.118}$$

$$\Box \iota^{\mu\nu}_{n,p} = \frac{[\log(r/r_0)]^p}{p!}\Lambda^{\mu\nu}_{(n)} \qquad \text{for} \quad p \geq 0. \tag{1.119}$$

We notice that $\iota^{\mu\nu}_{n,0}$, the coefficient of the term with $p = 0$ in the Laurent expansion of the analytically continued quantity (1.114), is a particular solution of Eq. (1.102). The series of operation that allowed us to compute $\iota^{\mu\nu}_{n,0}$ from the retarded integral $I^{\mu\nu}_n(B)$ is called *finite part* of $I^{\mu\nu}_n(B)$. In other words, denoting the operation of taking this finite part by the symbol $\mathcal{FP}_{B=0}$, we just found that a particular solution $u^{\mu\nu}_{(n)}$ to Eq. (1.102) can be computed as[11]

$$u^{\mu\nu}_{(n)} = \mathcal{FP}_{B=0}\Box^{-1}_{\rm ret}\left[\frac{r^B}{r_0^B}\Lambda^{\mu\nu}_{(n)}\right]. \tag{1.120}$$

The solution we want, however, must also satisfy the harmonic condition (1.103). Instead, from the solution above,

$$w^{\mu}_{(n)} \equiv \partial_\alpha u^{\alpha\mu}_{(n)} = \mathcal{FP}_{B=0}\Box^{-1}_{\rm ret}\left[B\frac{r^B}{r_0^B}\frac{n_i}{r}\Lambda^{\alpha i}_{(n)}\right], \tag{1.121}$$

where we used the conservation of the stress-energy pseudo tensor (1.10), which in vacuum becomes $\partial_\alpha \Lambda^{\alpha\mu} = 0$, and thus $\partial_\alpha \Lambda^{\alpha\mu}_{(n)} = 0$. We see that in general $w^{\mu}_{(n)} \neq 0$, as it is the case when the associated retarded integral, stripped of the explicit factor B, develops a simple pole $1/B$ in its Laurent expansion for $B \to 0$. Nevertheless, realizing that the finite part operation effectively identifies $w^{\mu}_{(n)}$ with the coefficient of this simple pole, we can infer, in

[11] For a source S with compact support and no divergences, we simply have

$$\mathcal{FP}_{B=0}\Box^{-1}_{\rm ret}\left[\frac{r^B}{r_0^B}S\right] = \Box^{-1}_{\rm ret}(S),$$

in compliance with the fact that no regularization is needed in this case.

analogy with Eq. (1.118), that it must solve the source-free equation $\Box w^{\mu}_{(n)} = 0$. This means that we can decompose it in terms of four set of STF multipoles, similarly to what we did in Eqs. (1.110)-(1.111) for ξ^{μ}. From the multipolar expression of $w^{\mu}_{(n)}$ is then possible to define another object $v^{\mu\nu}_{(n)}$ such that

$$\Box v^{\mu\nu}_{(n)} = 0, \qquad \partial_{\alpha} v^{\alpha\mu}_{(n)} = -w^{\mu}_{(n)}. \tag{1.122}$$

The resulting $v^{\mu\nu}_{(n)}$ is not unique, but each of its determinations, once added to $u^{\mu\nu}_{(n)}$, gives an object that is still a solution to Eq. (1.102) while also being divergence free, as we wanted. For the explicit expression commonly used for $v^{\mu\nu}_{(n)}$, given in terms of the multipoles of $w^{\mu}_{(n)}$, see, e.g., Eqs. (47)-(48) of Ref. [112].[12]

Summing up, the nPM metric coefficient $h^{\mu\nu}_{(n)}$, solution to Eqs. (1.102) and (1.103), is formally obtained as

$$h^{\mu\nu}_{(n)} = u^{\mu\nu}_{(n)} + v^{\mu\nu}_{(n)}, \tag{1.123}$$

with $u^{\mu\nu}_{(n)}$ defined in Eq. (1.120) and $v^{\mu\nu}_{(n)}$ defined from $w^{\mu}_{(n)}$ in Eq. (1.121), upon requesting the conditions (1.122). Moreover, this is the most general solution we can find for $h^{\mu\nu}_{(n)}$. As proved in Ref. [161], in fact, the most general solution to the associated homogeneous equation, $\Box h^{\mu\nu}_{(n)} = 0$, has necessarily the same multipolar structure of the 1PM solution $h^{\mu\nu}_{(1)}$, which is also a solution to this equation. Thus, we can always reabsorb any extra homogeneous term added to the solution (1.123) in a redefinition of the multipole moments used to parameterize $h^{\mu\nu}_{(1)}$.

As it is not difficult to imagine, the practical implementation of the MPM iterative algorithm presented above becomes very challenging already at low PM orders. To make things manageable, the usual strategy is to consider separately different multipole interactions, determined by the different multipole products that pop up in the MPM iterations. This is done by starting the iterative algorithm with a linear term $h^{\mu\nu}_{(1)}$ which only presents the pieces where some selected multipoles appear. For instance, to fix the mass monopole and mass quadrupole structure of $h^{\mu\nu}$ up to 2.5PN corrections, it is sufficient to consider a single iteration on the linear metric

$$\left[h^{\mu\nu}_{(1)}\right]_{M,M_{ij}} = h^{\mu\nu}_{(1,M)} + h^{\mu\nu}_{(1,M_{ij})}, \tag{1.124}$$

where, referring to Eqs. (1.107)-(1.109), rewritten in terms of the canonical moments (M_L, S_L), the multipolar components considered read[13]

$$h^{00}_{(1,M)} = -\frac{4M}{c^2 r}, \qquad h^{0i}_{(1,M)} = h^{ij}_{(1,M)} = 0, \tag{1.125}$$

[12] The procedure to compute $v^{\mu\nu}_{(n)}$ from the multipolar expression of $w^{\mu}_{(n)}$ is often called the *MPM harmonicity algorithm*.

[13] In our notation, for instance, $h^{\mu\nu}_{(1,M)}$ represents the term, in the multipolar decomposition of $h^{\mu\nu}_{(1)}$, that just involves the mass monopole M, whereas $h^{\mu\nu}_{(1,M_{ij})}$ is the one associated to the mass quadrupole M_{ij}.

and

$$h^{00}_{(1,M_{ij})} = -\frac{2}{c^2}\partial_{ab}\left[\frac{M_{ab}(t_r)}{r}\right], \tag{1.126}$$

$$h^{0i}_{(1,M_{ij})} = \frac{2}{c^3}\partial_{a}\left[\frac{M^{(1)}_{ai}(t_r)}{r}\right], \tag{1.127}$$

$$h^{ij}_{(1,M_{ij})} = -\frac{2}{c^4}\frac{M^{(2)}_{ij}(t_r)}{r}. \tag{1.128}$$

Then, by inserting the linear metric (1.124) in the right hand side of Eq. (1.104), we find the three quadratic interactions

$$\left[h^{\mu\nu}_{(2)}\right]_{M,M_{ij}} = h^{\mu\nu}_{(2,M^2)} + h^{\mu\nu}_{(2,M\times M_{ij})} + h^{\mu\nu}_{(2,M_{ij}\times M_{ij})}, \tag{1.129}$$

which can be separately determined by direct application of the MPM algorithm; for the explicit computation of these contributions see Sec. 5.3.4 of Ref. [163] and references therein.

An important aspect of the nonlinear MPM metric coefficients that result from the procedure we just outlined is the inevitable appearance in their expressions of time integrals, involving the canonical moments and spanning over all the instants before the retarded time t_r.[14] Contributions of this kind are called *hereditary*, in antithesis with the "standard" *instantaneous* terms which just depend on a specific time t_r, because they effectively impress in the exterior field the mark of the whole history of its (yet unspecified, at this point) source. Seen from another angle, these hereditary non-linearities are expression of the fact that the curved background spacetime affects the gravitational interaction as if the latter took place in flat spacetime and propagated at all possible speeds, lower or equal to c.

We finally mention a very important result, originally shown in Ref. [161], about the near-zone singular structure that each coefficient $h^{\mu\nu}_{(n)}$ must have to allow the analytic continuations in B underlying the MPM algorithm. For each $N \in \mathbb{N}$, in the limit $r \to 0$, we have

$$\begin{gathered} h^{\mu\nu}_{(n)}(t,\mathbf{x}) = \sum_{m,p} r^m (\log r)^p \hat{n}_L F^{\mu\nu}_{L,m,p,n}(t) + o(r^N), \\ \{m \in \mathbb{Z} \mid m_0(n) \leq m \leq N\,;\, p \in \mathbb{N} \mid p \leq n-1\}, \end{gathered} \tag{1.130}$$

where $m_0(n)$ is an integer that goes toward $-\infty$ as n increases, $F^{\mu\nu}_{L,m,p,n}(t)$ are multi-linear functionals of the source moments, and $o(r^N)$ is the standard Bachmann–Landau notation for a residual of order greater than r^N in the considered limit.

[14] This happens already at the level of the metric component $h^{00}_{(2,M\times M_{ij})}$; see Eq. (5.164) of Ref. [163].

1.3.2 PN expansion in the near region

We address now the problem of building a PN solution to the field equations (1.9), formally valid at each perturbative order but limited to the near region $r < \mathcal{R}$. Using a standard notation, the formal PN expansion, complete of all its infinite terms, of any given quantity is indicated with an overline. Focusing in particular on our field variable $h^{\mu\nu}$, its PN expansion reads[15]

$$\bar{h}^{\mu\nu}(t,\mathbf{x}) = \sum_{n=2}^{+\infty} \frac{1}{c^n} h_n^{\mu\nu}(t,\mathbf{x};\log c) \tag{1.131}$$

where we made explicit that the nPN coefficient, which multiplies the factor $1/c^n$, may also contain logarithms of c. Their presence is expected from the profile of the nth MPM metric coefficient in the limit $c \to \infty$, which is

$$h_{(n)}^{\mu\nu} \sim \sum_{p,q\in\mathbb{N}} \frac{(\log c)^p}{c^q}, \tag{1.132}$$

as implied by its near-zone structure (1.130), considering that each r therein comes with a factor $1/c$.

Accordingly, the PN-expanded stress-energy pseudo tensor (1.10) reads

$$\bar{\tau}^{\mu\nu}(t,\mathbf{x}) = \sum_{n=-2}^{+\infty} \frac{1}{c^n} \tau_n^{\mu\nu}(t,\mathbf{x};\log c), \tag{1.133}$$

where the starting term of order c^2 comes from the rest-mass contribution to the energy.

By inserting these expansions in Eq. (1.9), we find the recursive set of Poisson-like equations

$$\Delta h_n^{\mu\nu} = 16\pi G \tau_{n-4}^{\mu\nu} + \partial_t^2 h_{n-2}^{\mu\nu}, \tag{1.134}$$

where the last term comes from $\Box = \Delta + 1/c^2\partial_t^2$. We proceed again by induction: we try to formally compute $h_n^{\mu\nu}$ supposing the knowledge of all the previous PN coefficients of the metric and, with them, of $\tau^{\mu\nu}$. Here the Laplacian cannot be simply inverted via the Green's function (1.67), because the source term has a non-compact support, and diverges for $r \to +\infty$. This obstacle has been overcome in Ref. [178], which showed that an appropriate inversion of the Laplacian, for any source term $\tau_n^{\mu\nu}$, can be be defined in terms of a finite-part regularization, operationally similar to the one used in the MPM algorithm and thus denoted with the same symbol $\mathcal{FP}_{B=0}$. It reads

$$\Delta^{-1}[\tau_n^{\mu\nu}](t,\mathbf{x}) \equiv -\frac{1}{4\pi} \mathcal{FP}_{B=0} \int d^3\mathbf{x}' \, \frac{r'^B}{r_0^B} \frac{\tau_n^{\mu\nu}(t,\mathbf{x}')}{|\mathbf{x}-\mathbf{x}'|}. \tag{1.135}$$

[15] This should not be confused with the linear trace-reversed perturbation $\bar{h}_{\mu\nu}$, which plays no role in the non-linear formalism we hare presenting here.

We remark that in this case the regularization is needed for divergences at infinity, rather than at zero, therefore $\Re(B)$ must be sufficiently large and *negative* for the integral to be defined, before it is analytically continued everywhere in the complex B-plane except for, in this case, just $B = 0$.

The most general solution to Eq. (1.134) is then given by

$$h_n^{\mu\nu} = 16\pi G\Delta^{-1}[\tau_{n-4}^{\mu\nu}] + \partial_t^2\Delta^{-1}[h_{n-2}^{\mu\nu}] + \sum_{\ell=0}^{+\infty}\hat{x}_L\,\mathcal{B}_{L,n}^{\mu\nu}, \tag{1.136}$$

where in the last term we also added the most general solution of the homogeneous Laplace equation that is regular at $r = 0$, decomposed in STF tensorial functions $\mathcal{B}_{L,n}^{\mu\nu}$ as we did in Eq. (1.62). Indeed we can reinsert Eq. (1.136) in its own coefficient $h_{n-2}^{\mu\nu}$ and keep going recursively until we reach either $h_0^{\mu\nu}$ or $h_1^{\mu\nu}$, which are both zero.

Let us now introduce the operator

$$\Box_{\text{inst}}^{-1}[\bar{\tau}^{\mu\nu}] \equiv \sum_{k=0}^{+\infty}\frac{1}{c^{2k}}\partial_t^{2k}\Delta^{-k-1}[\bar{\tau}^{\mu\nu}], \tag{1.137}$$

where

$$\Delta^{-k-1}[\bar{\tau}^{\mu\nu}](t,\mathbf{x}) \equiv -\frac{1}{4\pi}\mathcal{FP}_{B=0}\int d^3\mathbf{x}'\,\frac{r'^B}{r_0^B}\frac{\left|\mathbf{x}-\mathbf{x}'\right|^{2k-1}\bar{\tau}_n^{\mu\nu}(t,\mathbf{x}')}{(2k)!} \tag{1.138}$$

is the kth iteration of the operator (1.135). Mind that the definition (1.137) is legitimate exclusively for PN expanded quantities such as $\bar{\tau}^{\mu\nu}$. Once all the metric coefficients are recursively replaced in the left hand side, neglecting for the moment the homogeneous terms, Eq. (1.136) can be generalized at every PN order in the compact form

$$\bar{h}_{\text{part}}^{\mu\nu} = \frac{16\pi G}{c^4}\Box_{\text{inst}}^{-1}[\bar{\tau}^{\mu\nu}]. \tag{1.139}$$

This is by construction a particular solution to Eq. (1.9), implying that

$$\Box(\Box_{\text{inst}}^{-1}[\bar{\tau}^{\mu\nu}]) = \bar{\tau}^{\mu\nu}, \tag{1.140}$$

and thus justifying a posteriori the notation $\Box_{\text{inst}}^{-1}$, where the label "inst" stands for *instantaneous*, namely not involving integrals in time as opposed to $\Box_{\text{ret}}^{-1}$. On parallel, we have the collection of homogeneous terms that comes from the infinite iterations required to obtain Eq. (1.139) from Eq. (1.136). It can be proved that this homogeneous part corresponds to the general solution of the source-free D'Alembertian equation regular at the origin, which must be composed by the difference between retarded and advanced waves. The

most general PN solution for the metric $h^{\mu\nu}$, formally encompassing all PN orders, can therefore be written as

$$\bar{h}^{\mu\nu} = \frac{16\pi G}{c^4}\Box^{-1}_{\rm inst}[\bar{\tau}^{\mu\nu}] - \frac{4G}{c^4}\sum_{\ell=0}^{+\infty}\frac{(-)^\ell}{\ell!}\hat{\partial}_L\left[\frac{\mathcal{A}^{\mu\nu}_L(t-r/c)-\mathcal{A}^{\mu\nu}_L(t+r/c)}{2r}\right]. \tag{1.141}$$

There is no way to further specify the quantities $\mathcal{A}^{\mu\nu}_L$ in the standard PN theory, we may just relate them to the functions $\mathcal{B}^{\mu\nu}_{L,n}$ that appear in Eq. (1.136) without gaining much. As we will see in the next section, the solution to this problem lies in the matching with the MPM solution in the exterior region.

1.3.3 PN-MPM matching in the overlapping region

We now come to the crucial point of the Blanchet-Damour generation formalism: enforcing the matching between the MPM and PN expansions in their common region of validity, the overlapping region $d < r < \mathcal{R}$. Similarly to what we did on the PN side with the notation $\bar{h}^{\mu\nu}$, let us denote by $\mathcal{M}(h^{\mu\nu})$ the formal MPM expansion

$$\mathcal{M}(h^{\mu\nu}) \equiv \sum_{n=1}^{+\infty} G^n h^{\mu\nu}_{(n)}[I_L, J_L, W_L, X_L, Y_L, Z_L], \tag{1.142}$$

which represents the exterior solution of Sec. 1.3.1, comprehensive of all PM orders and expressed in terms of the multipoles of the source. Indeed this is such that $\mathcal{M}(h^{\mu\nu}) = h^{\mu\nu}$ for $r > d$, just like $\bar{h}^{\mu\nu} = h^{\mu\nu}$ for $r < \mathcal{R}$. We thus have

$$\mathcal{M}(h^{\mu\nu}) = \bar{h}^{\mu\nu} \qquad \text{for } \; d < r < \mathcal{R}. \tag{1.143}$$

This is not yet a matching equation since it does not relate two mathematical expression of the same nature. The idea is then to take the formal PN expansion of $\mathcal{M}(h^{\mu\nu})$ and equate it to the formal multipolar expansion of $\bar{h}$. In our notation we get

$$\overline{\mathcal{M}(h^{\mu\nu})} = \mathcal{M}(\bar{h}^{\mu\nu}), \tag{1.144}$$

which is by all means a matching equation, to be intended as the infinite set of functional equations that make identical, term by term, the two double expansions, $\overline{\mathcal{M}(h^{\mu\nu})}$ and $\mathcal{M}(\bar{h}^{\mu\nu})$. Moreover, thanks to the known near-zone structure of $h^{\mu\nu}_{(n)}$, given in Eq. (1.130), we are able to infer the general shared structure of such double expansions, that is

$$\begin{gathered}\overline{\mathcal{M}(h^{\mu\nu})} = \sum_{m,\,p} r^m (\log r)^p \hat{n}_L F^{\mu\nu}_{L,m,p} = \mathcal{M}(\bar{h}^{\mu\nu}), \\ \{m \in \mathbb{Z}\,;\, p \in \mathbb{N}\},\end{gathered} \tag{1.145}$$

where, compared to Eq. (1.130), we have $F^{\mu\nu}_{L,m,p} = \sum_{n=1}^{+\infty} G^n F^{\mu\nu}_{L,m,p,n}$. Here the second equality can be seen as the specification of the singular structure of the PN expansion $\bar{h}$ in the limit $r \to +\infty$.

The first remarkable consequence of the matching equation (1.145) is that, given a PN source, which we know to always come with the necessary overlapping region, the solution to the Einstein field equations (1.9) in the exterior region can be proved to be[16]

$$\mathcal{M}(h^{\mu\nu}) = \mathcal{FP}_{B=0}\Box^{-1}_{\rm ret}\left[\frac{r^B}{r_0^B}\mathcal{M}(\Lambda^{\mu\nu})\right] - \frac{4G}{c^4}\sum_{\ell=0}^{+\infty}\hat{\partial}_L\left[\frac{\mathcal{F}_L^{\mu\nu}(t_r)}{r}\right], \tag{1.146}$$

where, in the first term, we find the formal MPM expansion

$$\mathcal{M}(\Lambda^{\mu\nu}) = \sum_{n=2}^{+\infty} G^n \Lambda^{\mu\nu}_{(n)} = \frac{16\pi G}{c^4}\mathcal{M}(\tau^{\mu\nu}), \tag{1.147}$$

while, in the second term, we have a set of STF tensorial functions $\mathcal{F}_L^{\mu\nu}(t_r)$ that are related to $\tau^{\mu\nu}$ by

$$\mathcal{F}_L^{\mu\nu}(t_r) = \mathcal{FP}_{B=0}\int d^3\mathbf{y}\,\frac{|\mathbf{y}|^B}{r_0^B}\hat{y}_L\int_{-1}^{+1} dz\,\delta_\ell(z)\bar{\tau}^{\mu\nu}(t_r + z|\mathbf{y}|/c, \mathbf{y}), \tag{1.148}$$

where the weighted integral in z is the same one seen in Eq. (1.76).[17] This second term represents the linear 1PM term of the exterior solution (1.146). As such, it can be further decomposed in irreducible STF representations of $SO(3)$ which correspond *precisely* to the source multipole moments $(I_L, J_L, W_L, X_L, Y_L, Z_L)$. One can thus invert the relations that substantiate this decomposition and express the source moments in terms of the components $\mathcal{F}_L^{00}(t_r)$, $\mathcal{F}_L^{0i}(t_r)$, and $\mathcal{F}_L^{ij}(t_r)$, finally relating them to $\bar{\tau}^{\mu\nu}$ via Eq. (1.148). The results is a set of source-rooted closed-form expressions for the source multipoles. For instance we have

$$\begin{aligned} I_L(t_r) = \mathcal{FP}_{B=0}\int d^3\mathbf{y}\,\frac{|\mathbf{y}|^B}{r_0^B}\int_{-1}^{+1} dz\,\Bigg\{&\delta_\ell\hat{y}_L\overline{\Sigma} - \frac{4(2\ell+1)}{c^2(\ell+1)(2\ell+3)}\delta_{\ell+1}\hat{y}_{iL}\overline{\Sigma}_i^{(1)} \\ &+ \frac{2(2\ell+1)}{c^4(\ell+1)(\ell+2)(2\ell+5)}\delta_{\ell+2}\hat{y}_{ijL}\overline{\Sigma}_{ij}^{(2)}\Bigg\}(t_r + z|\mathbf{y}|/c, \mathbf{y}), \end{aligned} \tag{1.149}$$

$$\begin{aligned} J_L(t_r) = \mathcal{FP}_{B=0}\int d^3\mathbf{y}\,\frac{|\mathbf{y}|^B}{r_0^B}\int_{-1}^{+1} dz\,\epsilon_{ab\langle i_\ell}\Bigg[&\delta_\ell\hat{y}_{L-1\rangle a}\overline{\Sigma}_b \\ &- \frac{2\ell+1}{c^2(\ell+2)(2\ell+3)}\delta_{\ell+1}\hat{y}_{L-1\rangle ac}\overline{\Sigma}_{bc}^{(1)}\Bigg](t_r + z|\mathbf{y}|/c, \mathbf{y}), \end{aligned} \tag{1.150}$$

[16] This poof is given e.g. in Sec. 4.2 of Ref. [112].

[17] This is no coincidence since the second term of the solution (1.146) is the only one that survives in the linear limit, therefore it must reproduce the linearized field studied below Eq. (1.80), once we replace $\bar{\tau}^{\mu\nu}$ by the compact-support matter tensor $T^{\mu\nu}$, whose regularity also allows us to remove $\mathcal{FP}_{B=0}$ and $|\mathbf{y}|^B/r_0^B$.

where we have defined $\overline{\Sigma} \equiv c^{-2}(\bar{\tau}^{00} + \bar{\tau}^{aa})$, $\overline{\Sigma}_i \equiv c^{-1}\bar{\tau}^{0i}$, and $\overline{\Sigma}_{ij} \equiv \bar{\tau}^{ij}$. Analogues relations are found for the gauge moments (W_L, X_L, Y_L, Z_L); see e.g. Eqs. (125a)-(125d) of Ref. [112]. Notably, the above expressions for I_L and J_L correspond to the linearized theory expressions (1.89)-(1.90) with the replacement $T^{\mu\nu} \to \bar{\tau}^{\mu\nu}$ and the addition of the necessary finite-part regularization. Beware that each z-integral in the source multipoles should be intended as a formal PN expansions in the sense of Eq. (1.79).

Essentially, the first important consequence of the matching is that it selects, among the general class of exterior solutions described by the MPM algorithm of Sec. 1.3.1, which we remind are not source-specific, the physical solution associated to the energy-momentum content of a given matter source, provided the latter is post-Newtonian. Indeed, to compute explicitly the source moments up to a target PN accuracy, we need to determine the PN-expanded sources $\overline{\Sigma}$, $\overline{\Sigma}_i$, and $\overline{\Sigma}_{ij}$, and thus $\bar{\tau}^{\mu\nu}$. We need therefore the near-zone field solution of section 1.3.2, which was however not completely determined, because of the unspecified homogeneous functions $\mathcal{A}_L^{\mu\nu}$ in Eq. (1.141). This brings us to the second remarkable accomplishment of the PN-MPM matching: as shown in Ref. [178], the matching equation also implies

$$\mathcal{A}_L^{\mu\nu}(t) = \mathcal{F}_L^{\mu\nu}(t) + \mathcal{R}_L^{\mu\nu}(t) \tag{1.151}$$

where $\mathcal{F}_L^{\mu\nu}$ are the functions of Eq. (1.148) and

$$\mathcal{R}_L^{\mu\nu}(t) = \mathcal{FP}_{B=0} \int d^3\mathbf{y} \frac{|\mathbf{y}|^B}{r_0^B} \hat{y}_L \int_1^{+\infty} dz\, (-2\delta_\ell) \mathcal{M}(\tau^{\mu\nu})(t + z|\mathbf{y}|/c, \mathbf{y}), \tag{1.152}$$

which we note to be given in terms of the formal MPM expansion $\mathcal{M}(\tau^{\mu\nu})$. The functions $\mathcal{F}_L^{\mu\nu}$ and $\mathcal{R}_L^{\mu\nu}$ in Eq. (1.151) completely characterize the radiation-reaction effects in the near field-solution, with the linear order contribution $\mathcal{F}_L^{\mu\nu}$ and the extra non-linear correction $\mathcal{R}_L^{\mu\nu}$ first entering, respectively, at 2.5PN order and 4PN order.

Remarkably, it is possible to rewrite Eq. (1.141) in the convenient form [179]

$$\bar{h}^{\mu\nu} = \frac{16\pi G}{c^4} \Box_{\text{ret}}^{-1}[\bar{\tau}^{\mu\nu}] - \frac{4G}{c^4} \sum_{\ell=0}^{+\infty} \frac{(-)^\ell}{\ell!} \hat{\partial}_L \left[\frac{\mathcal{R}_L^{\mu\nu}(t - r/c) - \mathcal{R}_L^{\mu\nu}(t + r/c)}{2r} \right]. \tag{1.153}$$

Here the first term is given by

$$\Box_{\text{ret}}^{-1}[\bar{\tau}^{\mu\nu}](t, \mathbf{x}) = -\frac{1}{4\pi} \sum_{n=0}^{+\infty} \frac{(-)^n}{n!} \left(\frac{\partial}{c\partial t} \right)^n \mathcal{FP}_{B=0} \int d^3\mathbf{y}\, |\mathbf{x} - \mathbf{y}|^{n-1}\, \bar{\tau}^{\mu\nu}(t, \mathbf{y}), \tag{1.154}$$

and corresponds to the formal PN expansion of the retardations in the integral (1.15), thus representing the most intuitive way of tackling (1.14) within PN

theory; recalling Eq. (1.137), one can furthermore prove that

$$\Box^{-1}_{\rm ret}[\bar\tau^{\mu\nu}] - \Box^{-1}_{\rm inst}[\bar\tau^{\mu\nu}] = -\frac{4G}{c^4}\sum_{\ell=0}^{+\infty}\frac{(-)^\ell}{\ell!}\hat\partial_L\left[\frac{\mathcal{F}^{\mu\nu}_L(t-r/c)-\mathcal{F}^{\mu\nu}_L(t+r/c)}{2r}\right]. \tag{1.155}$$

The second term of Eq. (1.153), with its dependence on $\mathcal{R}^{\mu\nu}_L$, conveys the inadequacy of the intuitive PN solution $\bar h^{\mu\nu} \sim \Box^{-1}_{\rm ret}[\bar\tau^{\mu\nu}]$ as one goes at the 4PN order and beyond, where it is no longer possible to completely expand the solution in instantaneous contributions but it is rather necessary to also factor in nonlinear radiation-reaction effects, complete of hereditary pieces, as prescribed by the MPM expansion entering $\mathcal{R}^{\mu\nu}_L$ through $\mathcal{M}(\tau^{\mu\nu})$. In fact, if restricted to its leading order, this term with $\mathcal{R}^{\mu\nu}_L$ of Eq. (1.153) reduces to the 4PN hereditary-type radiation-reaction originally found in Ref. [102].

In conclusion, Eq. (1.153) is what is generally considered to explicitly determine order by order $\bar h^{\mu\nu}$, and from it $\bar\tau^{\mu\nu}$, as it is needed for the evaluation of Eqs. (1.149), (1.150), and their gauge moment analogues. See for instance Refs. [109,110] for the application of this formalism up to the 3PN order, and Sec. 5.3 and Sec. 5.4 of Ref. [112] for its 3.5PN and, in part, 4PN extension.

1.3.4 Non-linear waveform at infinity

We conclude the Chapter by discussing the implication of the Blanchet-Damour formalism on the asymptotic waveform at future null infinity. We remind that this is the observationally relevant component of the GW, projected on the TT gauge and restricted to its leading $1/R$ component, R being the radial distance from the source in radiative coordinates. We also recall that the asymptotic waveform admits the general STF decomposition given in Eq. (1.91), in terms of the two sets of radiative multipoles $U_L(T_R)$ and $V_L(T_R)$.

Similarly to what we did in our linearized theory analysis, in Sec. 1.2.4, the strategy to compute (U_L, V_L) is to take the field solution valid outside the source we built in the previous sections, select its $1/R$ component, and finally read off, by comparison with Eq. (1.91), the structure of each radiative multipole (U_L, V_L) up to the available PN order (see the c factors in Eq. (1.91)). In practice, within the non-linear formalism we are exploring now, the exterior solution we have to consider for this procedure is the one computed via the MPM algorithm. The radiative multipoles are thus computed in the form of non-linear functionals of the canonical multipole moments (M_L, S_L), which are then rewritten in terms of the source moments $(I_L, J_L, W_L, X_L, Y_L, Z_L)$ as discussed below Eq. (1.111). Using the source-rooted expressions one has, thanks to the PN-MPM matching, for the source multipoles, we can ultimately relate the observable radiative multipoles (U_L, V_L) of the asymptotic waveform to the matter content of its source. In this derivation we have however to be careful about the difference between the radiative coordinates used in Eq. (1.91) and the harmonic coordinates adopted so far in each part of

the Blanchet-Damour formalism. In fact, if we ignore the problem and pretend that Eq. (1.91) is written in harmonic coordinates $(t, \mathbf{x})$, the resulting radiative moments are found to develop an explicit dependence on $\log r$ (and powers of it). For instance, stopping at the first non-linear correction, one computes

$$U_L(t_r, \log r) = M_L^{(\ell)}(t_r) + \frac{2GM}{c^3}\int_0^{+\infty} d\tau\, M_L^{(\ell+2)}(t_r-\tau)\left[\log\left(\frac{c\tau}{2r}\right) + \kappa_\ell\right] + \mathcal{O}(1/c^5), \tag{1.156}$$

$$V_L(t_r, \log r) = S_L^{(\ell)}(t_r) + \frac{2GM}{c^3}\int_0^{+\infty} d\tau\, S_L^{(\ell+2)}(t_r-\tau)\left[\log\left(\frac{c\tau}{2r}\right) + \pi_\ell\right] + \mathcal{O}(1/c^5), \tag{1.157}$$

with

$$\kappa_\ell = \frac{2\ell^2+5\ell+4}{\ell(\ell+1)(\ell+2)} + \sum_{k=1}^{\ell-2}\frac{1}{k}, \tag{1.158}$$

$$\pi_\ell = \frac{\ell-1}{\ell(\ell+1)} + \sum_{k=1}^{\ell-1}\frac{1}{k}. \tag{1.159}$$

Beside the presence of $\log r$, we see that the first non-linear effects in the radiative multipole expressions (1.156)-(1.157) are of hereditary type. In particular, these hereditary contributions are known as *tail integrals*, since the $\log\tau$ they contain tends to suppress them as τ goes toward the remote past before t_r. Coming back to the issue with the logarithms of r, it can be proved that they can all be removed with the linear gauge transformation

$$\begin{aligned} H^{\mu\nu}_{(1)} &= h^{\mu\nu}_{(1)} + \partial^\mu\chi^\nu_{(1)} + \partial^\nu\chi^\mu_{(1)} - \eta^{\mu\nu}\partial_\alpha\chi^\alpha_{(1)}, \\ \chi^\mu_{(1)} &\equiv \frac{2M}{c^2}\eta^{0\mu}\log\left(\frac{r}{r_0}\right), \end{aligned} \tag{1.160}$$

which results in the retarded-time shift

$$T_R = t_r - \frac{2GM}{c^3}\log\left(\frac{r}{r_0}\right) + \mathcal{O}(G^2), \tag{1.161}$$

where r_0 is the same constant length scale that appears in the finite part regularizations. The transformation (1.161) is actually enough to remove any radial logarithm in $U_L(t_r, \log r)$ and $V_L(t_r, \log r)$. For instance, by employing it in (1.156), we simply find

$$U_L(T_R) = M_L^{(\ell)}(T_R) + \frac{2GM}{c^3}\int_0^{+\infty} d\tau\, M_L^{(\ell+2)}(T_R-\tau)\left[\log\left(\frac{c\tau}{2r_0}\right) + \kappa_\ell\right]$$

$$+\mathcal{O}(1/c^5). \tag{1.162}$$

The same happens even if we consider non-linearities at higher PN order. By way of illustration, we provide below the 3PN-accurate expression for the radiative mass quadrupole:

$$\begin{aligned} U_{ij}(T_R) &= M_{ij}^{(2)} + \frac{2GM}{c^3}\int_0^{+\infty} d\tau\, M_{ij}^{(4)}(T_R-\tau)\left[\log\left(\frac{c\tau}{2r_0}\right)+\frac{11}{42}\right] \\ &+ \frac{G}{c^5}\left[\frac{1}{7}M_{a\langle i}^{(5)}M_{j\rangle a} - \frac{5}{7}M_{a\langle i}^{(4)}M_{j\rangle a}^{(1)} - \frac{2}{7}M_{a\langle i}^{(3)}M_{j\rangle a}^{(2)} + \frac{1}{3}\epsilon_{ab\langle i}M_{i\rangle a}^{(4)}S_b\right. \\ &\left. - \frac{2}{7}\int_0^{+\infty} d\tau\, M_{a\langle i}^{(3)}M_{j\rangle a}^{(3)}(T_R-\tau)\right] \\ &+ 2\left(\frac{GM}{c^3}\right)^2\int_0^{+\infty} d\tau\, M_{ij}^{(5)}(T_R-\tau)\left[\log^2\left(\frac{c\tau}{2r_0}\right)+\frac{57}{70}\log\left(\frac{c\tau}{2r_0}\right)+\frac{124627}{44100}\right] \\ &+ \mathcal{O}(1/c^7) \end{aligned} \tag{1.163}$$

Here, the term in the third row is the lowest order *memory integral* [105], a designation given to all the non-linear contribution where the remote past is not suppressed as in the tail integrals, because there are no logarithms of τ. The term in the last row is instead the *tail-of-tail* of the mass quadrupole, the first of the "second layer" hereditary effects that arise from more than quadratic multipolar interactions; more specifically, this is obtained from the cubic interaction $M \times M \times M_{ij}$ [180]. Mind that, with harmonic coordinates, the tail-of-tail logarithms would have r instead of r_0 in their argument, but the transformation (1.161) is enough to completely remove any $\log r$ here as well.

Concerning this aspect, we have also to mention that the presence of radial logarithms in harmonic coordinates may become an obstacle to the very application of the MPM algorithm: in highly non-linear terms like the *tail-of-memory*, a cubic-interaction effect whose leading 4PN contribution is currently under investigation, the standard MPM paradigm in harmonic coordinates leads to polylogarithmic terms which is quite hard to handle. The way out of this issue has been recently found in the adoption of a modified version of the MPM algorithm, which directly builds the exterior field solution in radiative coordinates; see the recent work [181] for more details.

In conclusion, the computational scheme that emerges from the Blanchet-Damour GW generation formalism is essentially

$$\begin{aligned} T^{\mu\nu} &\to \bar{\tau}^{\mu\nu} \to (I_L, J_L, W_L, X_L, Y_L, Z_L) \to (M_L, S_L) \\ &\to (U_L, V_L) \to h_{ij}^{TT}(T_R, \mathbf{N}), \end{aligned} \tag{1.164}$$

and constitutes the beyond-linear generalization of Eq. (1.95).

Before we end this Chapter, let us mention for later convenience that there is an alternative way of writing the general asymptotic waveform (1.91). In fact, introducing the pure-spin tensor harmonics $T_{ij}^{E2,\ell m}$ and $T_{ij}^{B2,\ell m}$, we can also write [174, 182]

$$h_{ij}^{TT}(T_R,\mathbf{N}) = \frac{G}{c^2 R}\sum_{\ell=2}^{\infty}\sum_{m=-\ell}^{\ell}\left[\frac{1}{c^\ell}U_{\ell m}(T_R)T_{ij}^{E2,\ell m} + \frac{1}{c^{\ell+1}}V_{\ell m}(T_R)T_{ij}^{B2,\ell m}\right], \tag{1.165}$$

where the two sets of spherical multipole moments $(U_{\ell m}, V_{\ell m})$, again referred to, respectively, as mass-type and current-type radiative multipole moments, are related to their STF counterparts (U_L, V_L) by

$$U_{\ell m} = \frac{4}{\ell!}\sqrt{\frac{(\ell+1)(\ell+2)}{2\ell(\ell-1)}}\,\mathcal{Y}_L^{\ell m}\,U_L, \tag{1.166}$$

$$V_{\ell m} = -\frac{8}{\ell!}\sqrt{\frac{\ell(\ell+2)}{2(\ell+1)(\ell-1)}}\,\mathcal{Y}_L^{\ell m}\,V_L, \tag{1.167}$$

where $*$ denotes complex conjugation and $\mathcal{Y}_L^{\ell m}$ are the STF spherical harmonics that connects the basis of the scalar spherical harmonics $Y^{\ell m}$ to the set of STF tensors $\hat{N}_L$. They can be computed in terms of the integral

$$\mathcal{Y}_L^{\ell m} = \int d\Omega\,\hat{N}_L(\Theta,\Phi)[Y^{\ell m}(\Theta,\Phi)]^*, \tag{1.168}$$

considering the angular parametrization $\mathbf{N}(\Theta,\Phi) = (\sin\Theta\cos\Phi, \sin\Theta\sin\Phi, \cos\Theta)$. Furthermore, the STF harmonics are related to the spin-weighted spherical harmonics ${}_{\pm2}Y_{\ell m}$ by

$$T_{ij}^{E2,\ell m} = \frac{1}{\sqrt{2}}\big({}_{-2}Y_{\ell m}m_i m_j + {}_2Y_{\ell m}m_i^* m_j^*\big), \tag{1.169}$$

$$T_{ij}^{B2,\ell m} = -\frac{i}{\sqrt{2}}\big({}_{-2}Y_{\ell m}m_i m_j - {}_2Y_{\ell m}m_i^* m_j^*\big), \tag{1.170}$$

where we used the vector $\mathbf{m}$ of Eq. (1.27). We recall that the general definition of the spin-weighted spherical harmonics is

$${}_{-s}Y_{\ell m} \equiv (-)^s\sqrt{\frac{2\ell+1}{4\pi}}d_{ms}^{\ell}(\Theta)e^{im\Phi}, \tag{1.171}$$

where the Wigner d-function are defined as

$$d_{ms}^{\ell}(\Theta) \equiv \sqrt{(\ell+m)!(\ell-m)!(\ell+s)!(\ell-s)!}$$

$$\times \sum_{k=k_i}^{k^f} (-)^k \frac{[\sin(\Theta/2)]^{2k+s-m}[\cos(\Theta/2)]^{2\ell+m-s-2k}}{k!(\ell+m-k)!(\ell-s-k)!(s-m+k)!}, \quad (1.172)$$

with $k_i = \max(0, m-s)$ and $k_f = \min(\ell+m, \ell-s)$. Plugging Eqs. (1.169)-(1.170) in Eq. (1.165), and remembering Eq. (1.28), yields

$$\begin{aligned} h_+ - ih_\times &= \frac{G}{\sqrt{2}Rc^2} \sum_{\ell=2}^{\infty} \sum_{m=-\ell}^{\ell} \frac{1}{c^\ell} \left[U_{\ell m}(T_R) - \frac{i}{c} V_{\ell m}(T_R) \right] {}_{-2}Y_{\ell m}(\Theta, \Phi) \\ &= \sum_{\ell=2}^{\infty} \sum_{m=-\ell}^{\ell} h_{\ell m} {}_{-2}Y_{\ell m}(\Theta, \Phi), \end{aligned} \quad (1.173)$$

in which we defined the spherical harmonic components

$$h_{\ell m} \equiv \frac{G}{\sqrt{2}Rc^{\ell+2}} \left[U_{\ell m}(T_R) - \frac{i}{c} V_{\ell m}(T_R) \right], \quad (1.174)$$

also known as spherical modes of the waveform. The latter encode all the relevant information of the waveform at infinity and are particularly convenient when one wants to compare analytical and numerical results for the GW waveform. As such, they are also at the basis of the formalism adopted by the EOB waveform models we will discuss in the next Chapter, since these models hybridize analytical results with non-perturbative information coming from NR simulations.

Relevantly, when one deals with GWs produced by non-precessing compact binaries (i.e. spin-less or with spins aligned/antialigned to the binary angular momentum), such as the ones we will mainly target in this Thesis, Eq. (1.174) further simplifies according to the mode separation

$$h_{\ell m} = -\frac{G}{\sqrt{2}Rc^{\ell+2}} U_{\ell m} \qquad \text{when } \ell+m \text{ is even}, \quad (1.175)$$

$$h_{\ell m} = i\frac{G}{\sqrt{2}Rc^{\ell+3}} V_{\ell m} \qquad \text{when } \ell+m \text{ is odd}, \quad (1.176)$$

as proved, e.g., in section IIIB of Ref. [164].

We finally highlight that, within this formalism, the fluxes of energy and angular momentum at infinity can be directly computed from the spherical modes $h_{\ell m}$. In fact, from Eqs. (1.54)-(1.55), one finds

$$\dot{E} = \frac{1}{16\pi} \sum_{\ell=2}^{\ell_{\max}} \sum_{m=-\ell}^{\ell} |\dot{h}_{\ell m}|^2, \quad (1.177)$$

$$\dot{J} = -\frac{1}{16\pi} \sum_{\ell=2}^{\ell_{\max}} \sum_{m=-\ell}^{\ell} m\, \Im\big(\dot{h}_{\ell m} h^*_{\ell m}\big) \quad (1.178)$$

Chapter 2

The effective one-body approach to coalescing compact binaries

The waveform modeling techniques we discussed so far are inherently limited in their application to post-Newtonian sources. As such, they have no means of adequately reproducing GW signals whenever these are radiated by astrophysical phenomena that elude the PN approximation, encompassing strong-gravity effects and high internal velocities. We think in particular about the last stages of the CBC evolution, starting from the late inspiral, when the two component objects become close to each other and their orbital velocity rises up to relativistic values. In order to build complete waveform templates for CBC signals, as it is required by GW data analysis, one has therefore to go beyond plain PN results, whether they are relative to the waveform or to the underlying compact binary dynamics. The effective one-body approach (EOB) we will review in this Chapter, which is at the root of the waveform modeling activity presented in the next one, has been devised precisely with this purpose: finding a proper analytical formalism to exploit the available information regarding the two-body problem, coming particularly but not exclusively from PN theory, and provide a description to the motion and radiation of coalescing compact binaries valid over their entire evolution, comprehensive of late inspiral, plunge, merger, and ringdown. As we will see, the key factors to achieve this goal are essentially two: (i) the systematic use of several *resummation methods*, which basically consist in replacing PN results, in their standard polynomial form, in powers of $1/c$, with suitable non-polynomial functions that incorporate expected non-perturbative features of their exact counterparts,[1] and that give back, once PN-expanded,

[1] In identifying these non-perturbative structures, a crucial role is played by the connection that the EOB approach establishes between the compact binary dynamics and the much simpler case of a test particle in motion around a Schwarzschild (or Kerr) black hole;

the original polynomial results; (ii) the calibration of several free parameters, either naturally present but analytically unknown or specifically added in the EOB description,[2] on the non-perturbative waveform information provided by numerical relativity (NR) simulations, which is exact modulo the small numerical error.

In general, we can single out three main building blocks in the EOB formalism [183, 184]:

- a prescription for the conservative dynamics of the compact binary, encoded in an Hamiltonian;
- a prescription for the radiation-reaction force that drives the dissipative effects in the dynamics, i.e. the loss of energy and angular momentum through the emission of GWs;
- a prescription for the corresponding GW waveform at infinity.

In this Chapter we will review each one of these fundamental aspects, referring specifically to the recipes that characterize the waveform model `TEOBResumS`, which will be the protagonist of the noncircular extensions at the core of the next Chapter. In doing so, we will mainly focus on the case of nonspinning binary black holes, although we specify that `TEOBResumS` can account for more general dynamics where spin and tidal deformations are present. We briefly review in Appendix B the measures taken in the model to make it viable also for spin-aligned (or antialigned) binary black holes, that is with individual spins parallel (or anti-parallel) to the angular momentum direction; for the application of `TEOBResumS` to binaries with generically oriented spins and associated precessing orbital planes, see the waveform twisting technique described in Refs. [185, 186]; for the inclusion in the model of tidal effects, relevant for binaries with neutron stars, see instead Refs. [187, 188].

Better specifying the structure of this Chapter, we will proceed as follows. In Sec. 2.1 we will present the EOB conservative dynamics, detailing its historical establishment at 2PN accuracy [140, 141] and its extensions at 3PN [142] and 4PN [189], with some mentions to the strategy recently devised to push it at even higher orders [190–193]. Then, in Sec. 2.2 we will discuss the prescriptions for the radiation reaction force and the waveform model before merger, specifically referring to the native quasi-circular version of `TEOBResumS`. Finally, in Sec. 2.3, we target how the EOB approach succeeds in completing the waveform model with the inclusion of a description for the merger and ringdown phases of the coalescence.

---

the nature of this link will be clarified in Sec. 2.1.

[2] The possibility of adding free tunable parameters in the EOB description is often referred to as the *EOB flexibility*.

2.1 Conservative dynamics in the EOB approach

It is widely known that, within Newtonian gravity, the two-body relative motion, in the center of mass frame, for a system of objects with masses m_1 and m_2, can be described in terms of a "test particle" of mass $\mu \equiv m_1 m_2/(m_1+m_2)$ orbiting in the gravitational potential generated by an external mass $M \equiv m_1 + m_2$ equal to the total mass of the system. The founding idea of the EOB approach, from which it takes its name, is a generalization of this logic to the general relativity case: describing the conservative dynamics of a compact binary of masses m_1 and m_2 in terms of the motion of a particle of mass μ in an effective external metric $g^{\rm eff}_{\mu\nu}(x^\lambda_{\rm eff}, M)$, which is *a priori* undetermined. Indeed, this effective description should be equivalent, once PN-expanded, to the corresponding "real" two-body dynamics obtained in PN theory. Moreover it should make contact to other approximation schemes in their regime of validity, such as the gravitational self force or the post Minkowskian formalism. Enforcing this requirements, we have thus to properly define the effective metric $g^{\rm eff}_{\mu\nu}(x^\lambda_{\rm eff}, M)$ and establish a dictionary between the EOB and the basic two-body dynamical descriptions. In what follows we will describe in details this procedure, initially limiting our discussion to the 2PN order, for historical and expositional reasons.

2.1.1 EOB conservative dynamics at 2PN

The motion of a gravitationally interacting systems of two compact objects of masses m_1 and m_2 is generally encoded in the action

$$S_{\rm tot}[x^\mu_1, x^\mu_2, g_{\mu\nu}] = S_{\rm EH}[g_{\mu\nu}] - \sum_{A=1,2} m_A c \int \sqrt{-g_{\mu\nu}(x^\lambda_A) dx^\mu_A dx^\nu_A}, \qquad (2.1)$$

where the first term is the Einstein-Hilbert action (1.3) and the second one is relative to the two component objects, seen as point particles with coordinates x^μ_1 and x^μ_2. In 1981, Damour & Deruelle computed the associated equations of motion at 2PN accuracy [194], using harmonic coordinates. Therein, they showed that those same equations equivalently follow from a generalized Lagrangian, 2PN-extension of the 1PN Lagrangian of Einstein, Infeld & Hoffman [53], that must depend also on the accelerations of the two particles. Afterwards, in Ref. [195], Damour & Schäfer proved that this acceleration dependence could be removed by rewriting the harmonic Lagrangian in ADM coordinates, which had been introduced in Ref. [196].[3] The so-obtained ordinary Lagrangian was then translated, via a Legendre transform, into a 2PN-accurate two-body ADM Hamiltonian. This PN-expanded Hamiltonian is of great importance to our discussion, as it represented the technical starting

[3] The contact transformation between harmonic and ADM coordinates is given at 2PN order in Eq. (35) of Ref. [197] and at 3PN order in Ref. [64].

point for the establishment of the EOB formalism in the seminal work [140], by Buonanno & Damour.

Let us denote the ADM coordinates of the two particles as $\mathbf{Q}_1$ and $\mathbf{Q}_2$, with conjugate momenta $\mathbf{P}_1$ and $\mathbf{P}_2$, where $\mathbf{P}_A = \partial S/\partial \mathbf{Q}_A$ for $A = 1, 2$. In the center-of-mass frame, the relative motion is described by the coordinates $\mathbf{Q} = \mathbf{Q}_1 - \mathbf{Q}_2$ and $\mathbf{P} = \mathbf{P}_1 = -\mathbf{P}_2$, such that $\mathbf{P} = \partial S/\partial \mathbf{Q}$. Introducing the rescalings

$$\mathbf{q} \equiv \frac{\mathbf{Q}}{GM}, \quad \mathbf{p} \equiv \frac{\mathbf{P}}{\mu}, \quad t \equiv \frac{T}{GM}, \tag{2.2}$$

the μ-rescaled 2PN Hamiltonian of Ref. [195] is written as

$$\hat{H}^{\rm nr}(\mathbf{q},\mathbf{p}) \equiv \frac{H^{\rm nr}(\mathbf{q},\mathbf{p})}{\mu} = \sum_{n=0} \frac{1}{c^{2n}} \hat{H}^{\rm nr}_{n\rm PN}(\mathbf{q},\mathbf{p}), \tag{2.3}$$

$$\hat{H}^{\rm nr}_{\rm N}(\mathbf{q},\mathbf{p}) = \frac{\mathbf{p}}{2} - \frac{1}{q}, \tag{2.4}$$

$$\hat{H}^{\rm nr}_{\rm 1PN}(\mathbf{q},\mathbf{p}) = -\frac{1-3\nu}{8}\mathbf{p}^4 - \frac{1}{2q}\big[(3+\nu)\mathbf{p}^2 + \nu(\mathbf{n}\cdot\mathbf{p})^2\big] + \frac{1}{2q^2}, \tag{2.5}$$

$$\begin{aligned}\hat{H}^{\rm nr}_{\rm 2PN}(\mathbf{q},\mathbf{p}) = {}& \frac{1-5\nu+5\nu^2}{16}\mathbf{p}^6 + \frac{1}{8q}\big[(5-20\nu-3\nu^2)\mathbf{p}^4 \\ & - 2\nu^2\mathbf{p}^2(\mathbf{n}\cdot\mathbf{p})^2 - 3\nu^2(\mathbf{n}\cdot\mathbf{p})^4\big] + \frac{1}{2q^2}\big[(5+8\nu)\mathbf{p}^2 + 3\nu(\mathbf{n}\cdot\mathbf{p})^2\big] \\ & - \frac{1+3\nu}{4q^3},\end{aligned} \tag{2.6}$$

where $H^{\rm nr} \equiv H - Mc^2$ is the "non-relativistic" Hamiltonian obtained by subtracting to the total one its rest-mass contribution, $\nu \equiv \mu/M = m_1 m_2/(m_1+m_2)^2$ is the symmetric mass ratio of the system, $q \equiv |\mathbf{q}|$, and $\mathbf{n} \equiv \mathbf{q}/q$. The invariance of this Hamiltonian under time translations and spatial rotations ensures the conservation of the quantities

$$\hat{H}^{\rm nr} = \hat{\mathcal{E}}^{\rm nr} \equiv \frac{\mathcal{E}^{\rm nr}}{\mu}, \qquad \mathbf{q}\times\mathbf{p} = \mathbf{j} \equiv \frac{\mathcal{J}}{\mu GM}, \tag{2.7}$$

respectively the reduced energy and angular momentum of the system in the center-of-mass frame.

We now move to rewriting the dynamical information above in a coordinate-invariant fashion, that will be helpful in establishing the connection with the effective problem. In the non-spinning (or spin-aligned) setting the motion is planar, and thus we can set $q_z = 0$. Using polar coordinates $\mathbf{q} = (r\cos\varphi, r\sin\varphi, 0)$ we can therefore write the reduced action as[4]

$$\hat{S} = \frac{S}{\mu GM} = -\hat{\mathcal{E}}^{\rm nr} t + j\varphi + \hat{S}_r(r, \hat{\mathcal{E}}^{\rm nr}, j) \tag{2.8}$$

[4]We work here, in particular, with the Fokker-type action that is obtained by eliminating the gravitational degrees of freedom in the total action (2.1)

where we used the conservation of the quantities (2.7) to separate the coordinates t and ϕ, with $j \equiv |\mathbf{j}|$. Here the radial action is defined as

$$\hat{S}_r(r, \hat{\mathcal{E}}^{\rm nr}, j) \equiv \int dr\, p_r(r, \hat{\mathcal{E}}^{\rm nr}, j), \tag{2.9}$$

where the radial-momentum function p_r can be computed by solving perturbatively Eq. (2.3) for $(\mathbf{n}\cdot\mathbf{p})^2 = p_r^2$, with $\hat{H} = \hat{\mathcal{E}}^{\rm nr}$ and $\mathbf{p}^2 = p_r^2 + j^2/r^2$. The resulting expression is a fifth-order polynomial in $1/r$ and is written in Eq. (3.4) of Ref. [195]. The associated radial action variable is determined by solving the integral

$$i_r(\hat{\mathcal{E}}^{\rm nr}, j) \equiv \frac{1}{\pi}\int_{r_{\rm min}}^{r_{\rm max}} dr\, p_r(r, \hat{\mathcal{E}}^{\rm nr}, j), \tag{2.10}$$

where $r_{\rm min}$ and $r_{\rm max}$ are the two turning points of the radial motion, real roots of $p_r(r, \hat{\mathcal{E}}^{\rm nr}, j) = 0$; see Appendix B of Ref. [195] for more details on this computation.

Coming back to unscaled variables, with $R = GMr$, $\alpha \equiv \mu GM$, and $I_R(\mathcal{E}^{\rm nr}, \mathcal{J}) = \alpha i_r(\mathcal{E}^{\rm nr}/\mu, \mathcal{J}/\alpha)$, the explicit 2PN result for the radial action variable is [195]

$$\begin{aligned} I_R(\mathcal{E}^{\rm nr}, \mathcal{J}) = \alpha\sqrt{\frac{\mu}{-2\mathcal{E}^{\rm nr}}}\Bigg[1 + \left(\frac{15}{4} - \frac{\nu}{4}\right)\frac{\mathcal{E}^{\rm nr}}{\mu c^2} + \left(\frac{35}{32} + \frac{15}{16}\nu \right.\\ \left. + \frac{3}{32}\nu^2\right)\left(\frac{\mathcal{E}^{\rm nr}}{\mu c^2}\right)^2\Bigg] - \mathcal{J} + \frac{\alpha^2}{\mathcal{J}c^2}\left[3 + \left(\frac{15}{2} - 3\nu\right)\frac{\mathcal{E}^{\rm nr}}{\mu c^2}\right]\\ + \frac{\alpha^4}{\mathcal{J}^2 c^4}\left(\frac{35}{4} - \frac{5}{2}\nu\right), \end{aligned} \tag{2.11}$$

This expression can be inverted perturbatively, order by order in the PN expansion, to derive $\mathcal{E}^{\rm nr}$ as a function of the action variables I_R and $\mathcal{J}$[5]. Doing so by trading I_R for the Delaunay action variable $\mathcal{N} \equiv I_R + \mathcal{J}$ yields the 2PN Delaunay Hamiltonian

$$\begin{aligned} \mathcal{E}^{\rm nr}_{\rm real}(\mathcal{N}, \mathcal{J}) = -\frac{1}{2}\frac{\mu\alpha^2}{\mathcal{N}^2}\Bigg[1 + \frac{\alpha^2}{c^2}\left(\frac{6}{\mathcal{N}\mathcal{J}} - \frac{15-\nu}{4\mathcal{N}^2}\right) + \frac{\alpha^4}{c^4}\left(\frac{5(7-2\nu)}{2\mathcal{N}\mathcal{J}^3}\right.\\ \left. + \frac{27}{\mathcal{N}^2\mathcal{J}^2} - \frac{3(35-4\nu)}{2\mathcal{N}^3\mathcal{J}} + \frac{145 - 15\nu + \nu^2}{8\mathcal{N}^4}\right)\Bigg], \end{aligned} \tag{2.12}$$

that we equip with the subscript "real" for future convenience, so as to highlight that it refers to the real two body dynamics we want to describe in EOB terms.

[5]Indeed $\mathcal{J}$ corresponds to the action variable

$$\mathcal{J} = \frac{1}{2\pi}\oint d\varphi\, P_\varphi.$$

For our purpose, the great utility of this objects resides in its coordinate invariance. In fact, if we see it through the lens of the semi-classical quantization of Bohr & Sommerfeld, $\mathcal{E}^{\rm nr}_{\rm real}(\mathcal{N},\mathcal{J})$ describes the discrete energy spectrum of the conservative two-body dynamics in terms of the integers values assumed by $\mathcal{N}/\hbar$, the principal quantum number, and $\mathcal{J}/\hbar$, the angular-momentum quantum number.

Let us now move to the effective problem and compute the analogue of Eq. (2.12) in the effective dynamics. In this case the action is simply given by

$$S_{\rm eff} = -\mu c \int \sqrt{-g^{\rm eff}_{\mu\nu}(x^\lambda_{\rm eff}) dx^\mu_{\rm eff} dx^\nu_{\rm eff}}. \tag{2.13}$$

Focusing on non-spinning dynamics, we can use a static and spherically symmetric ansatz for the metric, namely[6]

$$\begin{aligned} g^{\rm eff}_{\mu\nu} dx^\mu_{\rm eff} dx^\nu_{\rm eff} = &-A(R_{\rm eff})c^2 dT^2_{\rm eff} + B(R_{\rm eff}) dR^2_{\rm eff} \\ &+ R^2_{\rm eff}\left(d\theta^2_{\rm eff} + \sin^2\theta_{\rm eff} d\varphi_{\rm eff}\right), \end{aligned} \tag{2.14}$$

where the unknown metric functions $A(R_{\rm eff})$ and $B(R_{\rm eff})$ are conveniently organized in the generic expansions

$$A(R_{\rm eff}) = 1 + \sum_{n=1}^{+\infty} a_n \left(\frac{GM}{R_{\rm eff}c^2}\right)^n, \tag{2.15}$$

$$B(R_{\rm eff}) = 1 + \sum_{n=1}^{+\infty} b_n \left(\frac{GM}{R_{\rm eff}c^2}\right)^n, \tag{2.16}$$

which are parameterized by two sets of unknown mass-dependent parameters a_n and b_n. Notice that truncating $A(R_{\rm eff})$ and $B(R_{\rm eff})$ at the kPN order means to stop the respective series at $n_{\rm max} = k+1$ for the former and $n_{\rm max} = k$ for the latter.

To keep things as simple as possible, we assume that the motion of the effective test particle of mass μ can be constrained along the geodesics of the spacetime described by $g^{\rm eff}_{\mu\nu}$. We therefore have at our disposal the Hamilton-Jacobi equation

$$0 = \mu^2 c^2 + g^{\mu\nu}_{\rm eff} p^{\rm eff}_\mu p^{\rm eff}_\nu = \mu^2 c^2 + g^{\mu\nu}_{\rm eff} \frac{\partial S_{\rm eff}}{\partial x^\mu_{\rm eff}} \frac{\partial S_{\rm eff}}{\partial x^\nu_{\rm eff}}, \tag{2.17}$$

which we can solve by a separation of variable akin to the one of Eq. (2.8), that is

$$S_{\rm eff} = -\mathcal{E}_{\rm eff} T_{\rm eff} + \mathcal{J}_{\rm eff}\varphi_{\rm eff} + S_{R_{\rm eff}}(R_{\rm eff}, \mathcal{E}_{\rm eff}, \mathcal{J}_{\rm eff}), \tag{2.18}$$

[6] We use here Schwarzschild-like coordinates, which avoid the appearance of an extra radial potential multiplying the angular part of the metric.

where $\mathcal{E}_{\rm eff}$ is the energy in the effective problem, comprehensive of its rest-mass part, and $\mathcal{J}_{\rm eff}$ its angular momentum. Inserting Eqs. (2.14) and (2.18) in Eq. (2.17) yields

$$0 = -\frac{1}{A(R_{\rm eff})}\frac{\mathcal{E}_{\rm eff}^2}{c^2} + \frac{1}{B(R_{\rm eff})}\left(\frac{dS_{R_{\rm eff}}}{dR_{\rm eff}}\right)^2 + \frac{\mathcal{J}_{\rm eff}^2}{R_{\rm eff}^2} + \mu^2 c^2, \tag{2.19}$$

from which

$$S_{R_{\rm eff}}(R_{\rm eff}, \mathcal{E}_{\rm eff}, \mathcal{J}_{\rm eff}) = \int dR_{\rm eff}\, P_{R_{\rm eff}}(R_{\rm eff}, \mathcal{E}_{\rm eff}, \mathcal{J}_{\rm eff}), \tag{2.20}$$

with

$$P_{R_{\rm eff}}(R_{\rm eff}, \mathcal{E}_{\rm eff}, \mathcal{J}_{\rm eff}) = \sqrt{\frac{B(R_{\rm eff})}{A(R_{\rm eff})}\frac{\mathcal{E}_{\rm eff}^2}{c^2} - B(R_{\rm eff})\left(\mu^2 c^2 + \frac{\mathcal{J}_{\rm eff}^2}{R_{\rm eff}^2}\right)}. \tag{2.21}$$

We can now compute the effective radial action $I_{R_{\rm eff}}$ at 2PN order, by adopting the same method used to get Eq. (2.11). The result, in terms of $\mathcal{E}_{\rm eff}^{\rm nr} \equiv \mathcal{E}_{\rm eff} - \mu c^2$, reads

$$\begin{aligned} I_{R_{\rm eff}}(\mathcal{E}_{\rm eff}^{\rm nr}, \mathcal{J}_{\rm eff}) = \alpha\sqrt{\frac{\mu}{-2\mathcal{E}_{\rm eff}^{\rm nr}}}\left[C_1 + C_2\frac{\mathcal{E}_{\rm eff}^{\rm nr}}{\mu c^2} + C_3\left(\frac{\mathcal{E}_{\rm eff}^{\rm nr}}{\mu c^2}\right)^2\right] - \mathcal{J}_{\rm eff} \\ + \frac{\alpha^2}{\mathcal{J}_{\rm eff} c^2}\left[C_4 + C_5\frac{\mathcal{E}_{\rm eff}^{\rm nr}}{\mu c^2}\right] + \frac{\alpha^4}{\mathcal{J}_{\rm eff}^3 c^4} C_6, \end{aligned} \tag{2.22}$$

where

$$\begin{aligned} &C_1 = -\frac{a_1}{2}, \qquad C_2 = b_1 - \frac{7}{8}a_1, \qquad C_3 = \frac{b_1}{4} - \frac{19}{64}a_1, \\ &C_4 = \frac{a_1^2}{2} - \frac{a_2}{2} - \frac{a_1 b_1}{2}, \qquad C_5 = a_1^2 - a_2 - a_1 b_1 + b_2, \\ &C_6 = \frac{3}{8}a_1^4 - \frac{3}{4}a_1^2 a_2 + \frac{a_2^2}{8} + \frac{a_1 a_3}{4} - \frac{a_1^3 b_1}{2} + \frac{a_1 a_2 b_1}{2} + \frac{a_1^2 b_1^2}{8} + \frac{a_1^2 b_2}{4}. \end{aligned} \tag{2.23}$$

With the same perturbative inversion we used to get $\mathcal{E}_{\rm real}^{\rm nr}$ from Eq. (2.11), Eq. (2.22) results in the 2PN effective Delaunay Hamiltonian

$$\begin{aligned} \mathcal{E}_{\rm eff}^{\rm nr}(\mathcal{N}_{\rm eff}, \mathcal{J}_{\rm eff}) = -\frac{1}{2}\frac{\mu\alpha^2}{\mathcal{N}_{\rm eff}^2}\left[1 + \frac{\alpha^2}{c^2}\left(\frac{2C_4}{\mathcal{N}_{\rm eff}\mathcal{J}_{\rm eff}} - \frac{C_2}{\mathcal{N}_{\rm eff}^2}\right) + \frac{\alpha^4}{c^4}\left(\frac{2C_6}{\mathcal{N}_{\rm eff}\mathcal{J}_{\rm eff}^3}\right.\right. \\ \left.\left. + \frac{3C_4^2}{\mathcal{N}_{\rm eff}^2\mathcal{J}_{\rm eff}^2} - \frac{4C_2C_4 + C_5}{\mathcal{N}_{\rm eff}^3\mathcal{J}_{\rm eff}} + \frac{5C_2^2 + 2C_3}{4\mathcal{N}_{\rm eff}^4}\right)\right], \end{aligned} \tag{2.24}$$

where $\mathcal{N}_{\rm eff} \equiv I_{R_{\rm eff}} + \mathcal{J}_{\rm eff}$. Again, this is a coordinate-invariant object that represents, in a semi-classical sense, the possible energy levels in the effective dynamics, with quantum numbers $\mathcal{N}_{\rm eff}/\hbar$ and $\mathcal{J}_{\rm eff}/\hbar$.

It is now time to establish the connection between $\mathcal{E}^{\rm nr}_{\rm real}$ and $\mathcal{E}^{\rm nr}_{\rm eff}$ and use it to build the bridge between the real and the effective dynamics. In light of the coordinate invariance of these objects and their semi-classical interpretation, we start by imposing the natural identifications

$$\mathcal{N} = \mathcal{N}_{\rm eff}, \qquad \mathcal{J} = \mathcal{J}_{\rm eff}. \tag{2.25}$$

From here, the most straightforward path would be to directly identify the two Delaunay Hamiltonians. Accordingly, this was the first tentative energy map considered in Ref. [140]. There, however, it was proved that such an identification is incompatible with two basic requirements: that mass of the effective test particle is simply equal to μ and that the effective metric does not acquire any extra dependence on $\mathcal{E}^{\rm nr}_{\rm eff}$. The solution proposed therein is to consider instead a generalized energy map of the type

$$\frac{\mathcal{E}^{\rm nr}_{\rm eff}}{\mu c^2} = \frac{\mathcal{E}^{\rm nr}_{\rm real}}{\mu c^2}\left[1 + \sum_{n=1}^{+\infty} \alpha_n \left(\frac{\mathcal{E}^{\rm nr}_{\rm real}}{\mu c^2}\right)^n\right], \tag{2.26}$$

given in terms of another set of mass-dependent unknown parameters, α_n.

Stopping Eq. (2.26) at the 2PN order and plugging it in Eqs. (2.12) and (2.24), with the identification (2.25), returns an *underdetermined* system of five equations in the seven parameters $(a_1, a_2, a_2; b_1, b_2; \alpha_1, \alpha_2)$, which together completely specify the effective metric and the above energy-map at 2PN accuracy. The standard way of proceeding in their computation is to require $a_1 = -b_2 = -2$, i.e. that the effective metric coincides with the Schwarzschild metric at linear order in G.[7] The other parameters are thus *uniquely* fixed by the energy map equations and read

$$a_2 = 0, \quad a_3 = 2\nu, \quad b_2 = 2(2-3\nu), \quad \alpha_1 = \frac{\nu}{2}, \quad \alpha_2 = 0. \tag{2.27}$$

At the level of the metric functions (2.15)-(2.16), typically referred to as EOB potentials, this means

$$\begin{aligned} A_{\leq 2\rm PN}(u) &= 1 - 2u + 2\nu u^3, \\ B_{\leq 2\rm PN}(u) &= 1 + 2u + 2(2-3\nu)u^2, \end{aligned} \tag{2.28}$$

where we introduced the PN-counting radial variable $u \equiv GM/(R_{\rm eff}c^2)$. To better understand the properties of the effective metric, it is often advantageous to replace the potential $B(u)$ with

$$D(u) \equiv A(u)B(u) = 1 + \sum_{n=1}^{+\infty} d_n u^n, \tag{2.29}$$

$$D_{\leq 2\rm PN}(u) = 1 - 6\nu u^2, \tag{2.30}$$

[7] To be precise, the condition $a_1 = -2$ actually follows already from the Newtonian limit.

where, at 2PN, $d_1 = a_1 + b_1 = 0$ and $d_2 = a_2 + a_1 b_1 + b_2 = -6\nu$.

On the other hand, for the 2PN energy map one finds the simple result

$$\frac{\mathcal{E}^{\rm nr}_{\rm eff}}{\mu c^2} = \frac{\mathcal{E}^{\rm nr}_{\rm real}}{\mu c^2}\left(1 + \frac{\nu}{2}\frac{\mathcal{E}^{\rm nr}_{\rm real}}{\mu c^2}\right), \tag{2.31}$$

or equivalently, in terms of the total energies,

$$\frac{\mathcal{E}_{\rm eff}}{\mu c^2} = \frac{\mathcal{E}^2_{\rm real} - m_1^2 c^4 - m_2^2 c^4}{2 m_1 m_2 c^4}. \tag{2.32}$$

This is, remarkably, the simplest symmetric function of the Mandelstam invariant $s \equiv \mathcal{E}^2_{\rm real}$. Inverting Eq. (2.32) in terms of $\mathcal{E}_{\rm real}$, and introducing the Hamiltonians $H_{\rm real} = \mathcal{E}_{\rm real}$ and $H_{\rm eff} = \mathcal{E}_{\rm eff}$, we find

$$H_{\rm EOB}(\mathbf{Q}_e, \mathbf{P}_e) \equiv H_{\rm real}(\mathbf{Q}_e, \mathbf{P}_e) = Mc^2\sqrt{1 + 2\nu\left(\frac{H_{\rm eff}(\mathbf{Q}_e, \mathbf{P}_e)}{\mu c^2} - 1\right)}, \tag{2.33}$$

where $\mathbf{Q}_e$ and $\mathbf{P}_e$ are the effective analogue of the ADM center-of-mass canonical coordinate $\mathbf{Q}$ and $\mathbf{P}$; their expressions in terms of the effective polar coordinates we used up too now are

$$\begin{aligned} \mathbf{Q}_e &= (R_{\rm eff}\cos\varphi_{\rm eff}, R_{\rm eff}\sin\varphi_{\rm eff}, 0), \\ \mathbf{P}_e &= (P_{R_{\rm eff}}\cos\varphi_{\rm eff} - \frac{P_{\varphi_{\rm eff}}}{R_{\rm eff}}\sin\varphi_{\rm eff}, P_{R_{\rm eff}}\sin\varphi_{\rm eff} + \frac{P_{\varphi_{\rm eff}}}{R_{\rm eff}}\cos\varphi_{\rm eff}, 0). \end{aligned} \tag{2.34}$$

The effective Hamiltonian $H_{\rm eff}$, which encodes the dynamics of the test mass μ in the effective metric, can be computed from (2.19) with

$$P_{R_{\rm eff}} = \frac{\partial S}{\partial R_{\rm eff}} = \frac{dS_{R_{\rm eff}}}{dR_{\rm eff}}, \qquad P_{\varphi_{\rm eff}} = \frac{\partial S}{\partial \varphi_{\rm eff}} = \mathcal{J}_{\rm eff}, \tag{2.35}$$

and at 2PN accuracy it reads

$$H_{\rm eff}(R_{\rm eff}, P_{R_{\rm eff}}, P_{\varphi_{\rm eff}}) = \mu c^2\sqrt{A(u)\left[1 + \frac{P^2_{\varphi_{\rm eff}}}{\mu^2 c^2 R^2_{\rm eff}} + \frac{A(u)}{D(u)}\left(\frac{P^2_{R_{\rm eff}}}{\mu^2 c^2}\right)\right]}. \tag{2.36}$$

Some comments are in order. For starters, we stress that the EOB Hamiltonian (2.33), with $H_{\rm eff}$ given by Eq. (2.36), describes the two-body conservative motion in a form canonically equivalent to the 2PN ADM Hamiltonian (2.3). It is however remarkably simpler, since the many terms in Eq. (2.3) have been condensed in the Hamiltonian map (2.33) and in the two non-zero coefficients a_3 and d_2 in the 2PN potentials $A_{\le 2\rm PN}(u)$ and $D_{\le 2\rm PN}(u)$. Moreover, it is not given in the form of a PN expansion but rather it incorporates the PN-expanded information of the ADM Hamiltonian in resummed form. In fact, considering Eqs. (2.33) and (2.36), the PN-expanded quantities from which

$H_{\rm EOB}$ depends, i.e. the EOB potentials A and D, are manifestly nested in a double square root structure.

Let us now examine the distinctive features of the effective dynamics encoded in the Hamiltonian (2.36). A crucial aspect to notice is the closeness between the effective metric determined by the EOB potentials $A_{\leq 2\rm PN}(u)$ and $D_{\leq 2\rm PN}(u)$ and the Schwarzschild metric relative to a black hole with mass M, which in the language of Eq. (2.14) would be given by $A_{\rm Schw}(u) = 1-2u$ and $D_{\rm Schw}(u) = 1$. At the 1PN level, the two metrics do actually *coincide*, with the first differences appearing at 2PN, where the effective metric turns out to be given by a very simple smooth deformation of the Schwarzschild metric, with deformation parameter ν, the symmetric mass ratio of the system. We recall in this respect that $\nu \in [0, 1/4]$, where the maximum value $\nu = 1/4$ corresponds to the equal-mass case, $m_1 = m_2$, while the minimum $\nu = 0$ is the test-mass limit, approached when $m_1 \ll m_2$.[8]

The overall deviation of the 2PN effective metric from the Schwarzschild one is in general quite small, even in the extreme scenario where $\nu = 1/4$ and $R_{\rm eff} = 2GM/c^2$ (or $u = 1/2$), that is at the Schwarzschild event horizon. This implies that the effective dynamics is *qualitatively equivalent* to the motion of a particle around a Schwarzschild black hole, and thus presents the same non-perturbative features, including in particular:

(i) the existence of an innermost stable circular orbit (ISCO), below which the particle plunges, defined by the effective radius $R_{\rm ISCO}(\nu)$ such that

$$\frac{\partial W_{\mathcal{J}_{\rm ISCO}}}{\partial R_{\rm eff}}(R_{\rm ISCO}) = 0 = \frac{\partial^2 W_{\mathcal{J}_{\rm ISCO}}}{\partial R^2_{\rm eff}}(R_{\rm ISCO}), \tag{2.37}$$

namely the inflection point developed by the radial potential

$$W_{\mathcal{J}_{\rm eff}}(R_{\rm eff}) \equiv H_{\rm eff}(R_{\rm eff}, P_{R_{\rm eff}} = 0, P_{\varphi_{\rm eff}} = \mathcal{J}_{\rm eff}) \tag{2.38}$$

at the ISCO value $\mathcal{J}_{\rm ISCO}(\nu)$ of the angular momentum; see Fig. 1 of Ref. [140] for an illustration of this fact;

(ii) the existence of a last unstable circular orbit, or *light ring*, defined as the radius $R_{\rm LR}(\nu)$ at which the angular momentum $\mathcal{J}(R_{\rm eff})$, obtained from the circular-orbit condition $\partial_{R_{\rm eff}} W_{\mathcal{J}}(R_{\rm eff}) = 0$, becomes singular, i.e. $\mathcal{J}(R_{\rm LR})^{-1} = 0$;

(iii) the existence of a regular Killing horizon $R_H(\nu)$, defined by the real solution of $A(R_H) = 0$.

[8] The case $m_2 \ll m_1$ would be equivalent, although we always adopt the convention $m_1 \leq m_2$.

These quantities have been evaluated at 2PN accuracy In Refs. [140, 141], where they were shown to assume slightly lower values than in the Schwarzschild case; e.g., for $\nu = 1/4$, the values found are

$$\begin{aligned} &R^{\rm 2PN}_{\rm ISCO}(1/4) \simeq 0.953 R^{\rm Schw}_{\rm ISCO}, \qquad R^{\rm 2PN}_{\rm LR}(1/4) \simeq 0.948 R^{\rm Schw}_{\rm LR}, \\ &R^{\rm 2PN}_{\rm H}(1/4) \simeq 0.928 R^{\rm Schw}_{\rm H}, \end{aligned} \tag{2.39}$$

where we recall $R^{\rm Schw}_{\rm ISCO} = 6GM/c^2$, $R^{\rm Schw}_{\rm LR} = 3GM/c^2$, and $R^{\rm Schw}_{\rm H} = 2GM/c^2$.

Lastly, we deal with the link between the effective canonical coordinates $(\mathbf{Q}_e, \mathbf{P}_e)$ and their ADM counterparts $(\mathbf{Q}, \mathbf{P})$. As originally proved in Ref. [140], they are related by a canonical transformation; below we revisit its 2PN derivation, in view of its importance for the extension of the EOB approach at higher PN orders. Henceforth, both the effective and the ADM coordinates will be considered in their rescaled form, as per Eqs. (2.2), with the same lowercase letter notation to signal the rescaling.

The general procedure consists in looking for a generating function $G(\mathbf{q}, \mathbf{p}_e)$ such that

$$G(\mathbf{q}, \mathbf{p}_e) = (\mathbf{q} \cdot \mathbf{p}_e) + \bar{G}(\mathbf{q}, \mathbf{p}_e), \qquad \bar{G}(\mathbf{q}, \mathbf{p}_e) \equiv \sum_{n=1}^{+\infty} \frac{1}{c^{2n}} G_{n\rm PN}(\mathbf{q}, \mathbf{p}_e), \tag{2.40}$$

$$q^i_e = q^i + \frac{\partial \bar{G}(\mathbf{q}, \mathbf{p}_e)}{\partial p^i_e}, \qquad p^i_e = p^i - \frac{\partial \bar{G}(\mathbf{q}, \mathbf{p}_e)}{\partial q^i}. \tag{2.41}$$

For its determination at 2PN, we come back to Eq. (2.31) and insert therein $\mathcal{E}^{\rm nr}_{\rm real}/\mu = \hat{H}^{\rm nr}(\mathbf{q}, \mathbf{p})$, in its 2PN form given by Eqs. (2.4)-(2.6), and $\mathcal{E}^{\rm nr}_{\rm eff}/\mu = \hat{H}_{\rm eff}(\mathbf{q}_e, \mathbf{p}_e) - c^2$, where

$$\hat{H}_{\rm eff}(\mathbf{q}_e, \mathbf{p}_e) = c^2 \sqrt{A(u) \left[1 + \frac{\mathbf{p}^2_e}{c^2} + \left(\frac{A(u)}{D(u)} - 1 \right) \frac{(\mathbf{n}_e \cdot \mathbf{p}_e)^2}{c^2} \right]} \tag{2.42}$$

is the μ-rescaled version of Eq. (2.36), here written in rescaled effective Cartesian coordinates, with $q_e \equiv |\mathbf{q}_e|$, $\mathbf{n}_e \equiv \mathbf{q}_e/q_e$, and $u \equiv 1/(c^2 q_e)$. In this Hamiltonian we use the generating function relations (2.41) in iterated form, namely

$$\begin{aligned} q^i_e &= q^i + \frac{\partial \bar{G}(\mathbf{q}, \mathbf{p})}{\partial p^i} - \frac{\partial \bar{G}(\mathbf{q}, \mathbf{p})}{\partial q^a} \frac{\partial^2 \bar{G}(\mathbf{q}, \mathbf{p})}{\partial p^a \partial p^i} + \mathcal{O}(1/c^6), \\ p^i_e &= p^i - \frac{\partial \bar{G}(\mathbf{q}, \mathbf{p})}{\partial q^i} + \frac{\partial \bar{G}(\mathbf{q}, \mathbf{p})}{\partial q^a} \frac{\partial^2 \bar{G}(\mathbf{q}, \mathbf{p})}{\partial p^a \partial q^i} + \mathcal{O}(1/c^6), \end{aligned} \tag{2.43}$$

considering that with each $\bar{G}$ comes at least a factor $1/c^2$. At this point, both sides of our energy map are expressed in rescaled ADM coordinates. Its Taylor expansion in $1/c$ yields a series of differential equations for the PN coefficients of $\bar{G}$; more specifically, from the leading order differential equation we can

compute $G_{1\mathrm{PN}}(\mathbf{q},\mathbf{p})$ and, once it determined, we can plug it in the next one and solve for $G_{2\mathrm{PN}}(\mathbf{q},\mathbf{p})$. This procedure is greatly simplified by the fact that, given the structure of such differential equations, we can write in advance

$$G_{1\mathrm{PN}}(\mathbf{q},\mathbf{p}_e) = (\mathbf{q}\cdot\mathbf{p}_e)\left[c_{11}\mathbf{p}_e^2 + \frac{c_{12}}{q}\right], \tag{2.44}$$

$$G_{2\mathrm{PN}}(\mathbf{q},\mathbf{p}_e) = (\mathbf{q}\cdot\mathbf{p}_e)\left\{c_{21}\mathbf{p}_e^4 + \frac{1}{q}\left[c_{22}\mathbf{p}_e^2 + c_{23}(\mathbf{n}\cdot\mathbf{p}_e)^2\right] + \frac{c_{24}}{q^2}\right\}, \tag{2.45}$$

and recast them in a set of algebraic relations to solve for the mass dependent coefficients c_{mn}. The result is

$$c_{11} = -\frac{\nu}{2}, \qquad c_{12} = 1 + \frac{\nu}{2}, \tag{2.46}$$

for $G_{1\mathrm{PN}}$ and

$$\begin{aligned} c_{21} &= \frac{\nu}{8} + \frac{3\nu^2}{8}, \qquad c_{22} = \frac{2\nu}{8} - \frac{5\nu^2}{8}, \qquad c_{23} = \nu + \frac{3\nu^2}{8}, \\ c_{24} &= \frac{1}{4} - \frac{7\nu}{4} + \frac{\nu^2}{4}, \end{aligned} \tag{2.47}$$

for $G_{2\mathrm{PN}}$. Once inserted in Eq. (2.43), the 2PN generating function we just found completely determines the 2PN canonical transformation we were after; for the explicit result see Eqs. (6.22) and (6.23) of Ref. [140].[9]

Remarkably, it is possible to carry out the computation of the generating function (2.40) also *before* the parameters describing the effective metric and the energy map (2.31) have been determined. In this case the procedure detailed above fixes them to the same values found by matching the two Delaunay Hamiltonians, and therefore it constitutes a full-fledged alternative implementation of the EOB method. As we will see in the next sections, this route has been instrumental to define the EOB Hamiltonian at higher PN orders.

2.1.2 EOB Hamiltonian at 3PN

The 3PN extension of the reduced ADM Hamiltonian (2.3) has been computed by Damour, Jaranowski & Schäfer in Ref. [72], with some associated regularization ambiguities that have been finally fixed by the same authors in Ref. [73], via dimensional regularization. With the notation of Eq. (2.3), the resulting $1/c^6$ Hamiltonian coefficient reads

$$\begin{aligned} \hat{H}^{\mathrm{nr}}_{3\mathrm{PN}}(\mathbf{q},\mathbf{p}) = &-\frac{5 - 35\nu + 70\nu^2 - 35\nu^3}{128}\mathbf{p}^8 - \frac{1}{16q}\big[(7 - 42\nu + 53\nu^2 \\ &+ 5\nu^3)\mathbf{p}^6 - (2 - 3\nu)\nu^2(\mathbf{n}\cdot\mathbf{p})^2\mathbf{p}^4 - 3(1-\nu)\nu^2(\mathbf{n}\cdot\mathbf{p})^4\mathbf{p}^2 + 5\nu^3(\mathbf{n}\cdot\mathbf{p})^6\big] \end{aligned}$$

[9] Here the authors denote the rescaled EOB coordinates as $(\mathbf{q}',\mathbf{p}')$ instead of $(\mathbf{q}_e,\mathbf{p}_e)$.

$$
\begin{aligned}
&- \frac{1}{16q^2}\Big[(27-136\nu-109\nu^2)\mathbf{p}^2-(17+30\nu)\nu(\mathbf{n}\cdot\mathbf{p})^2\mathbf{p}^2 \\
&- \frac{4}{3}(5+43\nu)\nu(\mathbf{n}\cdot\mathbf{p})^4\Big] - \frac{1}{8q^3}\Big\{\Big[25-\Big(\frac{\pi^2}{8}-\frac{335}{6}\Big)\nu+23\nu^2\Big]\mathbf{p}^2 \\
&+ \Big(\frac{85}{2}+\frac{3\pi^2}{8}+14\nu\Big)\nu(\mathbf{n}\cdot\mathbf{p})^2\Big\} + \frac{1}{8q^4}\Big[1+\Big(\frac{218}{3}-\frac{21\pi^2}{4}\Big)\nu\Big]. \qquad (2.48)
\end{aligned}
$$

The corresponding EOB Hamiltonian has been derived in Ref. [142] by means of the generating function method we explored at the end of the previous section. There is however an important difference with respect to the 2PN order. In general, the number of equations we have to solve to establish a proper mapping between the real and the effective dynamics, at a given PN order, is determined by the number of combinations of the scalars $\mathbf{p}^2, (\mathbf{n}\cdot\mathbf{p})^2, 1/q$ (and their powers) in the starting ADM Hamiltonian at that PN order. In the present 3PN case, the Hamiltonian (2.48) has eleven combinations of this kind, so that a direct 3PN generalization of what we did at 2PN would yield eleven new equations to satisfy. However the additional free parameters we have at 3PN are:

(i) a_4 and d_3, in the 3PN order expansions of the potentials (2.15) and (2.29), respectively;

(ii) α_3, in the 3PN energy map (2.26);

(iii) the seven parameters $(c_{31}, ..., c_{37})$ in the 3PN term $G_{3\mathrm{PN}}(\mathbf{q}, \mathbf{p}_e)$ of Eq. (2.40), whose structure can be specified in advance, just like at the previous orders, in the form

$$
\begin{aligned}
G_{3\mathrm{PN}}(\mathbf{q},\mathbf{p}_e) = (\mathbf{q}\cdot\mathbf{p}_e)\Big\{&c_{31}\mathbf{p}_e^6 + \frac{1}{q}\big[c_{32}\mathbf{p}_e^4 + c_{33}\mathbf{p}_e^2(\mathbf{n}\cdot\mathbf{p}_e)^2 \\
&+ c_{34}(\mathbf{n}\cdot\mathbf{p}_e)^4\big] + \frac{1}{q^2}\big[c_{35}\mathbf{p}_e^2 + c_{36}(\mathbf{n}\cdot\mathbf{p}_e)^2\big] \\
&+ \frac{c_{37}}{q^3}\Big\}. \qquad (2.49)
\end{aligned}
$$

Consequently, we would have a system of eleven equations but just ten free parameters to solve them, a clear indication of the fact that the effective dynamics is being constrained too much.

One possible solution would be to relax the 1PN constraint $b_1 = 2$, or equivalently $d_1 = 0$, as explored in Appendix A of Ref. [142], but it would result in an unpleasant mixing of perturbative orders (the 1PN parameter d_1 would have to be determined together with the 3PN parameters) with no follow-up generalization to higher PN orders. The main proposal of Ref. [142] is, instead, to stop assuming that the motion of the μ-particle in the effective

metric is geodesic. Without this assumption, in fact, the Hamilton-Jacobi equation (2.17) we use to derive the effective Hamiltonian becomes

$$0 = \mu^2 c^2 + g^{\mu\nu}_{\rm eff}(x^\lambda_{\rm eff}) p^{\rm eff}_\mu p^{\rm eff}_\nu + Q_4^{\mu\nu\rho\sigma}(x^\lambda_{\rm eff}) p^{\rm eff}_\mu p^{\rm eff}_\nu p^{\rm eff}_\rho p^{\rm eff}_\sigma + \mathcal{O}(p^6), \tag{2.50}$$

namely it acquires additional non-geodesic terms, at least quartic in the momenta. The leading quartic deviation from the geodesic case, the only one we can have at the 3PN level, is generally described by a tensor $Q_4^{\mu\nu\rho\sigma}(x^\lambda_{\rm eff})$ which remains essentially undetermined. Nevertheless, considering that $0 = \mu^2 c^2 + g^{\mu\nu}_{\rm eff}(x^\lambda_{\rm eff}) p^{\rm eff}_\mu p^{\rm eff}_\nu$ holds in first approximation, we can restrict all the non-geodesic terms in Eq. (2.50) to be purely spatial, relevantly with no $p^{\rm eff}_0 = \mathcal{E}_{\rm eff}$. Therefore, we can rewrite the Hamilton-Jacobi equation as[10]

$$0 = \mu^2 c^2 + g^{\mu\nu}_{\rm eff}(x^\lambda_{\rm eff}) p^{\rm eff}_\mu p^{\rm eff}_\nu + \mu^2 Q(\mathbf{q}_e, \mathbf{p}_e), \tag{2.51}$$

where $Q(\mathbf{q}_e, \mathbf{p}_e)$ is a function of the rescaled effective coordinates, with the dimensions of a velocity squared, which formally collects all the possible non-geodesic deviations. Indeed the presence of the latter yields a modification in the effective Hamiltonian, which, now computed from Eq. (2.51), becomes

$$\hat{H}_{\rm eff}(\mathbf{q}_e, \mathbf{p}_e) = c^2 \sqrt{A(u)\left[1 + \frac{\mathbf{p}_e^2}{c^2} + \left(\frac{A(u)}{D(u)} - 1\right)\frac{(\mathbf{n}_e \cdot \mathbf{p}_e)^2}{c^2} + \frac{Q(\mathbf{q}_e, \mathbf{p}_e)}{c^2}\right]}. \tag{2.52}$$

Here, the non-geodesic corrections $Q(\mathbf{q}_e, \mathbf{p}_e)$ are given, in their leading 3PN component, by

$$Q_{\rm 3PN}(\mathbf{q}_e, \mathbf{p}_e) = \frac{u^2}{c^2}\left[z_1 \mathbf{p}_e^4 + z_2 \mathbf{p}_e^2 (\mathbf{n}_e \cdot \mathbf{p}_e)^2 + z_3 (\mathbf{n}_e \cdot \mathbf{p}_e)^4\right], \tag{2.53}$$

which is the most general scalar involving quartic combinations of the momentum $\mathbf{p}_e$, equipped with a factor u^2/c^2 for dimensional reasons. The three parameters z_n appearing in Eq. (2.53) are again free dimensionless functions of the binary masses, and indeed take part, through Eq. (2.52), in the matching with the ADM Hamiltonian: now this involves eleven equations and thirteen free parameters. To uniquely solve this system we have to make two additional assumptions. Following Ref. [142], we require $z_1 = z_2 = 0$, so that the two-body circular motion can still be mapped to a geodesic effective dynamics; in fact, the residual term in $Q_{\rm 3PN}$ is then proportional to $(\mathbf{n}_e \cdot \mathbf{p}_e) = p^{\rm eff}_r$, which vanishes when the motion is circular. The unique solution that follows is characterized by the parameters[11]

$$\begin{aligned} &a_4 = \left(\frac{93}{3} - \frac{41\pi^2}{32}\right)\nu, \qquad d_3 = 2(3\nu - 26)\nu, \qquad \alpha_3 = 0, \\ &z_3 = 2(4 - 3\nu)\nu, \end{aligned} \tag{2.54}$$

[10] To avoid confusion, we specify that the four-vectors $x^\mu_{\rm eff}$ and $p^{\rm eff}_\mu$ are never to be intended in rescaled form. Explicitly this means $x^\mu_{\rm eff} = (c\,T_{\rm eff}, \mathbf{Q}_e)$, $p^{\rm eff}_\mu = (\mathcal{E}_{\rm eff}/c, \mathbf{P}_e)$.

[11] The values of the parameters $(c_{31}, ..., c_{37})$ can be found in Eqs. (4.32) and (4.35) of Ref. [142]. Mind moreover that we have set the regularization ambiguity parameter $\omega_{\rm static}$ to zero, in compliance with what was later found in Ref. [73], using dimensional regularization.

where we notice in particular that the energy map does not receive any modification at 3PN, a result that follows regardless of the choices made in $Q_{3\mathrm{PN}}(\mathbf{q}_e, \mathbf{p}_e)$, whose final form is

$$Q_{3\mathrm{PN}}(\mathbf{q}_e, \mathbf{p}_e) = \frac{u^2}{c^2}\big[2(4-3\nu)\nu(\mathbf{n}_e \cdot \mathbf{p}_e)^4\big]. \tag{2.55}$$

Before we explore how to push the EOB description at higher PN orders, let us address a considerable issue in the 3PN EOB description we just outlined. The 3PN result for the potential $A(u)$ is

$$A_{\leq 3\mathrm{PN}}(u) = 1 - 2u + 2\nu u^3 + \left(\frac{93}{3} - \frac{41\pi^2}{32}\right)\nu u^4, \tag{2.56}$$

where in the 3PN coefficient we find the rather large number

$$\left(\frac{93}{3} - \frac{41\pi^2}{32}\right) \simeq 18.6879. \tag{2.57}$$

This implies that, for comparable-mass binaries where $\nu \simeq 1/4$, as R_{eff} gets smaller and u grows, $A_{\leq 3\mathrm{PN}}(u)$ strays away from the exact function $A(u)$ of which it is a truncated PN series. Such a problem is also confirmed by the fact that $A_{\leq 3\mathrm{PN}}(u)$ no longer has a simple zero when ν is too large, as depicted in Fig. 2.1 for $\nu = 1/4$. We lose therefore the possibility of defining an effective horizon and with it the expected continuity between the effective and the Schwarzschild motion: the resummation inherent to the EOB approach is not enough to cure the bad convergence properties of the PN series. The solution originally proposed in Ref. [73] is then to further resum the potential $A_{\leq 3\mathrm{PN}}(u)$ in Eq. (2.56) by replacing it with the *Padé approximant*

$$P^1_3[A_{\leq 3\mathrm{PN}}](u) = \frac{8 - 2\nu - (16 - 8\nu - a_4)u}{8 - 2\nu + (4\nu + a_4)\,u + 2\,(4\nu + a_4)\,u^2 + 4\left(\nu^2 + a_4\right)u^3} \tag{2.58}$$

a rational function that gives back $A_{\leq 3\mathrm{PN}}(u)$ when PN-expanded up to order u^4; more details on Padé approximants can be found in Appendix A.2. As shown in Fig. 2.1, this resummation heavily modifies the behavior in u of the potential $A_{\leq 3\mathrm{PN}}(u)$, recovering the monotonically decreasing trend of $A_{\leq 2\mathrm{PN}}(u)$ and the existence of a simple zero, which defines the effective horizon.

A similar fate awaits the potential $D(u)$, with

$$D_{\leq 3\mathrm{PN}}(u) = 1 - 6\nu u^2 + 2(3\nu - 26)\nu u^3 \tag{2.59}$$

that needs to be resummed to prevent it from going towards large and negative values, as u grows. In this case, the Padé of reference is [183]

$$P^0_3[D_{\leq 3\mathrm{PN}}](u) = \frac{1}{1 + 6\nu u^2 - 2(3\nu - 26)\nu u^3}, \tag{2.60}$$

whose effect is illustrated in Fig. 2.2.

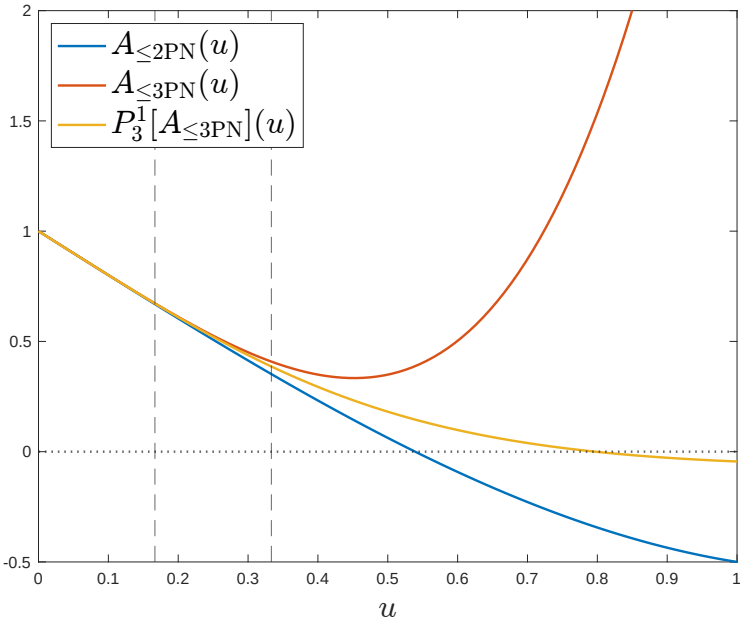

Figure 2.1: Profiles of the three approximations we considered so far for the EOB potential $A(u)$, for $\nu = 1/4$, adapted from Fig. 2 of Ref. [183]. The vertical dashed lines mark the positions of the ISCO and the light ring in Schwarzschild. The behavior of $A_{\leq 3\mathrm{PN}}(u)$ is dramatically different than $A_{\leq 2\mathrm{PN}}(u)$, in particular it has no zero as u grows. The approximant $P_3^1[A_{\leq 3\mathrm{PN}}](u)$, instead, decreases monotonically and reaches a simple zero, ensuring the continuity with the Schwarzschild case in the limit $\nu \to 0$.

2.1.3 EOB Hamiltonian at 4PN

Starting from the 4PN order, working out the two-body dynamics becomes significantly more challenging than at the previous orders. The main reason is that, as we already commented in Sec. 1.3.3 of Chapter 1, it becomes necessary to supplement the PN description of the near-zone metric with the correlations over arbitrarily large time differences induced by the tail-transported part of the radiation-reaction [102]. As a consequence, every 4PN dynamical description develops contributions that are *non-local* in time. The first complete derivation of the 4PN dynamics came only in 2014, when Damour, Jaranowski & Schäfer derived the full 4PN Hamiltonian in ADM coordinates [75]. Under the usual μ-rescaling and non-relativistic reduction, the corresponding 4PN coefficient of Eq. (2.3) reads

$$\hat{H}^{\mathrm{nr}}_{\mathrm{4PN}}(\mathbf{q},\mathbf{p}) = \hat{H}^{\mathrm{loc,c}}_{\mathrm{4PN}}(\mathbf{q},\mathbf{p}) + \hat{H}^{\mathrm{loc,log}}_{\mathrm{4PN}}(\mathbf{q},\mathbf{p}) + \hat{H}^{\mathrm{nl}}_{\mathrm{4PN}}(\mathbf{q},\mathbf{p}). \tag{2.61}$$

where:

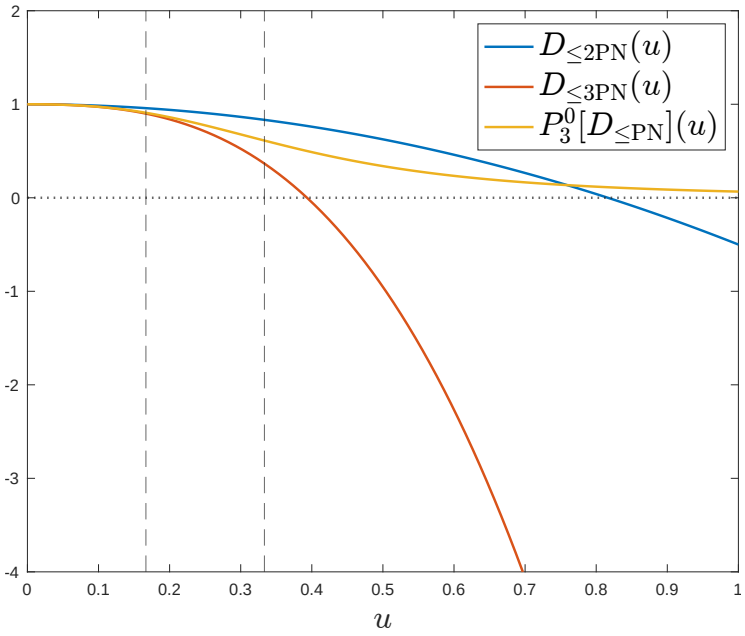

Figure 2.2: Analogue of Fig. 2.2 for the EOB potential $D(u)$, again with $\nu = 1/4$. The approximant $P^0_3[A_{\leq 3\mathrm{PN}}(u)]$ cures the tendency of $D_{\leq 3\mathrm{PN}}$ of going towards large negative values as u grows, remaining always positive.

- $\hat{H}^{\mathrm{loc,c}}_{4\mathrm{PN}}(\mathbf{q},\mathbf{p})$ is a local in time component whose profile is in continuity with the previous PN orders. See Eq. (5.13) of Ref. [75] for its (quite long) explicit expression.[12]

- $\hat{H}^{\mathrm{loc,log}}_{4\mathrm{PN}}(\mathbf{q},\mathbf{p})$ is another local in time term characterized by its proportionality to a factor $\log q$. In particular it is given by

$$\hat{H}^{\mathrm{loc,log}}_{4\mathrm{PN}}(\mathbf{q},\mathbf{p}) = \frac{2}{5}G^2 M \log\frac{q}{s}\left[(I_N)^{(3,\mathrm{red})}_{ij}(\mathbf{q},\mathbf{p})\right]^2, \tag{2.62}$$

  where s is a scale with the same dimensions of q ($1/\mathrm{velocity}^2$) that has to be introduced in the regularization of logarithmic infra-red divergences, while $(I_N)^{(3,\mathrm{red})}_{ij}$ is the order-reduced third time derivative of the Newtonian mass quadrupole of the binary system, whose original form can be found in Eq. (1.53). The result of this order-reduction procedure, which amounts to the replacement of each time derivative with the corresponding equation of motion, in this case truncated at Newtonian accuracy, reads

$$(I_N)^{(3,\mathrm{red})}_{ij}(\mathbf{q},\mathbf{p}) = -2\frac{\mu(GM)^2}{q^3}\left[4q_{\langle i}p_{j\rangle} - \frac{3}{q}(\mathbf{n}\cdot\mathbf{p})q_{\langle i}q_{j\rangle}\right]. \tag{2.63}$$

[12] Here, the variables $\mathbf{r}$ and r correspond to $\mathbf{q}$ and q in our notation.

- $\hat{H}^{\rm nl}_{\rm 4PN}(\mathbf{q},\mathbf{p})$ is the non-local in time part of the 4PN Hamiltonian and consists in a time-integral functional of the variables $\mathbf{q}$ and $\mathbf{p}$. Explicitly we have

$$\hat{H}^{\rm nl}_{\rm 4PN}(\mathbf{q},\mathbf{p}) = -\frac{G^2}{5\nu}{\rm Pf}_{T_s}\int_{-\infty}^{+\infty}\frac{d\tau}{|\tau|}(I_N)^{(3,{\rm red})}_{ij}(t)(I_N)^{(3,{\rm red})}_{ij}(t+\tau), \quad (2.64)$$

  where the integral is regularized by taking its *Hadamard partie finie* [61] ${\rm Pf}_{T_s}$, with time scale $T_s \equiv 2GMs/c$.

In view of the objective of translating this PN information in the EOB formalism, we have first to understand how to properly deal with the non-localities in time of Eq. (2.64). Ref. [189] has purposely introduced a method to recast the non-local Hamiltonian (2.64) in an ordinary local expression. The basic idea is to take advantage of the fact that $\hat{H}^{\rm nl}_{\rm 4PN}(\mathbf{q},\mathbf{p})$ is by itself a 4PN correction, so that, if we work at 4PN accuracy, we can rewrite it according to the Keplerian parametrization of the Newtonian orbital motion [198]. In particular, it is convenient to find the associated Delaunay expression in the action-angle variables $(\mathcal{L},\ell;\mathcal{G},g)$, where $\mathcal{L}$ and $\mathcal{G}$ are defined in terms of the semimajor axis a (GM-rescaled) and the eccentricity e of the orbit by

$$\mathcal{L} \equiv \sqrt{a}, \qquad \mathcal{G} \equiv \sqrt{a(1-e^2)}, \quad (2.65)$$

while their conjugate angle variable are the *mean anomaly* ℓ and the *argument of periastron* g. The Newtonian motion is then described by

$$\begin{aligned} q_x(\mathcal{L},\ell;\mathcal{G},g) &= q_{x_0}\cos g - q_{y_0}\sin g,\\ q_y(\mathcal{L},\ell;\mathcal{G},g) &= q_{x_0}\sin g - q_{y_0}\cos g, \end{aligned} \quad (2.66)$$

with

$$q_{x_0} \equiv \mathcal{L}^2\cos u_e - \mathcal{L}\sqrt{\mathcal{L}^2-\mathcal{G}^2}, \qquad q_{y_0} \equiv \mathcal{G}^2\sin u_e. \quad (2.67)$$

The *eccentric anomaly* u_e is related to ℓ and $e = \sqrt{1-\mathcal{G}^2/\mathcal{L}^2}$ by Kepler's equation,

$$u_e - e\sin u_e = \ell, \quad (2.68)$$

which admits the Bessel-Fourier expanded solution

$$u_e = \ell + \sum_{n=1}^{+\infty}\frac{2}{n}J_n(ne)\sin(n\ell), \quad (2.69)$$

in terms of the Bessel function of the first kind, J_n. This is in essence an expansion in e, where, for instance, up to order e^4, we have

$$u_e = \ell + \left(e - \frac{e^3}{8}\right)\sin\ell + \frac{e^2}{2}\sin(2\ell) + \frac{3e^3}{8}\sin(3\ell) + \frac{e^4}{3}\sin(4\ell) + \mathcal{O}(e^5). \quad (2.70)$$

Using this parametrization, the non-local Hamiltonian (2.64) becomes a functional of the type $\hat{H}^{\rm nl}_{\rm 4PN}(\mathcal{L},\mathcal{G},\ell)$, with no g dependence because of the

rotational invariance of $(I_N)_{ij}$, and an underlying expansion in powers of e, considered as a function of $\mathcal{L}$ and $\mathcal{G}$. Of course, it still involves the regularized integral in τ of the original expression (2.64). The crucial point proved in Ref. [189] is that this e-expanded Hamiltonian is canonically equivalent to (and thus can be replaced with) its ℓ-averaged value

$$\hat{\bar{H}}^{\rm nl}_{\rm 4PN}(\mathcal{L},\mathcal{G}) \equiv \frac{1}{2\pi}\int_0^{2\pi} d\ell\, \hat{H}^{\rm nl}_{\rm 4PN}(\mathcal{L},\mathcal{G},\ell), \tag{2.71}$$

which indeed is still organized in a power series in e. Since $\mathcal{L}$ and $\mathcal{G}$ are conserved quantities of the Newtonian motion, and so is e, the integral functional $\hat{\bar{H}}^{\rm nl}_{\rm 4PN}$ results in a series of simple integrals in τ over the coefficients of the underlying expansion in e. All these integrals can be readily evaluated, yielding a local, ordinary Delaunay Hamiltonian, expanded in even powers of e. For instance, up to order e^4, one finds [189][13]

$$\begin{aligned}\hat{\bar{H}}^{\rm nl}_{\rm 4PN}(\mathcal{L},\mathcal{G}) = \frac{\nu}{\mathcal{L}^{10}c^8}\Bigg\{&\frac{64}{5}\left[2\log 2+\log\left(\frac{\mathrm{e}^{\gamma_E}s}{c\mathcal{L}^3}\right)\right]+\frac{1}{5}\left[\frac{296}{3}\log 2\right.\\&+729\log 3+\frac{1256}{3}\log\left(\frac{\mathrm{e}^{\gamma_E}s}{c\mathcal{L}^3}\right)\Bigg]e^2+\Bigg[\frac{29966}{15}\log 2\\&\left.-\frac{13851}{20}\log 3+242\log\left(\frac{\mathrm{e}^{\gamma_E}s}{c\mathcal{L}^3}\right)\right]e^4\Bigg\}+\mathcal{O}(e^5),\end{aligned} \tag{2.72}$$

where the scale s enters through the partie finie operation regularizing the integrals in τ and the Euler–Mascheroni constant γ_E appears in their evaluation. We will refer to the series of operation detailed above, which reduces the non-local Hamiltonian (2.64) to the equivalent local expression (2.72), as *Delaunay time averaging*.

Let us now come to the corresponding 4PN generalization of the effective Hamiltonian. Even though we can still refer to the generic expression (2.52), we have to modify the structure of the building blocks $A(u)$, $D(u)$, and $Q(\mathbf{q}_e,\mathbf{p}_e)$, so as to take into account the presence of logarithms and time non-localities in the ADM Hamiltonian. It turns out that it is enough to consider the local versus non-local split

$$\begin{aligned}&A(u)=A^{\rm loc}(u)+A^{\rm nl}(u), \qquad D(u)=D^{\rm loc}(u)+D^{\rm nl}(u),\\&Q(\mathbf{q}_e,\mathbf{p}_e)=Q^{\rm loc}(\mathbf{q}_e,\mathbf{p}_e)+Q^{\rm nl}(\mathbf{q}_e,\mathbf{p}_e),\end{aligned} \tag{2.73}$$

where the 4PN-accurate local components are parameterized by

$$A^{\rm loc}_{\le 4\rm PN}(u) = A_{\le 3\rm PN}(u)+\left(a^{\rm loc}_{5,\rm c}+a^{\rm loc}_{5,\log}\log u\right)u^5, \tag{2.74}$$

$$D^{\rm loc}_{\le 4\rm PN}(u) = D_{\le 3\rm PN}(u)+\left(d^{\rm loc}_{4,\rm c}+d^{\rm loc}_{4,\log}\log u\right)u^4, \tag{2.75}$$

[13] To avoid confusion, in this equation Euler's number is denoted with the symbol e rather than e as in the rest of the text, which instead has here the meaning of eccentricity.

$$Q^{\rm loc}_{\le 4{\rm PN}}(\mathbf{q}_e,\mathbf{p}_e)=Q_{3{\rm PN}}(\mathbf{q}_e,\mathbf{p}_e)+\frac{1}{c^2}\Big[\big(z^{\rm loc}_{34,{\rm c}}+z^{\rm loc}_{34,\log}\log u\big)u^3(\mathbf{n}_e\cdot\mathbf{p}_e)^4 + \frac{1}{c^2}\big(z^{\rm loc}_{26,{\rm c}}+z^{\rm loc}_{26,\log}\log u\big)u^2(\mathbf{n}_e\cdot\mathbf{p}_e)^6\Big], \tag{2.76}$$

and similarly, on the non-local side,

$$A^{\rm nl}_{4{\rm PN}}(u)=\big(a^{\rm nl}_{5,{\rm c}}+a^{\rm nl}_{5,\log}\log u\big)u^5, \tag{2.77}$$

$$D^{\rm nl}_{4{\rm PN}}(u)=\big(d^{\rm nl}_{4,{\rm c}}+d^{\rm nl}_{4,\log}\log u\big)u^4, \tag{2.78}$$

$$Q^{\rm nl}_{4{\rm PN}}(\mathbf{q}_e,\mathbf{p}_e)=\frac{1}{c^2}\Big[\big(z^{\rm nl}_{34,{\rm c}}+z^{\rm nl}_{34,\log}\log u\big)u^3(\mathbf{n}_e\cdot\mathbf{p}_e)^4 + \frac{1}{c^2}\big(z^{\rm nl}_{26,{\rm c}}+z^{\rm nl}_{26,\log}\log u\big)u^2(\mathbf{n}_e\cdot\mathbf{p}_e)^6\Big]. \tag{2.79}$$

Correspondingly, the PN expansion of the effective Hamiltonian can be itself split in two parts: (i) a local piece $\hat{H}^{\rm loc}_{\rm eff}$, which only depends on the local components of A, D, and Q; (ii) a non-local 4PN piece, simply given by

$$\hat{H}^{\rm nl}_{\rm eff}=\frac{1}{2}\big[A^{\rm nl}_{4{\rm PN}}(u)-(\mathbf{n}_e\cdot\mathbf{p}_e)^2D^{\rm nl}_{4{\rm PN}}(u)+Q^{\rm nl}_{4{\rm PN}}(\mathbf{q}_e,\mathbf{p}_e)\big]. \tag{2.80}$$

Notice that we had to revise the profile of the PN series (2.15) and (2.29), by incorporating in their 4PN parameters, a_5 and d_5, the local/non-local split and a dependence on $\log u$. For example, the a_5 appearing in (2.15) is now

$$a_5=a^{\rm loc}_{5,{\rm c}}+a^{\rm nl}_{5,{\rm c}}+\big(a^{\rm loc}_{5,\log}+a^{\rm nl}_{5,\log}\big)\log u. \tag{2.81}$$

As for $Q(\mathbf{q}_e,\mathbf{p}_e)$, in continuity with the choice made for its leading term, it is written as a power series in the radial momentum $(\mathbf{n}_e\cdot\mathbf{p}_e)$, including all the dimensionally admitted combinations at least quartic in it.

Lastly, we point out that all the non-local components introduced above are, despite their name, actually local in time. Although the nomenclature may sound strange, the point is that we can match the effective Hamiltonian component $\hat{H}^{\rm nl}_{\rm eff}$, after this is rewritten in the action-angle variables $(\mathcal{L},\ell,\mathcal{G})$, ℓ-averaged as in Eq. (2.71) and finally expanded in powers of e, with the Delaunay time averaged Hamiltonian (2.72). This *uniquely* fixes the value of the 4PN "nl" coefficients. On parallel, all the 4PN local coefficients can be separately obtained by matching $\hat{H}^{\rm loc}_{\rm eff}(\mathbf{q}_e,\mathbf{p}_e)$ with the local part of the ADM Hamiltonian, given at 4PN by the sum $\hat{H}^{\rm loc,c}_{4{\rm PN}}(\mathbf{q},\mathbf{p})+\hat{H}^{\rm loc,log}_{4{\rm PN}}(\mathbf{q},\mathbf{p})$ seen in Eq. (2.61). This can be done, again, by means of the generating function method, with the energy map (2.26) stopped at the α_4 term and the 4PN component of the generating function expressed in the parametric form[14]

$$G_{4{\rm PN}}(\mathbf{q},\mathbf{p}_e)=(\mathbf{q}\cdot\mathbf{p}_e)\Big\{c^c_{4,1}\mathbf{p}_e^8+\frac{1}{q}\big[c^c_{4,2}\mathbf{p}_e^6+c^c_{4,3}\mathbf{p}_e^4(\mathbf{n}\cdot\mathbf{p}_e)^2+...\big]$$

[14] We do not show explicitly every term of $G_{4{\rm PN}}$, with the understanding that one has to include inside the braces all the dimensionally allowed combinations of $(1/q,\ \mathbf{p}_e^2,\ (\mathbf{n}\cdot\mathbf{p}_e)^2)$ and their powers, each with an associated coefficient $c_{4,n}$.

$$+ ... + \frac{c^{c}_{4,11}}{q^4}\Bigg\} + (\mathbf{q}\cdot\mathbf{p}_e)\log\left(\frac{q}{c^2}\right)\Bigg\{c^{\log}_{4,1}\mathbf{p}_e^8 + \frac{1}{q}\big[c^{\log}_{4,2}\mathbf{p}_e^6 + c^{\log}_{4,3}\mathbf{p}_e^4(\mathbf{n}\cdot\mathbf{p}_e)^2 + ...\big]$$
$$+ ... + \frac{c^{\log}_{4,11}}{q^4}\Bigg\}, \tag{2.82}$$

where we also need a logarithm-dependent part. The result is again unique and remarkably one finds $\alpha_4 = 0$, meaning that the simple energy map (2.31) is still unmodified at this order.

The final 4PN result for the EOB functions, found by assembling the local and non-local part of their separately determined coefficients, reads

$$A_{\rm 4PN}(u) = \left[\left(\frac{2275\pi^2}{512} - \frac{4237}{60} + \frac{128}{5}\gamma_E + \frac{256}{5}\log 2\right)\nu + \left(\frac{41\pi^2}{32} - \frac{221}{6}\right)\nu^2 + \frac{64}{5}\nu\log u\right]u^5, \tag{2.83}$$

$$D_{\rm 4PN}(u) = \left[\left(\frac{23761\pi^2}{1536} + \frac{533}{45} - \frac{1184}{15}\gamma_E + \frac{6496}{15}\log 2 - \frac{2916}{5}\log 3\right)\nu - \left(\frac{123\pi^2}{16} - 260\right)\nu^2 - \frac{592}{15}\nu\log u\right]u^4, \tag{2.84}$$

$$Q_{\rm 4PN}(\mathbf{q}_e,\mathbf{p}_e) = \frac{1}{c^2}\Bigg\{\Bigg[-\left(\frac{5308}{15} - \frac{496256}{45}\log 2 - \frac{33048}{5}\log 3\right)\nu - 83\nu^2 + 10\nu^3\Bigg]u^3(\mathbf{n}_e\cdot\mathbf{p}_e)^4 - \frac{1}{c^2}\Bigg[\left(\frac{827}{3} + \frac{2358912}{25}\log 2 - \frac{1399437}{50}\log 3 - \frac{390625}{18}\log 5\right)\nu + \frac{27}{5}\nu^2 - 6\nu^3\Bigg]u^2(\mathbf{n}_e\cdot\mathbf{p}_e)^6\Bigg\}. \tag{2.85}$$

We see that the regularization scale s has disappeared from the final results, even tough, as shown in Ref. [189], it is present in the individual local and non-local pieces of a_5 and d_4: this amounts to a non-trivial consistency check. Moreover, we notice that the function $Q_{\rm 4PN}(\mathbf{q}_e,\mathbf{p}_e)$ does not develop any $\log u$ dependence, which a priori could not be excluded.

2.1.4 EOB conservative dynamics beyond the 4PN order

The PN knowledge of the two-body conservative dynamics does not go beyond the 4PN order, with only partial results obtained at the 5PN level [85,199]. In this case, the EOB formalism has been used in a series of works [190–193] as a receptacle for collecting and organizing complementary dynamical information derived within different perturbative schemes beside the PN one: MPM results

for the non local contributions, $\mathcal{O}(\nu)$ information from gravitational self-force, and post-Minkowskian (PM) results for the scattering angle. Without entering too much into the quite intricate details of this machinery, we present here below the main steps of its implementation, which has ultimately pushed the EOB dynamical description up to the 6PN order, modulo some undetermined coefficients in the effective Hamiltonian.

(i) Using the results for the hereditary pieces of the radiation-reaction, coming from the PN-matched MPM formalism of Sec. 1.3, the non-local Hamiltonian is completely determined up to the 6PN order.

(ii) With a 2PN generalization of the Delaunay averaging procedure, outlined at Newtonian accuracy in the previous section, the information encoded in the 6PN non-local Hamiltonian is translated into the knowledge of the 6PN non-local component of the effective Hamiltonian. The latter is singled out from the total effective Hamiltonian through the same local/non-local split used at the 4PN level.

(iii) In the context of gravitational self force, it is possible to compute the $\mathcal{O}(\nu)$ correction to the orbital averaged redshift invariant $\langle z_1\rangle$ [200], redefinition of the one introduce by Barack & Sago in Ref. [201]. Once such a correction, usually denoted as $\langle \delta z_1\rangle$, is expanded in powers of the eccentricity, it turns out to contain all the information needed to fix the total (local+non-local) $\mathcal{O}(\nu)$ component of, in principle, each coefficient in the PN series of the EOB potentials, Q included.

(iv) Subtracting the result of point (i) from the one of point (iii), the local $\mathcal{O}(\nu)$ component of the EOB potential coefficients is determined. Beyond the 4PN order, the local components more than linear in ν remain still unknown at this point.

(v) In Ref. [202] it has been found that the coefficients in the PM expansion of the scattering angle $\chi(\mathcal{E}_{\rm eff}, j_{\rm eff})$ in the effective dynamics have a specific dependence on ν; see e.g. Sec. IX of Ref. [191]. By exploiting the latter it is ultimately possible to compute the vast majority of the missing components, $O(\nu^2)$ and beyond, of the coefficients in the EOB potentials.

At 5PN accuracy, the resulting values for the EOB potential parameters are separately listed in their non-local and local parts respectively in Table IV and Table VII of Ref. [191]. For instance, at the level of the $A(u)$ potential, with local and non-local parts combined, we have

$$A_{\rm 5PN}(u) = \big(a_{6,\rm c} + a_{6,\log}\log u\big)u^6, \tag{2.86}$$

with

$$a_{6,\rm c} = \nu\bigg[-\frac{1066621}{1575} + \frac{246367\pi^2}{3072} - \frac{14008}{105}\gamma_E - \frac{31736}{105}\ln 2 + \frac{243}{7}\ln 3$$

$$+\left(\frac{64}{5}-\frac{288}{5}\gamma_E+\frac{928}{35}\ln 2-\frac{972}{7}\ln 3+a_{6,\mathrm{c}}^{\nu^2}\right)\nu+4\nu^2\Bigg], \tag{2.87}$$

$$a_{6,\log}=-\frac{7004}{105}\nu-\frac{144}{5}\nu^2. \tag{2.88}$$

Here $a_{6,\mathrm{c}}^{\nu^2}$ is a missing numerical parameter in the $\mathcal{O}(\nu^2)$ component of $a_{6,\mathrm{c}}$, specifically coming from its local part. This and another similar parameter $d_{5,\mathrm{c}}^{\nu^2}$ in the local part of $D_{5\mathrm{PN}}(u)$ are the only two 5PN components of the EOB Hamiltonian that are left undetermined by the procedure sketched above. Correspondingly, at the 6PN order, we just have four missing numerical parameters: $a_{7,\mathrm{c}}^{\nu^2}$ and $a_{7,\mathrm{c}}^{\nu^3}$ in $A_{6PN}(u)$, $d_{6,\mathrm{c}}^{\nu^2}$ in $D_{6PN}(u)$, and $z_{54}^{\nu^2}$ in the local part of $Q_{6\mathrm{PN}}(\mathbf{q}_e,\mathbf{p}_e)$ proportional to $u^5(\mathbf{n}_e\cdot\mathbf{p}_e)^4$. All the other 6PN parameters are uniquely determined and can be found in Tables VI and X of Ref. [192].

If this represents the state-of-the-art knowledge of the EOB conservative dynamics (and of the two body motion in general), only part of this information is effectively implemented in EOB waveform models. Examining the case of `TEOBResumS`, and more in particular of its non-spinning sector, the EOB effective Hamiltonian it employs has the EOB potentials $D(u)$ and $Q(\mathbf{q}_e,\mathbf{p}_e)$ stopped at the 3PN order, with $Q(\mathbf{q}_e,\mathbf{p}_e)$ containing only its leading contribution (2.55), and $D(u)$ included in the resummed Padé form (2.60). As for the potential $A(u)$, the model incorporates it at 5PN accuracy, specifically through the Padé approximant $P_5^1[A_{\leq 5\mathrm{PN}}](u)$,[15] direct generalization of the 3PN approximant (2.58) discussed in Sec. 2.1.2. However, the 5PN contribution (2.86) is included considering the parameter $a_{6,\mathrm{c}}$ therein as a free ν-dependent tunable parameter, which is then fixed by minimizing the dephasing at merger between waveform model and numerical relativity simulations [203]. The reason for this is in part chronological, since the logarithmic contribution $a_{6,\log}$ was made available already in Ref. [189], in Sec. IXA, while the analytical result for $a_{6,\mathrm{c}}$ only came with Ref. [191]. On the other hand, the recent work [157] assessed the impact of including in `TEOBResumS` the extra analytical information of Eq. (2.87), along with higher order terms in the other EOB potentials, and showed that the numerically fitted expression for $a_{6,\mathrm{c}}$ has better performances than its analytical counterpart.

2.2 Radiation reaction and inspiral-plunge waveform in the EOB approach

In the previous section we have been concerned with the EOB prescription for the conservative dynamics of non-spinning compact binaries. Summing up, we saw that this part of the dynamics can be fully encoded in a μ-rescaled

[15] When computing log-dependent Padé approximant like this one, the $\log u$ are treated as numerical constants.

EOB Hamiltonian given by

$$\hat{H}_{\rm EOB} = \frac{c^2}{\nu}\sqrt{1+2\nu\left(\frac{\hat{H}_{\rm eff}}{c^2}-1\right)}, \tag{2.89}$$

$$\hat{H}_{\rm eff} = c^2\sqrt{\frac{p_{r_*}^2}{c^2}+A(u)\left[1+p_\varphi^2u^2c^2+\frac{Q(u,p_{r_*})}{c^2}\right]}, \tag{2.90}$$

which we have conveniently rewritten here in rescaled phase-space variables, associated to the polar coordinates in the plane $\theta_{\rm eff} = \pi/2$. In particular we consider $r \equiv R_{\rm eff}/GM = c^2/u$, $\varphi \equiv \varphi_{\rm eff}$, $p_r \equiv P_{R_{\rm eff}}/\mu.$, and $p_\varphi \equiv P_{\varphi_{\rm eff}}/(\mu GM)$. Moreover, the radial momentum p_r has been replaced with $p_{r_*} = A/D^{1/2}\,p_r$, the momentum conjugate to the tortoise radial coordinate $r_* \equiv \int dr\,(D^{1/2}/A)$, as it is often done in analytical and numerical work to bypass the diverging behavior of $p_r(r)$ for $r \to 0$.

Adopting this notation, we now want to discuss how to complete the EOB dynamics with dissipative effects, as they are induced by the emission of gravitational radiation at infinity during the pre-merger part of the CBC evolution. To do so, we will see that we also need to specify the contextual EOB waveform model for the inspiral and plunge phases. More precisely, in this section we will address such topics in the specific context of *circularized binaries*, whose inspiral and, for the most part, plunge are modeled after a sequence of circular orbits, shrinking adiabatically up to the last part of the plunge. This *quasi-circular* assumption is motivated by the long-known fact that inspiralling binaries are very efficient in circulating through the emission of GWs [204], so much that, when isolated, they are expected to have become practically circular, irrespective of their initial eccentricity, by the time their orbital frequency has increased enough to allow the detection of the associated GW signal. In Chapter 3 we will have the chance to comment on the limits of this assumption and explore the strategies that can be used to extend `TEOBResumS` beyond its borders, finally coming to the main original contribution of this Thesis.

Considering the Hamiltonian nature of the EOB approach, the EOB dynamics is indeed determined by solving Hamilton's equations, relative to $\hat{H}_{\rm EOB}$, for the variables $(r, \varphi, p_{r_*}, p_\varphi)$ we selected to describe the motion. The basic strategy to include dissipative effects in the dynamics is then to equip such Hamilton's equations with a *radiation-reaction force* $\boldsymbol{\mathcal{F}}$ of components $\mathcal{F}_r$ and $\mathcal{F}_\varphi$, specifically added in the evolution equations of the momenta p_{r_*} and p_φ, respectively. More explicitly, the general EOB equations of motion are

$$\frac{dr}{dt} = \frac{A}{\sqrt{D}}\frac{\partial \hat{H}_{\rm EOB}}{\partial r_*}, \tag{2.91}$$

$$\frac{d\varphi}{dt} = \frac{\partial \hat{H}_{\rm EOB}}{\partial \varphi} \equiv \Omega, \tag{2.92}$$

$$\frac{dp_{r_*}}{dt} = \frac{A}{\sqrt{D}}\left(\hat{\mathcal{F}}_r - \frac{\partial \hat{H}_{\rm EOB}}{\partial r}\right), \tag{2.93}$$

$$\frac{dp_\varphi}{dt} = \hat{\mathcal{F}}_\varphi, \tag{2.94}$$

where $\hat{\mathcal{F}}_{\varphi,r} \equiv \mathcal{F}_{\varphi,r}/\nu$ and $t \equiv T_{\rm eff}/(GM)$. In the quasi-circular case, we actually need to include just $\hat{\mathcal{F}}_\varphi$, with $\hat{\mathcal{F}}_r$ either set to 0, as in `TEOBResumS-GIOTTO` [154, 156], the native quasi-circular branch of `TEOBResumS`, or expressed in terms of $\hat{\mathcal{F}}_\varphi$ as in the quasi-circular model `SEOBNRv4HM` [150, 152].[16]

The computation of PN-expanded results for the radiation-reaction force $\boldsymbol{\mathcal{F}}$ has been the subject of several works using different approaches, see Ref. [205] and references therein. Since the initial development of the EOB formalism, it was understood that these results could not be included in the equations of motion in their original Taylor-expanded form, but they needed some suitable resummation. Ref. [116] in particular, shortly before the birth of the EOB approach, proposed a resummation technique for $\hat{\mathcal{F}}_\varphi$ that was based on a parameter-dependent Padé approximant, building upon the test-mass limit case $\nu \to 0$; this technique was then extensively used to model the radiation-reaction force in early-stage EOB models [141, 206–210]. Nevertheless, the resummation method adopted in modern EOB models, `TEOBResumS` included, builds upon a different, parameter-free procedure, proposed in Refs. [211, 212] and refined in Ref. [213]. In this more sophisticated paradigm, the radiation-reaction force $\hat{\mathcal{F}}_\varphi$ is modeled after the resummed (quasi-circular) prescription for the spherical modes $h_{\ell m}$ of the inspiral-plunge (hereafter *insplunge*) waveform, which was laid down in those same works. Let us first specify the link between the radiation-reaction force and the spherical modes of the waveform, which we recall have been defined in Eq. (1.173). The radiation-reaction force components $(\mathcal{F}_r, \mathcal{F}_\varphi)$ are related, via Eqs. (2.91)-(2.94), to the system loss of energy ($\dot{E}_{\rm S}$) and angular momentum ($\dot{J}_{\rm S}$); we have in particular

$$\dot{E}_{\rm S} \equiv \frac{d\hat{H}_{\rm EOB}}{dt} = \dot{r}\hat{\mathcal{F}}_r + \Omega\hat{\mathcal{F}}_\varphi, \tag{2.95}$$

$$\dot{J}_{\rm S} \equiv \frac{dp_\varphi}{dt} = \hat{\mathcal{F}}_\varphi, \tag{2.96}$$

here in rescaled form. These, in turn, are connected to the energy and angular momentum fluxes at infinity, $\dot{E}$ and $\dot{J}$, by two balance equations, which read [205]

$$\dot{r}\hat{\mathcal{F}}_r + \Omega\hat{\mathcal{F}}_\varphi + \dot{E}_{\rm Schott} + \dot{E} = 0, \tag{2.97}$$

[16] In particular `SEOBNRv4HM` prescribes

$$\hat{\mathcal{F}}_r = \frac{p_r}{p_\varphi}\hat{\mathcal{F}}_\varphi.$$

$$\hat{\mathcal{F}}_\varphi + \dot{J} = 0, \tag{2.98}$$

where $\dot{E}_{\rm Schott}$ is the Schott contribution to the energy loss of the system $\dot{E}_{\rm S}$, which cannot be directly identified with $\dot{E}$ due to the interactions with the local field. In general there is an additional Schott contribution $\dot{J}_{\rm Schott}$ also in Eq. (2.98), but in Sec. II of Ref. [205] it has been shown that such a term can be always set to zero. Focusing on the quasi-circular case, thanks to the expression (1.178) of $\dot{J}$ in terms of the spherical modes $h_{\ell m}$, we can write the φ-component of the radiation-reaction force as

$$\hat{\mathcal{F}}_\varphi = -\dot{J} = \frac{1}{16\pi} \sum_{\ell=2}^{\ell_{\rm max}} \sum_{m=-\ell}^{\ell} m\, \Im\big(\dot{h}_{\ell m} h^*_{\ell m}\big), \tag{2.99}$$

with $\ell_{\rm max}$ determined by the desired PN accuracy, considering the powers of c in Eqs. (1.175)-(1.176).

Let us now clarify the resummation prescription used in `TEOBResumSGIOTTO` for the multipolar insplunge waveform. Under the quasi-circular approximation, the PN Taylor-expanded results for the modes $h_{\ell m}$, which stem from the PN-matched MPM formalism we explored in the previous Chapter, can be written in the form of polynomials (modulo some logarithmic terms) of the PN-counting frequency parameter $x \equiv (\Omega/c^3)^{2/3}$ [182].[17] This is the only dynamical variable required, besides φ, to model the waveform in the quasi-circular case,[18] where it has the advantage of being gauge invariant (just like φ), so that there is no need to worry about the difference between harmonic and EOB coordinates. As we go towards the merger and x increases in magnitude, however, the modes $h_{\ell m}$ in their original polynomial form exhibit an unsatisfactory converging behavior. Therefore, instead of incorporating these results as they are, modern EOB models use them as input in the construction of corresponding resummed avatars, one for each spherical mode, given by the *product* of several factors:

$$h_{\ell m} = h^{(N,\epsilon)}_{\ell m} \hat{h}^{(\epsilon)}_{\ell m} \equiv h^{(N,\epsilon)}_{\ell m} \hat{S}^{(\epsilon)}_{\rm eff}\, T_{\ell m} e^{i\delta_{\ell m}} f_{\ell m} \hat{h}^{\rm NQC}_{\ell m}. \tag{2.100}$$

[17] Our definition of x has a missing GM factor with respect to the one of Ref. [182], since we are using $t = T/(GM)$ and thus $\Omega(t) = GM\Omega(T)$.

[18] More specifically, with respect of our canonical variables, in the quasi-circular limit we have $p_{r_*} = 0$, $p_\varphi = p_\varphi(u)$, obtained by solving for p_φ

$$0 = \dot{p}_{r_*} = \frac{\partial \hat{H}_{\rm EOB}}{\partial r}\big(p_{r_*} = 0, p_\varphi, u\big),$$

and $u = u(x)$, obtained by inverting perturbatively

$$x = \frac{1}{c^2}\dot{\varphi}^{2/3} = \frac{1}{c^2}\left[\frac{\partial \hat{H}_{\rm EOB}}{\partial p_\varphi}\big(p_{r_*} = 0, p_\varphi(u), u\big)\right]^{2/3},$$

which indeed also implies $p_\varphi = p_\varphi(x)$.

We outline below the definition and the rationale behind each one of these factors.

- The *Newtonian factor* $h^{(N,\epsilon)}_{\ell m}$ represents the leading order term in the PN expansion (in x) of $h_{\ell m}$. By factoring out this term, one can define a *residual PN factor* $\hat{h}^{(\epsilon)}_{\ell m}$ that is stripped off the overall constants and φ-dependence of $h_{\ell m}$, thus resulting, at this level, in a simple polynomial in x (modulo $\log x$ terms) of the type $1+\mathcal{O}(x)$. The explicit form of $h^{(N,\epsilon)}_{\ell m}$ reads

$$h^{(N,\epsilon)}_{\ell m} = \frac{GM\nu}{D_L} n^{(\epsilon)}_{\ell m} c_{\ell+\epsilon}(\nu) x^{(\ell+\epsilon)/2} Y_{\ell-\epsilon,-m}\left(\frac{\pi}{2},\varphi\right), \tag{2.101}$$

where D_L is the luminosity distance (the physical value of the radial separation R between source and observer), ϵ depends on the parity of the spherical mode and is either 0, when $\ell+m$ is even, or 1, when $\ell+m$ is odd, while for the rest

$$\begin{aligned} n^{(0)}_{\ell m} &\equiv (im)^\ell \frac{8\pi}{(2\ell+1)!!}\sqrt{\frac{(\ell+1)(\ell+2)}{\ell(\ell-1)}}, \\ n^{(1)}_{\ell m} &\equiv -i(im)^\ell \frac{16\pi}{(2\ell+1)!!}\sqrt{\frac{(2\ell+1)(\ell+2)(\ell^2-m^2)}{(2\ell-1)(\ell+1)\ell(\ell-1)}}, \end{aligned} \tag{2.102}$$

$$c_{\ell+\epsilon}(\nu) \equiv 2^{1-\ell-\epsilon}\left[\left(\sqrt{1-4\nu}+1\right)^{\ell+\epsilon-1} - \left(\sqrt{1-4\nu}-1\right)^{\ell+\epsilon-1}\right]. \tag{2.103}$$

We finally mention that it is standard to improve the behavior during the plunge of $h^{(N,\epsilon)}_{\ell m}$ by replacing the variable x therein with v^2_φ, the square of the azimuthal velocity $v_\varphi \equiv r_\omega \Omega$ defined in terms of the modified EOB radius $r_\omega \equiv r\psi^{1/3}$, where [147, 214]

$$\psi \equiv -2\left(\frac{dA}{du}\right)^{-1}\left[1+2\nu\left(\sqrt{A\left(1+p^2_\varphi u^2\right)}-1\right)\right]. \tag{2.104}$$

These quantities are such that they generalize to the comparable-mass case the Keplerian law $\Omega^2 r^3_\omega = v^2_\varphi r_\omega = 1$. In the last avatar of `TEOBResumS-GIOTTO`, however, for some subdominant spherical multipoles the replacement $x \to v^2_\varphi$ is not performed on all the powers of x in Eq. (2.101); the specific choices made in this regard are listed, e.g., in Sec. IIIC of Ref. [203].

- $\hat{S}^{(\epsilon)}_{\rm eff}$ is the so-called *effective source* and is given by

$$\begin{aligned} \hat{S}^{(0)}_{\rm eff} &\equiv \hat{H}_{\rm eff}, \\ \hat{S}^{(1)}_{\rm eff} &\equiv \frac{p_\varphi}{r_\omega v_\varphi}, \end{aligned} \tag{2.105}$$

which can be expressed in x through the relations mentioned in footnote 18. These quantities are the EOB generalizations for arbitrary ν of factors appearing in the source of the Regge-Wheeler-Zerilli equations [117, 118], from which one computes the spherical modes $h_{\ell m}$ in the test-mass limit $\nu \to 0$. By factoring out each of the two, we are actually removing a square root singularity $\propto 1/\sqrt{1-3x}$ of the test-mass limit, with the singular value $x = 1/3$ reached at the light-ring; such a singularity would otherwise cause the numerical coefficient of x^n in $\hat{h}^{(\epsilon)}_{\ell m}$ to grow as 3^n for large n.[19]

- $T_{\ell m}$ is a factor that resums an infinite series of tail-rooted logarithmic terms that enters the MPM expression of (U_L, V_L) in terms of the canonical moments (M_L, S_L), and thus the spherical modes $h_{\ell m}$ via Eqs. (1.166)-(1.167). Such terms are in particular those proportional to

$$(GM)^n \int_0^{+\infty} d\tau \, C_L^{(\ell+1+n)}(T_R - \tau) \log^n \left(\frac{c\tau}{2r_0} \right), \tag{2.106}$$

with C_L equal to either M_L or S_L, depending on the spherical multipole. In Eq. (1.163), for instance, one can easily find the pertaining terms for $n = 1, 2$ in the case of the mass quadrupole U_{ij}, which shapes the dominant mode h_{22}. The explicit definition of $T_{\ell m}$ is

$$T_{\ell m} \equiv \frac{\Gamma\big(\ell + 1 - 2i\hat{\hat{k}}\big)}{\Gamma\big(\ell + 1\big)} \, e^{\pi \hat{\hat{k}}} \, e^{2i\hat{\hat{k}} \log (2kr_0)}, \tag{2.107}$$

where $\hat{\hat{k}} \equiv GH_{\rm EOB} m\Omega$, $k \equiv m\Omega$, and r_0, the length scale introduced in the Blanchet-Damour waveform generation formalism, is fixed here to the value $r_0 = 2GM/\sqrt{e}$, so as to match test-mass limit results. Again, the original proposal of the factor (2.107), advanced in Ref. [212], is the outcome of the EOB generalization of a related test-mass waveform factor, first singled out in Ref. [211]. Concerning the utility of factoring out $T_{\ell m}$, it is done to absorb powers of $m\pi$ that would otherwise end up in the coefficients of the PN-expanded quantity $\hat{h}^{(\epsilon)}_{\ell m}$, making them bigger and thus spoiling its convergence properties towards merger.

- The factor $e^{i\delta_{\ell m}}$ collects all the subleading *phase* corrections not captured by $T_{\ell m}$, with $\delta_{\ell m}$ defined as the argument of the PN-expanded

[19] More in general, if $f(x) = \sum_n c_n x^n$ has a radius of convergence x_s, corresponding to the closest singularity to $x = 0$ of $f(x)$, then

$$\lim_{n\to\infty} \left| \frac{c_{n+1}}{c_n} \right| = \frac{1}{x_s}.$$

complex ratio

$$T_{\rm PN}\left[\frac{\hat{h}^{(\epsilon)}_{\ell m}}{\hat{S}^{(\epsilon)}_{\rm eff}\,T_{\ell m}}\right], \tag{2.108}$$

where we introduced the operator $T_{\rm PN}$, which applies the required PN expansion, in this case a Taylor-series in x; mind however that the quantity $\delta_{\ell m}$ is usually rewritten in terms of the variable $y \equiv (\hat{H}_{\rm EOB}\Omega/c^3)^{2/3}$ [211]. As for the PN orders considered, `TEOBResumS-GIOTTO` employs a 3.5PN-accurate expression for $\delta_{\ell m}$, with the addition of higher order test-mass contributions, up to the 4.5PN order. For the majority of the spherical modes $\delta_{\ell m}$ is further resummed through Padé approximants, selected individually, spherical mode by spherical mode, to improve the EOB/NR frequency agreement before merger [154].

- The factor $f_{\ell m}$, on the other hand, collects all the residual *amplitude* corrections and is defined as

$$f_{\ell m} \equiv T_{\rm PN}\left[\frac{\left|\hat{h}^{(\epsilon)}_{\ell m}\right|}{\hat{S}^{(\epsilon)}_{\rm eff}\,|T_{\ell m}|}\right], \tag{2.109}$$

where, recalling Eq. (2.107) and using the properties of the Γ function, we have

$$|T_{\ell m}|^2 = \frac{1}{(\ell!)^2}\frac{4\pi\hat{\hat{k}}}{1-e^{-4\pi\hat{\hat{k}}}}\prod_{n=1}^{\ell}\left[n^2+(2\hat{\hat{k}})^2\right]. \tag{2.110}$$

Among the various terms appearing in the resulting expression of $f_{\ell m}$, which is again a power series of the type $1+\mathcal{O}(x)$ with some logarithms of x, there are contributions $\propto \ell x$ that become problematically large as ℓ grows. Therefore, already in Ref. [213], it was proposed to consider the replacement

$$f_{\ell m} \to (\rho_{\ell m})^{\ell}, \qquad \rho_{\ell m} \equiv T_{\rm PN}\left[f^{1/\ell}_{\ell m}\right], \tag{2.111}$$

devised so that the quantity $\rho_{\ell m}$ does not present anymore the aforementioned ℓ-growing terms of $f_{\ell m}$. This is what is used also in `TEOBResumS-GIOTTO` where, similarly to what is done for $\delta_{\ell m}$, the generic-in-ν results for $\rho_{\ell m}$, included up to the 3PN order, are hybridized with test-mass information up to 5PN or 6PN accuracy, depending on the given spherical mode, and later Padé resummed [154]; see also Ref. [215] for an extension of this hybridization and resummation process at higher PN orders.

- The last factor, $\hat{h}^{\rm NQC}_{\ell m}$, is called *Next-to-Quasi-Circular* (NQC) factor and, as the name may suggest, it is specifically included in the waveform

to incorporate the modulating effects induced by the deviations from circularity that necessarily appear, also for quasi-circular binaries, during the last part of the plunge, right before merger. In `TEOBResumS-GIOTTO` it is given by the phenomenological expression [148]

$$\hat{h}^{\rm NQC}_{\ell m} = \left(1 + a^{\ell m}_1 n^{\ell m}_1 + a^{\ell m}_2 n^{\ell m}_2\right) e^{i\left(b^{\ell m}_1 n^{\ell m}_3 + b^{\ell m}_2 n^{\ell m}_4\right)}, \tag{2.112}$$

where $(a^{\ell m}_1, a^{\ell m}_2, b^{\ell m}_1, b^{\ell m}_2)$ are free parameters and $(n^{\ell m}_1, n^{\ell m}_2, n^{\ell m}_3, n^{\ell m}_4)$ is a basis of functions of the radial momentum and acceleration. More specifically, they read [203]

$$n^{\ell m}_1 = \left(\frac{p_{r_*}}{r\Omega}\right)^2 \quad \forall \ell, m \quad , \tag{2.113}$$

$$n^{22}_2 = \frac{\dot{p}_{r_*}}{r\Omega^2}\frac{\partial \dot{r}}{\partial p_{r_*}}, \quad n^{21}_2 = \frac{p^2_{r_*}}{r^2\Omega^{4/3}}, \quad n^{\ell\geq 3,m}_2 = n^{22}_2, \tag{2.114}$$

$$n^{\ell m}_3 = \frac{p_{r_*}}{r\Omega} \quad \forall \ell, m \quad , \tag{2.115}$$

$$n^{22}_4 = (r\Omega)p_{r_*}, \quad n^{21}_4 = n^{\ell\geq 3,m}_4 = \frac{p_{r_*}}{r\Omega^{1/3}}, \tag{2.116}$$

where their specific definitions are chosen to control as much as possible the behavior of the corresponding factor $\hat{h}^{\rm NQC}_{\ell m}$. The parameters $(a^{\ell m}_1, a^{\ell m}_2, b^{\ell m}_1, b^{\ell m}_2)$ are fixed by imposing a C^2 contact condition, at a specific ν-dependent extraction time, between the EOB and NR spherical modes, precisely at the level of their amplitude and frequency. We underline in this respect that, being $h_{\ell m}$ a complex quantity, it can be decomposed in amplitude and phase as $h_{\ell m} = A_{\ell m} e^{-i\phi_{\ell m}}$, with associated frequency $\omega_{\ell m} \equiv -\dot{\phi}_{\ell m}$. The C^2 contact condition mentioned above can thus be written as

$$A^{\rm EOB}_{\ell m}(t^{\rm EOB}_{\rm extr}) = A^{\rm NR}_{\ell m}(t^{\rm NR}_{\rm extr}), \qquad \dot{A}^{\rm EOB}_{\ell m}(t^{\rm EOB}_{\rm extr}) = \dot{A}^{\rm NR}_{\ell m}(t^{\rm NR}_{\rm extr}), \tag{2.117}$$

$$\omega^{\rm EOB}_{\ell m}(t^{\rm EOB}_{\rm extr}) = \omega^{\rm NR}_{\ell m}(t^{\rm NR}_{\rm extr}), \qquad \dot{\omega}^{\rm EOB}_{\ell m}(t^{\rm EOB}_{\rm extr}) = \dot{\omega}^{\rm NR}_{\ell m}(t^{\rm NR}_{\rm extr}), \tag{2.118}$$

where the choices for the extraction times are [203]

$$t^{\rm EOB}_{\rm extr} = t^{\rm peak}_{\Omega} - 1 + \Delta t^{\rm NR}_{\ell m}, \qquad \Delta t^{\rm NR}_{\ell m} \equiv t^{\rm peak}_{A^{\rm NR}_{\ell m}} - t^{\rm peak}_{A^{\rm NR}_{22}}; \tag{2.119}$$

$$t^{\rm NR}_{\rm extr} = t^{\rm peak}_{A^{\rm NR}_{\ell m}} + 2, \tag{2.120}$$

in general we denote as $t^{\rm peak}_X$ the instant at which every given quantity X reaches its maximum. For more details on these choices we refer the reader to Sec. IIID of Ref. [203] and references therein.

Coming back to the associated factorization of the radiation-reaction force $\hat{\mathcal{F}}_\varphi$, `TEOBResumS-GIOTTO` does not use directly Eq. (2.99), but rather

$$\hat{\mathcal{F}}_\varphi = -\frac{32}{5c^5}\nu r^4_\omega \Omega^5 \hat{f}, \tag{2.121}$$

where $\hat{f}$ is the Newton-normalized flux

$$\hat{f} \equiv \sum_{\ell=2}^{8} \sum_{m=1}^{\ell} (F_{22}^{N})^{-1} F_{\ell m}, \tag{2.122}$$

explicitly given by

$$F_{\ell m} \equiv \frac{1}{8\pi} m^2 \Omega^2 |h_{\ell m}(x)|^2, \tag{2.123}$$

$$F_{22}^{N} \equiv \frac{32}{5} x^5, \tag{2.124}$$

F_{22}^{N} being the leading Newtonian part of the dominant mode F_{22}. We notice that to obtain this form of $\hat{\mathcal{F}}_{\varphi}$ from Eq. (2.99), in addition to the required factorizations, one has to use the parity condition $h_{\ell,-m} = (-)^{\ell} h^{*}_{\ell m}$ and the circular-limit relations $\dot{h}_{\ell m} = -im\Omega h_{\ell m}$ and $h_{\ell 0} = 0$. Evidently, it is actually in Eq. (2.123) that the factorized and resummed insplunge waveform of Eq. (2.100) enters the radiation-reaction force, defining a resummation for its spherical modes $F_{\ell m}$.[20]

2.3 EOB description of merger and ringdown

To complete the discussion on the EOB approach, we have now to outline its prescription for merger and ringdown. Once again, the guiding principle is the closeness between the EOB dynamics and the test-mass motion in the Schwarzschild metric, which is recovered from it for $\nu \to 0$. The pioneering works of Davis, Ruffini, Press, Price & Tiomno [216–218] showed that, in the simple case of a test-particle plunging radially on a Schwarzschild black hole, the associated GW signal at infinity is composed by an initial quadrupolar-like part suddenly followed by exponentially dumped oscillations. The latter were interpreted in Ref. [217] as the vibrational modes, or *quasi-normal-modes* (QNMs), of the black hole perturbed by the plunging particle, which relaxes to stability with the emission of GWs. Building upon these works and the "close limit" analysis of Ref. [219], the proposal of the EOB waveform formalism is to use, up to merger, the insplunge model we discussed in the previous section, and then prescribes a sharp transition to a different waveform model, specific of the ringdown phase. This was originally implemented in the form of a linear superposition of the QNMs of the final Kerr black hole, born out of

[20] In this process, we point out that the NQC factor of the waveform is only used for the dominant quadrupolar mode F_{22}, while it is neglected in the factorization of any other spherical mode of $\hat{\mathcal{F}}_{\varphi}$. Moreover, the parameters (a_1^{22}, a_2^{22}), which end up in F_{22}, have through the latter an impact on the EOB dynamics that is used to compute them. They must therefore be determined using an iterative process, which stops when an acceptable degree of convergence is reached.

the coalescence, whose mass ($M_{\rm BH}$) and spin ($J_{\rm BH}$) can be either determined from the insplunge EOB dynamics or, more accurately, via NR fits [220].

Going into more details, let us first specify that the merger time $t_{\rm mrg}$, at which the waveform description is prescribed to sharply change, is chosen as the time where the amplitude of the quadrupolar mode h_{22} reaches its maximum. Accordingly, for each spherical mode of the waveform, we can write a *complete EOB model*, covering the whole CBC evolution, as

$$h^{\rm tot}_{\ell m}(t) = \theta(t - t_{\rm mrg}) h^{\rm insplunge}_{\ell m}(t) + \theta(t_{\rm mrg} - t) h^{\rm ringdown}_{\ell m}(t), \tag{2.125}$$

where $\theta(t)$ is Heaviside's step function, $h^{\rm insplunge}_{\ell m}(t)$ is the insplunge model given by Eq. (2.100), and $h^{\rm ringdown}_{\ell m}(t)$ is the corresponding ringdown model, that we will now proceed to illustrate.

The linear superposition of QNMs after which the ringdown signal was originally modeled reads

$$h^{\rm QNM}_{\ell m} \equiv \sum_n \left(C^+_{\ell m n} e^{-\sigma^+_{\ell n}\tau} + C^-_{\ell m n} e^{-\sigma^-_{\ell n}\tau} \right). \tag{2.126}$$

Here the index n is the overtone number and labels the different QNMs in the decomposition, starting from the fundamental one with $n = 1$. Each QNM is given in terms of two complex coefficients $C^\pm_{\ell m n}$ and two complex frequencies $\sigma^\pm_{\ell n} \equiv \alpha_{\ell n} \pm i\omega_{\ell n}$, made of a real frequency $\omega_{\ell n}$ and an inverse dumping time $\alpha_{\ell n}$. The dimensionless time parameter appearing on the exponentials of Eq. (2.126) is defined as

$$\tau \equiv \frac{c^3}{G M_{\rm BH}} (T - T^{\rm peak}_{A^{\rm NR}_{\ell m}}), \tag{2.127}$$

and counts the time passed from the instant $T^{\rm peak}_{A^{\rm NR}_{\ell m}}$, at which the amplitude $A^{\rm NR}_{\ell m}$ of the numerical waveform reaches its peak, in unit of the final black hole mass $M_{\rm BH}$.

Actually, with the test-mass analysis of Ref. [211] on the physical excitation of QNMs, it was understood that the above superposition could be simplified by setting $C^-_{\ell m n} = 0$ and retaining just the components with positive frequencies ($\sigma^+_{\ell n}$). The procedure consisted then in determining these QNM complex frequencies from (M_{BH}, J_{BH}) [221] and the coefficients $C^+_{\ell m n}$ from specific matching conditions between $h^{\rm QNM}_{\ell m}$ and the insplunge waveform, for instance by imposing that the two waveforms do coincide at a specific set of instants, selected by discretizing into equally spaced points a time interval around $t_{\rm mrg}$ [211]. However, Ref. [149] proved that, in order for Eq. (2.126) to be a faithful representation of the ringdown signal, the coefficients appearing therein should be promoted to τ-dependent functions, as a consequence of the fact that in general the QNM excitation is not yet completed at merger. This additional layer of complexity led to the proposal, in that same paper,

of an alternative approach, which is now the basis of the ringdown modeling strategy of `TEOBResumS`.

The idea is to consider a factorized ringdown waveform of the type

$$h_{\ell m}^{\rm ringdown} = e^{-\sigma_1 \tau - i\phi_{\ell m}^{\rm peak}} \bar{h}_{\ell m}(\tau), \tag{2.128}$$

where $\phi_{\ell m}^{\rm peak}$ is the value of the waveform phase at $\tau = 0$. Then, instead of deriving $\bar{h}_{\ell m}(\tau)$ from Eq. (2.126), this is replaced with a suitable parametric template. Omitting the indices (ℓ, m) for readability, this reads[21]

$$\bar{h}(\tau) = A_{\bar{h}}(\tau) e^{i\phi_{\bar{h}}(\tau)}, \tag{2.129}$$

$$A_{\bar{h}}(\tau) = \left(\frac{c_1^A}{1 + e^{-c_2^A \tau + c_3^A}} + c_4^A \right)^{\frac{1}{c_5^A}}, \tag{2.130}$$

$$\phi_{\bar{h}}(\tau) = -c_1^\phi \ln \left(\frac{1 + c_3^\phi e^{-c_2^\phi \tau} + c_4^\phi e^{-2c_2^\phi \tau}}{1 + c_3^\phi + c_4^\phi} \right), \tag{2.131}$$

given in terms of two sets of parameters, c_i^A and c_i^ϕ. However, not all of these are free: there are five constraints that ensure the correct behavior of $\bar{h}(\tau)$ for $\tau = 0$ and late times, namely

$$c_1^A = \frac{c_5^A \alpha_{21}}{c_2^A} (A_{\rm peak})^{c_5^A} e^{-c_3^A} \left(1 + e^{c_3^A}\right)^2, \tag{2.132}$$

$$c_4^A = (A_{\rm peak})^{c_5^A} - \frac{c_1^A}{1 + e^{c_3^A}}, \tag{2.133}$$

$$c_5^A = -\frac{\ddot{A}_{\rm peak}}{A_{\rm peak} \alpha_{21}^2} + \frac{c_2^A}{\alpha_{21}} \frac{e^{c_3^A} - 1}{1 + e^{c_3^A}}, \tag{2.134}$$

$$c_1^\phi = \frac{1 + c_3^\phi + c_4^\phi}{c_2^\phi (c_3^\phi + 2c_4^\phi)} (\omega_1 - M_{\rm BH} \omega_{\rm peak}), \tag{2.135}$$

$$c_2^\phi = \alpha_{21}, \tag{2.136}$$

where α_n and ω_n are the real and imaginary components of the QNM complex frequency σ_n (n being the overtone number), $\alpha_{21} \equiv \alpha_2 - \alpha_1$, and finally $(A_{\rm peak}, \omega_{\rm peak})$ are the numerically-determined amplitude and frequency of the given waveform mode at $\tau = 0$, with $\ddot{A}_{\rm peak}$ second time-derivative computed at that instant. Consequently, the free parameters that remain to be determined by fits on the numerical data are actually just $(c_2^A, c_3^A, c_3^\phi, c_4^\phi)$.

[21] We report here the updated prescription of Ref. [215], which improves the one in Ref. [203] by replacing with Eq. (2.130) the old amplitude template

$$A_{\bar{h}}(\tau) = c_1^A \tanh\left(c_2^A \tau + c_3^A\right) + c_4^A.$$

.

We conclude by noticing that the NR waveform information, incorporated (i) in $h^{\rm insplunge}_{\ell m}$ through $\hat{h}^{\rm NQC}_{\ell m}$ and (ii) in $h^{\rm ringdown}_{\ell m}$ through $\bar{h}_{\ell m}$ (here written with explicit indices ℓ and m), is enough to guarantee that the complete waveform modes (2.125) are smooth at $t = t_{\rm mrg}$, where there is the sudden shift between the insplunge and the ringdown model.

Chapter 3

Eccentricity effects in EOB waveform models

In this Chapter we finally discuss the main theme of the Thesis: how to best extend EOB models to the case of *eccentric binaries*. We refer with this term to binary systems that have escaped, at least partially, the circularization process typical of isolated binaries [204, 222], and thus still present non-negligible orbital eccentricity in their late inspiral, when the GWs they emit enter the frequency band sensitivity of our detectors. The motivation behind this line of work is essentially twofold. On the one hand, measuring eccentricity with GWs can shed light on the unknown mechanisms behind the generation of binary black holes, with valuable indications on the actual plausibility and weight of the different formation channels that have been so far proposed for their origin. If in fact isolated binary black holes, result of the evolution of isolated binary stars, are expected to efficiently circularize via GW emissions, in recent years population synthesis studies [223–230] have shown that dynamical captures in dense stellar environments, primarily globular clusters and galactic nuclei, and the Lidov-Kozai mechanism in compact triples, isolated or in dense environments like those cited above, should lead to a substantial fraction of CBCs with measurable eccentricity during their pre-merger evolution, notably with different eccentricity distributions depending on the given astrophysical scenario considered. See, e.g., the illustrative scheme in Fig. 3.1, taken from Ref. [229], that puts together the expected distributions of eccentric binaries, relative to three relevant formation scenarios, with the minimum distinguishable eccentricity for several GW detectors.

On the other hand, even if we are not interested in the astrophysical implications of eccentricity signatures in the GWs we detect, dedicated analysis [233, 234] have shown that neglecting eccentricity in GW models is likely to cause systematic errors in the inference of the other binary parameters, especially the component masses of the system. This is due to the fact that, in the presence of eccentricity, the parameter that determines the leading order

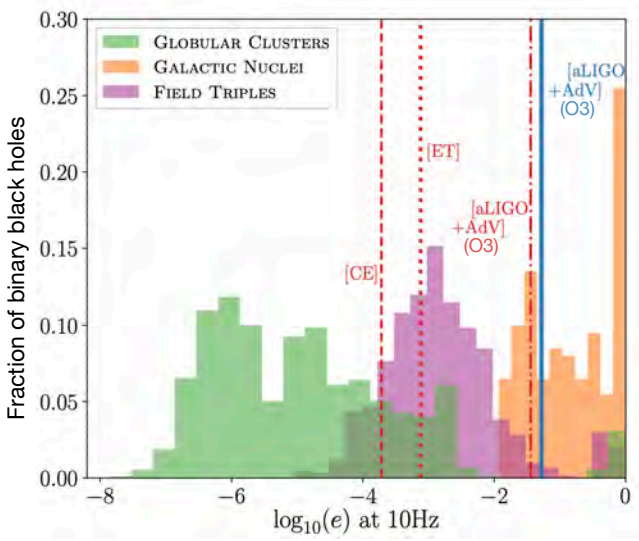

Figure 3.1: Expected fractional distributions of eccentric binary black holes for three relevant astrophysical scenarios, credits to Ref. [229]. Considering as a reference the eccentricity at an orbital frequency of 10Hz, we find in different colors (i) the globular cluster distribution of Refs. [227, 228] (green), (ii) the galactic nuclei one of Ref. [231] (orange), and (iii) the one relative to field triples (i.e. isolated three-body systems), taken from Ref. [232] (purple). The vertical lines represent the minimum detectable eccentricity, estimated in Ref. [229], for the ground-based detectors Advanced LIGO and Advanced Virgo, Einstein Telescope, and Cosmic Explorer. On these lines, different colors mark different estimation techniques: the Bayesian (blue) and the waveform overlap method (red); see Sec. III of Ref. [229] for more details on these techniques.

evolution of the GW phase, and thus is measured with the highest precision, is no longer the chirp mass

$$M_{\rm ch} \equiv \frac{(m_1 m_2)^{3/5}}{(m_1+m+2)^{1/5}}, \tag{3.1}$$

but an "eccentric chirp mass", combination of $M_{\rm ch}$ and the eccentricity e, that around a reference frequency of 10Hz can be approximately defined as [234]

$$M_{\rm ch}^{\rm ecc} \equiv M_{\rm ch}\left(1+\frac{157}{40}e_0^2\right), \tag{3.2}$$

e_0 being the eccentricity at that frequency. We have therefore a degeneracy between $M_{\rm ch}$ and e_0, similar to the well-known circular case degeneracy

between m_1 and m_2, in which the primary parameter that drives the GW phasing is simply $M_{\rm ch}$. This has been also proved to be impactful for the validity of GR tests performed on GW data, with arising systematic biases that become comparable with the statistical errors even when small eccentricities are neglected; see for instance the analysis of Refs. [235, 236].

Prompted by all this, and with the additional prospect of many future detections of eccentric stellar-mass binaries, thanks to the forthcoming space-based interferometer such as LISA [237, 238], the GW community has embarked on developing new waveform models that go beyond the quasi-circular approximation, both on the numerical [239–242] and the analytical side [243–251].Regarding EOB-based waveform models, the first eccentricity modulations have been incorporated in the circular model `SEOBNRv1` [145] in a series of works [252, 253], which ultimately led to the proposal of a new model, dubbed `SEOBNRE`. This was later improved, building upon the next generation circular model `SEOBNRv4HM` [152], with the inclusion of analytical noncircular waveform information up to the 2PN order [251], thus yielding the recent eccentric model `SEOBNRv4EHM` [153]. On the `TEOBResumS` side, noncircular corrections to the insplunge waveform have been first introduced in Ref. [254], generalizing to non-circularized orbits the quasi-circular Newtonian prefactor (2.101). This laid the foundation for the development, in several follow-up works [155, 157, 215, 255] of a new highly accurate EOB model for generic planar orbits, now referred to as `TEOBResumS-DALI`, which has also been used to analyze the GW source GW190521 [256, 257] under the hypothesis of a hyperbolic capture [258].

In this Chapter, after a brief review, in Sec. 3.1, of the crucial noncircular generalizations that define `TEOBResumS-DALI`, we will present, discuss and test some strategies to incorporate in this model, while preserving its factorization and resummation prescriptions, currently known analytical waveform results for generic planar orbits, at 2PN accuracy. More specifically, the rest of the Chapter is organized as follows. In Sec. 3.2 we review the 2PN waveform results we used as an input and explain how their information can be recasted into new 2PN noncircular waveform factors, presenting the dedicated factorization procedure. Their performance in the waveform model is probed in Sec. 3.3, by comparing the predictions of the latter against several numerical waveforms, relative to a test particle inspiralling and plunging on a Kerr black hole along eccentric orbits. This gives rise to the need of implementing additional resummation strategies, necessary to obtain noncircular corrections that are reliable *also* for large eccentricities, $e \sim 0.9$. In the same section we also perform similar test-mass analyses for a few of illustrative hyperbolic encounter dynamics. The testing process continues in Sec. 3.4, where we focus on comparable-mass binaries and provide direct phasing comparisons between numerical relativity (NR) simulations and our EOB eccentric model, complete of the new 2PN-accurate resummed factors. An analogues factorization strategy is used in Sec. 3.5 for the proposal of associated noncircular correcting

factors to include in the radiation-reaction force component $\hat{\mathcal{F}}_\varphi$; their impact is then numerically investigated in the test-mass limit. In Sec. 3.6, focusing again on the test-mass limit case, we provide waveform comparisons with the factorization scheme proposed in Ref. [251] (and used in Ref. [259]). Motivated by the results of these comparisons, in Sec. 3.7 we finally devise and test an alternative prescription for some of the noncircular waveform factors introduced in Sec. 3.2, focusing on the dominant mode $\ell = m = 2$.

We mention in closing that a big portion of the content presented in this Chapter has been originally released to the public in our series of papers [158–160].

3.1 The eccentric insplunge of `TEOBResumS-DALI`

We dedicate this section to a concise review of the noncircular generalizations that distinguish the eccentric model `TEOBResumS-DALI` from the native quasi-circular model `TEOBResumS-GIOTTO`, outlined in its non-spinning sector in the previous Chapter. We will focus in particular on the noncircular analytical prescription for the insplunge waveform factorization and, correspondingly, for the radiation-reaction force, although we mention that `TEOBResumS-DALI` also entails a new determination of the NR-informed flexibility parameters in the EOB dynamics, like the $a_{6,\mathrm{c}}$ mentioned at the end of Sec. 2.1.4,[1] and new suitable choices for the initial conditions, such that the modulations due to eccentricity of the EOB waveform are consistent with their homologues in eccentric NR simulations; for more details on these aspects see Ref. [155].

The noncircular insplunge waveform model proposed by Ref. [254] is simply obtained by performing, in the factorized quasi-circular waveform (2.100), a general redefinition of its Newtonian factor $h_{\ell m}^{(N,\epsilon)}$, i.e. of Eq. (2.101). Considering the chain of relations (1.175)-(1.176) and (1.166)-(1.167), which connects the spherical modes $h_{\ell m}$ to the STF radiative multipoles (U_L, V_L), and remembering that at Newtonian order we have

$$(U_L)_{\mathrm{Newt}} = \frac{d^\ell}{dt^\ell}(I_L)_{\mathrm{Newt}}, \qquad (V_L)_{\mathrm{Newt}} = \frac{d^\ell}{dt^\ell}(J_L)_{\mathrm{Newt}}, \tag{3.3}$$

where (I_L, J_L) are the STF multipoles of the source, the most general definition of the Newtonian factor of each $h_{\ell m}$ is[2]

$$h_{\ell m}^{(N,0)} = -\frac{2\sqrt{2}G}{D_L c^{\ell+2}(\ell!)}\sqrt{\frac{(\ell+1)(\ell+2)}{2\ell(\ell-1)}}\,\frac{d^\ell}{dt^\ell}\left[\mathcal{Y}_L^{\ell m}\,(I_L)_{\mathrm{Newt}}\right], \tag{3.4}$$

[1] The other one is the mass-dependent parameter c_3 appearing in the spin-orbit part of the effective Hamiltonian for spinning binaries; see Sec. B.1 of Appendix B.

[2] The tensors $\mathcal{Y}_L^{\ell m}$ can be freely brought inside the time derivatives, since they are purely numerical.

$$h^{(N,1)}_{\ell m} = -i\frac{4\sqrt{2}G}{D_L c^{\ell+3}(\ell!)}\sqrt{\frac{\ell(\ell+2)}{2(\ell+1)(\ell-1)}}\,\frac{d^\ell}{dt^\ell}\left[\mathcal{Y}^{\ell m}_L\,(J_L)_{\rm Newt}\right] \tag{3.5}$$

We notice that in general

$$\left[\mathcal{Y}^{\ell m}_L\,(I_L)_{\rm Newt}\right] \propto M\nu\, r^\ell e^{-im\varphi}, \tag{3.6}$$

$$\left[\mathcal{Y}^{\ell m}_L\,(J_L)_{\rm Newt}\right] \propto M\nu\, r^{\ell+1}\Omega e^{-im\varphi}, \tag{3.7}$$

implying that the general Newtonian prefactor $h^{(N,\epsilon)}_{\ell m}$ defined above involves time derivatives of r and Ω, up to $r^{(\ell)}$ and $\Omega^{(\ell)}$. All these time derivatives vanish for circular orbits; moreover, the usual approach used in their regards when computing PN noncircular results for the modes $h_{\ell m}$ is to order-reduce them by means of the PN-expanded equations of motion, truncated at the target PN accuracy. Here they are instead kept explicit and evaluated using the resummed EOB equations of motion, which become exactly known in the test-mass limit $\nu \to 0$.[3] In this sense, we can regard these explicit time derivatives as a resummation of the noncircular contributions that would appear in the PN-expanded noncircular expression of $h_{\ell m}$ by performing the usual order-reduction procedure. Moreover, each Newtonian factor $h^{(N,\epsilon)}_{\ell m}$ is written as

$$h^{(N,\epsilon)}_{\ell m} = h^{(N,\epsilon)_{\rm c}}_{\ell m} h^{(N,\epsilon)_{\rm nc}}_{\ell m} \tag{3.8}$$

i.e. as the product of its circular limit part $h^{(N,\epsilon)_{\rm c}}_{\ell m}$, which gives back Eq. (2.101) when expressed in terms of x, and a *Newtonian noncircular factor*,

$$h^{(N,\epsilon)_{\rm nc}}_{\ell m} \equiv \frac{h^{(N,\epsilon)}_{\ell m}}{h^{(N,\epsilon)_{\rm c}}_{\ell m}}, \tag{3.9}$$

which collects all the noncircular contributions and reduces to 1 for circular orbits; for instance, focusing on the dominant quadrupolar mode h_{22}, we have

$$h^{(N,0)_{\rm c}}_{22} = -\frac{8GM}{D_L c^4}\sqrt{\frac{\pi}{5}}\nu r^2\Omega^2 e^{-2{\rm i}\varphi}, \tag{3.10}$$

$$\hat{h}^{(N,0)_{\rm nc}}_{22} = 1 - \frac{1}{2}\left(\frac{\dot{r}^2}{r^2\Omega^2} + \frac{\ddot{r}}{r\Omega^2}\right) + {\rm i}\left(\frac{2\dot{r}}{r\Omega} + \frac{\dot{\Omega}}{2\Omega^2}\right). \tag{3.11}$$

Let us now outline the corresponding noncircular modifications on the radiation-reaction force. To begin with, the radial component $\hat{\mathcal{F}}_r$ can no longer be set to zero: the noncircular prescription for it, introduced in Ref. [254], is

[3] In practice, the evaluation of all these time derivatives follows from a generalization of the iterative analytical approach outlined in Appendix A of Ref. [147].

to use the 2PN instantaneous result of Ref. [205] in Padé resummed form. Explicitly we have

$$\hat{\mathcal{F}}_r = \frac{\nu}{c^5}\frac{p_{r_*}}{r^4}\hat{f}_r^{\rm N} P_2^0\big[\hat{f}_r/\hat{f}_r^{\rm N}\big], \tag{3.12}$$

where, from Eqs. (3.70) and (D9)-(D11) of Ref. [205],

$$\hat{f}_r = \hat{f}_r^{\rm N} + \frac{1}{c^2}\hat{f}_r^{\rm 1PN} + \frac{1}{c^4}\hat{f}_r^{\rm 2PN}, \tag{3.13}$$

$$\hat{f}_r^{\rm N} = -\frac{8}{15} + \frac{56p_\varphi^2}{5r}, \tag{3.14}$$

$$\begin{aligned}\hat{f}_r^{\rm 1PN} = {}& p_{r_*}^2\left(-\frac{1228}{105}+\frac{556\nu}{105}\right)+\frac{1}{r}\left[-\frac{1984}{105}+\frac{16\nu}{21}+p_{r_*}^2p_\varphi^2\left(-\frac{124}{105}\right.\right.\\ &\left.\left.-\frac{436\nu}{105}\right)\right]+\frac{p_\varphi^2}{r^2}\left(-\frac{1696}{35}-\frac{1268\nu}{105}\right)+\frac{p_\varphi^4}{r^3}\left(\frac{1252}{105}-\frac{2588\nu}{105}\right),\end{aligned} \tag{3.15}$$

$$\begin{aligned}\hat{f}_r^{\rm 2PN} = {}& p_{r_*}^4\left(\frac{323}{315}+\frac{1061\nu}{315}-\frac{1273\nu^2}{315}\right)+\frac{1}{r}\left[p_{r_*}^2\left(\frac{20666}{315}+\frac{17590\nu}{189}-\frac{218\nu^2}{189}\right)\right.\\ &\left.+p_{r_*}^4p_\varphi^2\left(-\frac{461}{315}-\frac{983\nu}{315}+\frac{131\nu^2}{63}\right)\right]+\frac{1}{r^2}\left[\frac{59554}{2835}+\frac{9854\nu}{105}-\frac{3548\nu^2}{315}\right.\\ &\left.+p_{r_*}^2p_\varphi^2\left(-\frac{1774}{21}+\frac{10292\nu}{315}-\frac{8804\nu^2}{315}\right)\right]+\frac{1}{r^3}\left[-\frac{29438}{315}+\frac{9568\nu}{63}\right.\\ &\left.-\frac{1752\nu^2}{35}+p_{r_*}^2p_\varphi^4\left(-\frac{628}{105}-\frac{1052\nu}{105}+\frac{194\nu^2}{7}\right)\right]+\frac{p_\varphi^4}{r^4}\left(-\frac{35209}{315}\right.\\ &\left.+\frac{1606\nu}{15}+\frac{25217\nu^2}{315}\right)+\frac{p_\varphi^6}{r^5}\left(-\frac{3229}{315}-\frac{718\nu}{63}+\frac{3277\nu^2}{105}\right).\end{aligned} \tag{3.16}$$

Regarding the other component $\hat{\mathcal{F}}_\varphi$, the noncircular generalization of Eq. (2.121) used in `TEOBResumS-DALI` consists in dressing the dominant multipole F_{22} in $\hat{f}$ with the noncircular factor $\hat{f}_{\varphi,22}^{\rm N_{nc}}$, compute from $\hat{h}_{22}^{(N,0)_{\rm nc}}$. More explicitly, we have

$$\hat{\mathcal{F}}_\varphi = -\frac{32}{5c^5}\nu r_\omega^4\Omega^5\hat{f}_{\rm nc_{22}}, \tag{3.17}$$

where

$$\hat{f}_{\rm nc_{22}} \equiv \hat{F}_{22}\hat{f}_{\varphi,22}^{\rm N_{nc}} + \hat{F}_{21} + \sum_{\ell\geq 3}^{8}\sum_{m=1}^{\ell}\hat{F}_{\ell m}, \tag{3.18}$$

$$\begin{aligned}\hat{f}_{\varphi,22}^{\rm N_{nc}} = {}& \frac{1}{8\pi}\Im\left[\dot{\hat{h}}_{22}^{(N,0)_{\rm nc}}\big(\hat{h}_{22}^{(N,0)_{\rm nc}}\big)^*\right] = 1+\frac{3\dot{r}^4}{4r^4\Omega^4}+\frac{3\dot{r}^3\dot{\Omega}}{4r^3\Omega^5}+\frac{3\ddot{r}^2}{4r^2\Omega^4}\\ &+\frac{3\ddot{r}\dot{r}\dot{\Omega}}{8r^2\Omega^5}-\frac{r^{(3)}\dot{r}}{2r^2\Omega^4}+\frac{\dot{r}^2\ddot{\Omega}}{8r^2\Omega^5}+\frac{4\dot{r}^2}{r^2\Omega^2}+\frac{\ddot{r}\ddot{\Omega}}{8r\Omega^5}-\frac{2\ddot{r}}{r\Omega^2}-\frac{r^{(3)}\dot{\Omega}}{8r\Omega^5}\\ &+\frac{3\dot{r}\dot{\Omega}}{r\Omega^3}+\frac{3\dot{\Omega}^2}{4\Omega^4}-\frac{\ddot{\Omega}}{4\Omega^3}.\end{aligned} \tag{3.19}$$

Here the noncircular factor (3.19) is obtained from Eq. (2.99) after the parity condition $h_{\ell,-m} = (-)^\ell h^*_{\ell m}$ is used in it.

We finally mention that a particularly useful way of testing different radiation-reaction force prescriptions is to compare the corresponding fluxes at infinity with their numerical analogues. In this respect, we remind that the energy flux at infinity is obtained via the balance equation (2.97), where in addition to $\hat{\mathcal{F}}_r$ and $\hat{\mathcal{F}}_\varphi$ also the Schott contribution $\dot{E}_{\rm Schott}$ appears. To compute the latter, following Ref. [254], it is useful to reorganize the 2PN result for $E_{\rm Schott}$, given in Eqs. (C1)-(C4) of Ref. [205], in the factorized and resummed form

$$E_{\rm Schott} = \frac{16}{5}\frac{p_{r_*}}{c^5 r^3} P_2^0[E^{\rm c}_{\rm Schott}] P_2^0[E^{\rm nc}_{\rm Schott}], \tag{3.20}$$

where $E^{\rm c}_{\rm Schott}$ is the circular component of the Schott energy, which can be read off Eq. (3.56) of Ref. [205], while $E^{\rm nc}_{\rm Schott}$ is the corresponding noncircular factor obtained by computing $E_{\rm Schott}/E^{\rm c}_{\rm Schott}$.

3.2 Factorized 2PN noncircular corrections in the insplunge waveform

The spherical modes of the 2PN waveform for generic planar orbits have been recently obtained in EOB coordinates by Khalil *et al.* [251]. Here, the expression for the instantaneous contributions have been computed by translating in EOB coordinates the waveform results of Ref. [246], which obtained them in harmonic coordinates trough an application, for noncircularized orbits, of the non-linear waveform generation formalism we outlined in Sec. 1.3 of Chapter 1. Within the same framework, the tail contributions have been derived starting from the results of Ref. [253], and then subsequently extended to include higher-order corrections in the eccentricity, notably also for higher spherical modes than the dominant one, the $\ell = m = 2$ mode. In this section we want ot exploit this 2PN waveform information (neglecting noncircular spin contributions) to define alternative noncircular corrections that fit properly in the waveform factorization scheme of `TEOBResumS-DALI`. The procedure we followed to define these corrections, in the form of extra noncircular factors, is presented in Sec. 3.2.2, focusing initially on the case of the dominant spherical mode $\ell = m = 2$ and then moving to all the subdominant modes that enter the 2PN accurate waveform. Before that, we find useful to recall, in Sec. 3.2.1, the last steps in the derivation of the 2PN waveform results cited above, so as to fix the notation and keep the discussion as self-contained as possible. Separately, in Sec. 3.2.3, we discuss the main issues of the modes with $m = 0$ and propose a specific 2PN-accurate model to circumvent them.

3.2.1 2PN noncircular waveform in EOB coordinates

To start with, let us specify that we consider here the waveform mode structure [246]

$$h_{\ell m} = \frac{4GM\nu}{c^4 D_L}\sqrt{\frac{\pi}{5}}e^{-im\varphi}\hat{H}_{\ell m}, \tag{3.21}$$

where each $\hat{H}_{\ell m}$ mode is decomposed in the sum of instantaneous and hereditary (or tail) terms

$$\hat{H}_{\ell m} = \hat{H}^{\rm inst}_{\ell m} + \hat{H}^{\rm tail}_{\ell m}, \tag{3.22}$$

which enter at different PN orders and thus will be discussed separately.

Instantaneous contributions

The instantaneous contributions to the modes for non-spinning binaries have been derived in Ref. [97, 260] up to 2PN order and in Ref. [246] up to 3PN order, where they can be found in terms of harmonic coordinates. By way of illustration, the 2PN-accurate $\ell = m = 2$ mode in harmonic coordinates explicitly reads

$$\begin{aligned}
\left(\hat{H}^{\rm inst}_{22}\right)_h &= \frac{1}{r_h} + r_h^2\dot{\varphi}_h^2 + 2ir\dot{r}_h\dot{\varphi}_h - \dot{r}_h^2 + \frac{1}{c^2}\left\{\frac{1}{r_h^2}\left(\frac{\nu}{2}-5\right) + r_h\left[\dot{\varphi}_h^2\left(\frac{78\nu}{21}+\frac{11}{42}\right)\right.\right.\\
&\left. - i\dot{r}_h\dot{\varphi}_h(\dot{r}_h^2 + r_h^2\dot{\varphi}_h^2)\left(\frac{27\nu}{7}-\frac{9}{7}\right)\right] - \frac{\dot{r}_h^2}{r_h}\left(\frac{16\nu}{7}+\frac{15}{14}\right) + i\dot{r}_h\dot{\varphi}_h\left(\frac{45\nu}{7}+\frac{25}{21}\right)\\
&+ (\dot{r}_h^4 - r_h^4\dot{\varphi}_h^4)\left(\frac{27\nu}{14}-\frac{9}{14}\right)\Bigg\} + \frac{1}{c^4}\left\{\frac{1}{r_h^3}\left(\frac{79\nu^2}{126}+\frac{181\nu}{36}+\frac{757}{63}\right)\right.\\
&+ \dot{\varphi}_h^2\left(\frac{13133\nu^2}{1512}-\frac{5225\nu}{216}-\frac{11891}{1512}\right) + \frac{\dot{r}_h^4}{r_h}\left(\frac{214\nu^2}{21}+\frac{83\nu}{21}-\frac{557}{168}\right)\\
&+ \frac{i\dot{r}_h\dot{\varphi}_h}{r_h}\left(\frac{2852\nu^2}{189}-\frac{3767\nu}{189}-\frac{773}{189}\right) - \frac{\dot{r}_h^2}{r_h^2}\left(\frac{467\nu^2}{126}+\frac{2789\nu}{252}-\frac{619}{252}\right)\\
&+ (\dot{r}_h^2 r_h^4\dot{\varphi}_h^4 - \dot{r}_h^6 + r_h^6\dot{\varphi}_h^6 - r_h^2\dot{r}_h^4\dot{\varphi}_h^2)\left(\frac{1111\nu^2}{168}-\frac{589\nu}{168}+\frac{83}{168}\right)\\
&- ir_h^2\dot{r}_h\dot{\varphi}_h^3\left(\frac{1703\nu^2}{84}-\frac{103\nu}{12}-\frac{433}{84}\right) - i\dot{r}_h^3\dot{\varphi}_h\left(\frac{211\nu^2}{9}+\frac{731\nu}{63}-\frac{863}{126}\right)\\
&+ r_h^3\dot{\varphi}_h^4\left(-\frac{2995\nu^2}{252}+\frac{19\nu}{252}+\frac{835}{252}\right) + ir_h^3\dot{r}_h^3\dot{\varphi}_h^3\left(\frac{1111\nu^2}{42}-\frac{589\nu}{42}+\frac{83}{42}\right)\\
&- r_h\dot{r}_h^2\dot{\varphi}_h^2\left(\frac{58\nu^2}{21}+\frac{169\nu}{14}-\frac{11}{28}\right) + i(r_h\dot{r}_h^5\dot{\varphi}_h + \dot{r}_h r_h^5\dot{\varphi}_h^5)\left(\frac{1111\nu^2}{84}-\frac{589\nu}{84}\right.\\
&\left.\left.+\frac{83}{84}\right)\right\} + \mathcal{O}\left(\frac{1}{c^6}\right),
\end{aligned} \tag{3.23}$$

where φ_h is the harmonic orbital phase and r_h is the GM-reduced radial harmonic coordinate, $r_h \equiv R_h/GM$. For completeness, we explicitly report below the transformation from the harmonic set $(r_h, \dot{r}_h, \varphi_h, \dot{\varphi}_h)$ to the EOB canonical set $(u, \varphi, p_r, p_\varphi)$, as we derived, independently of Ref. [251], from the coordinate relations given in Appendix E of Ref. [205]. We highlight that, in order to make clearer the PN structure, we henceforth redefine the variable u by stripping it of the usual c^{-2} factor; therefore, if not otherwise specified, we consider $u \equiv 1/r$. We find

$$\begin{aligned} r_h &= \frac{1}{u} + \frac{1}{c^2}\left[\frac{1}{2}\nu\left(\frac{3p_r^2}{u} + p_\varphi^2 u - 1\right) - 1\right] - \frac{\nu}{8c^4 u}\Bigg[(5-3\nu)p_r^4 \\ &\quad + 2p_r^2 u\left(28 - 3(\nu-1)p_\varphi^2 u\right) + u^2\Big(2(\nu-19) + (\nu+1)p_\varphi^4 u^2 \\ &\quad + p_\varphi^2 u(1-3\nu)\Big)\Bigg] + \mathcal{O}\left(\frac{1}{c^6}\right), \end{aligned} \tag{3.24}$$

$$\begin{aligned} \dot{r}_h &= p_r + \frac{1}{2c^2}p_r\left[(2\nu-1)p_r^2 + u\left((4\nu-1)p_\varphi^2 u - 6 - 4\nu\right)\right] \\ &\quad + \frac{1}{8c^4}\Bigg\{(3-8\nu)p_r^5 - 2p_r^3 u\left[2(8\nu-5) + \left(2\nu^2 + 12\nu - 3\right)p_\varphi^2 u\right] \\ &\quad + p_r u^2\Big[-10\nu^2 + 78\nu + 12 + \left(8\nu^2 - 16\nu + 3\right)p_\varphi^4 u^2 \\ &\quad + 2\left(\nu^2 - 55\nu + 6\right)p_\varphi^2 u\Big]\Bigg\} + \mathcal{O}\left(\frac{1}{c^6}\right), \end{aligned} \tag{3.25}$$

$$\begin{aligned} \varphi_h &= \varphi + \frac{1}{c^2}\nu p_r p_\varphi u - \frac{1}{4c^4}\nu p_r p_\varphi u\Big[(4\nu+2)p_r^2 + u\Big(-3\nu + 15 \\ &\quad + 2p_\varphi^2 u\Big)\Big] + \mathcal{O}\left(\frac{1}{c^6}\right), \end{aligned} \tag{3.26}$$

$$\begin{aligned} \dot{\varphi}_h &= p_\varphi u^2 + \frac{1}{2c^2}p_\varphi u^2\left[u\left((\nu-1)p_\varphi^2 u - 2\right) - (3\nu+1)p_r^2\right] \\ &\quad - \frac{1}{8c^4}p_\varphi u^2\Bigg\{-\left(15\nu^2 + 11\nu + 3\right)p_r^4 + 2p_r^2 u\Big[2\left(\nu^2 - 24\nu - 3\right) \\ &\quad + 3\left(3\nu^2 - \nu - 1\right)p_\varphi^2 u\Big] + u^2\Big[2\left(\nu^2 - 9\nu + 2\right) + \left(\nu^2 + 5\nu - 3\right)p_\varphi^4 u^2 \\ &\quad - 2\left(3\nu^2 - 17\nu + 2\right)p_\varphi^2 u\Big]\Bigg\} + \mathcal{O}\left(\frac{1}{c^6}\right). \end{aligned} \tag{3.27}$$

Then, replacing the relations (3.24)-(3.27) into Eq. (3.23) yields

$$\begin{aligned} \hat{H}_{22}^{\rm inst} &= u - p_r^2 + 2ip_r p_\varphi u + p_\varphi^2 u^2 + \frac{1}{c^2}\Bigg\{i\left(\frac{\nu}{7} - \frac{5}{7}\right)p_r^3 p_\varphi u \\ &\quad - ip_r p_\varphi u^2\left[\left(\frac{4\nu}{7} + \frac{185}{21}\right) - \left(\frac{\nu}{7} - \frac{5}{7}\right)p_\varphi^2 u\right] + \left(\frac{\nu}{14} - \frac{5}{14}\right)(p_\varphi^4 u^4 - p_r^4) \end{aligned}$$

$$
\begin{aligned}
&+\left(\frac{3\nu}{14}+\frac{64}{14}\right)p_r^2u+u^2\left[(\nu-4)+\left(\frac{31\nu}{14}-\frac{157}{42}\right)p_\varphi^2u\right]\Bigg\}\\
&+\frac{1}{c^4}\Bigg\{\left(\frac{17\nu^2}{168}+\frac{13\nu}{168}-\frac{5}{24}\right)(p_r^6+p_r^4p_\varphi^2u^2-p_\varphi^6u^6)-i\left(\frac{17\nu^2}{84}+\frac{13\nu}{84}\right.\\
&\left.-\frac{5}{12}\right)p_rp_\varphi u(p_r^4+p_\varphi^4u^4)-p_r^2u^2\left[\left(\frac{13\nu^2}{63}+\frac{151\nu}{18}+\frac{1055}{252}\right)+\left(\frac{17\nu^2}{504}\right.\right.\\
&\left.+\frac{13\nu}{504}-\frac{5}{72}\right)p_\varphi^4u^2+\left(\frac{313\nu^2}{252}+\frac{85\nu}{252}-\frac{101}{252}\right)p_\varphi^2u\Bigg]\\
&-\left(\frac{85\nu^2}{168}+\frac{55\nu}{168}+\frac{425}{168}\right)p_r^4u+ip_r^3p_\varphi u^2\left[\left(\frac{62\nu^2}{63}+\frac{11\nu}{126}+\frac{695}{126}\right)\right.\\
&\left.-\left(\frac{17\nu^2}{42}+\frac{13\nu}{42}-\frac{5}{6}\right)p_\varphi^2u\right]-ip_rp_\varphi u^3\left[\left(\frac{523\nu^2}{189}+\frac{2452\nu}{189}-\frac{193}{27}\right)\right.\\
&\left.+\left(\frac{8\nu^2}{21}-\frac{29\nu}{14}-\frac{67}{28}\right)p_\varphi^2u\right]+u^3\left[\left(\frac{205\nu^2}{126}-\frac{49\nu}{18}+\frac{190}{63}\right)\right.\\
&\left.-\left(\frac{671\nu^2}{504}+\frac{1375\nu}{504}-\frac{481}{72}\right)p_\varphi^4u^2+\left(\frac{127\nu^2}{27}-\frac{2710\nu}{189}-\frac{5519}{1512}\right)p_\varphi^2u\right]\Bigg\}\\
&+\mathcal{O}\left(\frac{1}{c^6}\right). \qquad (3.28)
\end{aligned}
$$

This result coincides with Eq. (83) of Ref. [251], as long as we replace $p_\varphi^2u^2 = p^2-p_r^2$. The canonical transformations above have also been applied to higher multipoles, up to $\ell = m = 6$, and their EOB coordinate expressions have been checked to precisely coincide with the corresponding ones provided in the supplementary material of Ref. [251]. Moreover, for an additional, independent, validation of these transformations, we have verified that the 2PN instantaneous angular momentum flux given in Eq. (3.70) of Ref. [205] could be obtained, by means of Eq. (2.99), from the 2PN noncircular instantaneous component of $h_{\ell m}$, once rewritten in EOB coordinates.[4]

Hereditary contributions

For the hereditary components $\hat{H}^{\rm tail}_{\ell m}$ we adopt the results of Ref. [251]. These contributions comes from the evaluation of the leading tail integrals that appear in the relations between radiative and source multipole moments; see Eqs. (1.156)-(1.157). In particular their evaluation is performed using the Keplerian parametrization and considering an expansion for small eccentricity, according to the method outlined in Ref. [253]. The resulting tail contributions are initially expressed in terms of the frequency parameter $x \equiv (\Omega/c^3)^{2/3}$, the eccentricity e and the phase variable χ, which, together with the semilatus

[4] More specifically, we found that the spherical modes that bring a nonzero contribution to $\hat{\mathcal{F}}_\varphi$ are: $(2,1)$, $(2,2)$, $(3,1)$, $(3,2)$, $(3,3)$, $(4,2)$, and $(4,4)$.

rectum p, parametrize the motion according to

$$r = \frac{p}{1 + e\cos\chi}. \tag{3.29}$$

To be precise, the dynamical parameters p and e used in Refs. [251, 253] and by us are defined, in analogy with Newtonian mechanics, as[5]

$$e \equiv \frac{r_+ - r_-}{r_+ + r_-}, \qquad p \equiv \frac{2r_+r_-}{r_+ + r_-}, \tag{3.30}$$

where r_+ and r_- are the turning point of the radial motion, respectively apastron and periastron, which can be determined from the EOB Hamiltonian $\hat{H}_{\rm EOB}$. We also specify that, for stable orbits, p must satisfy the condition $p > p_s(e, \hat{a})$ where $p_s(e, \hat{a})$ is the *separatrix*, real root of [262, 263]

$$\begin{aligned} &p_s^2(p_s - 6 - 2e)^2 + \hat{a}^4(e-3)^2(e+1)^2 - 2\hat{a}^2(1+e)p_s\big[14 + 2e^2 \\ &+ p_s(3-e)\big] = 0. \end{aligned} \tag{3.31}$$

Here $\hat{a}$ is the dimensionless spin parameter of the Kerr black hole that lies at the core of the EOB dynamics when spinning binaries are concerned; see appendix B. In the non spinning case $\hat{a} = 0$, we have simply $p_s = 3(2 + e)$.

From Ref. [251], the $\ell = m = 2$ dominant tail component at 2PN accuracy, and up to $\mathcal{O}(e^6)$, reads

$$\begin{aligned} \left(\hat{H}_{22}^{\rm tail}\right)_{KP} = \frac{2\pi x^{5/2}}{c^3}\Bigg[1 &+ e\left(\frac{11\mathrm{e}^{-i\chi}}{8} + \frac{13\mathrm{e}^{i\chi}}{8}\right) + e^2\left(\frac{5}{8}\mathrm{e}^{-2i\chi} + \frac{7}{8}\mathrm{e}^{2i\chi}\right. \\ &\left. + 4\right) + e^3\left(\frac{121\mathrm{e}^{-i\chi}}{32} + \frac{143\mathrm{e}^{i\chi}}{32} + \frac{3\mathrm{e}^{-3i\chi}}{32} + \frac{\mathrm{e}^{3i\chi}}{12}\right) + e^4\left(\frac{25\mathrm{e}^{-2i\chi}}{16} + \frac{203\mathrm{e}^{2i\chi}}{96}\right. \\ &\left. - \frac{5\mathrm{e}^{4i\chi}}{96} + \frac{65}{8}\right) + e^5\left(\frac{55\mathrm{e}^{-i\chi}}{8} + \frac{6233\mathrm{e}^{i\chi}}{768} + \frac{15\mathrm{e}^{-3i\chi}}{64} + \frac{281\mathrm{e}^{3i\chi}}{1536} + \frac{53\mathrm{e}^{5\chi}}{7680}\right) \\ &+ e^6\left(\frac{175\mathrm{e}^{-2i\chi}}{64} + \frac{1869\mathrm{e}^{2i\chi}}{512} - \frac{449\mathrm{e}^{4i\chi}}{3840} + \frac{31\mathrm{e}^{6i\chi}}{23040} + \frac{30247}{2304}\right)\Bigg]. \end{aligned} \tag{3.32}$$

Analogously to Ref. [251], we want to recast all the tail components like Eq. (3.32) in terms of EOB phase-space variables. However, as opposed to Ref. [251], we want to adopt just the variables (u, p_r, p_φ), avoiding the use of $\dot{p}_r$, in order to simplify the numerical implementation of the consequential model. Since we are working at 2PN accuracy, we can resort to the following Newtonian relations:[6]

$$x = \frac{1 - e^2}{p}, \tag{3.33}$$

[5] We warn the reader that the eccentricity e defined here is different from the time eccentricity e_t that appears in the context of the quasi-Keplerian parametrization [195, 261].

[6] The first corrections to the leading Newtonian order would enter at 2.5PN order in the waveform.

$$u = \frac{1 + e\cos\chi}{p}, \tag{3.34}$$

$$p_\varphi = \sqrt{p}, \tag{3.35}$$

$$p_r = \frac{e\sin\chi}{\sqrt{p}}. \tag{3.36}$$

Then, since Eq. (3.32) is given in an expansion for small eccentricity e, it is important to identify the combinations of the variable (u, p_r, p_φ) that are of the same order of e. These are easily found in p_r and $\dot{p}_r$, with the latter related to p_φ and u through the Newtonian equation of motion

$$\dot{p}_r = u^2(p_\varphi^2 u - 1). \tag{3.37}$$

In fact, using Eqs. (3.33)–(3.36), we find $p_r \sim e$ and $(p_\varphi^2 u - 1) \sim e$. Therefore, the expansion in e of Eq. (3.32) translates into a simultaneous expansion in p_r and $\dot{p}_r$. This reads[7]

$$\begin{aligned}\hat{H}_{22}^{\rm tail} = \frac{2\pi u^{5/2}}{c^3}\Bigg[1 &+ \left(\frac{\dot{p}_r}{2u^2} + \frac{ip_r}{4\sqrt{u}}\right) - \frac{\dot{p}_r^2}{8u^4} - \left(\frac{\dot{p}_r^3}{96u^6} + \frac{7ip_r\dot{p}_r^2}{32u^{9/2}}\right.\\
&\left. - \frac{7p_r^2\dot{p}_r}{32u^3} - \frac{7ip_r^3}{96u^{3/2}}\right) + \left(\frac{7\dot{p}_r^4}{384u^8} + \frac{ip_r\dot{p}_r^3}{12u^{13/2}} - \frac{p_r^2\dot{p}_r^2}{64u^5} - \frac{ip_r^3\dot{p}_r}{96u^{7/2}} + \frac{p_r^4}{48u^2}\right)\\
&- \left(\frac{13\dot{p}_r^5}{1920u^{10}} - \frac{ip_r\dot{p}_r^4}{768u^{17/2}} + \frac{73p_r^2\dot{p}_r^3}{768u^7} + \frac{49ip_r^3\dot{p}_r^2}{384u^{11/2}} - \frac{35p_r^4\dot{p}_r}{384u^4} - \frac{89ip_r^5}{3840u^{5/2}}\right)\\
&+ \left(\frac{109\dot{p}_r^6}{46080u^{12}} - \frac{ip_r\dot{p}_r^5}{64u^{21/2}} + \frac{137p_r^2\dot{p}_r^4}{1536u^9} + \frac{137ip_r^3\dot{p}_r^3}{1152u^{15/2}} - \frac{65p_r^4\dot{p}_r^2}{768u^6}\right.\\
&\left. - \frac{23ip_r^5\dot{p}_r}{640u^{9/2}} + \frac{p_r^6}{96u^3}\right)\Bigg],\end{aligned} \tag{3.38}$$

where we also find half-integer powers of u. These can be eliminated by means of Eq. (3.37), which, after an expansion in $\dot{p}_r$, gives

$$\begin{aligned}p_\varphi = &\frac{1}{\sqrt{u}} + \frac{\dot{p}_r}{2u^{5/2}} - \frac{\dot{p}_r^2}{8u^{9/2}} + \frac{\dot{p}_r^3}{16u^{13/2}} - \frac{5\dot{p}_r^4}{128u^{17/2}} + \frac{7\dot{p}_r^5}{256u^{21/2}}\\
&- \frac{21\dot{p}_r^6}{1024u^{25/2}} + \mathcal{O}(\dot{p}_r^7),\end{aligned} \tag{3.39}$$

and thus

$$\frac{1}{\sqrt{u}} = p_\varphi\left(1 - \frac{\dot{p}_r}{2u^2} + \frac{3\dot{p}_r^2}{8u^4} - \frac{5\dot{p}_r^3}{16u^6} + \frac{35\dot{p}_r^4}{128u^8} - \frac{63\dot{p}_r^5}{256u^{10}} + \frac{231\dot{p}_r^6}{1024u^{12}}\right) + \mathcal{O}(\dot{p}_r^7). \tag{3.40}$$

Once this is inserted into Eq. (3.38), one precisely obtains Eq. (102) of Ref. [251], which we rewrite here in our notation:

$$\hat{H}_{22}^{\rm tail} = \frac{2\pi}{c^3}\left[p_\varphi u^3 + \frac{1}{4}ip_r u^2 - \left(\frac{7\dot{p}_r^3 p_\varphi}{96u^3} + \frac{7ip_r\dot{p}_r^2}{32u^2} - \frac{7}{32}p_r^2\dot{p}_r p_\varphi\right.\right.$$

[7] Here the parentheses () collect terms at the same order in eccentricity

$$
\begin{aligned}
&- \frac{7}{96} i p_r^3 u \Big) + \Big(\frac{3 \dot{p}_r^4 p_\varphi}{32 u^5} + \frac{i p_r \dot{p}_r^3}{12 u^4} - \frac{p_r^2 \dot{p}_r^2 p_\varphi}{8 u^2} - \frac{i p_r^3 \dot{p}_r}{96 u} + \frac{1}{48} p_r^4 p_\varphi u \Big) \\
&- \Big(\frac{173 \dot{p}_r^5 p_\varphi}{1920 u^7} - \frac{i p_r \dot{p}_r^4}{768 u^6} + \frac{p_r^2 \dot{p}_r^3 p_\varphi}{192 u^4} + \frac{49 i p_r^3 \dot{p}_r^2}{384 u^3} - \frac{31 p_r^4 \dot{p}_r p_\varphi}{384 u} - \frac{89 i p_r^5}{3840} \Big) \\
&+ \Big(\frac{97 \dot{p}_r^6 p_\varphi}{1152 u^9} - \frac{i p_r \dot{p}_r^5}{64 u^8} + \frac{p_r^2 \dot{p}_r^4 p_\varphi}{16 u^6} + \frac{137 i p_r^3 \dot{p}_r^3}{1152 u^5} - \frac{47 p_r^4 \dot{p}_r^2 p_\varphi}{384 u^3} - \frac{23 i p_r^5 \dot{p}_r}{640 u^2} \\
&+ \frac{p_r^6 p_\varphi}{96} \Big) \Big] . \qquad (3.41)
\end{aligned}
$$

Note that this expression, if interpreted within the EOB framework, may be ambiguous, since here $\dot{p}_r$ actually only refers to the time derivative of the *Newtonian* radial momentum, obtained from the Newtonian reduction of its PN-expanded equation of motion. Although there are no strong arguments that may prevent one from promoting it to the derivative of the *relativistic* radial momentum as defined within the resummed EOB dynamics, we prefer here to simplify the logic and have an expression that *avoids* $\dot{p}_r$, only using (u, p_r, p_φ) as in the instantaneous components $\hat{H}^{\rm inst}_{\ell m}$. We therefore insert Eq. (3.37) in Eq. (3.41), obtaining

$$
\begin{aligned}
\hat{H}^{\rm tail}_{22} = \frac{2\pi}{c^3} \Big[& p_\varphi u^3 \Big(\frac{1931}{1440} - \frac{595 p_\varphi^2 u}{384} + \frac{377 p_\varphi^4 u^2}{128} - \frac{1747 p_\varphi^6 u^3}{576} \\
&+ \frac{347 p_\varphi^8 u^4}{192} - \frac{381 p_\varphi^{10} u^5}{640} + \frac{97 p_\varphi^{12} u^6}{1152} \Big) - i p_r u^2 \Big(\frac{9}{256} - \frac{29 p_\varphi^2 u}{48} + \frac{39 p_\varphi^4 u^2}{128} \\
&+ \frac{5 p_\varphi^6 u^3}{64} - \frac{61 p_\varphi^8 u^4}{768} + \frac{p_\varphi^{10} u^5}{64} \Big) - p_r^2 p_\varphi u^2 \Big(\frac{53}{192} - \frac{13 p_\varphi^2 u}{64} - \frac{17 p_\varphi^4 u^2}{64} \\
&+ \frac{49 p_\varphi^6 u^3}{192} - \frac{p_\varphi^8 u^4}{16} \Big) - i p_r^3 u \Big(\frac{47}{288} - \frac{77 p_\varphi^2 u}{128} + \frac{31 p_\varphi^4 u^2}{64} - \frac{137 p_\varphi^6 u^3}{1152} \Big) \\
&- p_r^4 p_\varphi u \Big(\frac{35}{192} - \frac{125 p_\varphi^2 u}{384} + \frac{47 p_\varphi^4 u^2}{384} \Big) + i p_r^5 \Big(\frac{227}{3840} - \frac{23 p_\varphi^2 u}{640} \Big) \\
&+ \frac{p_r^6 p_\varphi}{96} \Big] . \qquad (3.42)
\end{aligned}
$$

Indeed, the same is repeated for all the subdominant spherical multipoles relevant at 2PN, that is up to $\ell = m = 6$.

We finally point out that the absence of logarithmic terms in Eq. (3.42) is due to a dedicated phase redefinition, performed already at the level of Eq. (3.32), which completely reabsorbs them at this PN order; see Sec. IIIC of Ref. [253] for further details on this.

3.2.2 New noncircular waveform factors at 2PN accuracy ($m \neq 0$)

We now want to incorporate the 2PN waveform results of the previous section in the factorization prescription for the insplunge waveform used in `TEOBResumS-DALI`, which we remember is given by substituting the general Newtonian prefactor of Eqs. (3.4)-(3.5) and (3.8) in the quasi-circular factorized waveform (2.100).

We do so according to the generalized factorization scheme

$$h_{\ell m} = h_{\ell m}^{(N,\epsilon)_{\rm c}} \hat{h}_{\ell m}^{(N,\epsilon)_{\rm nc}} \hat{S}_{\rm eff}^{(\epsilon)} \hat{h}_{\ell m}^{(\epsilon)_{\rm c}} \hat{h}_{\ell m}^{\rm nc}, \tag{3.43}$$

where: the first two factors are the circular and noncircular part of the general Newtonian factor (3.8); $\hat{S}_{\rm eff}^{(\epsilon)}$ is the effective source, here considered in its generic orbit form (2.105); $\hat{h}_{\ell m}^{(\epsilon)_{\rm c}}$ is the PN residual circular correction, i.e. $\hat{h}_{\ell m}^{(\epsilon)}$ of Eq. (2.100) (without $\hat{S}_{\rm eff}^{(\epsilon)}$), equipped here with a "c" to make manifest its circular nature; $\hat{h}_{\ell m}^{\rm nc}$ is the PN residual noncircular correction, which collects the novel information we propose to integrate in the model. Essentially, our aim here is to explicitly determine the noncircular correcting factors $\hat{h}_{\ell m}^{\rm nc}$ at 2PN accuracy, for each mode relevant at this PN order, by factorizing the PN-expanded generic-orbit results for $h_{\ell m}$ of the previous section, following the trail of Eq. (3.43). The procedure is rather straightforward, although it needs the 2PN-expanded EOB equations of motion to be correctly executed. It consists in three steps: (i) starting from the 2PN noncircular results for $h_{\ell m}$, we factor out the generic Newtonian prefactor and the effective source; (ii) in the denominator, we order-reduce the associated derivatives with the 2PN-expanded equations of motion and we expand the residual at 2PN; (iii) we factor out the circular part of the residual in order to single out the 2PN noncircular factor $\hat{h}_{\ell m}^{\rm nc}$. Indeed, for this prescription to work properly, one has to be sure that no spurious poles are introduced by the factorization. Even though this is not the case for the majority of the spherical modes, all the modes with $m = 0$ happen to show this kind of problematic behavior, since their Newtonian factor is entirely noncircular and thus goes to zero in the circular limit. We defer to the next section the discussion of a possible alternative prescription for these modes and focus here on the $m \neq 0$ case.

In formulas, we can write the total PN residual factor as

$$\hat{h}_{\ell m}^{(\epsilon)} \equiv T_{\rm 2PN} \left[\frac{h_{\ell m}}{\left(h_{\ell m}^{(N,\epsilon)_{\rm c}} \hat{h}_{\ell m}^{(N,\epsilon)_{\rm nc}} \right)_{\rm EOMs} \hat{S}_{\rm eff}^{(\epsilon)}} \right], \tag{3.44}$$

where $T_{\rm 2PN}$ applies to its argument a Taylor-expansion in $1/c$ up to $\mathcal{O}(1/c^4)$ and the subscript "EOMs" indicates that inside the parenthesis where it appears we order-reduce all the time derivatives with the corresponding PN-

expanded equations of motion.[8] This is needed to avoid considering two times the noncircular terms already resummed, in the form of time derivatives, by the general Newtonian prefactor that precedes the PN residual we are computing here. The resulting expression (3.44) is a rational function of (u, p_r, p_φ) of the type $1 + \mathcal{O}(1/c^2)$.

Now that the PN factor is singled out, we can also factor out from it its circular component

$$\hat{h}^{(\epsilon)_{\rm c}}_{\ell m} \equiv \lim_{p_r \to 0} \hat{h}^{(\epsilon)}_{\ell m}, \tag{3.45}$$

so as to obtain the total noncircular PN factor we are interested in, that is

$$\hat{h}^{\rm nc}_{\ell m} \equiv T_{\rm 2PN} \left[\frac{\hat{h}^{(\epsilon)}_{\ell m}}{\hat{h}^{(\epsilon)_{\rm c}}_{\ell m}} \right], \tag{3.46}$$

which amounts to a collection of all the relativistic noncircular contributions not yet included in `TEOBResumS-DALI`. Moreover, we can split $\hat{h}^{\rm nc}_{\ell m}$ into a tail factor and an instantaneous factor,[9] considering

$$\hat{h}^{\rm nc}_{\ell m} = \hat{h}^{\rm nc_{tail}}_{\ell m} \hat{h}^{\rm nc_{inst}}_{\ell m}. \tag{3.47}$$

Then, we trade the radial momentum p_r for $p_{r_*} \equiv (A/\sqrt{D})\, p_r$, with $A/\sqrt{D}$ truncated at the 2PN order. Finally, to simplify the structure of the analytical expressions we are using, we expand each of the new factors in p_{r_*} up to $\mathcal{O}(p^4_{r_*})$.[10]

Focusing now on the dominant $\ell = m = 2$ mode, the tail factor that follows from the procedure detailed above reads

$$\begin{aligned} \hat{h}^{\rm nc_{tail}}_{22} = 1 + \frac{1}{c^3} \frac{\pi}{(p^2_\varphi u + 1)^2} \Bigg[- i \left(\frac{9 p_{r_*} u}{64} \hat{t}^{22}_{p_{r_*}} + \frac{457}{456} \frac{p^3_{r_*}}{(p^2_\varphi u + 1)^2} \hat{t}^{22}_{p^3_{r_*}} \right) \\ + \frac{5729}{1440} \frac{p^2_{r_*} p_\varphi u}{(p^2_\varphi u + 1)} \hat{t}^{22}_{p^2_{r_*}} + \frac{133}{80} \frac{p^4_{r_*} p_\varphi}{(p^2_\varphi u + 1)^3} \hat{t}^{22}_{p^4_{r_*}} \Bigg], \end{aligned} \tag{3.48}$$

where $(\hat{t}^{22}_{p_{r_*}}, \hat{t}^{22}_{p^3_{r_*}}, \hat{t}^{22}_{p^2_{r_*}}, \hat{t}^{22}_{p^4_{r_*}})$ are the following polynomials in $y \equiv p^2_\varphi u$ (with alternate signs):

$$\hat{t}^{22}_{p_{r_*}} = 1 + \frac{24341}{405} y - \frac{290}{3} y^2 + \frac{1606}{9} y^3 - \frac{13979}{81} y^4$$

[8] The PN-expanded equations of motion for the first time derivatives can be computed directly from the EOB Hamiltonian, by Taylor-expanding Eqs. (2.91)-(2.94); see Appendix B of Ref. [205] for their explicit expressions at 2PN order. Then, the computation of the PN-expanded equations of motion for the higher order derivatives follows from a straightforward iteration.

[9] This splitting can be performed with ease since tail and instantaneous contributions are consistently well separated by the PN ordering.

[10] We have verified that this choice gives an excellent approximation to the full expressions for all cases considered.

$$+ 101y^5 - \frac{1504}{45}y^6 + \frac{388}{81}y^7, \tag{3.49}$$

$$\begin{aligned}\hat{t}^{22}_{p^3_{r_*}} &= 1 + \frac{46372}{2285}y - \frac{134587}{2285}y^2 + \frac{45492}{457}y^3 \\ &- \frac{54397}{457}y^4 + \frac{43924}{457}y^5 - \frac{112697}{2285}y^6 \\ &+ \frac{32212}{2285}y^7 - \frac{776}{457}y^8,\end{aligned} \tag{3.50}$$

$$\begin{aligned}\hat{t}^{22}_{p^2_{r_*}} &= 1 - \frac{27552}{5729}y + \frac{2910}{337}y^2 - \frac{70015}{5729}y^3 \\ &+ \frac{61785}{5729}y^4 - \frac{34674}{5729}y^5 + \frac{10952}{5729}y^6 - \frac{1455}{5729}y^7,\end{aligned} \tag{3.51}$$

$$\begin{aligned}\hat{t}^{22}_{p^4_{r_*}} &= 1 - \frac{35260}{1197}y + \frac{78500}{1197}y^2 - \frac{34825}{342}y^3 \\ &+ \frac{265975}{2394}y^4 - \frac{96727}{1107}y^5 + \frac{6305}{171}y^6 \\ &- \frac{3245}{342}y^7 + \frac{2425}{2394}y^8.\end{aligned} \tag{3.52}$$

The resulting instantaneous factor is conveniently separated in amplitude and phase,

$$h^{\mathrm{nc_{inst}}}_{22} = f^{\mathrm{nc_{inst}}}_{22} e^{\mathrm{i}\delta^{\mathrm{nc_{inst}}}_{22}}, \tag{3.53}$$

which are given by

$$\begin{aligned}f^{\mathrm{nc_{inst}}}_{22} &= 1 - \frac{p^2_{r_*}}{c^2\left(p^2_\varphi u+1\right)^3}\left[\left(\frac{1}{14}-\frac{31\nu}{14}\right)\hat{f}^{22}_{1^{\mathrm{1PN}}} + \frac{p^2_{r_*}}{u\left(p^2_\varphi u+1\right)^2}\left(\frac{5}{7}-\frac{8\nu}{7}\right)\hat{f}^{22}_{p^{\mathrm{1PN}}_{r_*}}\right] \\ &+ \frac{p^2_{r_*}}{c^4\left(p^2_\varphi u+1\right)^4}\left[u\left(\frac{65}{252}+\frac{211\nu}{126}+\frac{139\nu^2}{63}\right)\hat{f}^{22}_{u^{\mathrm{2PN}}}\right. \\ &\left. + \frac{p^2_{r_*}}{\left(p^2_\varphi u+1\right)^2}\left(\frac{1613}{504}-\frac{1567\nu}{504}-\frac{71\nu^2}{72}\right)\hat{f}^{22}_{p^{\mathrm{1PN}}_{r_*}}\right],\end{aligned} \tag{3.54}$$

$$\begin{aligned}\delta^{\mathrm{nc_{inst}}}_{22} &= \frac{p_{r_*}p_\varphi}{c^2\left(p^2_\varphi u+1\right)^2}\left[u\left(\frac{25}{21}-\frac{18}{7}\nu\right)\hat{\delta}^{22}_{u^{\mathrm{1PN}}} + \frac{p^2_{r_*}}{\left(p^2_\varphi u+1\right)^2}\left(\frac{55}{21}-\frac{34\nu}{7}\right)\hat{\delta}^{22}_{p^{\mathrm{1PN}}_{r_*}}\right] \\ &+ \frac{p_{r_*}p_\varphi u}{c^4\left(p^2_\varphi u+1\right)^3}\left[u\left(\frac{7}{27}-\frac{416}{189}\nu-\frac{652}{189}\nu^2\right)\hat{\delta}^{22}_{u^{\mathrm{2PN}}}\right. \\ &\left. + \frac{p^2_{r_*}}{\left(p^2_\varphi u+1\right)^2}\left(\frac{20945}{2646}-\frac{17321}{1323}\nu+\frac{134}{1323}\nu^2\right)\hat{\delta}^{22}_{p^{\mathrm{2PN}}_{r_*}}\right].\end{aligned} \tag{3.55}$$

Similarly to the tail factor, all the functions $(\hat{f}^{22}_i, \hat{\delta}^{22}_i)$ are polynomials in y; their explicit expressions are

$$\hat{f}^{22}_{1^{\mathrm{1PN}}} = 1 - \frac{7(1+3\nu)}{1-31\nu}y - \frac{(451-177\nu)}{3-93\nu}y^2 - \frac{3(3+5\nu)}{1-31\nu}y^3, \tag{3.56}$$

$$\hat{f}^{22}_{p^{1\mathrm{PN}}_{r_*}} = 1 - \frac{65-216\nu}{3(5-8\nu)}y - \frac{5(115-72\nu)}{3(5-8\nu)}y^2 + \frac{305-264\nu}{3(5-8\nu)}y^3, \tag{3.57}$$

$$\begin{aligned}\hat{f}^{22}_{u^{2\mathrm{PN}}} &= 1 - \frac{44767+28618\nu-7276\nu^2}{42\left(65+422\nu+556\nu^2\right)}y \\ &+ \frac{132507-87244\nu-29672\nu^2}{14\left(65+422\nu+556\nu^2\right)}y^2 - \frac{134789+27920\nu+9472\nu^2}{42\left(65+422\nu+556\nu^2\right)}y^3 \\ &- \frac{3\left(637-1448\nu+512\nu^2\right)}{2\left(65+422\nu+556\nu^2\right)}y^4 - \frac{3\left(418+355\nu+710\nu^2\right)}{7\left(65+422\nu+556\nu^2\right)}y^5,\end{aligned} \tag{3.58}$$

$$\begin{aligned}\hat{f}^{22}_{p^{2\mathrm{PN}}_{r_*}} &= 1 - \frac{16399-169738\nu-9902\nu^2}{7\left(1613-1567\nu-497\nu^2\right)}y \\ &- \frac{256835-145513\nu+7405\nu^2}{4839-4701\nu-1491\nu^2}y^2 + \frac{4\left(292018-194489\nu-76057\nu^2\right)}{21\left(1613-1567\nu-497\nu^2\right)}y^3 \\ &- \frac{449937+29671\nu-80119\nu^2}{7\left(1613-1567\nu-497\nu^2\right)}y^4 - \frac{34361-33826\nu-3518\nu^2}{7\left(1613-1567\nu-497\nu^2\right)}y^5 \\ &+ \frac{15\left(5-13\nu+\nu^2\right)}{1613-1567\nu-497\nu^2}y^6,\end{aligned} \tag{3.59}$$

$$\hat{\delta}^{22}_{u^{1\mathrm{PN}}} = 1 + \frac{125-102\nu}{25-54\nu}y, \tag{3.60}$$

$$\hat{\delta}^{22}_{p^{1\mathrm{PN}}_{r_*}} = 1 + \frac{42\left(5-2\nu\right)}{55-102\nu}y - \frac{35\left(7-6\nu\right)}{55-102\nu}y^2, \tag{3.61}$$

$$\begin{aligned}\hat{\delta}^{22}_{u^{2\mathrm{PN}}} &= 1 + \frac{39761-20950\nu-21236\nu^2}{14\left(49-416\nu-652\nu^2\right)}y - \frac{3\left(3709-2556\nu-408\nu^2\right)}{14\left(49-416\nu-652\nu^2\right)}y^2 \\ &- \frac{3\left(767-2551\nu-1070\nu^2\right)}{7\left(49-416\nu-652\nu^2\right)}y^3\ ,\end{aligned} \tag{3.62}$$

$$\begin{aligned}\hat{\delta}^{22}_{p^{2\mathrm{PN}}_{r_*}} &= 1 + \frac{66624-84120\nu+300789\nu^2}{41890-69284\nu+536\nu^2}y \\ &- \frac{292601-298528\nu-144464\nu^2}{41890-69284\nu+536\nu^2}y^2 + \frac{7\left(28217+17672\nu-1664\nu^2\right)}{41890-69284\nu+536\nu^2}y^3 \\ &+ \frac{3\left(6473-23284\nu+6856\nu^2\right)}{41890-69284\nu+536\nu^2}y^4\ .\end{aligned} \tag{3.63}$$

We anticipate here that in Sec. 3.3.2 these polynomials in y, especially the various $\hat{t}^{22}_{p^n_{r_*}}(y)$ of the tail factor, will be found to require a suitable resummation process, necessary to make robust the corresponding noncircular corrections in the strong field regime. The same will follow for the subdominant spherical modes of the waveform, in Sec. 3.3.4.

3.2.3 2PN noncircular corrections for the $m = 0$ modes

As mentioned in the previous section, the factorization scheme presented therein cannot be applied successfully to the spherical modes with $m = 0$,

because of the vanishing of their Newtonian factor in the circular limit. Nevertheless, we can still devise a model for them that is well behaved and incorporates the 2PN noncircular waveform information outlined in Sec. 3.2.1. In particular, the alternative to Eq. (3.43) we propose in this case is

$$h_{\ell 0} = \hat{S}_{\rm eff} \left(h_{\ell 0}^{(N,\epsilon)} + \hat{\hat{h}}_{\ell 0} \right), \tag{3.64}$$

where the PN correction, which indeed is fully noncircular, is given by

$$\hat{\hat{h}}_{\ell 0} = T_{\rm 2PN} \left[\frac{h_{\ell 0} - \left(h_{\ell 0}^{(N,\epsilon)}\right)_{\rm EOMs}}{\hat{S}_{\rm eff}} \right]. \tag{3.65}$$

Similarly to the other prescription, this quantity comes out naturally split into an instantaneous and a tail part,

$$\hat{\hat{h}}_{\ell 0} = \hat{\hat{h}}_{\ell 0}^{\rm tail} + \hat{\hat{h}}_{\ell 0}^{\rm inst}. \tag{3.66}$$

Here however it is convenient to express the PN corrections using $(u, p_{r_*}, \dot{p}_{r_*})$ instead of (u, p_{r_*}, p_φ). The reason is that, in this case, writing the corrections in p_φ leads to issues in their numerical evaluation along the EOB dynamics, since they present noncircular combinations of p_φ and u that do not vanish automatically in the circular limit, but need p_φ to be replaced with its corresponding quasi-circular PN expansion in u. Therefore, we remove p_φ in favor of $(u, p_{r_*}, \dot{p}_{r_*})$ by inverting the 2PN-accurate EOB equation of motion of $\dot{p}_{r_*}$, Eq. (2.93).

We report here the corresponding PN corrections for the mode $(2,0)$:

$$\begin{aligned}
\hat{\hat{h}}_{20}^{\rm tail} &= -\frac{\pi}{960u^{10}c^3}\sqrt{\frac{\dot{p}_{r_*}+u^2}{6u}}\Big[960\dot{p}_{r_*}u^{10} + 960\dot{p}_{r_*}^2u^8 + 240\left(-3\dot{p}_{r_*}^3u^6\right.\\
&\left.+p_{r_*}^2\dot{p}_{r_*}u^9\right) + 80u^4\left(7\dot{p}_{r_*}^4 + 2p_{r_*}^4u^6\right) - 5\left(95\dot{p}_{r_*}^5u^2 + 26p_{r_*}^2\dot{p}_{r_*}^3u^5\right.\\
&\left.+11p_{r_*}^4\dot{p}_{r_*}u^8\right) + \left(417\dot{p}_{r_*}^6 + 110p_{r_*}^2\dot{p}_{r_*}^4u^3 - 45p_{r_*}^4\dot{p}_{r_*}^2u^6 + 2p_{r_*}^6u^9\right)\Big] \qquad (3.67)\\
\hat{\hat{h}}_{20}^{\rm inst} &= \frac{1}{14\sqrt{6}u^2c^2}\Big[\dot{p}_{r_*}u^2(-19+\nu) + 3\left(\dot{p}_{r_*}^2 - p_{r_*}^2u^3\right)(3+5\nu)\\
&+ 6p_{r_*}^2\dot{p}_{r_*}u(3+5\nu) + 3p_{r_*}^4u^2(3+5\nu)\Big]\\
&+ \frac{1}{504\sqrt{6}u^3c^4}\Big[\dot{p}_{r_*}u^4\left(1052 - 2803\nu - 53\nu^2\right) + p_{r_*}^2u^5\left(-743 + 7009\nu\right.\\
&\left.-571\nu^2\right) + 3\dot{p}_{r_*}^2u^2\left(545 - 430\nu + 28\nu^2\right) - 3\dot{p}_{r_*}^3\left(79 + 25\nu + 5\nu^2\right)\\
&+ 18p_{r_*}^2\dot{p}_{r_*}u^3\left(81 + 404\nu + 65\nu^2\right) - 9p_{r_*}^2\dot{p}_{r_*}^2u\left(115 + 121\nu + 65\nu^2\right)
\end{aligned}$$

$$+ 6p_{r_*}^4 u^4 \left(79 + 133\nu + 185\nu^2\right) - 9p_{r_*}^4 \dot{p}_{r_*} u^2 \left(151 + 217\nu + 125\nu^2\right)$$
$$- 3p_{r_*}^6 u^3 \left(187 + 313\nu + 185\nu^2\right)\Big]. \tag{3.68}$$

3.3 Waveform validation: test-mass limit

Let us now proceed to assess the performance of our new factorized waveform model, starting from the test-mass case, $\nu \to 0$. As we mentioned multiple times in our presentation of the EOB approach, in Chapter 2, this extreme case has always been of great importance in the development of essentially every aspect of EOB models: on the one hand, because it is closely related, via the EOB approach, to the general case of binary systems with arbitrary mass-ratio ν; on the other hand, because it is much easier to handle from an analytical and numerical point of view. Focusing in particular on the numerical side, in the test-mass limit we have the great advantage of being able to rapidly generate exact waveforms (modulo numerical errors) for essentially *any* dynamics we want, without the need of computationally expensive simulations as in the comparable-mass case. This offers a convenient and flexible methodology to thoroughly test our waveform model and individuate possible paths of improvement. Accordingly, in Sec. 3.3.1 we explore the case of test-mass eccentric insplunges, focusing on the dominant $\ell = m = 2$ mode, and we show the emergent need of adopting specific resummation techniques on our noncircular factors. These are discussed and tested in Sec. 3.3.2 and Sec. 3.3.3, and later extended to higher (ℓ, m) modes in Sec. 3.3.4. In Sec. 3.3.5 we test the 2PN noncircular corrections for the $m = 0$ modes, presented in Sec. 3.2.3, focusing in particular on the mode h_{20}. Finally, in Sec. 3.3.6 we use the flexibility of the test-mass limit to validate our model in the case of dynamical capture dynamics.

3.3.1 Eccentric insplunge in the test-mass limit

Let us start our waveform checks in the test-mass limit with the case of elliptic inspirals . We proceed by following Ref. [215], which extensively explored this limit to validate the waveform prescription of `TEOBResumS-DALI`, indeed now considering also the 2PN noncircular factors at the center of our study. Focusing on the motion of a test particle around a Kerr black hole, such validation procedure relies on comparisons between the analytic EOB waveform and the numerical solution of the Teukolsky equation, obtained using the 2+1 time-domain code `Teukode` [264]. In particular Ref. [215] considered both (i) the geodesic motion along elliptic orbits and (ii) the full transition from the eccentric inspiral up to merger and ringdown. The outcome of that study was that, even without the 2PN corrections, the analytic waveform delivers a rather accurate approximation of the exact waveform up to mild values of

the initial eccentricity, both for its amplitude and phase (see, e.g., Fig. 13 of Ref. [215]).

On our side, we use precisely the expressions for $(\hat{h}_{22}^{\mathrm{nc_{tail}}}, h_{22}^{\mathrm{nc_{inst}}})$ given in Eqs. (3.48) and (3.53) and repeat the comparisons of Ref. [215]. The eccentric numerical waveforms we compare with are listed in Table 3.1. We

Table 3.1: Numerical eccentric simulations considered in our comparisons. We use $\nu = 10^{-3}$ to drive the transition from inspiral to merger. For each eccentric simulation, we report the spin parameter $\hat{a}$, the initial/final values of eccentricity and semilatus rectum, and the merger time t_{mrg}. The final values of eccentricity and semilatus rectum are evaluated at t_s since they are not defined for later times, where t_s is the time when the semilatus rectum equals the separatrix and the radial turning points cease to exist. The definitions of e and p written in terms of the radial turning points can be found in Eq. (3.30), while the separatrix is defined by Eq. (3.31).

$\hat{a}$	e_0	p_0	e_s	p_s	t_s	t_{mrg}
0.0	0.1	6.700	0.107	6.213	1459	1890
0.0	0.3	7.000	0.305	6.611	1382	1731
0.0	0.7	7.700	0.694	7.388	1916	2049
0.0	0.9	8.050	0.891	7.783	4570	4663
−0.4	0.5	8.800	0.501	8.426	2182	2387
0.4	0.5	5.900	0.490	5.415	2092	2192

also recall that the quasi-circular part of the waveform we adopt is precisely the same of Ref. [215]. In Fig. 3.2, we report different configurations aiming at comprehensively covering the parameter space. The first four panels from left to right refer to non-spinning binaries with increasing eccentricity $e_0 = (0.1, 0.3, 0.7, 0.9)$, while the last two panels refer to two spinning binaries with $\hat{a} = \pm 0.4$ and initial eccentricity $e_0 = 0.5$. For low eccentricity, up to $e \simeq 0.3$, the 2PN corrections improve the phase agreement during the inspiral, but for higher eccentricity, the phase of the wave with only Newtonian corrections is more accurate. Moreover, in all the cases, the analytical/numerical agreement visibly deteriorates as one gets closer to plunge and merger, both at the level of the waveform phase and amplitude. Careful analysis of the geodesic case highlights that the reliable behavior of the waveform during the eccentric inspiral is related to *cancellations* between the tail and instantaneous factors. By contrast, the inaccurate behavior of the analytical waveform during the plunge is related to the fact that the quantity $y \equiv p_\varphi^2 u$, which appears everywhere in Eq. (3.48), becomes rather large during the late plunge, as shown in Fig. 3.3. The growth of $p_\varphi^2 u$ makes the eccentric noncircular tail factors too large with respect to the instantaneous ones, and the cancellations mentioned above are no longer possible, leading to the observed loss in accu-

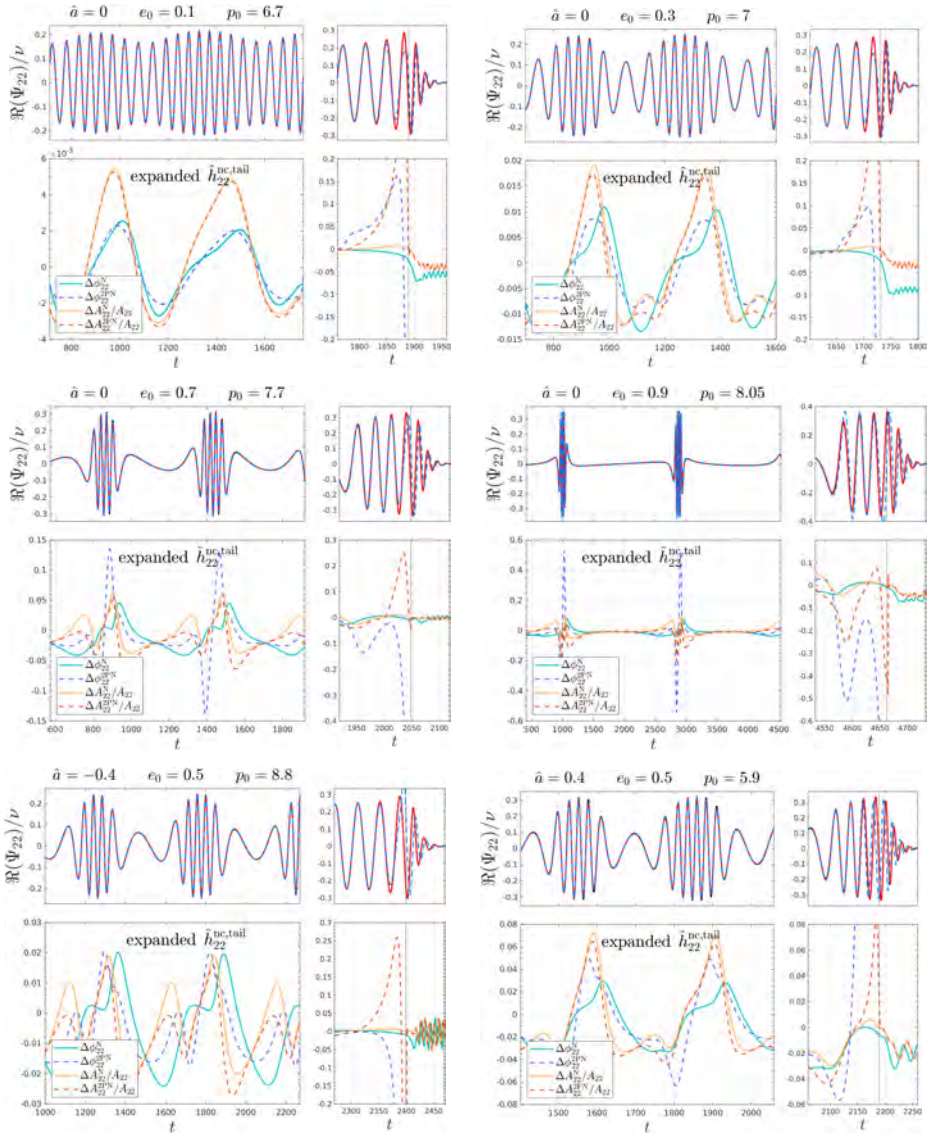

Figure 3.2: Comparisons with *nonresummed* noncircular tail factor: comparing analytical and numerical $\ell = m = 2$ waveforms for the transition from inspiral to plunge of a test particle on a Kerr black hole with spin parameter $\hat{a}$. We consider different orbital configurations, determined by the values of initial eccentricity e_0 and initial semilatus rectum p_0, with $\nu = 10^{-3}$. Each panel displays the numerical waveform (black line, indistinguishable) and two EOB waveforms: (i) the solid-red one, with noncircular information only in the Newtonian prefactor and (ii) the dashed-blue one, with also the noncircular 2PN factor, here without any resummation. The bottom panel shows both the phase differences and the relative amplitude differences with respect to the numerical waveform. We use dashed lines for the differences corresponding to the wave with 2PN corrections. The vertical line marks the merger time, corresponding to the peak of the numerical amplitude.

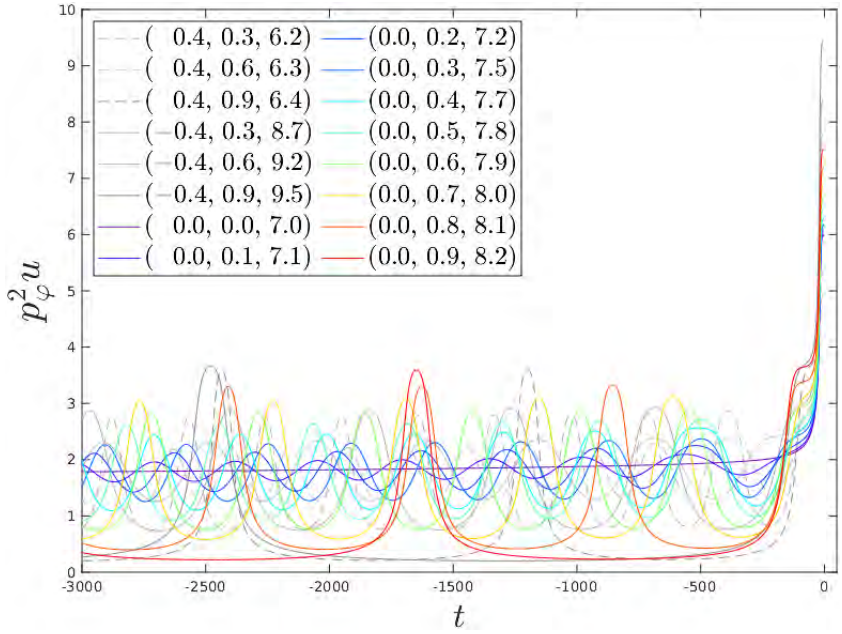

Figure 3.3: Last part of the time evolution of $p_\varphi^2 u$ for different combinations of $(\hat{a}, e_0, p_0)$. Notice that, during the plunge, $p_\varphi^2 u$ can grow up to ~ 10. This growth is mostly responsible for the unacceptably large analytical/numerical phase disagreement during the plunge exhibited by the waveform model with 2PN noncircular corrections, see Fig. 3.2.

racy. This issue is also responsible for the large phase disagreement near the periastra of configurations with high eccentricity.

To cure this behavior, we need to implement specific resummation strategies, which will discuss in the following.

3.3.2 Resummation of the noncircular tail factor

Let us start this section by going back to the structure of the tail factor for $\ell = m = 2$. In its native form, it is a 1.5PN order term that is expanded in eccentricity up to e^6. We have seen above that this expansion in eccentricity, after the factorization of the Newtonian contribution, can be recast in a rational function of (u, p_r, p_φ), see e.g. Eq. (3.48). In particular, the expansion in the eccentricity e can be rewritten as an expansion in the radial momentum p_r and $\dot{p}_r$, which can be subsequently recast in a form where one can single out several polynomials in $y \equiv p_\varphi^2 u$ that are all, formally, at *Newtonian order*. Figure 3.3 shows the behavior of y versus time for different eccentric configurations: y *is not* a small quantity.[11] For the non-spinning configurations

[11] Note that $y = p_\varphi^2 u = 1$ at Newtonian order and for circular orbits, since $p_\varphi^{\mathrm{N,circ}} = 1/\sqrt{u}$.

considered in Fig. 3.3, it oscillates between 0 and 4 during the eccentric inspiral and may reach values ~ 7 approaching merger. We thus wonder whether an argument that can be so large may eventually generate some nonphysical behavior for the functions $(\hat{t}^{22}_{p_{r_*}}, \hat{t}^{22}_{p^3_{r_*}}, \hat{t}^{22}_{p^2_{r_*}}, \hat{t}^{22}_{p^4_{r_*}})$, especially given the fact that they stem from an expansion in eccentricity within a PN expansion.

As an example, Fig. 3.4 shows various truncations of $\hat{t}^{22}_{p_{r_*}}$. One sees that

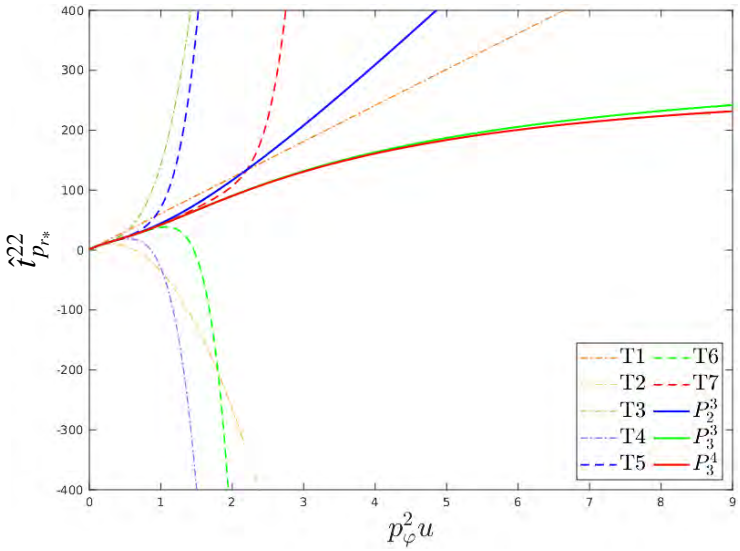

Figure 3.4: Behavior of various truncations and several Padé resummation for the polynomial $\hat{t}^{22}_{p_{r_*}}$, appearing in Eq. (3.49). Tn represents a truncation at y^n. The various truncations of $\hat{t}^{22}_{p_{r_*}}$ oscillate and become very large for values of $p^2_\varphi u$ of the order of those reached during the plunge; see Fig. 3.3. A straightforward diagonal Padé approximant (P^3_3 or P^4_3) tapers the behavior of the polynomial in strong field and eventually improves the performance of the noncircular factor where it appears.

(i) the various polynomial truncations become very large for values of y of the order of those of the late inspiral and (ii) the sign alternation gives an oscillatory behavior that visually resembles the one that is typically observed for the truncated PN expansions of the energy flux of a test particle orbiting a Schwarzschild black hole on circular orbits; see e.g. Ref. [116]. On the basis of this analogy, and with the understanding that $\hat{t}^{22}_{p_{r_*}}$ is the product of an expansion in the eccentricity (or in p_{r_*} and $\dot{p}_r$), we *interpret* the polynomial expression of $\hat{t}^{22}_{p_{r_*}}$ as the *truncated expansion* of an unknown function of y around $y = 0$. As such, this function can be resummed, and we do it straightforwardly by applying Padé approximants. In Fig. 3.4 we also exhibit several (diagonal

or nearly diagonal) Padé approximant that resum different truncations of this polynomial. The Padé stabilizes the truncated series (e.g. the results obtained resumming the truncation up to y^6 is close to the Padé of the full polynomial up to y^7) and considerably lowers the value it reaches after $y \simeq 3$, in particular with respect to the full nonresummed polynomial (T7 in Fig. 3.4). Although we do not have a formal proof, the consistency between the P^3_2, P^3_3, and P^4_3 approximants seems to suggest that the residual polynomial $\hat{t}^{22}_{p_{r_*}}$ is indeed the Taylor expansion of some unknown function and its resummation does make sense. A completely analogous behavior is found for the other three polynomial functions ($\hat{t}^{22}_{p^3_{r_*}}, \hat{t}^{22}_{p^2_{r_*}}, \hat{t}^{22}_{p^4_{r_*}}$), which are thus similarly resummed. More specifically, the Padé approximants we consider to replace the Taylor-expanded polynomials of the tail factor are ($P^4_3[\hat{t}^{22}_{p_{r_*}}], P^4_4[\hat{t}^{22}_{p^3_{r_*}}], P^4_3[\hat{t}^{22}_{p^2_{r_*}}], P^4_4[\hat{t}^{22}_{p^4_{r_*}}]$). The quality of this resummation is probed in Fig. 3.5, which is the analog of Fig. 3.2 in which the polynomials in the noncircular tail factor have been Padé resummed as clarified above. The analytical/numerical phase agreement not only improves (and largely) during the plunge and merger phase, but also improves during the eccentric inspiral. Moreover, the overall improvement with respect to the simple Newtonian prefactor is evident, and there is no longer any hint of pathological behaviors towards merger.

3.3.3 Resummation of the noncircular instantaneous factor

A priori, the same resummation strategy should be implemented for the residual instantaneous 2PN corrections, which present as well expressions where one can single out polynomials in y with alternate signs. We explored this both at the level of the amplitude and phase corrections, $f^{\rm nc_{inst}}_{22}$ and $\delta^{\rm nc_{inst}}_{22}$. For the amplitude, we found that any choice of Padé approximant for the various residual polynomials in y of Eq. (3.54) develops spurious poles in the equal-mass case (i.e. for $\nu = 1/4$), implying that our resummation strategy cannot be pursued here.[12] This is not of great concern, since the generic Newtonian prefactor alone already gives an excellent approximation to the numerical waveform amplitude. This can be clearly seen in Fig. 3.5, where the amplitudes, with and without 2PN noncircular corrections, are seen to produce analytical/numerical relative differences that are comparable.

By contrast, for the instantaneous residual noncircular phase given in Eq. (3.55) the procedure is robust. More precisely, we resum the polynomials in y appearing in Eq. (3.55) with the Padé approximants $P^1_0[\hat{\delta}^{22}_{u^{\rm 1PN}}]$, $P^1_1[\hat{\delta}^{22}_{p^{\rm 1PN}_{r_*}}]$, $P^1_2[\hat{\delta}^{22}_{u^{\rm 2PN}}]$, and $P^1_1[\hat{\delta}^{22}_{p^{\rm 2PN}_{r_*}}]$. Note that the polynomial $\hat{\delta}^{22}_{p^{\rm 2PN}_{r_*}}$, written explicitly in Eq. (3.63), is of degree four in y, but we only use $O(y^2)$ terms since the P^2_1 approximant produces unphysical behaviors for large y and the other higher-order Padé approximants have spurious poles in the equal-mass

[12] This is the current situation with the 2PN-accurate noncircular waveform. The procedure will have to be investigated again in the future using results at 3PN order.

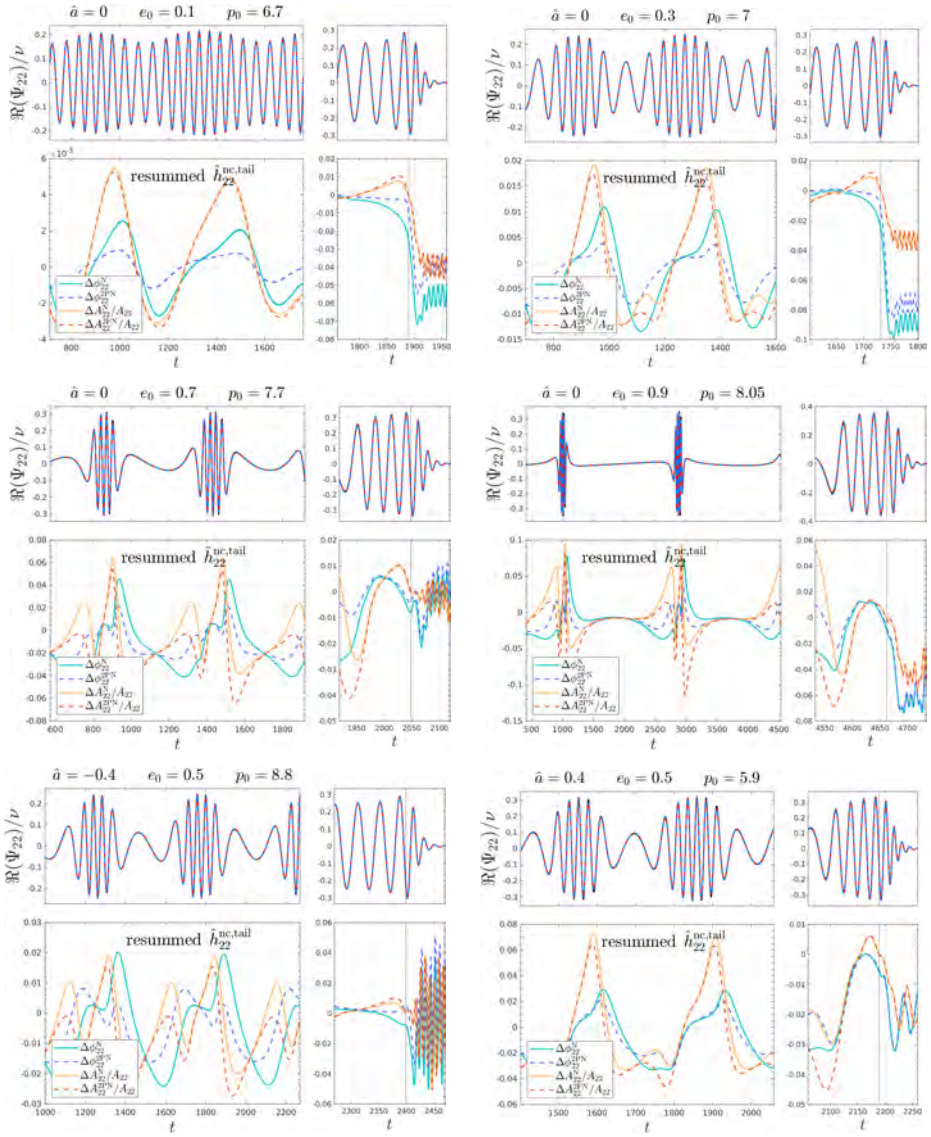

Figure 3.5: Comparisons with *resummed* noncircular tail factor: comparing analytical and numerical $\ell = m = 2$ waveforms for the transition from inspiral to plunge of a test particle on a Kerr black hole with spin parameter $\hat{a}$. We consider different orbital configurations with $\nu = 10^{-3}$. Each of the top panels displays the numerical waveform (black line, indistinguishable) and two EOB waveforms: (i) the solid-red one, with noncircular information only in the Newtonian prefactor and (ii) the dashed-blue one, with noncircular 2PN corrections that include the tail factor $\hat{h}_{22}^{\rm nc_{tail}}$ of Eq. (3.48) in the *resummed* form introduced in Sec. 3.3.2. The bottom panel shows both the phase differences and the relative amplitude differences with respect to the numerical waveform. We use dashed lines for the differences corresponding to the wave with 2PN corrections. The vertical line marks the merger time, corresponding to the peak of the numerical amplitude. The resummation strongly improves the analytical/numerical agreement with respect to Fig. 3.2.

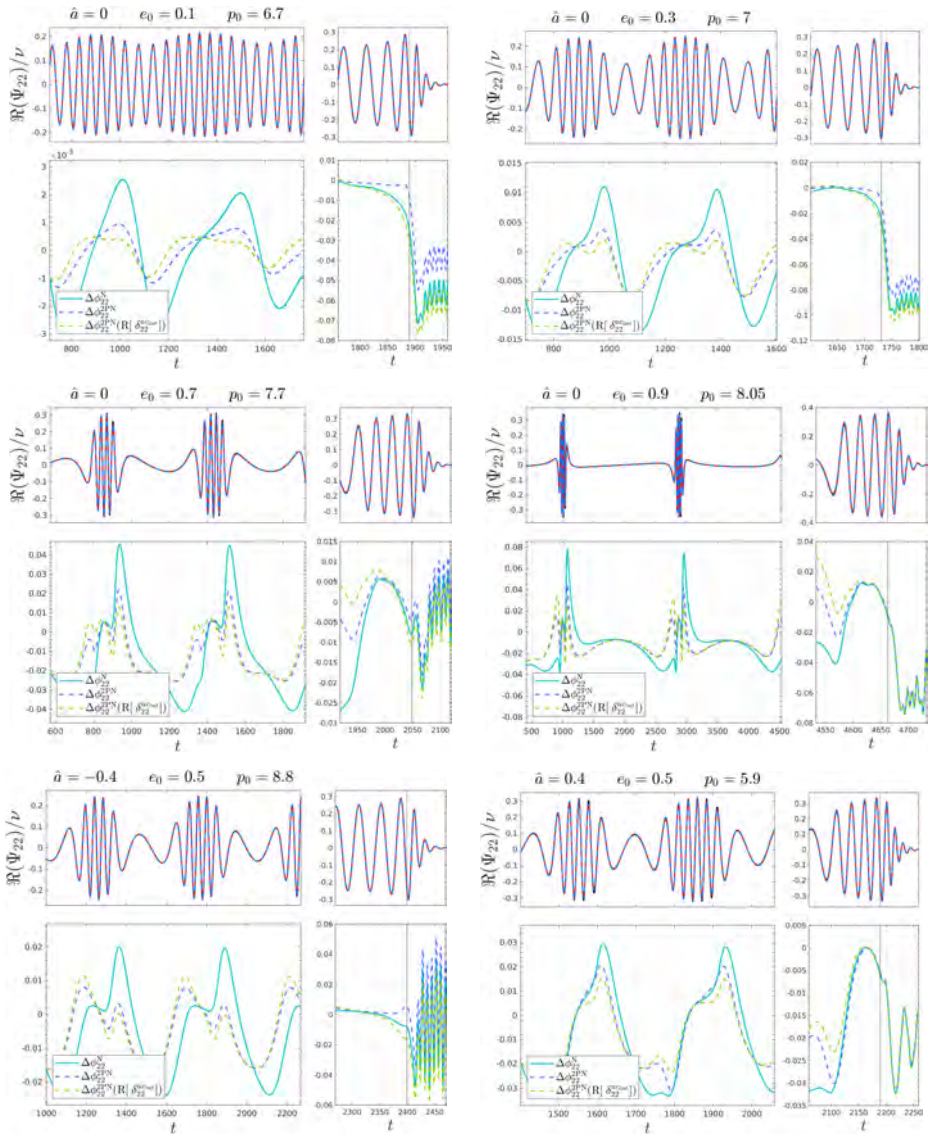

Figure 3.6: Same configurations of Fig. 3.5, but here we focus on the phase, and we show also the analytical/numerical agreement obtained considering the resummed noncircular tail and the resummed instantaneous noncircular correction (dashed light green line). The color scheme of the other differences is the same of Fig. 3.5: solid light blue line for the wave with only the generic Newtonian prefactor and dashed blue line for the wave with 2PN corrections with resummed tail and Taylor-expanded instantaneous corrections.

case. The improvements introduced by this resummation are shown in Fig. 3.6, where we compare the analytical/numerical phase differences of the waveforms with and without the resummations of the polynomials in $\delta_{22}^{\mathrm{nc}_{\mathrm{inst}}}$, while always adopting the resummed version of the noncircular tail factor. While a slight improvement in the phase accuracy can be seen in the reported cases,[13] the resummation of the instantaneous phase corrections appears to be less relevant than the resummation of the eccentric tail.

As noted in previous works [215, 254], the general Newtonian prefactor is quite effective in capturing the eccentric modulation of the waveform, both in amplitude and phase. As a consequence, the missing analytical information we are adding here is bound to bring rather tiny corrections, so that special resummation procedures become essential to make the 2PN noncircular correcting factors really useful. By separately analyzing the cumulative action of the instantaneous and hereditary contributions to the waveform, one finds that the good performance of our resummed waveform is due to *compensations* between the two. This eventually yields only a tiny correction to the Newtonian noncircular prefactor. More importantly, one notices that the instantaneous contributions alone tend to *overestimate* the analytical phase, eventually yielding phase differences, with respect to the numerical waveform, that are *larger* than those obtained with the simple Newtonian prefactor. This is very clear when inspecting Fig. 3.7, which illustrates this effect for four different geodesic configurations (i.e. with $\hat{\mathcal{F}}_r = \hat{\mathcal{F}}_\varphi = 0$): $(e, p) = (0.3, 9), (0.5, 9), (0.9, 9), (0.9, 13)$. Indeed, at high eccentricity and relatively small semilatus rectum, the resummation of the tail factor is a crucial aspect in order to have a compensation between instantaneous and hereditary terms. The benefits of the resummation can be seen even at milder eccentricities or larger semilatera recta, even if it is less pronounced. In Fig. 3.8, we also show the effect of resumming the polynomials in the instantaneous factors for the same configurations considered in Fig. 3.7. While the effect of the resummation is clearly visible, it is also evident that the resummation of the instantaneous factors is less significant than that of the tail factor.

3.3.4 Resummed noncircular corrections for the subdominant modes

The resummation procedure we just outlined can be similarly applied to the 2PN noncircular corrections of the other waveform modes, whose expressions are collected in Appendix C.1, notably in the form that we get before any resummation is applied. Here we specifically discuss resummations and analytical/numerical comparisons for the (ℓ, m) modes $(2, 1)$, $(3, 3)$, $(3, 2)$ and $(4, 4)$. We choose this illustrative set by observing that, at 2PN order, while for the modes $(2, 1)$ and $(3, 3)$ the noncircular tail contribution is present, for

[13] The only exception is the $\hat{a} = -0.4$ case, but bear in mind that we are not including spin terms in the noncircular corrections.

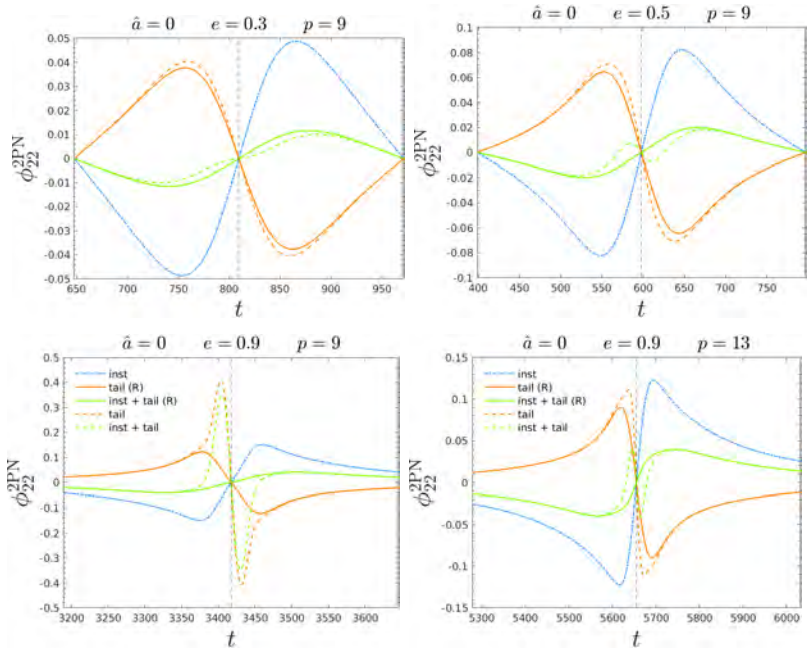

Figure 3.7: Instantaneous and hereditary noncircular 2PN corrections to the quadrupolar phase for four non-spinning geodesic cases $(e,p) = (0.3,9),(0.5,9),(0.9,9),(0.9,13)$. The instantaneous phase corrections are shown with dot-dashed blue lines, while the orange lines are for the phase contributions of the resummed eccentric tail (dashed for the expanded results and solid for the resummed ones). The corresponding sums between instantaneous and tail terms are shown in green with the same line style scheme for the expanded and resummed version. The vertical dashed line marks the periastron passage. For $e = 0.9$, we do not show the whole radial period in order to highlight the neighborhood of the periastron.

the modes $(3,2)$ and $(4,4)$ it is absent, since it would appear as a 2.5PN term in the complete waveform. This has implications on the performance of the respective noncircular corrections, as we will see below. To make the discussion clearer, it is convenient to rewrite here explicitly the tail factors at 2PN order for the modes $(2,1)$ and $(3,3)$:

$$\begin{aligned}\hat{h}^{\rm nc_{tail}}_{21} &= 1+\frac{1}{c^3}\pi\Bigg[-i\left(\frac{3029}{1920}up_{r_*}\,\hat{t}^{21}_{p_{r_*}}+\frac{619}{576}p^3_{r_*}\,\hat{t}^{21}_{p^3_{r_*}}\right)+\frac{635}{768}\frac{p^2_{r_*}}{p_\varphi}\,\hat{t}^{21}_{p^2_{r_*}}\\ &\quad-\frac{61}{256}\frac{p^4_{r_*}}{p_\varphi u}\,\hat{t}^{21}_{p^4_{r_*}}\Bigg],\\ \hat{h}^{\rm nc_{tail}}_{33} &= 1+\frac{1}{c^3}\frac{\pi}{p^2_\varphi\left(7+2p^2_\varphi u\right)^2}\Bigg[-i\left(\frac{4763}{384}p_{r_*}\hat{t}^{33}_{p_{r_*}}\right.\end{aligned} \tag{3.69}$$

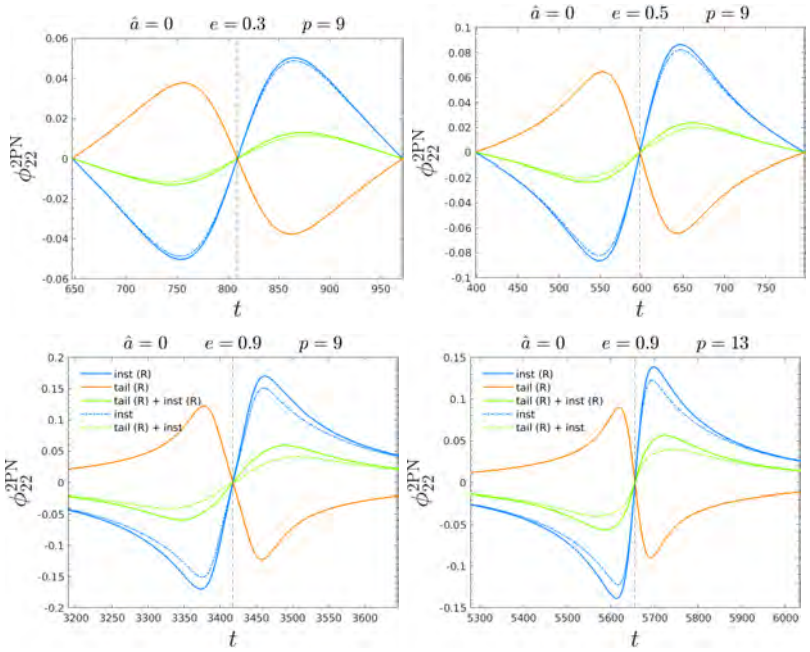

Figure 3.8: Analogous to Fig. 3.7, but here we focus on the relevance of the resummation for the instantaneous part. The orange solid line is the phase contribution of the resummed eccentric tail, while the blue lines correspond to the instantaneous phase contributions, solid when they are resummed and dot-dashed when they are not. The corresponding sums between tail and instantaneous contributions are shown in green with the same line style scheme. The vertical dashed line marks the periastron passage. For $e=0.9$, we do not show the whole radial period in order to highlight the neighborhood of the periastron.

$$
\begin{aligned}
&- \frac{4763}{24}\frac{p_\varphi^2 p_{r_*}^3}{p_\varphi^2 u^2\left(7+2p_\varphi^2 u\right)^2}\,\hat{t}^{33}_{p^3_{r_*}}\Big) + \frac{4763}{96}\frac{p_{r_*}^2}{p_\varphi u\left(7+2p_\varphi^2 u\right)}\,\hat{t}^{33}_{p^2_{r_*}} \\
&+ \frac{4763}{6}\frac{p_\varphi^3 p_{r_*}^4}{p_\varphi^3 u^3\left(7+2p_\varphi^2 u\right)^3}\,\hat{t}^{33}_{p^4_{r_*}}\Big],
\end{aligned}
\tag{3.70}
$$

where

$$\hat{t}^{21}_{p_{r_*}} = 1 + \frac{6035y}{3029} - \frac{10870y^2}{3029} + \frac{8350y^3}{3029} - \frac{3215y^4}{3029} + \frac{511y^5}{3029}, \tag{3.71}$$

$$\hat{t}^{21}_{p^2_{r_*}} = 1 - \frac{1388y}{635} + \frac{666y^2}{635} - \frac{92y^3}{635} - \frac{13y^4}{635}, \tag{3.72}$$

$$\hat{t}^{21}_{p^3_{r_*}} = 1 - \frac{981y}{619} + \frac{573y^2}{619} - \frac{115y^3}{619}, \tag{3.73}$$

$$\hat{t}^{21}_{p^4_{r_*}} = 1 - \frac{82y}{183} - \frac{17y^2}{183}, \tag{3.74}$$

$$\hat{t}^{33}_{p_{r_*}} = 1 + \frac{67183y}{23815} + \frac{721737y^2}{47630} - \frac{85973y^3}{9526} + \frac{30812y^4}{4763} - \frac{10722y^5}{4763} + \frac{16769y^6}{47630} - \frac{337y^7}{47630}, \tag{3.75}$$

$$\hat{t}^{33}_{p^3_{r_*}} = 1 + \frac{3125521y}{762080} + \frac{5675333y^2}{762080} - \frac{2623521y^3}{69280} + \frac{3513777y^4}{95260} - \frac{2943211y^5}{152416} + \frac{7128059y^6}{762080} - \frac{2725303y^7}{762080} + \frac{35247y^8}{95260} + \frac{5233y^9}{95260}, \tag{3.76}$$

$$\hat{t}^{33}_{p^2_{r_*}} = 1 + \frac{1407963y}{381040} - \frac{343943y^2}{47630} + \frac{2036583y^3}{95260} - \frac{271775y^4}{19052} + \frac{602219y^5}{76208} - \frac{268357y^6}{95260} + \frac{85037y^7}{190520} + \frac{918y^8}{23815}, \tag{3.77}$$

$$\hat{t}^{33}_{p^4_{r_*}} = 1 + \frac{858779y}{190520} + \frac{92901791y^2}{6096640} + \frac{66769y^3}{7040} - \frac{94475723y^4}{1219328} + \frac{9400891y^5}{152416} - \frac{82481269y^6}{3048320} + \frac{17880961y^7}{1524160} - \frac{6096411y^8}{1524160} + \frac{2935y^9}{13856} + \frac{4009y^{10}}{76208}. \tag{3.78}$$

Each of these polynomials in y is resummed using Padé approximants: the choices we made are summarized in Table 3.2. The results of this procedure for

Table 3.2: Padé used for the resummation of the tail 2PN noncircular corrections for the modes $(2,2)$, $(2,1)$, and $(3,3)$. Note that $\hat{t}^{33}_{p^3_{r_*}}$ has terms up to y^8, but we use the Padé P^3_2.

	Selected Padé			
(ℓ, m)	$\hat{t}^{\ell m}_{p_{r_*}}$	$\hat{t}^{\ell m}_{p^2_{r_*}}$	$\hat{t}^{\ell m}_{p^3_{r_*}}$	$\hat{t}^{\ell m}_{p^4_{r_*}}$
$(2,2)$	P^4_3	P^4_3	P^4_4	P^4_4
$(2,1)$	P^2_3	P^1_3	P^0_3	P^2_0
$(3,3)$	P^4_3	P^5_4	P^3_2	P^5_5

the modes $(2,1)$ and $(3,3)$ are collected in Fig. 3.9, which compares analytical and numerical waveforms for an illustrative, but significative, set of configurations. The same is done in Fig. 3.10 for the modes $(3,2)$ and $(4,4)$. When analyzing the phasing during the inspiral, a few comments are in order. First, the phase and amplitude agreement for the modes $(2,1)$ and $(3,3)$ is in this case comparable to the $(2,2)$ mode, and the 2PN corrections are found to yield a notable reduction of the analytical/numerical phase difference with respect to the simple Newtonian prefactor prescription. This is true for any value of the eccentricity considered. When moving to the modes $(3,2)$ and $(4,4)$, one

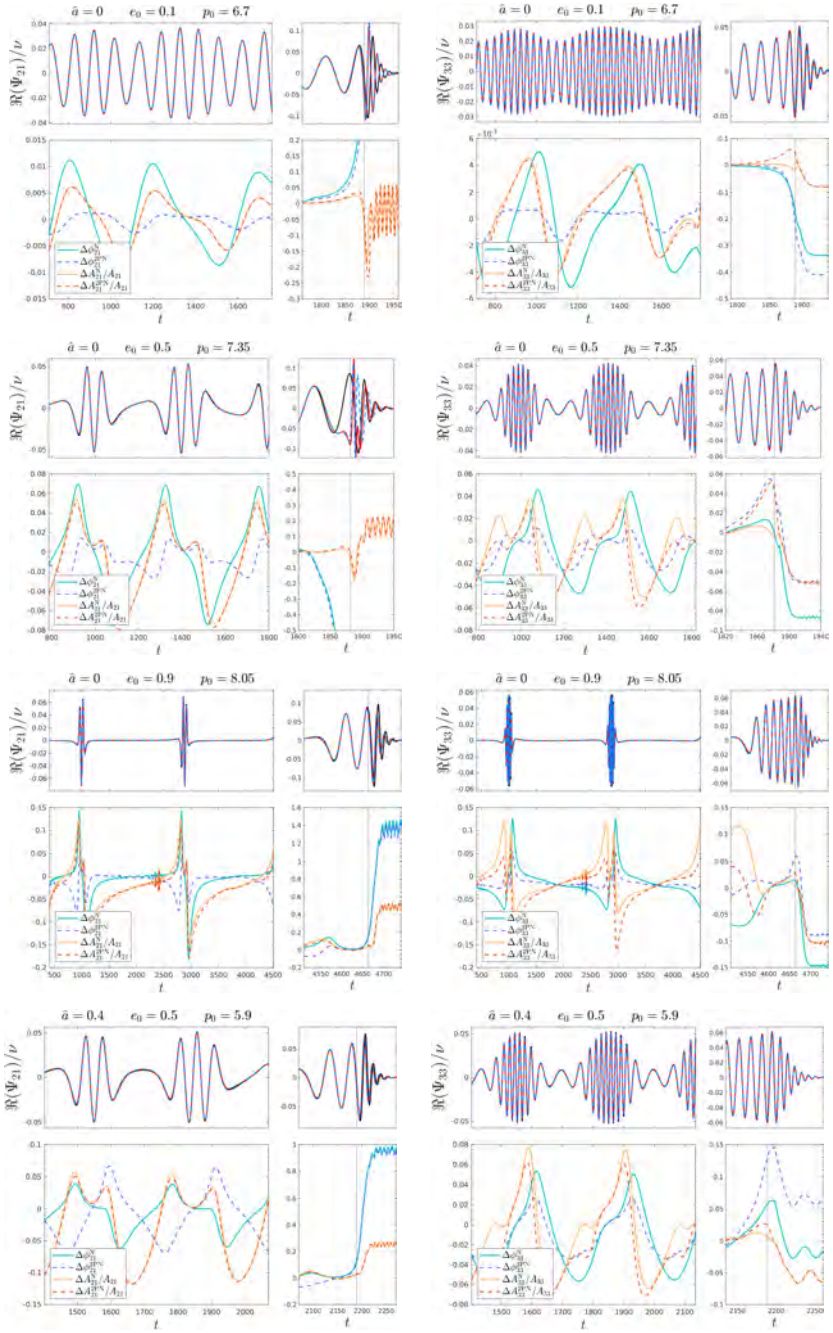

Figure 3.9: Same type of plots (and same color scheme) of Fig. 3.5, but here we collect in different columns our test-mass results for the subdominant modes (2,1) and (3,3), for the illustrative configurations $(e_0, \hat{a}, p_0) = (0.1, 0, 6.7), (0.5, 0, 7.35), (0.9, 0, 8.05), (0.5, 0.4, 5.9)$.

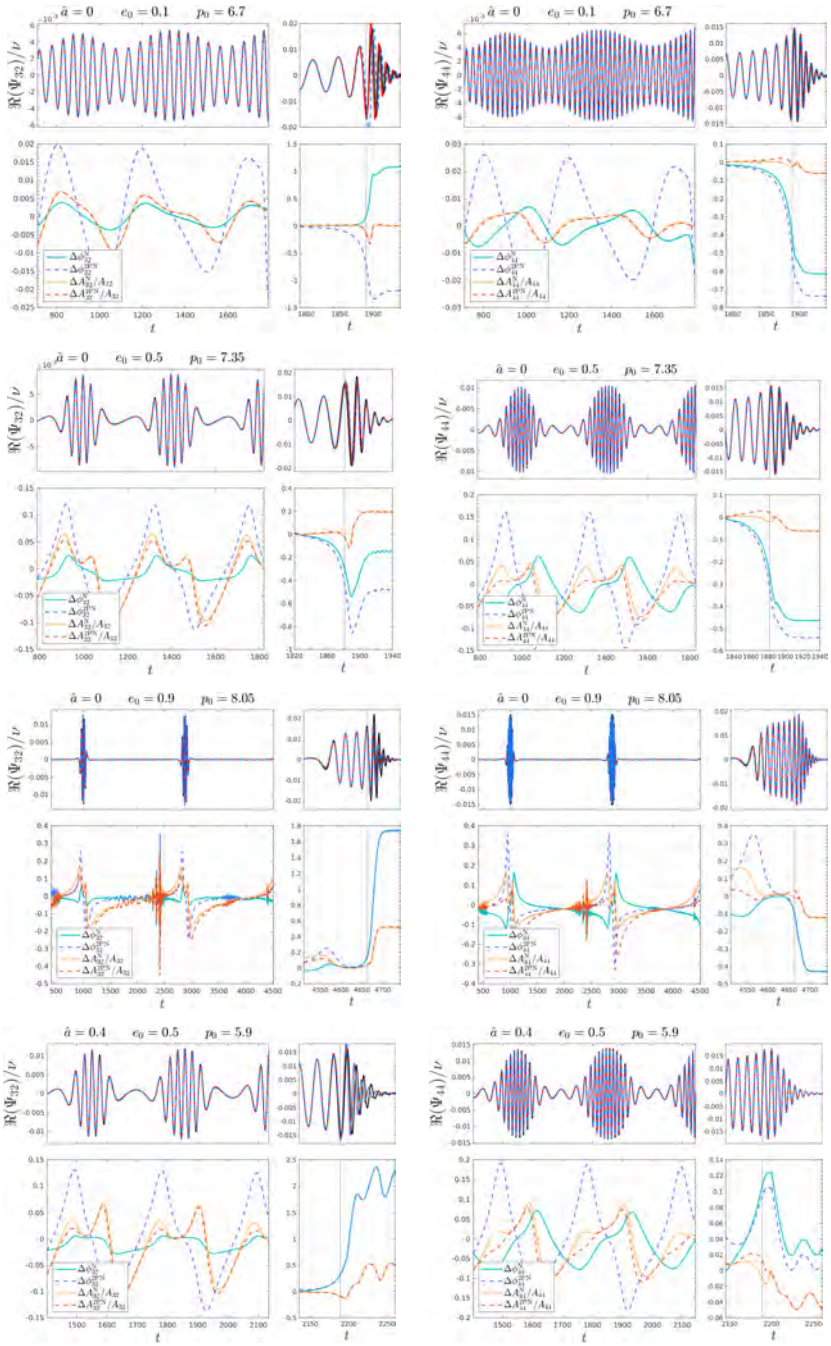

Figure 3.10: Same plots of Fig. 3.9 for the subdominant modes (3,2) and (4,4).

observes instead the rather surprising evidence that the waveforms with 2PN noncircular corrections perform *worse* than the ones without. In light of our above analysis regarding the compensation between tail and instantaneous factors, we understand this result as a consequence of the fact that these modes do not have a tail factor at 2PN order, in contrast to what happens for the modes $(2,2)$, $(3,3)$, and $(2,1)$, where the aforementioned compensation can take place. A confirmation of this interpretation can be found in Fig. 3.11, where we analyze an exemplifying orbital configuration with $e_0 = 0.7$.

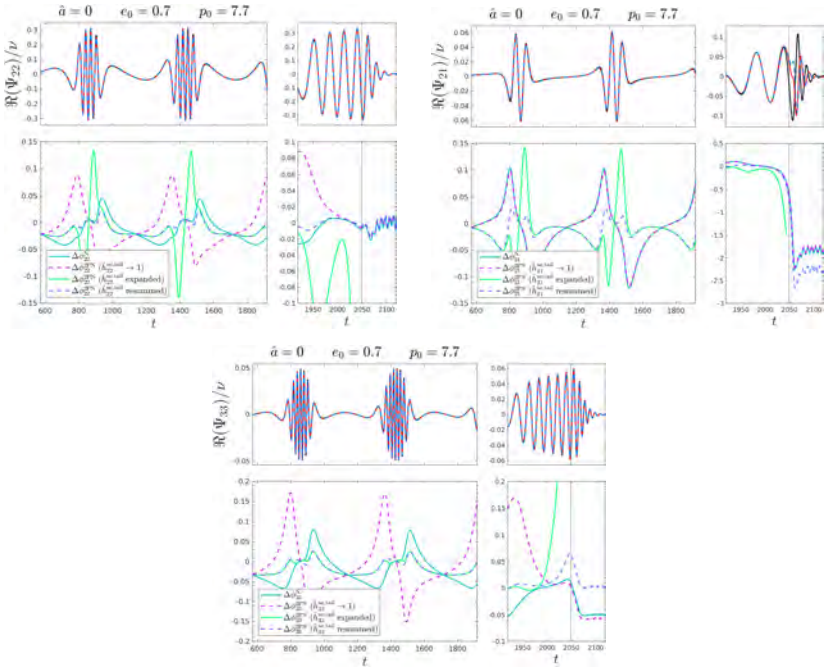

Figure 3.11: Comparisons of the waveform modes (2,2), (2,1), and (3,3) for the non-spinning configuration $(e_0, \hat{a}, p_0) = (0.7, 0, 7.7)$. Top panels: numerical waveforms (solid black line), analytical waveforms with only Newtonian noncircular corrections (solid red line), and analytical waveforms with complete 2PN noncircular corrections, with the resummed eccentric tail factor (dashed blue line). Bottom panels: analytical/numerical phase differences (in radians) for different prescriptions: (i) Newtonian noncircular corrections only (solid light blue line); (ii) with the addition of the 2PN instantaneous noncircular corrections without noncircular tail factor (dashed purple line); (iii) waveform with the complete 2PN noncircular corrections, with instantaneous and tail terms in expanded form (solid aqua-green line); and (iv) waveform with the complete 2PN noncircular corrections, with tail terms in resummed form (dashed blue line). Notice the huge impact of the resummed tail factor in the PN noncircular corrections.

Qualitatively, including noncircular waveform result up to at least the

2.5PN order, the same behavior should be found also for the modes $(3,2)$ and $(4,4)$. Future work, which aims at incorporating noncircular corrections at higher PN orders in our factorized and resummed waveform, will hopefully clarify these issues.

3.3.5 Testing the noncircular corrections for the $m = 0$ modes

In Sec. 3.2.3, we have already pointed out that we have to use an alternative factorization for the modes with $m = 0$. In Fig. 3.12, we test the factorization proposed in Eq. (3.43) for different geodesic configurations around a Schwarzschild black hole, in the case of the mode $(2,0)$. As one can see, the

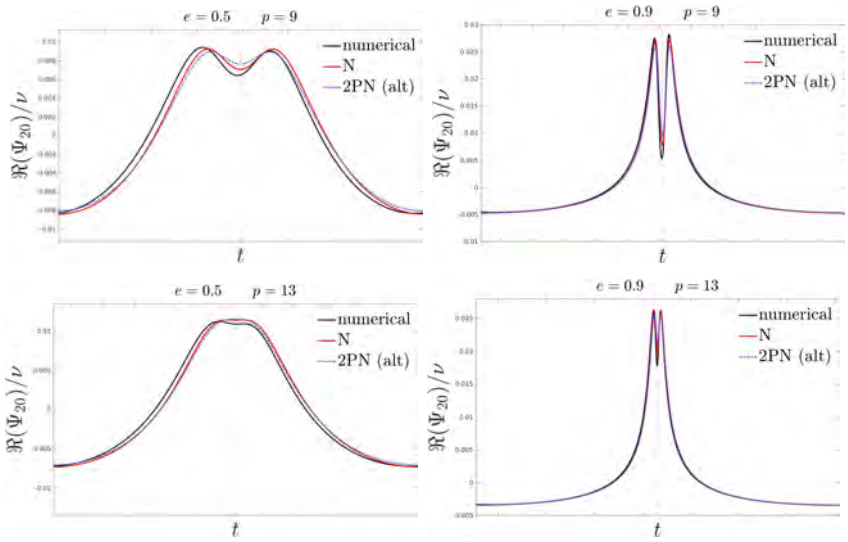

Figure 3.12: Comparisons for the mode $(2,0)$ on non-spinning geodesic orbits with $e = (0.5, 0.9)$ and $p = (9, 13)$. We show the numerical waveform (solid black line), the EOB waveform with noncircular corrections only at the Newtonian level (solid red line), and the one with corrections at 2PN order as discussed in Sec. 3.2.3 (dashed blue line).

agreement between numerical and analytical results is still qualitatively good, even if the accuracy reached by the $m \neq 0$ modes discussed above is evidently higher. Here, in addition to the different factorization scheme, a source of disagreement is that the asymmetry of the $m = 0$ numerical modes with respect to the apastron is not negligible, even for geodesic dynamics. In any case, for the $m = 0$ modes, the 2PN corrections do not seem to bring a definite improvement over the analytical waveform with only the generic Newtonian prefactor.

3.3.6 Dynamical captures in the test-mass limit

We now turn our attention to the case of *dynamical*, or *hyperbolic*, captures. In particular, we consider the same dynamical configurations that appear in Fig. 14 of Ref. [215], whose parameters are also listed in Table 3.3 below. The analytical/numerical comparisons for the new prescriptions, compared

Table 3.3: Reference hyperbolic capture configurations in the large-mass-ratio limit. The symmetric mass ratio used to drive the dynamics is $\nu = 10^{-2}$. For each configuration, we report the Kerr dimensionless spin parameter $\hat{a}$, the initial energy E_0, the initial angular momentum $p_{\varphi,0}$, the initial separation r_0, the number of peaks of the orbital frequency $N_\Omega^{\rm peaks}$, and the merger time $t_{\rm mrg}$.

$\hat{a}$	E_0	$p_{\varphi,0}$	r_0	$N_\Omega^{\rm peaks}$	$t_{\rm mrg}$
0	1.000711	4.01	120	2	2133
0	1.000712	4.01	120	1	819
0	1.001240	4.01	120	1	731

with the original Newtonian case, are shown in Fig. 3.13. We report both the waveforms with expanded and resummed instantaneous noncircular phase at 2PN order. We also recall that, in the hyperbolic case, the parameters of the ringdown model, the NQC corrections, and the merger time are extracted directly from the numerical waveform. This is due to the fact that a fit over the parameter space of these quantities is not currently available; see Sec. VC of Ref. [215] for further details. For this reason, the last part of the waveform is artificially more accurate than what we would have obtained with the same fitting procedure adopted for eccentric orbits. Nonetheless, this aspect is not very relevant for our discussion since, in order to test the reliability of the 2PN corrections, one should focus on the inspiral and plunge parts of the waveform. The phase differences of Fig. 3.13 show that, in this hyperbolic scenario, the 2PN noncircular corrections do not provide a remarkable improvement in the analytical/numerical agreement with respect to the original waveform of `TEOBResumS-DALI`. Moreover, the resummation of the instantaneous noncircular phase factor seems here to worsen the analytical/numerical agreement of the wave with respect to the one where such factor is left in expanded form. This may be an indication that the resummation of the instantaneous phase is not uniformly reliable in every corner of the parameter space and hence, considering the small effect it has in the elliptic inspiral case, that it may be preferable to just avoid it. We hope that adding noncircular analytical information beyond the 2PN order may conclusively clarify whether this particular resummation is convenient or not.

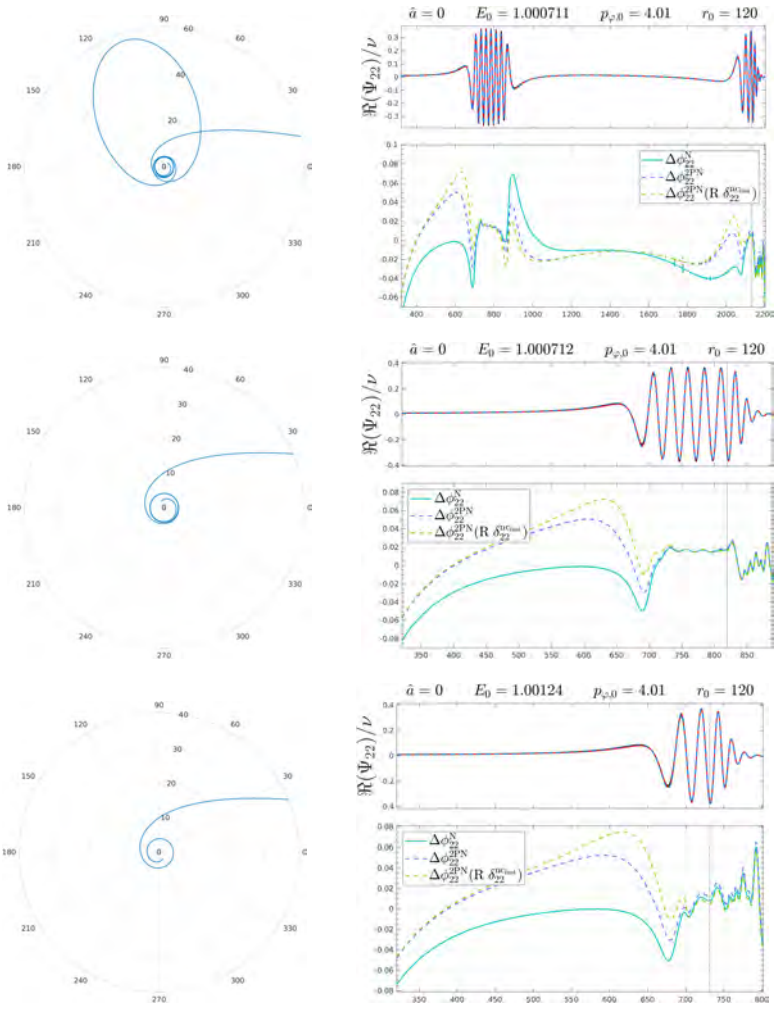

Figure 3.13: Dynamical captures of a particle on a Schwarzschild black hole with $\nu = 10^{-2}$, initial angular momentum $p_{\varphi,0} = 4.01$, and three different initial energies, $E_0 = (1.000711, 1.000712, 1.00124)$. Left column: relative trajectories, all starting from $r_0 = 120$, although the plot only focuses on the last part before the capture. Right column: In the upper panels we compare the real part of the numerical waveform (black line, barely distinguishable) with two analytical waveforms: the one with only the Newtonian noncircular factor (red line) and the one with the 2PN corrections where the tail factor is resummed while the instantaneous factor is not (dashed blue line). The corresponding phase differences are reported in the bottom panels (solid clear blue and dashed blue lines, respectively). The same panels also show the analytical/numerical phase difference obtained with the resummation applied to *both* the tail and the instantaneous 2PN noncircular phase $\delta_{22}^{\mathrm{nc_{inst}}}$ (dashed green line). The parameters of the ringdown and of the next-to-quasi-circular corrections, as well the merger time (marked by the vertical line), are extracted from numerical data, as in Ref. [215]. The closest analytical/numerical agreement is observed when only the noncircular tail factor is resummed.

3.4 Waveform validation: the comparable-mass case

Let us now shift our focus on comparable-mass binaries. In this case, we incorporate our 2PN-improved noncircular waveform within the EOB eccentric model of Ref. [157], which is currently the latest avatar of `TEOBResumS-DALI`. In doing so, we keep the same dynamics, informed by NR quasi-circular simulations, of Ref. [157]. The 2PN noncircular corrections to the waveform have an essentially negligible impact on quasi-circular configurations and it is not worth to provide a new, optimized, determination of (a_6^c, c_3) using the 2PN resummed waveform. Under these conditions, we explore here the performance of our new waveform model with both time-domain (phase-alignment) and frequency-domain (unfaithfulness) comparisons, reported respectively in Sec. 3.4.1 and Sec. 3.4.2.

3.4.1 Phase comparisons in the time domain

Let us consider first the time-domain phasing comparisons with the 28 public eccentric datasets of the SXS catalog [239]. We have 20 non-spinning datasets, with initial nominal eccentricities up to 0.3, and 8 spin-aligned datasets. Ref. [155] presented specific analyses of these data, aimed at complementing the information available in previous work [239], in particular (i) computing a gauge-invariant estimate of the eccentricity during the evolution and (ii) giving two different estimates on the NR uncertainty from the two highest resolutions available. For completeness, the datasets we consider are listed in Table 3.4. The table reports the time-domain phase uncertainty at merger $\delta\phi^{\rm NR}_{\rm mrg}$ as well as the analogous quantities for the unfaithfulness $\bar{F}^{\rm max}_{\rm NR/NR}$ on Advanced LIGO noise, as detailed in Ref. [155], according to the definitions that we will recall below in Sec. 3.4.2. Table 3.4 also reports, for each configuration, the parameters $(e^{\rm EOB}_{\omega_a}, \omega^{\rm EOB}_a)$ used to initialize each EOB evolution at apastron (see Refs. [155, 254]). These values are updated with respect to previous works, as they are determined by inspecting the EOB/NR phase difference in the time domain and are tuned manually so to reduce as much as possible the difference between EOB and NR instantaneous GW frequencies [155]. Let us note that our procedure for setting up initial data can be optimized. On the one hand, the manual procedure for determining $(e^{\rm EOB}_{\omega_a}, \omega^{\rm EOB}_a)$ could have been automatized. On the other hand, the initial conditions we use are the analogous of the adiabatic initial conditions for circular orbits. As such, they do not reduce to the (iterated) postadiabatic ones [147, 265] in the quasi-circular limit, and some spurious eccentricity would be present in that case. These improvements are discussed in Ref. [259] and will be taken into consideration for future developments. It is anyway understood that their eventual effect is to improve systematically the EOB/NR agreement, and thus they do not interfere with the model validation analysis we want to perform here.

Table 3.4: SXS simulations with non-zero eccentricity analyzed in this section. From left to right: the identification string of the simulation (ID); the mass ratio $q \equiv m_1/m_2 \geq 1$ and the individual dimensionless spins (χ_1, χ_2); the time-domain NR phasing uncertainty at merger $\delta\phi^{\rm NR}_{\rm mrg}$; the estimated NR eccentricity at first apastron, $e^{\rm NR}_{\omega_a}$; the NR frequency of first apastron $\omega^{\rm NR}_a$; the initial EOB eccentricity $e^{\rm EOB}_{\omega_a}$ and apastron frequency $\omega^{\rm EOB}_a$ used to start the EOB evolution; the maximal NR unfaithfulness uncertainty $\bar{F}^{\rm max}_{\rm NR/NR}$; the initial frequency used in the EOB/NR unfaithfulness computation $Mf_{\rm min}$; the maximal EOB/NR unfaithfulness $\bar{F}^{\rm max}_{\rm EOB/NR}$.

#	ID	(q, χ_1, χ_2)	$\delta\phi^{\rm NR}_{\rm mrg}$(rad)	$e^{\rm NR}_{\omega_a}$	$\omega^{\rm NR}_a$	$e^{\rm EOB}_{\omega_a}$	$\omega^{\rm EOB}_a$	$\bar{F}^{\rm max}_{\rm NR/NR}(\%)$	$Mf_{\rm min}$	$\bar{F}^{\rm max}_{\rm EOB/NR}(\%)$
1	SXS:BBH:1355	$(1, 0, 0)$	$+0.92$	0.0620	0.03278728	0.0888	0.02805750	0.012	0.0055	0.13
2	SXS:BBH:1356	$(1, 0, 0)$	$+0.95$	0.1000	0.02482006	0.15038	0.019077	0.0077	0.0044	0.24
3	SXS:BBH:1358	$(1, 0, 0)$	$+0.25$	0.1023	0.03108936	0.18082	0.021238	0.016	0.0061	0.22
4	SXS:BBH:1359	$(1, 0, 0)$	$+0.25$	0.1125	0.03708305	0.18240	0.021387	0.0024	0.0065	0.17
5	SXS:BBH:1357	$(1, 0, 0)$	-0.44	0.1096	0.03990101	0.19201	0.01960	0.028	0.0061	0.15
6	SXS:BBH:1361	$(1, 0, 0)$	$+0.39$	0.1634	0.03269520	0.23557	0.020991	0.057	0.0065	0.35
7	SXS:BBH:1360	$(1, 0, 0)$	-0.22	0.1604	0.03138220	0.2440	0.019508	0.0094	0.0065	0.31
8	SXS:BBH:1362	$(1, 0, 0)$	-0.09	0.1999	0.05624375	0.3019	0.01914	0.0098	0.0065	0.15
9	SXS:BBH:1363	$(1, 0, 0)$	$+0.58$	0.2048	0.05778104	0.30479	0.01908	0.07	0.006	0.25
10	SXS:BBH:1364	$(2, 0, 0)$	-0.91	0.0518	0.03265995	0.0844	0.025231	0.049	0.062	0.15
11	SXS:BBH:1365	$(2, 0, 0)$	-0.90	0.0650	0.03305974	0.110	0.023987	0.027	0.062	0.12
12	SXS:BBH:1366	$(2, 0, 0)$	-6×10^{-4}	0.1109	0.03089493	0.14989	0.02577	0.017	0.0052	0.20
13	SXS:BBH:1367	$(2, 0, 0)$	$+0.60$	0.1102	0.02975257	0.15095	0.0260	0.0076	0.0055	0.15
14	SXS:BBH:1368	$(2, 0, 0)$	-0.71	0.1043	0.02930360	0.14951	0.02512	0.026	0.0065	0.13
15	SXS:BBH:1369	$(2, 0, 0)$	-0.06	0.2053	0.04263738	0.3134	0.0173386	0.011	0.0041	0.25
16	SXS:BBH:1370	$(2, 0, 0)$	$+0.12$	0.1854	0.02422231	0.31708	0.016779	0.07	0.006	0.37
17	SXS:BBH:1371	$(3, 0, 0)$	$+0.92$	0.0628	0.03263026	0.0912	0.029058	0.12	0.006	0.19
18	SXS:BBH:1372	$(3, 0, 0)$	$+0.01$	0.1035	0.03273944	0.14915	0.026070	0.06	0.006	0.09
19	SXS:BBH:1373	$(3, 0, 0)$	-0.41	0.1028	0.03666911	0.15035	0.02529	0.0034	0.0061	0.13
20	SXS:BBH:1374	$(3, 0, 0)$	$+0.98$	0.1956	0.02702594	0.314	0.016938	0.067	0.0059	0.1
21	SXS:BBH:89	$(1, -0.50, 0)$	...	0.0469	0.02516870	0.07194	0.01779	...	0.0025	0.18
22	SXS:BBH:1136	$(1, -0.75, -0.75)$	-1.90	0.0777	0.04288969	0.1209	0.02728	0.074	0.0058	0.12
23	SXS:BBH:321	$(1.22, +0.33, -0.44)$	$+1.47$	0.0527	0.03239001	0.07621	0.02694	0.015	0.0045	0.27
24	SXS:BBH:322	$(1.22, +0.33, -0.44)$	-2.02	0.0658	0.03396319	0.0984	0.026895	0.016	0.0061	0.26
25	SXS:BBH:323	$(1.22, +0.33, -0.44)$	-1.41	0.1033	0.03498377	0.1438	0.02584	0.019	0.0058	0.17
26	SXS:BBH:324	$(1.22, +0.33, -0.44)$	-0.04	0.2018	0.02464165	0.29425	0.01894	0.098	0.0058	0.19
27	SXS:BBH:1149	$(3, +0.70, +0.60)$	$+3.00$	0.0371	0.03535964	0.06237	0.02664	0.025	0.005	1.07
28	SXS:BBH:1169	$(3, -0.70, -0.60)$	$+3.01$	0.0364	0.02759632	0.04895	0.024285	0.033	0.004	0.10

To convey all available information, we find it useful to explicitly show the time-domain phasing comparisons in Fig. 3.14 (for the non-spinning datasets) and in Fig. 3.15 (for the spinning dataset). One appreciates that, for several cases, the careful choice of $(e^{\rm EOB}_{\omega_a}, \omega^{\rm EOB}_a)$ allows one to obtain a rather flat EOB/NR phase difference and residual oscillations of the order of 0.01 rad, with accumulated phase difference at merger compatible with the nominal NR uncertainty listed in Table 3.4. However, for some datasets, notably those with larger initial eccentricities, the choice of the initial parameters looks suboptimal, and the phase difference still shows a linear drift. Typically, this effect is more prominent for dataset with larger initial eccentricity; it might be related to either missing physics in the dynamics[14] or to the need of further

[14]We remind the reader that the azimuthal radiation-reaction force we are using here

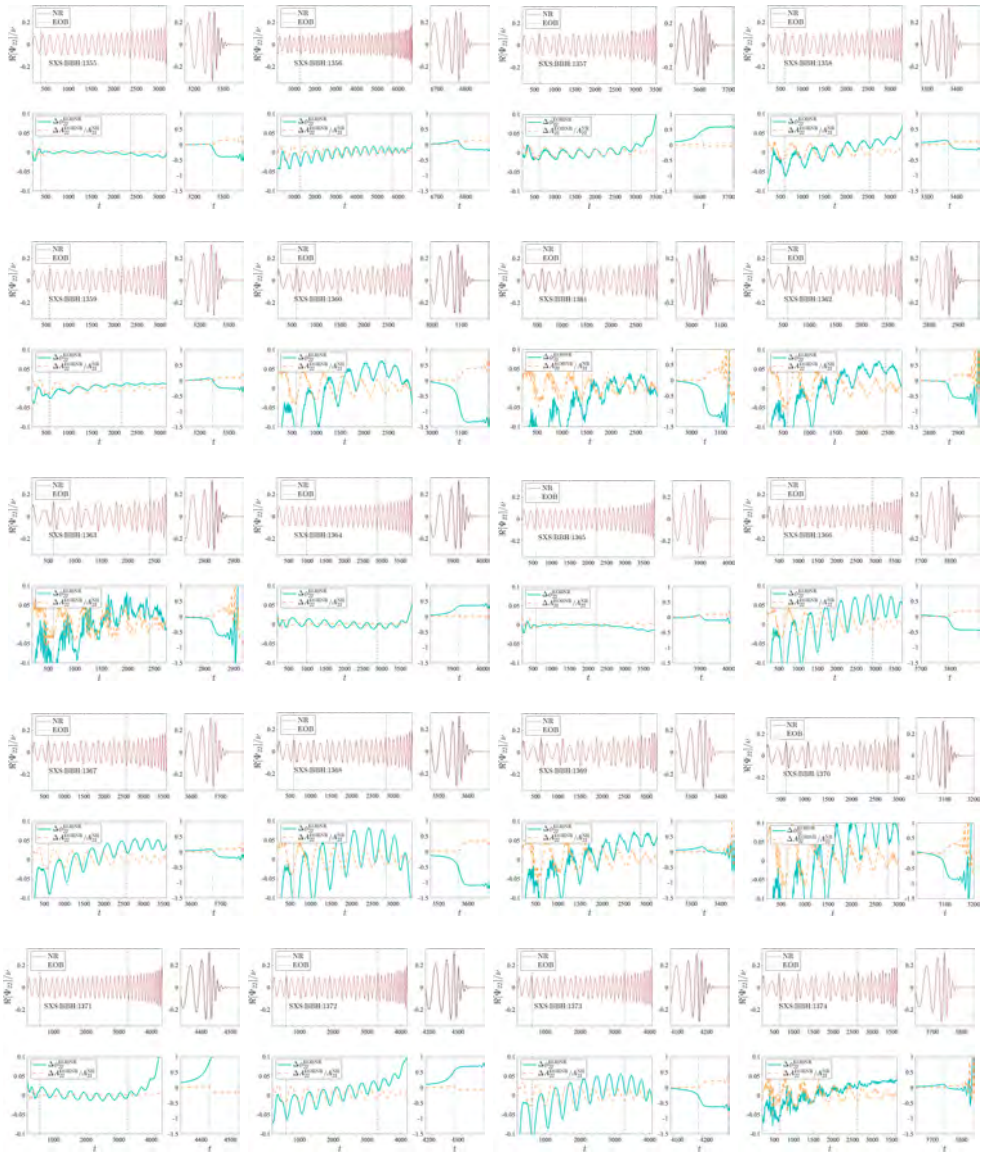

Figure 3.14: EOB/NR time-domain phasing for all the non-spinning datasets considered. The dashed vertical lines indicate the alignment window. For each configuration, in the top panel we show the real part of the NR waveform (black line, barely distinguishable) and the EOB one supplemented by our 2PN noncircular corrections (red line); in the bottom panel we report the associated phase difference (light blue line) and relative amplitude difference (orange line).

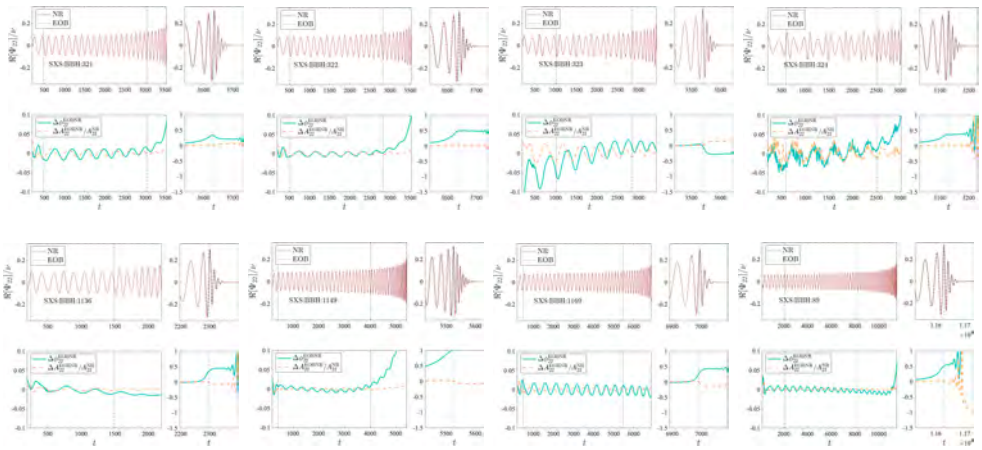

Figure 3.15: EOB/NR time-domain phasing, analogous to those of Fig. 3.14, for all the spinning datasets considered.

improving the initial data choice. Note, however, that this happens for NR simulations that are especially noisy in the frequency at early times, so this might prevent us from an optimal determination of the initial data that is based on the time-alignment procedure, which is in turn affected by the noise in the frequency. In any case, our choice of $(e^{\rm EOB}_{\omega_a}, \omega^{\rm EOB}_a)$ can be considered *conservative* for all the datasets considered and actually suggests that the analytical model can match the NR waveforms even better than what shown in Figs. 3.14 and 3.15. The understanding that this might be the case is motivated by the observation that there are datasets with high eccentricity, e.g., SXS:BBH:1362 or SXS:BBH:1363, whose EOB/NR phase agreement is practically equivalent to that of less eccentric dataset (e.g., SXS:BBH:1358).

3.4.2 EOB/NR unfaithfulness

As an additional figure of merit, we evaluate the quality of our EOB waveform by computing the EOB/NR unfaithfulness weighted by the Advanced LIGO noise over all the available configurations. Here we update the analogous calculation done in Ref. [157] that was only relying on the simple Newton-factorized waveform without the 2PN-accurate eccentric corrections. Considering two waveforms (h_1, h_2), let us recall that the unfaithfulness is a function of the total mass M of the binary and is defined as

$$\bar{F}(M) \equiv 1 - F = 1 - \max_{t_0,\phi_0} \frac{\langle h_1, h_2 \rangle}{||h_1||||h_2||}, \tag{3.79}$$

is the one of Sec. 3.1, which only incorporates the noncircular Newtonian prefactor in its $\ell = m = 2$ mode. See section 3.5 for the proposal and testing of an updated prescription which also incorporates the 2PN noncircular corrections we are adding here to the insplunge waveform.

where (t_0, ϕ_0) are the initial time and phase. We used $||h|| \equiv \sqrt{\langle h, h\rangle}$, and the inner product between two waveforms is defined as

$$\langle h_1, h_2\rangle \equiv 4\Re \int_{f_{\rm min}}^{\infty} \frac{\tilde{h}_1(f)\tilde{h}_2^*(f)}{S_n(f)}\, df, \tag{3.80}$$

where $\tilde{h}(f)$ denotes the Fourier transform of $h(t)$, $S_n(f)$ is the zero-detuned, high-power noise spectral density of Advanced LIGO [266] and $f_{\rm min}$ is the initial frequency, approximately corresponding to the frequency of the first apastron on each NR simulation, after the initial junk radiation has been cleared. In practice, the integral is done up to a maximal frequency $f_{\rm end}$ that corresponds to $|\tilde{h}(f_{\rm end})| \sim 10^{-2}$. Both EOB and NR waveforms are tapered[15] in the time domain so as to reduce high-frequency oscillations in the corresponding Fourier transforms. In addition, as originally pointed out in Ref. [239], the accurate calculation of the Fourier transform of eccentric waveforms is a delicate matter, and it may affect the calculation of the EOB/NR unfaithfulness, $\bar{F}_{\rm EOB/NR}$, if not optimally chosen. These issues have been discussed to some extent in Sec. IV of Ref. [157]; see in particular Figs. 15 and 16 therein. Here, we only recall that the original waveform is padded with zeros in order to increase the frequency resolution and capture all the details of the Fourier transform. Similarly, we were careful to tune the tapering parameters so that the EOB and NR Fourier transforms for each dataset visually agree, likewise to the case shown in Fig. 16 of Ref. [157]. The final outcome of the EOB/NR unfaithfulness computation versus M is shown in Fig. 3.16. The maximum values $\bar{F}^{\max_{\rm EOB/NR}}$ are also listed in the last column of Table 3.4, together with the value of the initial frequency $Mf_{\rm min}$ used in the integral. Figure 3.16, complemented by Table 3.4, shows a small improvement with respect to Fig. 14 of Ref. [157], especially for low masses. Since we are using here a new choice of the parameters $(e^{\rm EOB}_{\omega_a}, \omega^{\rm EOB}_a)$, and consequently new tapering parameters, it is not really possible, within the context of equal-mass binaries, to precisely state to which extent the small improvements found depend on these new choices or on the additional PN corrections in the waveforms. Globally, in view of the similarities between Fig. 14 of Ref. [157] and our current Fig. 3.16, we are prone to conservatively state that, even when in factorized and resummed form, the 2PN noncircular waveform corrections do not improve noticeably the `TEOBResumS-DALI` model on this specific corner of the parameter space.

3.5 2PN noncircular corrections in $\hat{\mathcal{F}}_\varphi$

In the previous sections we proposed and tested an extension of the `TEOBResumS-DALI` insplunge waveform that additionally incorporates 2PN-accurate non-

[15] We use a hyperbolic tangent function function, with two tunable parameters (α, τ), of the form $w(t) = \left[1 + \tanh(\alpha t - \tau)\right]/2$; this multiplies both the NR and EOB waveforms.

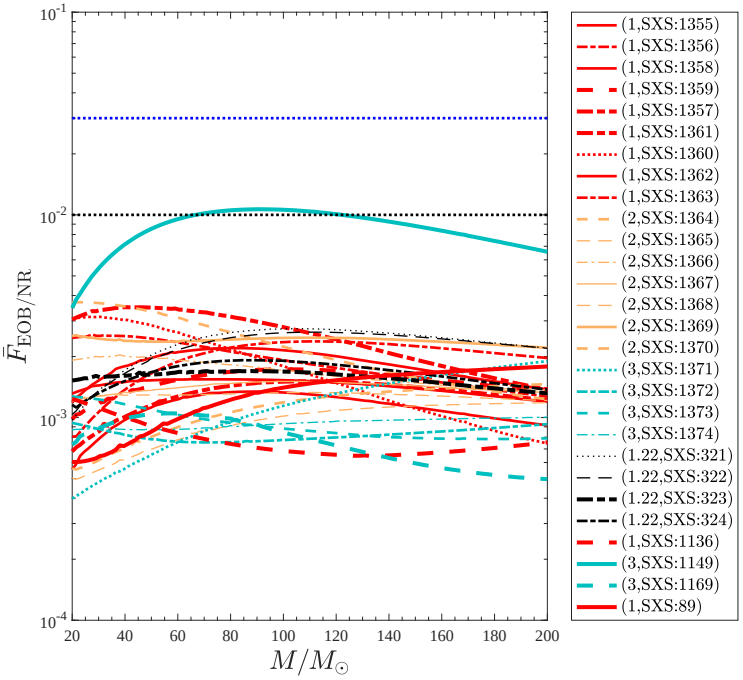

Figure 3.16: EOB/NR unfaithfulness for the $\ell = m = 2$ mode computed over the 28 eccentric SXS simulations we are considering, see Table 3.4. The horizontal lines mark the 0.03 and 0.01 values. The value of $\bar{F}^{\rm max}_{\rm EOB/NR}$ does not exceed the 0.7%, except for the single outlier given by SXS:BBH:1149, corresponding to $(3, +0.70, +0.60)$ with $e^{\rm NR}_{\omega_a} = 0.037$, which is around the 1%. This is consistent with the slight degradation of the `TEOBResumS` performance for large positive spins already found in the quasi-circular limit, and pointed out in Ref. [157].

circular correcting factors. After suitable resummations, in particular those introduced in Sec. 3.3.2, this yielded an improved analytical/numerical waveform agreement with respect to the simple use of the generic Newtonian prefactor, especially at the level of the phase. The aim of this section is to explore the performance of an analogous procedure applied to the radiation-reaction component $\hat{\mathcal{F}}_\varphi$. For simplicity, and since in any case the $\hat{\mathcal{F}}_\varphi$ used in `TEOBResumS-DALI` is noncircularly flexed only in the $\ell = m = 2$ mode (see Eq. (3.18)), we focus our radiation-reaction analysis on its quadrupolar component. Regarding the organization of the contents of this section, in Sec. 3.5.1 we present the 2PN noncircular expression for the $\ell = m = 2$ mode of $\hat{\mathcal{F}}_\varphi$, which is then used in Sec. 3.5.2 to build a properly resummed correcting factor. Finally, the new radiation-reaction prescription is tested in Sec. 3.5.3.

3.5.1 2PN-accurate noncircular quadrupolar flux

In analogy with the case of the waveform, the starting point for our extended noncircular prescription for $\hat{\mathcal{F}}_\varphi$ is to compute the generic planar orbit expression for its spherical multipoles, in PN-expanded form. We did so at 2PN accuracy, considering $F_{\ell m} = m\,\Im\big(\dot{h}_{\ell m} h^*_{\ell m}\big)$ with $h_{\ell m}$ given by the noncircular 2PN result of Sec. 3.2.1.

For our current purposes, we show here explicitly just the $\ell = m = 2$ flux multipole, up to 2PN order,[16] including *both* the instantaneous and tail parts:

$$
\begin{aligned}
F_{22}^{\rm 2PN} &= p_{r_*}^2 p_\varphi u^3 - 2p_\varphi^3 u^5 - 2p_\varphi u^4 + \frac{1}{c^2}\Bigg\{ p_\varphi u^5 \left[\frac{689}{42} - \frac{33\nu}{7} + \left(\frac{109}{7}\right.\right.\\
&\left. - \frac{61\nu}{7}\right) p_\varphi^2 u + \left(\frac{17}{42} - \frac{12\nu}{7}\right) p_\varphi^4 u^2 \Big] - p_{r_*}^2 p_\varphi u^4 \left[\frac{148}{21} - \frac{36\nu}{7}\right.\\
&\left. + p_\varphi^2 u \left(\frac{7}{3} - \frac{21\nu}{2}\right)\right] - p_{r_*}^4 p_\varphi u^3 \left(\frac{145}{42} + \frac{9\nu}{14}\right)\Bigg\} + \frac{\pi}{c^3}\Bigg[u^5\left(\frac{9}{128}\right.\\
&- \frac{173 p_\varphi^2 u}{10} + \frac{79309 p_\varphi^4 u^2}{5760} - \frac{889 p_\varphi^6 u^3}{32} + \frac{9157 p_\varphi^8 u^4}{384} - \frac{697 p_\varphi^{10} u^5}{72}\\
&\left. + \frac{47 p_\varphi^{12} u^6}{640} + \frac{643 p_\varphi^{14} u^7}{480} - \frac{97 p_\varphi^{16} u^8}{288}\right) + p_{r_*}^2 u^4 \left(\frac{215}{192} + \frac{91109 p_\varphi^2 u}{5760}\right.\\
&- \frac{811 p_\varphi^4 u^2}{24} + \frac{14659 p_\varphi^6 u^3}{192} - \frac{51487 p_\varphi^8 u^4}{576} + \frac{22975 p_\varphi^{10} u^5}{384} - \frac{3489 p_\varphi^{12} u^6}{160}\\
&\left. + \frac{485 p_\varphi^{14} u^7}{144}\right) - p_{r_*}^4 u^3 \left(\frac{1219}{1152} - \frac{1471 p_\varphi^2 u}{576} + \frac{449 p_\varphi^4 u^2}{128} - \frac{3677 p_\varphi^6 u^3}{576}\right.\\
&\left. + \frac{769 p_\varphi^8 u^4}{144} - \frac{49 p_\varphi^{10} u^5}{32}\right)\Bigg] - \frac{1}{c^4}\Bigg\{ p_\varphi u^6 \left[\frac{8852}{189} - \frac{12335\nu}{378} + \frac{268\nu^2}{27}\right.\\
&+ p_\varphi^2 u \left(\frac{21001}{882} - \frac{52147\nu}{588} + \frac{7661\nu^2}{294}\right) + p_\varphi^4 u^2 \left(\frac{59}{882} - \frac{60901\nu}{1764}\right.\\
&\left. + \frac{7663\nu^2}{1764}\right) + p_\varphi^6 u^3 \left(\frac{851}{882} - \frac{4987\nu}{882} - \frac{3295\nu^2}{1764}\right)\Big] - p_{r_*}^2 p_\varphi u^5 \left[\frac{10277}{882}\right.\\
&- \frac{60065\nu}{1764} + \frac{7799\nu^2}{441} + p_\varphi^2 u \left(-\frac{6465}{392} - \frac{48385\nu}{441} + \frac{22237\nu^2}{441}\right)\\
&\left. + p_\varphi^4 u^2 \left(\frac{709}{84} - \frac{685\nu}{24} + \frac{463\nu^2}{168}\right)\right] - p_{r_*}^4 p_\varphi u^4 \left[\frac{6527}{441} + \frac{6809\nu}{1764}\right.\\
&\left. - \frac{14921\nu^2}{1764} + p_\varphi^2 u \left(\frac{2923}{588} - \frac{4889\nu}{588} - \frac{6317\nu^2}{294}\right)\right]\Bigg\}, \qquad (3.81)
\end{aligned}
$$

where, for simplicity and to be consistent with we what we did on the noncircular waveform factors, we performed an expansion around 0 of p_{r_*} up to

[16] We refer here to PN orders counted from the leading order of $\hat{\mathcal{F}}_\varphi$, which we remember being, at leading order, a 2.5PN quantity in the EOB equations of motion.

order $\mathcal{O}(p_{r_*}^4)$; notice moreover that we are omitting an overall factor c^{-5}. We actually performed the same computation for all the subdominant (ℓ, m) multipoles of $\hat{\mathcal{F}}_\varphi$ that are relevant at 2PN accuracy; their explicit expressions can be found in Appendix C.2.

3.5.2 Factorization and resummation

Our aim here is to add 2PN-accurate noncircular corrections to the azimuthal radiation-reaction force $\hat{\mathcal{F}}_\varphi$. This is achieved by dressing the first term of Eq. (3.18) with an additional correcting factor $\hat{F}^{\mathrm{2PN_{nc}}}_{\varphi,22}$ derived from the full noncircular 2PN flux $\hat{F}^{\mathrm{2PN}}_{22}$ written in Eq. (3.81). Following the same methodology we adopted for the insplunge waveform in the previous sections, our factorization scheme is the following:

(i) starting from the Taylor expanded flux F^{2PN}_{22}, we factorize the full Newtonian contribution, given by $F^{N}_{22}\hat{f}^{\mathrm{N_{nc}}}_{\varphi,22}$, while using in the latter the 2PN-accurate EOB equations of motion, so to remove from our corrections the contribution already accounted for by the time derivatives in $\hat{f}^{\mathrm{N_{nc}}}_{\varphi,22}$, and finally we expand the residual up to $\mathcal{O}(1/c^4)$;

(ii) we single out the circular part $\hat{F}^{\mathrm{2PN_c}}_{22}$ of the Newton-factorized flux by simply taking on it the limit $p_{r_*} \to 0$;

(iii) we factorize the circular part computed in the previous step and compute the desired noncircular correction $\hat{F}^{\mathrm{2PN_{nc}}}_{22}$.

In formulas we have

$$\hat{F}^{\mathrm{2PN_c}}_{22} \equiv \lim_{p_{r_*}\to 0} T_{\mathrm{2PN}}\left[\frac{F^{\mathrm{2PN}}_{22}}{\left(F^{N}_{22}\hat{f}^{\mathrm{N_{nc}}}_{\varphi,22}\right)_{\mathrm{EOMs}}}\right], \tag{3.82}$$

$$\hat{F}^{\mathrm{2PN_{nc}}}_{22} \equiv T_{\mathrm{2PN}}\left[\frac{F^{\mathrm{2PN}}_{22}}{\left(F^{N}_{22}\hat{f}^{\mathrm{N_{nc}}}_{\varphi,22}\right)_{\mathrm{EOMs}}\hat{F}^{\mathrm{2PN_c}}_{22}}\right], \tag{3.83}$$

where we use the same notation of Sec. 3.2.2. Again, the resulting noncircular factor (3.83) comes out naturally split in an instantaneous and a tail component, which appear at different PN orders. For this reason we can readily factorize it further in an instantaneous and a tail factor,

$$\hat{F}^{\mathrm{2PN_{nc}}}_{22} = \hat{F}^{\mathrm{2PN_{nc,inst}}}_{22}\hat{F}^{\mathrm{2PN_{nc,tail}}}_{22}, \tag{3.84}$$

which explicitly read[17]

$$\hat{F}^{\mathrm{2PN_{nc,inst}}}_{22} = 1 + \frac{1}{c^2}\left[\frac{p^2_{r_*}}{\left(1+p^2_\varphi u\right)^2}\left(\frac{281}{168}+\frac{31\nu}{28}\right)\hat{f}^{\mathrm{1PN}}_{p^2_{r_*}}\right.$$

[17] For consistency we have again to expand in p_{r_*} up to order $\mathcal{O}(p_{r_*}^4)$.

$$+\frac{p_{r_*}^4}{u\big(1+p_\varphi^2u\big)^3}\left(\frac{5}{16}-\frac{3\nu}{8}\right)\hat{f}^{1\mathrm{PN}}_{p^4_{r_*}}\Bigg] \tag{3.85}$$

$$+\frac{1}{c^4}\Bigg[\frac{p_{r_*}^2u}{\big(1+p_\varphi^2u\big)^3}\left(\frac{159697}{42336}-\frac{2081\nu}{10584}+\frac{20345\nu^2}{10584}\right)\hat{f}^{2\mathrm{PN}}_{p^2_{r_*}}$$

$$+\frac{p_{r_*}^4}{p_\varphi\big(1+p_\varphi^2u\big)^4}\left(\frac{225067}{84672}+\frac{18119\nu}{10584}+\frac{6893\nu^2}{21168}\right)\hat{f}^{2\mathrm{PN}}_{p^4_{r_*}}\Bigg],$$

$$\hat{F}_{22}^{2\mathrm{PN}_{\mathrm{nc,tail}}}=1+\frac{\pi}{c^3}\Bigg[-\frac{p_{r_*}^2}{p_\varphi\big(1+p_\varphi^2u\big)^2}\frac{887}{1536}\hat{t}^{1.5\mathrm{PN}}_{p^2_{r_*}}$$

$$+\frac{p_{r_*}^4}{p_\varphi u\big(1+p_\varphi^2u\big)^3}\frac{2215}{9216}\hat{t}^{1.5\mathrm{PN}}_{p^2_{r_*}}\Bigg]. \tag{3.86}$$

The quantities $\hat{f}^{\mathrm{PN}}_{p^n_{r_*}}$ and $\hat{t}^{1.5\mathrm{PN}}_{p^n_{r_*}}$ are polynomials in the Newtonian-order variable $y=p_\varphi^2u$. For the instantaneous part, the coefficients of the polynomials contain also the symmetric-mass ratio ν and read

$$\hat{f}^{1\mathrm{PN}}_{p^2_{r_*}}=1+\frac{2(571-54\nu)}{281+186\nu}y+\frac{1061-390\nu}{281+186\nu}y^2, \tag{3.87}$$

$$\hat{f}^{1\mathrm{PN}}_{p^4_{r_*}}=1+\frac{2(395-366\nu)}{21(5-6\nu)}y+\frac{295-234\nu}{7(5-6\nu)}y^2, \tag{3.88}$$

$$\begin{aligned}\hat{f}^{2\mathrm{PN}}_{p^2_{r_*}}=1&+\frac{2\left(503861-236326\nu-42992\nu^2\right)}{159697-8324\nu+81380\nu^2}y\\&+\frac{6\left(144635-100862\nu-59260\nu^2\right)}{159697-8324\nu+81380\nu^2}y^2\\&-\frac{6\left(119807-50090\nu+28256\nu^2\right)}{159697-8324\nu+81380\nu^2}y^3\\&-\frac{21\left(26487-19592\nu+428\nu^2\right)}{159697-8324\nu+81380\nu^2}y^4,\end{aligned} \tag{3.89}$$

$$\begin{aligned}\hat{f}^{2\mathrm{PN}}_{p^4_{r_*}}=1&+\frac{2\left(1028891+66902\nu-13616\nu^2\right)}{225067+144952\nu+27572\nu^2}y\\&+\frac{6\left(670405+13630\nu+8948\nu^2\right)}{225067+144952\nu+27572\nu^2}y^2\\&+\frac{6\left(548563+5454\nu+42912\nu^2\right)}{225067+144952\nu+27572\nu^2}y^3\\&+\frac{3\left(478421-54244\nu+40444\nu^2\right)}{225067+144952\nu+27572\nu^2}y^4,\end{aligned} \tag{3.90}$$

while in the tail factor there are no ν-contributions and the two polynomials simply read

$$\hat{t}^{1.5\mathrm{PN}}_{p^2_{r_*}}=1+\frac{19094}{2661}y-\frac{127753}{13305}y^2+\frac{22016}{887}y^3-\frac{2569}{2661}y^4-\frac{79250}{2661}y^5$$

$$+\frac{29231}{887}y^6-\frac{204692}{13305}y^7+\frac{7372}{2661}y^8, \tag{3.91}$$

$$\hat{t}^{1.5\mathrm{PN}}_{p^4_{r_*}}=1-\frac{4222}{443}y+\frac{115273}{11075}y^2-\frac{74904}{2215}y^3-\frac{15491}{2215}y^4+\frac{91994}{2215}y^5 -\frac{77197}{2215}y^6+\frac{169412}{11075}y^7-\frac{7372}{2215}y^8. \tag{3.92}$$

Note that the analytical structure of the 2PN correction $\hat{F}_{22}^{2\mathrm{PN}_{\mathrm{nc}}}$ is similar to the one of the 2PN correcting factors of the waveform multipoles, discussed in Sec. 3.2.2. As already argued there, the polynomials in y need to be resummed in order to provide reliable results in the strong field regime. More specifically, we find convenient to use diagonal Padé approximants for the polynomials in Eq. (3.86) and in the 2PN part of Eq. (3.85), while leaving the other polynomials in Taylor-expanded form.

3.5.3 Testing the 2PN noncircular correction of $\hat{\mathcal{F}}_\varphi$

We test the reliability of the resummed factor $\hat{F}_{22}^{2\mathrm{PN}}$ in the test-mass limit, focusing on the associated quadrupolar contributions to the angular momentum and energy fluxes, which we denote respectively by $\dot{J}_{22}$ and $\dot{E}_{22}$. Since we are interested in comparing different prescriptions for $\hat{\mathcal{F}}_\varphi$, the analytical fluxes are not computed through Eqs. (1.178)-(1.177) but via the balance equations (2.97)-(2.97), with the Schott energy in the resummed form (3.20). Indeed this is not the case for the numerical results we use as a reference, which instead are computed using in Eqs. (1.178)-(1.177) the numerical test-mass quadrupolar waveform associated to the given dynamics selected for each comparison.

We start by considering two non-spinning geodesic dynamics with eccentricities $e=0.1,0.9$, in Fig. 3.17. In the rightmost panels, we show the 2PN noncircular correction $\hat{F}_{22}^{2\mathrm{PN}_{\mathrm{nc}}}$ with different resummation procedures: in Taylor expanded form, with resummations only on the tail factor $\hat{F}_{22}^{2\mathrm{PN}_{\mathrm{nc,tail}}}$, and with resummation on both $\hat{F}_{22}^{2\mathrm{PN}_{\mathrm{nc,inst}}}$ and $\hat{F}_{22}^{2\mathrm{PN}_{\mathrm{nc,tail}}}$. The latter is used to compute the fluxes that we label as NCN2PN. In the case with $e=0.1$, the three prescriptions considered are similar, while in the other configuration with $e=0.9$ the effects of the resummations is more evident. Moreover, it is possible to see that, again, the resummation is more relevant for the tail factor than for the instantaneous one. This is also a consequence of the fact that the polynomials $\hat{t}^{1.5\mathrm{PN}}_{p^n_{r_*}}$ are of order eight in y, while $\hat{f}^{2\mathrm{PN}}_{p^n_{r_*}}$ are fourth-order polynomials. Nevertheless, as shown in the middle panels of Fig. 3.17, the improvement brought by the resummed 2PN corrections to the angular flux $\dot{J}_{22}$ is rather small, even for $e=0.9$.

Deeper insight on its impact on the angular radiation-reaction force is obtained considering the averages of the quadrupolar fluxes over an entire

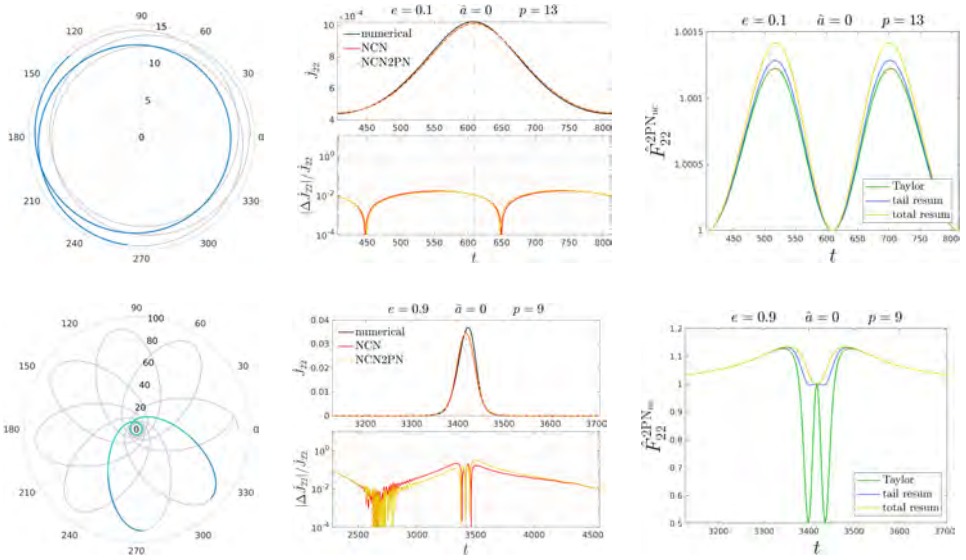

Figure 3.17: Trajectories, quadrupolar angular momentum fluxes, and 2PN factor $\hat{F}_{22}^{\mathrm{2PN_{nc}}}$ of Eq. (3.84) for two geodesic configurations. In the middle we show the numerical flux (black line, dubbed numerical), the standard flux from `TEOBResumS-DALI` (red line, dubbed NCN), and the result of our 2PN noncircular corrections in resummed form (yellow line, dubbed NCN2PN); below we plot the corresponding analytical/numerical relative differences. These plots refer to the radial periods that are highlighted in blue in the orbital trajectory plot, on the left column. More precisely, for the configuration with $e = 0.9$, the fluxes and the 2PN corrections are shown over just a portion of the radial period, in order to highlight the burst of radiation at periastron (vertical dashed line in the flux plots); in the corresponding trajectory plot this is highlighted in aqua-green. On the rightmost panels we show the 2PN corrections to the flux in Taylor expanded form (Taylor), with resummations in the tail factor (tail resum), and with resummations either in the instantaneous and tail terms (total resum).

orbital period $T_{\rm orb}$, that is

$$\langle \dot{J}_{22} \rangle \equiv \frac{1}{T_{\rm orb}} \int_0^{T_{\rm orb}} \dot{J}_{22} dt, \tag{3.93}$$

$$\langle \dot{E}_{22} \rangle \equiv \frac{1}{T_{\rm orb}} \int_0^{T_{\rm orb}} \dot{E}_{22} dt. \tag{3.94}$$

In particular, Table 3.5 and Fig. 3.18 show the relative analytical/numerical differences for these quantities, further averaged over several geodesic dynamics with the same eccentricity, and denoted as $\langle \Delta J_{22}/J_{22} \rangle_e$ and $\langle \Delta E_{22}/E_{22} \rangle_e$. The prescriptions we test are again the standard `TEOBResumS-DALI` prescrip-

Table 3.5: Absolute analytical/numerical relative differences for orbit averaged quadrupolar fluxes, further averaged over several dynamical configurations at fixed eccentricity. We consider in particular $\hat{a} = (0, \pm 0.2, \pm 0.6, \pm 0.9)$ and $p = (9p_s(e,\hat{a})/p_s(e,0), 13p_s(e,\hat{a})/p_s(e,0))$, where $p_s(e,\hat{a})$ is the separatrix given by Eq. (3.31). Moreover, we adopt the shorthand notation $\langle \delta F_{22} \rangle_e \equiv \langle |\Delta F_{22}|/F_{22} \rangle_e$, with $F = J, E$. The radiation-reaction prescriptions we compare are the NCN, NCN2PN(Taylor) and NCN2PN defined in the main text. Mind that each value in the table is reported as a percentage.

	NCN		NCN2PN (Taylor)		NCN2PN	
	$\langle \delta J_{22} \rangle_e$	$\langle \delta E_{22} \rangle_e$	$\langle \delta J_{22} \rangle_e$	$\langle \delta E_{22} \rangle_e$	$\langle \delta J_{22} \rangle_e$	$\langle \delta E_{22} \rangle_e$
$e = 0.1$	0.31	0.39	0.26	0.34	0.24	0.32
$e = 0.3$	2.03	2.52	1.70	2.23	1.47	1.98
$e = 0.5$	4.70	5.41	4.24	5.17	3.40	4.26
$e = 0.7$	7.41	8.10	8.75	10.05	5.45	6.49
$e = 0.9$	9.66	10.36	24.36	26.91	7.37	8.44

tion (NCN), the one upgraded with $\hat{F}_{22}^{\rm 2PN_{nc}}$ in Taylor-expanded form (NCN2PN (Taylor)), and the one where $\hat{F}_{22}^{\rm 2PN_{nc}}$ is Padé resummed. As can be seen, the 2PN noncircular correction improves the radiation-reaction NCN, but the resummation is needed in order to obtain accurate results also for $e \gtrsim 0.6$. Indeed, for high eccentricity the periastron gets closer to the central black hole, making the y-polynomials of $\hat{F}_{22}^{\rm 2PN_{nc}}$ grow too much in their original form. The resummation prevents this issue and leads also to better results for lower eccentricities.

3.6 Comparisons with others eccentric EOB models

Ref. [251], besides providing the analytical expressions of the generic-orbit tail terms we adopted for our model, also proposed a different waveform factorization where only the *quasi-circular* Newtonian prefactor (2.101) is used and

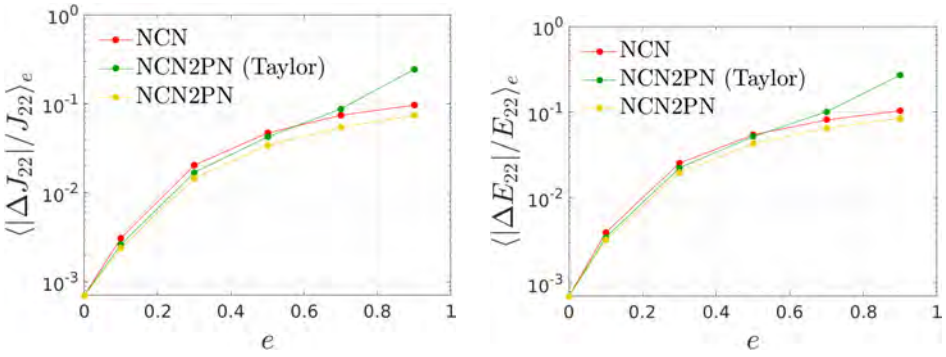

Figure 3.18: Illustrative plot for the absolute analytical/numerical relative differences of the averaged fluxes, as they are given by Table 3.5, for the three prescription NCN, NCN2PN(Taylor), and NCN2PN, specified in the main text. Each point is an average over 14 configurations, with $\langle\delta J_{22}\rangle_0 = \langle\delta E_{22}\rangle_0 = 0.07\%$ in the circular case $e = 0$. The NCN2PN prescription for the radiation-reaction force, which incorporates resummed 2PN noncircular corrections, is the one that has consistently the best performance.

all the 2PN noncircular contributions are included in additive form on top of the respective quasi-circular factors.

The scope of this section is to thoroughly test this analytical waveform proposal and compare it with ours, outlined in Sec. 3.2.2, using as a benchmark the numerical test-mass waveforms we already used throughout Sec. 3.3. To this end, we carefully follow Sec. IIIB of Ref. [251] and recap here the results that are relevant to our analysis. For modes with $m \neq 0$, Ref. [251] advocates the waveform prescription

$$h_{\ell m}^{\mathrm{2PN_{qc}}} = h_{\ell m}^{(N,\epsilon)_c} \hat{S}_{\mathrm{eff}} \left(T_{\ell m} + T_{\ell m}^{\mathrm{ecc}}\right) e^{i\delta_{\ell m}} \left(f_{\ell m} + f_{\ell m}^{\mathrm{ecc}}\right), \tag{3.95}$$

where the eccentric terms $f_{\ell m}^{\mathrm{ecc}}$ and $T_{\ell m}^{\mathrm{ecc}}$ are written as functions of $(r, p_r, \dot{p}_r)$. The quasi-circular terms $h_{\ell m}^{(N,\epsilon)_c}$, $T_{\ell m}$, $\delta_{\ell m}$, and $f_{\ell m}$, are here identified with their `TEOBResumS` counterparts, detailed in Sec. 2.2. Focusing just on the $(2, 2)$ mode, we use the expressions of T_{22}^{ecc} and f_{22}^{ecc} provided in the supplemental material of Ref. [251]. The full expression of the former reads

$$\begin{aligned}
T_{22}^{\mathrm{ecc}} = \eta^3\pi\Bigg[&-\frac{3ip_r}{2r} - \dot{p}_r\sqrt{r} - \frac{p_r\left(2p_r + i\dot{p}_r r^{3/2}\right)}{4\sqrt{r}} + \frac{1}{48}\Big(-5ip_r^3 - 15p_r^2\dot{p}_r r^{3/2} \\
&+ 9ip_r\dot{p}_r^2 r^3 - \dot{p}_r^3 r^{9/2}\Big) + \frac{1}{32}\sqrt{r}\Big(-10p_r^4 + 15ip_r^3\dot{p}_r r^{3/2} + 8p_r^2\dot{p}_r^2 r^3 - ip_r\dot{p}_r^3 r^{9/2} \\
&+ 2\dot{p}_r^4 r^6\Big) + \frac{r}{1920}\Big(589ip_r^5 + 1150p_r^4\dot{p}_r r^{3/2} - 1060ip_r^3\dot{p}_r^2 r^3 - 505p_r^2\dot{p}_r^3 r^{9/2} \\
&+ 55ip_r\dot{p}_r^4 r^6 - 116\dot{p}_r^5 r^{15/2}\Big) + \frac{r^{3/2}}{11520}\Big(1974p_r^6 - 4995ip_r^5\dot{p}_r r^{3/2} - 7470p_r^4\dot{p}_r^2 r^3
\end{aligned}$$

$$+ 7240 i p_r^3 \dot{p}_r^3 r^{9/2} + 3855 p_r^2 \dot{p}_r^4 r^6 - 669 i p_r \dot{p}_r^5 r^{15/2} + 560 \dot{p}_r^6 r^9 \Big) \Big], \tag{3.96}$$

while $f_{22}^{\rm ecc}$, specified to the test-mass limit case, results

$$\begin{aligned} f_{22}^{\rm ecc} = & -\frac{p_r^2}{2v_0^2} + i p_r r v_0 + \frac{r^2 v_0^4}{2} + \frac{1}{2 r v_0^2} - 1 + \frac{1}{c^2}\Bigg(\frac{p_r^4}{4 r^3 v_0^8} + \frac{29 p_r^4}{84 v_0^2} \\ & + \frac{i p_r^3}{4 r^2 v_0^5} - \frac{37}{84} i p_r^3 r v_0 - \frac{p_r^2}{12 r^4 v_0^8} + \frac{1}{4} p_r^2 r^2 v_0^4 + \frac{31 p_r^2}{14 r v_0^2} - \frac{37}{84} i p_r r^3 v_0^7 \\ & + \frac{i p_r}{6 r^3 v_0^5} - \frac{209 i p_r v_0}{84} - \frac{1}{6 r^5 v_0^8} - \frac{2}{21} r^4 v_0^{10} - \frac{13}{12 r^2 v_0^2} - \frac{59 r v_0^4}{84} + \frac{43 v_0^2}{21} \Bigg) + \\ & \frac{1}{c^3}\Bigg(- \frac{\hat{a} p_r^2}{3 r^3 v_0^5} - \frac{4 i \hat{a} p_r}{3 r^2 v_0^2} + \frac{\hat{a}}{3 r^4 v_0^5} - \frac{5 \hat{a} v_0}{3 r} + \frac{4 \hat{a} v_0^3}{3} \Bigg) + \frac{1}{c^4}\Bigg(- \frac{\hat{a}^2 p_r^4}{6 r^4 v_0^8} \\ & - \frac{i \hat{a}^2 p_r^3}{6 r^3 v_0^5} + \frac{\hat{a}^2 p_r^2}{6 r^5 v_0^8} - \frac{5 \hat{a}^2 p_r^2}{6 r^2 v_0^2} + \frac{i \hat{a}^2 p_r v_0}{r} + \frac{\hat{a}^2}{2 r^3 v_0^2} - \frac{\hat{a}^2 v_0^4}{2} - \frac{p_r^6}{4 r^6 v_0^{14}} \\ & - \frac{31 p_r^6}{112 r^3 v_0^8} - \frac{277 p_r^6}{1008 v_0^2} - \frac{5 i p_r^5}{32 r^5 v_0^{11}} - \frac{3 i p_r^5}{14 r^2 v_0^5} + \frac{571 i p_r^5 r v_0}{2016} - \frac{p_r^4}{12 r^7 v_0^{14}} \\ & - \frac{179 p_r^4}{144 r^4 v_0^8} - \frac{85}{252} p_r^4 r^2 v_0^4 - \frac{1963 p_r^4}{1008 r v_0^2} - \frac{5 i p_r^3}{24 r^6 v_0^{11}} + \frac{349 i p_r^3 r^3 v_0^7}{1008} \\ & - \frac{953 i p_r^3}{1008 r^3 v_0^5} + \frac{803}{504} i p_r^3 v_0 + \frac{2 p_r^2}{9 r^8 v_0^{14}} + \frac{79 p_r^2}{168 r^5 v_0^8} - \frac{71 p_r^2 r^4 v_0^{10}}{1008} + \frac{43 p_r^2}{42 r^3 v_0^4} \\ & - \frac{31 p_r^2}{168 r^2 v_0^2} - \frac{31}{112} p_r^2 r v_0^4 - \frac{43 p_r^2 v_0^2}{126} - \frac{5 i p_r}{72 r^7 v_0^{11}} + \frac{127 i p_r r^5 v_0^{13}}{2016} \\ & - \frac{83 i p_r}{504 r^4 v_0^5} + \frac{5}{63} i p_r r^2 v_0^7 - \frac{9221 i p_r v_0}{6048 r} + \frac{1}{9 r^9 v_0^{14}} - \frac{1}{126} r^6 v_0^{16} + \frac{1}{6 r^6 v_0^8} \\ & + \frac{43}{63 r^4 v_0^4} + \frac{53 r^3 v_0^{10}}{168} + \frac{13}{504 r^3 v_0^2} - \frac{43 r^2 v_0^8}{126} - \frac{43 v_0^2}{126 r} - \frac{11 v_0^4}{18} \Bigg), \end{aligned} \tag{3.97}$$

where

$$v_0 \equiv \frac{(1 + \dot{p}_r r^2)^{1/6}}{\sqrt{r}} \tag{3.98}$$

is the Newtonian orbital velocity.

These are then recasted in terms of $(p_{r_*},\ \dot{p}_{r_*})$ considering (see also Appendix E of Ref. [251])

$$p_r = \frac{\sqrt{D}}{A} p_{r_*}, \tag{3.99}$$

$$\dot{p}_r = -\Bigg[\left(\frac{\partial H}{\partial r} \right)_{p_{r_*}} + p_{r_*} \left(\frac{\partial H}{\partial p_{r_*}} \right)_r \frac{\sqrt{D}}{A} \frac{d}{dr} \frac{A}{\sqrt{D}} \Bigg]. \tag{3.100}$$

Figure 3.19 shows a comparison between (i) the numerical waveform, (ii) the analytical waveform of `TEOBResumS-DALI`, here without 2PN noncircular

corrections, and (iii) the 2PN-corrected waveform of Eq. (3.95). We observe that the amplitude differences during the inspiral become more relevant as we go towards large eccentricities and near the apastra. Moreover, even at small eccentricity, the waveform of `TEOBResumS-DALI` seems to perform globally better than the one of Eq. (3.95).

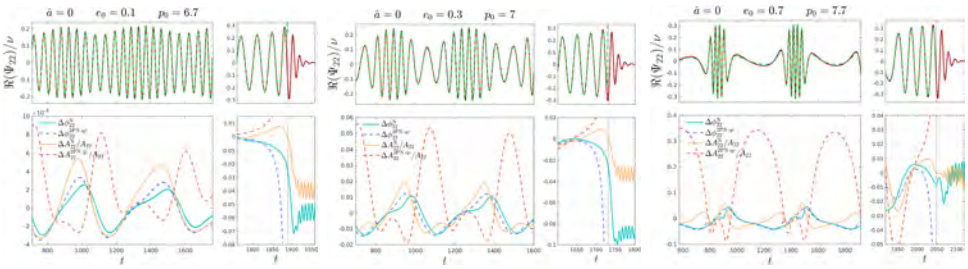

Figure 3.19: Comparisons between the $\ell = m = 2$ numerical and analytical waveforms emitted by the eccentric inspiral of a test particle on a Schwarzschild black hole. The initial eccentricities and semilatera recta are (e_0, p_0) =(0.1, 6.7), (0.3, 7), (0.7, 7.7). The top panels display the numerical waveform (black line, indistinguishable), `TEOBResumS-DALI` waveform (dot-dashed red line, labeled N) and the waveform of Eq. (3.95) (dot-dashed green line, labeled 2PN_{qc}). The corresponding phase differences and relative amplitude differences are shown in the bottom panels. The vertical black line marks the merger time, corresponding to the peak of the numerical waveform amplitude. Since we are interested on the inspiral, for simplicity the 2PN_{qc} waveform is not completed by NQC corrections and ringdown part. The analytical/numerical phase agreement is comparable for the two choices (blue lines); by contrast, the amplitude disagreement (orange lines) is always larger for the 2PN_{qc} prescription, for which worsens up to 30% when the eccentricity increases.

Figure 3.19 also highlights an aspect that is *a priori* unexpected: the largest amplitude differences occur at *apastron* and not at periastron. This might look puzzling because PN expansions are more accurate in weak field than in strong field, while the plot seems to indicate the opposite.

The reason for this behavior can be understood by inspecting Figs. 3.20 and 3.21. In the first one we compare (i) the quasi-circular EOB waveform, (ii) the waveform with the general Newtonian prefactor, (iii) the waveform of Eq. (3.43), and (iv) the waveform of Eq. (3.95). Moreover, we plot all the respective analytical/numerical relative amplitude differences. On parallel, the second figure focuses on the noncircular *instantaneous* corrections to the amplitude and to the phase for each analytical prescription, illustrating their evolution along the dynamics. As shown in the middle panel of Fig. 3.21, all the noncircular instantaneous factors provide a relevant correction to the phase. The effect of these corrections is evident in the top panel of Fig. 3.20,

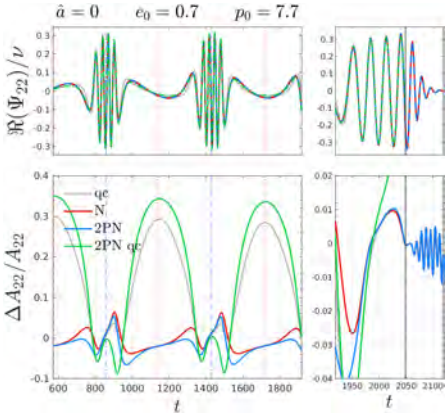

Figure 3.20: Comparing waveforms generated by a test particle inspiralling and plunging into a Schwarzschild black hole, with $(e_0, p_0) = (0.7, 7.7)$. Top panel: the numerical waveforms (black line, indistinguishable), the quasi-circular EOB waveform (gray line, dubbed qc), the waveform of `TEOBResumS-DALI` with just the Newtonian noncircular corrections (red line, dubbed N), the waveform of Eq. (3.43) with the 2PN correcting factor (blue line, dubbed 2PN), and the waveform of Eq. (3.95) (green line, dubbed 2PN_{qc}, without NQC terms and ringdown). Bottom panel: relative amplitude differences with the numerical waveforms. Apastra are marked by dotted red vertical lines, while periastra are marked with dot-dashed blue lines.

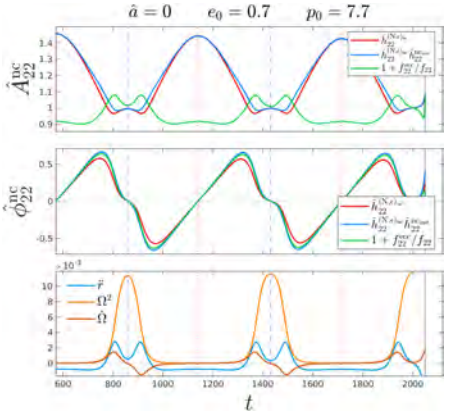

Figure 3.21: Contrasting different noncircular corrections for the same configuration of Fig. 3.20. Top and middle panels: the noncircular contributions to amplitude and phase. We consider: the noncircular Newtonian factor $\hat{h}^{(\text{N},0)_{\text{nc}}}_{22}$ of Eq. (3.11) (red); the noncircular factors $\hat{h}^{(\text{N},0)_{\text{nc}}}_{22}\hat{h}^{\text{nc}_{\text{inst}}}_{22}$ appearing in our prescription (blue); the 2PN noncircular corrections of Eq. (3.95), written as $1 + f^{\text{ecc}}_{22}/f_{22}$ for formal consistency with the other noncircular corrections (green). The bottom panel shows the values assumed by $\ddot{r}$, Ω^2, and $\dot{\Omega}$ along the dynamics. The correction proportional to $\ddot{r}/(r\Omega^2)$ in $\hat{h}^{(\text{N},0)_{\text{nc}}}_{22}$ yields larger values at apastron than $1+f^{\text{ecc}}_{22}/f_{22}$, since Ω^2 approaches 0 there.

where the quasi-circular waveform (gray line) is visibly dephased with respect to the other curves. This indicates that the noncircular waveform information has consistently the effect of improving the numerical/analytical phase agreement with respect to the quasi-circular EOB waveform. By contrast, the noncircular correction given in Eq. (3.95), at 2PN accuracy, does not provide a reliable amplitude description around the apastra, with differences that are rather close to those obtained using the standard circular waveform.

To understand this aspect, let us focus for a moment on the Newtonian noncircular prefactor, whose time evolution is shown, for the case considered, in Fig. 3.21. The figure shows that the contribution of the Newtonian prefactor is larger at apastron than at periastron. This is due to the fact that in $\hat{h}_{22}^{(\mathrm{N},0)_{\mathrm{nc}}}$ the orbital frequency Ω appears squared and at the denominator of the noncircular correction, as a consequence of having factorized the circular Newtonian contribution. This eventually amplifies the contribution of the whole function in correspondence of the lowest values of Ω, i.e. in the neighborhood of the apastra. Note, however, that the only nonvanishing contribution of $\hat{h}_{22}^{(\mathrm{N},0)_{\mathrm{nc}}}$ at apastron is the one proportional to $\ddot{r}$, whose presence is thus the main reason behind the behavior seen in Fig. 3.21. The hierarchy between $\ddot{r}$ and Ω^2 is clarified by the bottom panel of Fig. 3.21. By contrast, when considering Eq. (3.95), without the crucial factorization of the general Newtonian prefactor, the amplitude correction remains substantially constant, and small, for the whole radial evolution. This leads to the large analytical/numerical discrepancies for the amplitude, as shown in Figs. 3.19 and Fig. 3.20. In fact, the prescription of Eq. (3.95) incorporates the PN expansion of $\hat{h}_{22}^{(\mathrm{N},0)_{\mathrm{nc}}}$ through the replacement of Ω and $\ddot{r}$ via the 2PN equation of motion, so that the crucial amplification related to the exact $\ddot{r}/\Omega^2$ contribution is lost.

This trend is even more evident if we inspect dynamical capture dynamics. Figure 3.22 provides an example of this, by referring to the uppermost configuration of Fig. 3.13. The waveform of Ref. [251], Eq. (3.95), yields fractional amplitude differences $\sim 60\%$ at the apastron of the quasi-elliptic orbit following the first encounter.

We conclude by noting that the analysis we just carried out also indicates that, given the recipes we are following to build our 2PN noncircular corrections, it is structurally impossible for them to improve the analytical/numerical agreement at periastron and apastron, since the two radial turning points are characterized by $p_{r_*} = 0$, for which $\hat{F}_{\ell m}^{2\mathrm{PN}_{\mathrm{nc}}}$ and $\hat{h}_{\ell m}^{\mathrm{nc}}$ reduce to unity. Considering that in the vicinity of the periastra we have the biggest contribution to the fluxes, we see this as a first indication that using the PN-expanded EOB equations of motion to define the 2PN noncircular corrections, and thus getting rid of terms like $\ddot{r}$ that do not vanish at the radial turning points (see the bottom panel of Fig. 3.21), may not be the best way to proceed. We follow up on this note in the next section, where we reassess our noncircular insplunge waveform recipe in light of what we highlighted here.

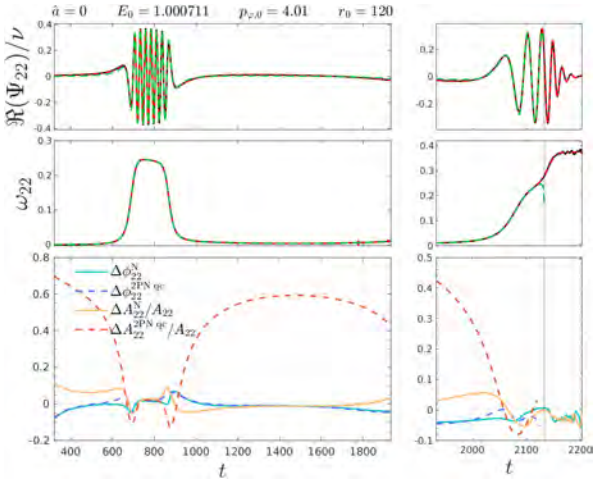

Figure 3.22: Same type of comparison of Fig. 3.19 but considering the dynamical capture configuration in the upper panels of Fig. 3.13. Top panel: real part of the quadrupolar waveform. Middle panel: quadrupolar frequency. Bottom panel: phase and fractional amplitude differences. The waveform of Ref. [251], Eq. (3.95), accumulates rather large amplitude differences up to the apastron of the quasi-elliptic orbit following the first encounter.

3.7 Alternative prescription for the quadrupolar noncircular instantaneous factor

The noncircular corrections we discussed and tested in the previous sections are all fundamentally based on PN expanded spherical multipoles of the waveform that, once recasted in EOB coordinates, are functions of the variables $(u, \varphi, p_{r_*}, p_\varphi)$. In our prescription, this leads to noncircular factors organized in powers of p_{r_*} that reduce to 1 when $p_{r_*} \to 0$. As a consequence, all of them tend to disappear whenever the radial momentum dynamically evolves to small values, notably near the apastra and periastra of the orbital motion.

Let us make a step back and dwell for a moment on the origin of the 2PN noncircular expression of $h_{\ell m}$, and thus of $(U_{\ell m}, V_{\ell m})$, which we are using as an input to devise our waveform corrections. Setting aside the tail contributions, the remaining 2PN-accurate instantaneous terms in $(U_{\ell m}, V_{\ell m})$ are completely determined by the ℓth time derivatives of the source multipoles (I_L, J_L), specified to their 2PN expressions for generic planar dynamics. Then, in the standard procedure, also followed by Ref. [246] for the derivation of the waveform results we used in Sec. 3.2.2 to define our noncircular instantaneous factors, these time derivatives are systematically order reduced by means of the PN-expanded equations of motion. Stated differently, at the 2PN order we are considering here, the instantaneous part of $h_{\ell m}$ is simply given by a straightforward generalization of Eqs. (3.4)-(3.5) where the Newto-

nian multipoles $(I_L)_{\rm Newt}$ and $(J_L)_{\rm Newt}$ are replaced with their 2PN-accurate counterparts. However, contrary to the rationale behind the definition of the general Newtonian prefactor, the natural occurring time derivatives of the dynamical variables appearing therein are all order reduced with the equations of motion.

In what follows we compute an alternative version of the 2PN instantaneous noncircular factor of Sec. 3.2.2 where we crucially skip this order-reduction procedure, in what can be regarded as the 2PN generalization of what is done in `TEOBResumS-DALI` for the Newtonian factor. The result is a noncircular instantaneous correction that also depends on the time derivatives of the EOB variables $(u, \varphi, p_{r_*}, p_\varphi)$, remarkably including terms, such as $\ddot{r}$, that despite being purely noncircular do not vanish in proximity of the radial turning points of the orbital motion (see Fig. 3.21), and thus should capture extra noncircular waveform modulations with respect to the previous prescription. Focusing again on the dominant spherical mode $\ell = m = 2$, we outline the new noncircular factor in Sec. 3.7.1, and then we test its performance in the waveform model in Sec. 3.7.2.

3.7.1 Time-derivative dependent noncircular instantaneous factor

In the case of the quadrupolar mode of the waveform, the 2PN generalization of (3.4) giving the 2PN instantaneous piece of h_{22} reads

$$h_{22}^{\rm inst} = -\frac{\sqrt{6}}{c^4}\frac{d^2}{dt^2}\left(\mathcal{Y}_L^{22}\, I_{ij}\right) \tag{3.101}$$

where, from Eq. (1.168),

$$\mathcal{Y}_{ij}^{22} = \sqrt{\frac{2\pi}{15}}\left(\delta_{1\langle i} - i\delta_{2\langle i}\right)\left(\delta_{j\rangle 1} - i\delta_{j\rangle 2}\right). \tag{3.102}$$

To obtain our new noncircular instantaneous factor, we proceed as follows: (i) we recover the 2PN accurate expressions for I_{ij}, valid for noncircular binaries, from Sec. IIIB of Ref. [246]; (ii) we trade the harmonic coordinates used therein for the EOB phase space variables $(u, \varphi, p_{r_*}, p_\varphi)$, using the transformation laws given in Eqs. (3.24)-(3.27); (iii) we compute $h_{22}^{\rm inst}$ from Eq. (3.101), crucially keeping as they are the occurring time derivatives of the EOB variables, *without* replacing them with the PN-expanded equations of motion; (iv) we factorize the Newtonian part, which is precisely $h_{22}^{(N,0)}$ of Eq. (3.10), and the generic-orbit source term $\hat{S}_{\rm eff}^{(0)} \equiv \hat{H}_{\rm eff}$; (v) we finally factorize the quasi-circular part of the residual, obtained by setting to zero p_{r_*} and all the time derivatives of the EOB variables except for $\Omega \equiv \dot{\varphi}$.

To be more precise, the expression we find for $h_{22}^{\rm inst}$, before the factorization process, has the structure

$$h_{22}^{\rm inst} = h_{22}^{(N,0)}(u, \dot{r}, \ddot{r}, \Omega, \dot{\Omega})$$

$$+\frac{1}{c^2}h_{22}^{(1\mathrm{PN},0)}(u,\dot{r},\ddot{r},\Omega,\dot{\Omega},p_{r_*},\dot{p}_{r_*},\ddot{p}_{r_*},p_\varphi,\dot{p}_\varphi,\ddot{p}_\varphi)$$
$$+\frac{1}{c^4}h_{22}^{(2\mathrm{PN},0)}(u,\dot{r},\ddot{r},\Omega,\dot{\Omega},p_{r_*},\dot{p}_{r_*},\ddot{p}_{r_*},p_\varphi,\dot{p}_\varphi,\ddot{p}_\varphi), \tag{3.103}$$

where $h_{22}^{(N,0)}$ corresponds to Eq. (3.10) and $(h_{22}^{(1\mathrm{PN},0)}, h_{22}^{(2\mathrm{PN},0)})$ formally address the contributions obtained by taking the time derivatives (in this case second order derivatives) of the corresponding PN terms of the source multipoles, while keeping all the derivatives explicit. We thus compute

$$\hat{h}_{22}^{\mathrm{inst}} \equiv T_{2\mathrm{PN}}\left[\frac{h_{22}^{\mathrm{inst}}}{h_{22}^{(N,0)}\hat{S}_{\mathrm{eff}}^{(0)}}\right]. \tag{3.104}$$

The quasi-circular part of this quantity reads

$$\hat{h}_{22}^{\mathrm{c_{inst}}} = 1+\frac{u}{c^2}\left[-\frac{12}{7}-\frac{p_\varphi^2 u}{3}+\left(\frac{1}{7}+\frac{p_\varphi^2 u}{2}\right)\nu\right]+\frac{u^2}{c^4}\left[-\frac{229}{252}\right.$$
$$-\frac{929p_\varphi^2 u}{756}+\frac{19p_\varphi^4 u^2}{63}+\left(\frac{289}{126}-\frac{1741p_\varphi^2 u}{378}-\frac{235p_\varphi^4 u^2}{504}\right)\nu$$
$$\left.+\left(\frac{65}{126}+\frac{31p_\varphi^2 u}{54}-\frac{143p_\varphi^4 u^2}{504}\right)\nu^2\right], \tag{3.105}$$

with p_φ left explicit, instead of being rewritten in terms of its quasi-circular orbit expansion in u. The sought for 2PN noncircular instantaneous factor is then obtained as

$$\hat{h}_{22}^{\mathrm{nc_{inst}}} = T_{2\mathrm{PN}}\left[\frac{\hat{h}_{22}^{\mathrm{inst}}}{\hat{h}_{22}^{\mathrm{c_{inst}}}}\right], \tag{3.106}$$

and results in a rather long function of the variables $(u,\dot{r},\ddot{r},\Omega,\dot{\Omega},p_{r_*},\dot{p}_{r_*},\ddot{p}_{r_*},p_\varphi,\dot{p}_\varphi,\ddot{p}_\varphi)$, which we report explicitly in Appendix C.3. Because of its involved analytical structure, we find here convenient not to split this factor in amplitude and phase.

Thanks to the fact that tail and instantaneous terms appear at different PN orders and that the factorization procedure leading to Eq. (C.22) is analogous to the one considered in Sec. (3.2.2), we can directly employ the new instantaneous noncircular factor (C.22) in the waveform model of Sec. (3.2.2) in place of its previous counterpart with order-reduced derivatives; relevantly, this means that we do not have the need of recomputing the noncircular tail factor, which remains in the resummed form outlined in Sec. 3.3.2. We test the so obtained alternative version of our 2PN-corrected waveform model in the next section.

3.7.2 Assessment of the new waveform factor

The new prescription for the 2PN noncircular correcting factor is tested by examining the performance of the respective waveform in the test-mass limit, for

several dynamical configurations, and in the comparable-mass case. To set the stage, we consider a particle inspiralling and plunging around a Schwarzschild black hole in Fig. 3.23, which refers to a configuration with initial eccentricity $e_0 = 0.5$ and semilatus rectum $p_0 = 7.35$. At the level of the phase, the

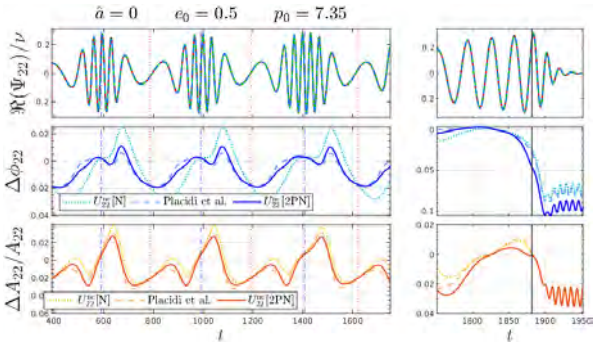

Figure 3.23: Quadrupolar waveform generated by a test-mass plunging into a Schwarzschild black hole along an orbit with initial eccentricity $e_0 = 0.5$ and semilatus rectum $p_0 = 7.35$. In the top panel the numerical waveform (black line) is shown alongside the EOB waveform of `TEOBResumS-DALI` (dashed red line, below dubbed $U_{22}^{\rm nc}[\rm N]$), the one with the prescription of Sec. (3.2.2) (dashed green line, below dubbed "Placidi et al." after the paper where we introduced it), and to the one proposed in the present section (dash-dotted blue line, dubbed $U_{22}^{\rm nc}[\rm 2PN]$). The middle and bottom panels show the phase and relative amplitude differences for the three analytical waveform considered.

performance of the new noncircular factor and the one of Sec. (3.2.2) are substantially equivalent; see the dashed and solid blue lines in the middle panel of Fig. 3.23. For the amplitude, instead, the new approach yields a reduced maximum analytical/numerical difference during the evolution, as well as a slight improvement as the orbital motion approaches the periastra; see bottom panel of Fig. 3.23. In view of our previous considerations, we attribute the cause of this difference to the nonvanishing of the new noncircular correction at the radial turning points. This is further highlighted in Fig. 3.24, which compares the amplitude and phase of the noncircular instantaneous factor used in the different prescriptions of Fig. 3.23. The bottom panel shows that the 2PN factor we are considering here does not vanish at the radial turning points and is especially relevant at periastron. Note that the noncircular instantaneous phase corrections at 2PN differ sensibly from the Newtonian one; however, part of this difference is compensated by the hereditary phase correction, as already highlighted in Fig. 3.7.

To better evaluate the impact of the difference at periastron between the two 2PN noncircular factors, it is convenient to compare how the respective quadrupolar waveforms reproduce the fluxes $\dot{J}_{22} = -\dfrac{1}{4\pi}\Im\left(\dot{h}_{22}h_{22}^{*}\right)$ and $\dot{E}_{22} =$

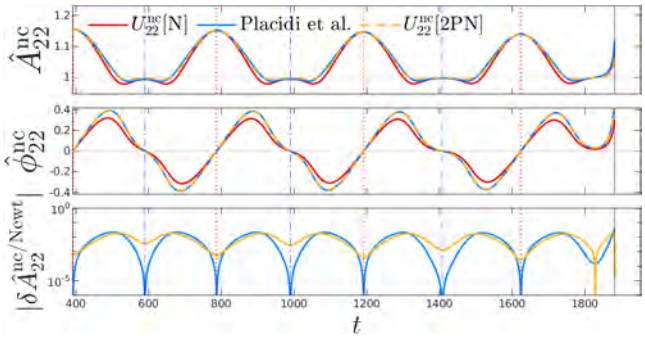

Figure 3.24: Comparing the instantaneous noncircular correction to the amplitude (top panel) and phase (middle panel) of the quadrupolar waveform, considering the same dynamical configuration and analytical prescriptions of Fig. 3.23. Bottom panel: amplitude relative difference of the two 2PN-corrected prescriptions with respect to the Newtonian contribution. The noncircular factor introduced here is nonzero at the apastron (red dotted vertical lines) and periastron (blue dash-dotted vertical lines). The black vertical line marks merger time.

$\frac{1}{8\pi}|\dot{h}_{22}|^2$. More specifically, we consider the set of 14 geodesic eccentric orbits of Table 3.5, already employed for Fig. 3.18 in Sec. 3.5.3. For instance, in Fig. 3.25 we compare the fluxes for one of these configurations, with $e = 0.5$. From the analytical/numerical relative differences, one finds that the 2PN noncircular corrections with explicit derivatives perform better at periastron than the one of Sec. 3.2.2. The upper panels show instead a slightly stronger emission at periastron than before, implying that, once the new waveform prescription is recasted in an angular radiation-reaction force correction, as we did in Sec. 3.5, and the latter is incorporated within the EOB dynamics, we would eventually have an additional acceleration of the eccentric inspiral. The development and testing of this radiation-reaction corrections is deferred to future work.

To draw a more global picture, it is useful to compare the orbital-averaged analytical fluxes with the corresponding, averaged, numerical ones, mirroring what we did in Fig. 3.18. This is done in Fig. 3.26. As showed therein, the new 2PN noncircular correction with explicit time derivatives yields (on average) the best analytical/numerical agreement: even when such a correction is truncated at 1PN, the respective waveform reproduces more accurate fluxes than the one of Sec. (3.2.2). Note however that the average over all spinning configurations can hide some information. In particular, for highly eccentric configurations ($e = 0.9$), the Newtonian prescription yields a better analytical/numerical agreement when averaged only on negative spins. However, in the Schwarzschild case, the hierarchy of the different prescriptions is the same

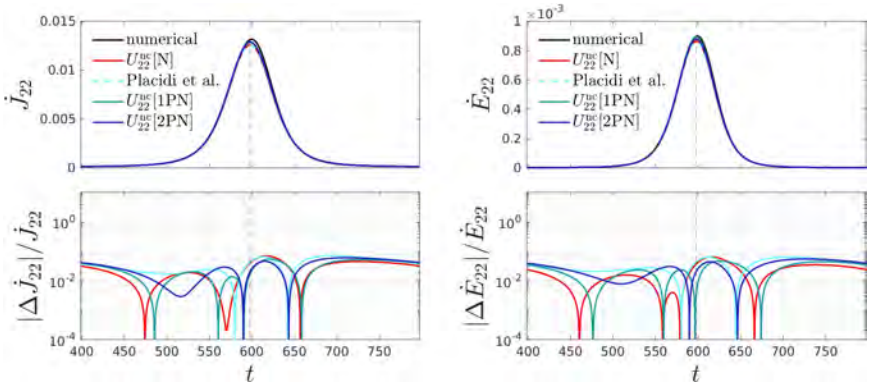

Figure 3.25: Quadrupolar fluxes at infinity of angular momentum and energy, generated by a test-particle in Schwarzschild spacetime along a geodesic with $e = 0.5$ and $p = 9$. To mark the different prescription we use the same notation of Fig. 3.23, with the addition of $U_{22}^{\rm nc}$[1PN], that represent the prescription with the time-derivative dependent noncircular factor truncated at 1PN. The vertical dashed line in the middle marks the periastron. The relative differences in the bottom panels shows that the prescription $U_{22}^{\rm nc}$[2PN] is the one with the best analytical/numerical agreement at periastron.

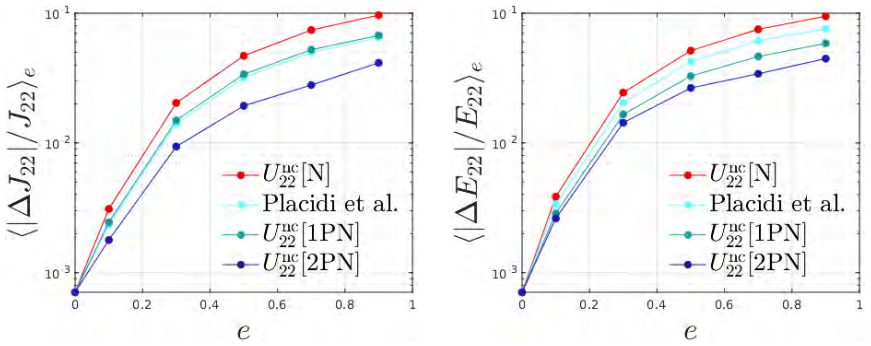

Figure 3.26: Analytical/numerical fractional differences between the averaged quadrupolar fluxes versus eccentricity. Each point is obtained from the mean of the orbital averaged fluxes of all the configurations at a given eccentricity e, taken from the set we previously considered for Fig. 3.18. We see that the analytical/numerical agreement of the fluxes is consistently improved with respect to the previous prescription, more evidently as we go towards high eccentricities.

as that of Fig. 3.26.

The new noncircular correcting factor with explicit time derivatives seems quantitatively superior to all the other prescriptions. This is further corroborated by the following: the instantaneous amplitude correction presented in Eq. (3.54) contains a 1PN term $\propto -p_{r_*}^2/u = -p_{r_*}^2 r$ that can become extremely large when considering hyperbolic or eccentric orbits with large initial radius. While this issue is not relevant for any of the configurations considered in Sec. 3.2.2, such an amplitude correction can become even negative, and thus unphysical, for large separations, e.g. those occurring in hyperbolic encounters. By contrast, the new noncircular correction is well-behaved *also* for a hyperbolic encounter or a scattering configuration starting from any, arbitrarily large, initial separation.

The same behavior carries over to the comparable-mass case, with the test-mass dynamics replaced by the resummed EOB dynamics in the evaluation of the explicit time derivatives. Figure 3.27 exhibits the time evolution of the different noncircular waveform corrections along the EOB dynamics of a binary corresponding to the illustrative NR configuration SXS:BBH:321 of the SXS catalog [267], row #23 in Table 3.4. In this case, the mass ratio is $q = 1.22$ while the dimensionless spins (χ_1, χ_2), aligned with the orbital angular momentum, are $\chi_1 = +0.33$ and $\chi_2 = -0.44$. The initial EOB eccentricity at the apastron is small, $e_{\omega_a}^{\rm EOB} = 0.07621$, but large enough to probe whether the new waveform model brings an improvement with respect to the one of Sec. 3.2.2 or not. Fig. 3.27 indicates that, in the comparable-mass case, the amplitude

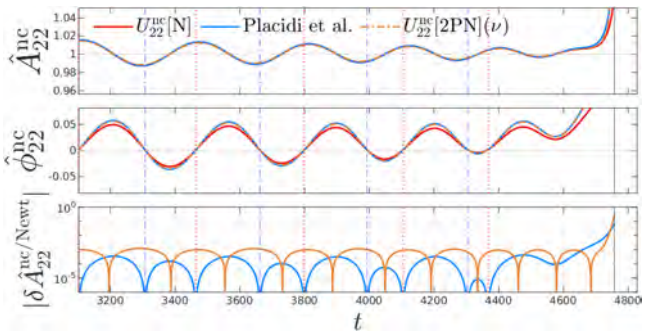

Figure 3.27: Same scheme as in Fig. 3.24, but relative to an eccentric inspiral binary with $e_0 = 0.07621$ and $q = 1.22$, corresponding to the illustrative NR configuration SXS:BBH:321 of the SXS catalog [267], row #23 in Table 3.4.

correction at the radial turning points is more relevant than in the test-mass case (compare with Fig. 3.24), although the extra correction with respect to the Newtonian one is still quite small. It is also informative to look at the EOB/NR phasing comparison for SXS:BBH:321, that we report in Fig. 3.28. The top panels compare the EOB and NR real parts of the waveform, while the bottom panels show the EOB/NR phase difference $\Delta\phi_{22}^{\rm EOBNR} \equiv \phi_{22}^{\rm EOB} - \phi_{22}^{\rm NR}$

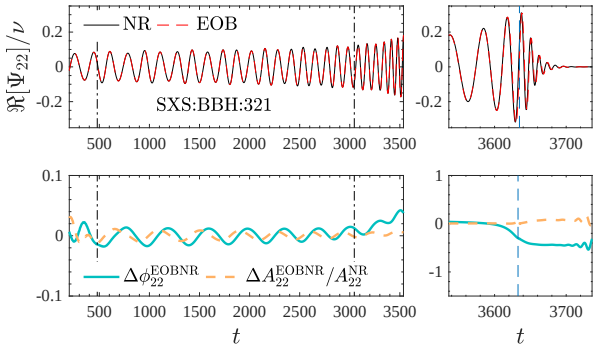

Figure 3.28: Illustrative EOB/NR phasing comparison with the NR dataset SXS:BBH:321 of the SXS catalog [267]; see row #23 in Table 3.4 for the relevant data. The EOB waveform is aligned to the NR one by minimizing the phase difference in the frequency interval corresponding to the two vertical lines in the left panels of the figure. Here, the EOB/NR phase difference is reduced during the plunge with respect to the corresponding plot in the upper right corner of Fig.3.15, in Sec. 3.4.1. The associated noncircular waveform correction is shown in Fig. 3.27.

and relative amplitude difference, with $\Delta A_{22}^{\rm EOBNR} \equiv A_{22}^{\rm EOB} - A_{22}^{\rm NR}$. The picture illustrates that $\Delta\phi_{22}^{\rm EOBNR}$ is reduced, during the late-inspiral and plunge, with respect to the corresponding plot with the model of Sec. 3.2.2, in the upper right corner of Fig. 3.15, which uses the same waveform alignment interval. A similar behavior is also found with higher eccentricities. However, it must be noted that, since the waveform is different, the choice of the initial parameters, which we are currently not changing, might be optimized further. Investigations on this aspect, together with the extension of this prescription to higher modes, is postponed to future work.

Conclusions

In this Thesis we addressed the problem of building accurate analytical models for GW signals that had their origin in the coalescence of non-circularized compact binary systems, i.e. binaries of compact objects whose orbital eccentricity remains non-negligible during their whole inspiral motion. We started out with an in-depth exploration of the general theory of GWs produced by PN sources, in Chapter 1, where we laid down the basic theoretical concepts and methodologies that are at the heart of any analytical waveform model. Then, in Chapter 2, we specialized our discussion to the case of EOB models, probing in details how the EOB approach describes the evolution of compact binaries and the associated emission of gravitational radiation. Here, we paid particular attention to the prescriptions of `TEOBResumS`, the faithful and physically complete EOB model upon which we based our waveform modeling activity, which represents the core content of Chapter 3, and, more in general, of our original contributions to the field. In particular, after having reviewed `TEOBResumS-DALI`, the state of the art eccentric branch of the aforementioned model, we dedicated the rest of Chapter 3 to propose and thoroughly test several extensions of it, which revolve around the inclusion of 2PN noncircular waveform information, with the goal of better capturing GW modulations induced by the eventual noncircularity in the underlying binary dynamics.

More specifically, in what follows we recap our proposals and set out the conclusions we can draw from their performance assessment:

(i) We have exploited 2PN waveform results for generic planar orbits to come up with the definition of associated correcting factors that can be directly used to improve the waveform of `TEOBResumS-DALI`, within the paradigm of the factorization of the generic Newtonian prefactor. In particular we split these corrections in instantaneous and tail factors, on the basis of the character of the waveform information they respectively incorporate.

(ii) We tested the performance of these analytical correcting factors by performing comparisons with numerical waveforms from eccentric inspirals (also through plunge and merger) in the test-mass limit. We showed

that the analytical/numerical agreement through the plunge phase, especially for large eccentricity, can be largely improved by implementing a straightforward resummation scheme, via Padé approximants, of the residual polynomials in $p_\varphi^2 u$ entering the noncircular factors; this was found to be particularly important for the tail factors. With this procedure, we obtained an analytical/numerical phase disagreements of ± 0.04 rad for $e = 0.9$ and disagreements at most within 0.02 rad for smaller eccentricities; see Figs. 3.5 and 3.6. Similar improvements are also found for the test-mass limit hyperbolic captures analyzed in Sec. 3.3.6.

(iii) Moving to the comparable-mass case, we provided a new comparison for our upgraded version of `TEOBResumS-DALI` with 28 public NR simulations of eccentric inspirals, from the SXS catalog. For most of the configurations, the phase difference during the inspiral is mostly within the ± 0.05 bandwidth. The related EOB/NR unfaithfulness computations (using aLIGO noise for $20M_\odot \leq M \leq 200M_\odot$) are below the 1% threshold, grazing at most the 0.7%, except for a single outlier, SXS:BBH:1149, which reaches this limit because of limitations inherited by the underlying quasi-circular model, as explained in Ref. [157]. It should be noted that the new 2PN factor discussed here are found to be small corrections to the `TEOBResumS-DALI` avatar of Ref. [157]. As such, the use of well controlled test-mass limit numerical data is crucial for determining the actual importance of this additional analytical information.

(iv) Adopting factorization and resummation strategies analogues to those used for the waveform, we have also built 2PN noncircular correcting factors with which to dress the quadrupolar component of the angular radiation-reaction force of `TEOBResumS-DALI`. Our flux tests indicate that employing this new radiation-reaction force prescription yields a small but visible improvement in the analytical/numerical agreement for each value of the eccentricity; see Fig. 3.18.

(v) The availability of test-mass waveform data has also allowed us to thoroughly compare our waveform prescription with the one proposed in Ref. [251], whose main difference from ours is that the the Newtonian prefactor is left in its original quasi-circular form. We found that the factorization of the general Newtonian-factor, even before the inclusion of our 2PN noncircular factors, yields more accurate and robust predictions all over the parameter space. This is particularly relevant at the level of the waveform amplitude, with differences that can reach up to 60%, versus the 6% at most of our model; see Figs. 3.19 and 3.20.

(vi) The origin of the reliable behavior found for the amplitude of the waveform with the general Newtonian factor $h_{\ell m}^{(N,\epsilon)}$, somehow not precisely understood in past works, has been traced back to the crucial presence

in the latter of contributions like $\ddot{r}/r\Omega^2$ that do not vanish at the radial turning point of the binary motion. This prompted the proposal of an alternative version of our 2PN noncircular instantaneous factors where, similarly to $h_{\ell m}^{(N,\epsilon)}$, the time derivatives of the EOB variables are left explicit. We comprehensively tested this prescription, focusing on the mode $\ell = m = 2$, against a large set of numerical data, with waveforms and fluxes emitted by a test-mass orbiting a Kerr black hole and with comparable-mass simulations. The corresponding waveform model has been observed to increase consistently the analytical/numerical agreement with respect its previous 2PN-corrected iteration; this is particularly evident at the level of the fluxes, which are reported in Fig. 3.26.

To wrap up, our results indicate that the incorporation of high-PN noncircular waveform information within EOB models is more effective if, on the one hand, suitable factorizations and resummation procedures are implemented, and if, on the other hand, the time derivatives of the EOB variables, naturally occurring in the formal expression of the analytical waveform, are not replaced, whenever possible, with the PN-expanded equations of motion, but rather evaluated using their resummed EOB counterparts. This also explains why the use of the general Newtonian prefactor, as originally proposed in Ref. [254], seems to be an essential element for constructing highly accurate analytical waveforms for noncircular dynamics.

Appendix

Appendix A

Useful mathematical tools

A.1 Symmetric-trace-free projection of a generic tensor

Given a Cartesian tensor $T_P \equiv T_{i_1 \dots i_p}$, its explicit STF part reads

$$\hat{T}_P = \sum_{k=0}^{[p/2]} a_k^p \delta_{(i_1 i_2} \delta_{i_3 i_4} \dots \delta_{i_{2k-1} i_{2k}} S_{i_{2k+1} \dots i_p) a_1 a_1 \dots a_k a_k} \,, \tag{A.1}$$

where the parenthesis () denote a symmetrization over the indices they enclose,

$$S_P \equiv T_{(P)}, \tag{A.2}$$

$$a_k^p \equiv \frac{p!}{(2p-1)!!} (-)^k \frac{(2p-2k-1)!!}{(p-2k)!(2k)!!}, \tag{A.3}$$

and $[p/2]$ is the integer part of $p/2$.

For example we have

$$\hat{T}_{ij} = T_{(ij)} - \frac{1}{3} \delta_{ij} T_{aa}, \tag{A.4}$$

$$\hat{T}_{ijk} = T_{(ijk)} - \frac{1}{5} \big(\delta_{ij} T_{(kaa)} + \delta_{jk} T_{(iaa)} + \delta_{ik} T_{(jaa)} \big). \tag{A.5}$$

A.2 Padé approximants

Given the truncated Taylor series of an arbitrary function, we define its Padé approximants as the rational polynomials that, written in terms of the same number of coefficients of the original truncated series, reduce to the latter when it is correspondingly Taylor-expanded and truncated.

Let us consider, by way of illustration, a function f of the variable u and the associated Taylor series in u truncated at order n,

$$S_n(u) \equiv T_n \big[f(u) \big] = f_0 + f_1 u + f_2 u^2 + ... + f_n u^n, \tag{A.6}$$

where, as in the main text, T_n is the operator that applies on its argument a Taylor series truncated at order n, here on the variable u. Introducing two integers (k, m) such that $m + k = n$, the $n + 1$ possible Padé approximants associated to the truncated series (A.6) are the rational functions $P^k_m\big[S_n(u)\big]$ such that

$$P^k_m\big[S_n(u)\big] = \frac{N_k(u)}{D_m(u)}, \tag{A.7}$$

$$T_n\big[P^k_m\big[S_n(u)\big]\big] = T_n\big[f(u)\big], \tag{A.8}$$

where $N_k(u)$ and $D_m(u)$ are polynomials in u, respectively of order k and m, with $D_m(0) = 1$; their coefficients are *uniquely* determined by Eq. (A.8) in terms of those of the original series (A.6), i.e. $(f_0, f_1, ..., f_n)$. For instance, given $S_3(u) = f_0 + f_1 u + f_2 u^2 + f^3 u^3$, we have

$$P^3_0\big[S_3(u)\big] = S_3(u), \tag{A.9}$$

$$P^2_1\big[S_3(u)\big] = \frac{a_0 + a_1 u + a_2 u^2}{1 + a_3 u}, \tag{A.10}$$

$$P^1_2\big[S_3(u)\big] = \frac{b_0 + b_1 u}{1 + b_2 u + b_3 u^2}, \tag{A.11}$$

$$P^0_3\big[S_3(u)\big] = \frac{c_0}{1 + c_1 u + c_2 u^2 + c_3 u^3}, \tag{A.12}$$

where $a_0 = b_0 = c_0 = f_0$ and

$$a_1 = \frac{f_1 f_2 - f_0 f_3}{f_2}, \quad a_2 = \frac{f_2^2 - f_1 f_3}{f_2}, \quad a_3 = -\frac{f_3}{f_2}; \tag{A.13}$$

$$b_1 = \frac{f_1^3 - 2 f_0 f_2 f_1 + f_0^3 f_3}{f_1^2 - f_0 f_2}, \quad b_2 = \frac{f_0 f_3 - f_1 f_2}{f_1^2 - f_0 f_2}, \quad b_3 = \frac{f_2^2 - f_1 f_3}{f_1^2 - f_0 f_2}; \tag{A.14}$$

$$c_1 = -f_1, \quad c_2 = f_1^2 - f_2, \quad c_3 = -f_1^3 + 2 f_2 f_1 - f_3. \tag{A.15}$$

Notice that Padé approximants are really useful only when $(k, m) \neq (n, 0)$, otherwise we simply recover the starting truncated series.

Concerning the relevant properties of Padé approximants, in general they satisfy

$$P^k_m\big[T_n\big[f(u)\big]\big] = \big(P^m_k\big[T_n\big[f^{-1}(u)\big]\big]\big)^{-1}, \tag{A.16}$$

$$P^{n/2}_{n/2}\big[S_n(u)\big] = f_0 + f_1 u\, P^{n/2-1}_{n/2}\big[\tilde{S}_{n-1}(u)\big] \qquad \text{if } n \text{ is even}, \tag{A.17}$$

$$P^{(n+1)/2}_{(n-1)/2}\big[S_n(u)\big] = f_0 + f_1 u\, P^{(n-1)/2}_{(n-1)/2}\big[\tilde{S}_{n-1}(u)\big] \qquad \text{if } n \text{ is odd}, \tag{A.18}$$

where

$$\tilde{S}_{n-1}(u) \equiv \frac{S_n(u) - f_0}{f_1 u}. \tag{A.19}$$

Appendix B

TEOBResumS for spin-aligned coalescing binaries

Even though spinning compact binaries do not represent the main source of reference for the waveform modeling activity discussed in this Thesis, specifically in Chapter 3, the basic version of the TEOBResumS model upon which the latter is based is actually capable of reproducing GW waveforms emitted by spinning binaries whose component objects have spins *aligned* or *anti-aligned* to the direction of their total angular momentum. This is made possible by a series of dedicated generalizations with respect to the non-spinning sector of the model we reviewed in Chapter 2, both at the level of the dynamical description and the pre-merger waveform model. In the following we will go through these generalizations, specifically targeting the spin-related modifications to the EOB Hamiltonian, in Sec. B.1, and to the insplunge waveform and radiation reaction force, in Sec. B.2.

B.1 Spin effects in the EOB Hamiltonian

Let us start by recalling the structure of the Hamiltonian of a spinning test μ-mass, with spin vector $\mathbf{S}_*$, in equatorial ($\theta = \pi/2$) motion around a Kerr black hole with mass M and spin vector $\mathbf{S}$. If we use, as usual, rescaled polar coordinates, with $\hat{a} \equiv |\mathbf{S}|/(cGM^2)$ and $\hat{a}_* \equiv |\mathbf{S}_*|/(cGM^2)$, the corresponding μ-rescaled Hamiltonian can be written according to the structure

$$\hat{H}_{\rm Kerr} = \hat{H}^{\rm orb}_{\rm Kerr}(r, p_r, p_\varphi, \hat{a}) + \frac{p_\varphi}{c}\left(g^{\rm K}_S \hat{a} + g^{\rm K}_{S_*} \hat{a_*}\right). \tag{B.1}$$

The first therm is the "orbital" component of the Hamiltonian and collects all the terms that are even in the spins. In the equatorial case we can conveniently write it as

$$\hat{H}^{\rm orb}_{\rm Kerr} = c^2 \sqrt{A_{\rm K}(r, \hat{a})\left(1 + \frac{p_r^2}{c^2 B_{\rm K}(r, \hat{a})} + \frac{p_\varphi^2}{c^2 r_c^2}\right)} \tag{B.2}$$

where we introduced the *centrifugal radius*

$$r_c^2 \equiv r^2 + \hat{a}^2 + \frac{2\hat{a}^2}{c^2 r}, \tag{B.3}$$

so to recast $H^{\rm orb}_{\rm Kerr}$ in a form that structurally mirrors the one of the test-particle Hamiltonian in the Schwarzschild case. The functions $A_{\rm K}$ and $B_{\rm K}$ appearing in Eq. (B.2) are explicitly given by

$$A_{\rm K}(r,\hat{a}) = \frac{r^2 + \hat{a}^2 + \dfrac{2r}{c^2}}{r_c^2}, \qquad B_{\rm K}(r,\hat{a}) = \frac{r^2}{r^2 + \hat{a}^2 + \dfrac{2r}{c^2}}, \tag{B.4}$$

and are such that

$$D_{\rm K}(r,r_c) \equiv A_{\rm K}(r,\hat{a}) B_{\rm K}(r,\hat{a}) = \frac{r^2}{r_c^2}. \tag{B.5}$$

Focusing on $A_{\rm K}(r,\hat{a})$, we notice that the use of r_c allows us to rewrite it in the form [148]

$$A_{\rm K}(r,\hat{a}) = A_{\rm Schw}(r_c)\hat{A}(r,r_c), \tag{B.6}$$

where we singled out

$$A_{\rm Schw}(r_c) = 1 - \frac{2}{c^2 r_c}, \tag{B.7}$$

the usual radial potential A in Schwarzschild, here with the replacement $r \to r_c$, and a residual correcting factor

$$\hat{A}(r,r_c) = \frac{1 + \dfrac{2}{c^2 r_c}}{1 + \dfrac{2}{c^2 r}}. \tag{B.8}$$

The last two terms of Eq. (B.1) are instead expression of the spin-orbit couplings between the spins $(\mathbf{S},\mathbf{S}_*)$ and the reduced angular momentum of the particle. They are determined by the two gyrogravitomagnetic functions $(g_S^{\rm K}, g_{S_*}^{\rm K})$ [268, 269], where for instance

$$g_S^{\rm K} = \frac{2G^3M^3}{r r_c^2}. \tag{B.9}$$

Mirroring what is done in the non-spinning case, the EOB Hamiltonian for spin-aligned (or anti-aligned) binaries featured by the `TEOBResumS` model is engineered as a generalization to arbitrary ν of the test-mass limit case given by Eq. (B.1), which must be recovered for $\nu \to 0$. First of all, we specify that, given the two individual spin vectors of a spinning compact binary, $(\mathbf{S}_1,\mathbf{S}_2)$,

the spin vectors $(\mathbf{S}, \mathbf{S}_*)$, here respectively relative to the effective metric and the EOB test particle, can be defined as

$$\mathbf{S} = \mathbf{S}_1 + \mathbf{S}_2, \qquad \mathbf{S}_* = \frac{m_2}{m_1}\mathbf{S}_1 + \frac{m_1}{m_2}\mathbf{S}_2. \tag{B.10}$$

Moreover, it is assumed [143] that the presence of spin does not alter the energy map (2.89), found in the non-spinning case, which thus still remains as the defining relation between the EOB Hamiltonian and the effective one. As the latter encodes the actual dynamical description (in its conservative part) of the effective problem, where now there are also spins, one has indeed to include in it some extra spin-induced term. This is done by maintaining the structure of the Kerr Hamiltonian given in Eq. (B.1), namely defining the spinning effective Hamiltonian according to

$$\hat{H}_{\rm eff} = \hat{H}^{\rm orb}_{\rm eff} + \frac{p_\varphi}{c}\left(g^{\rm eff}_S \hat{a} + g^{\rm eff}_{S_*}\hat{a}_*\right), \tag{B.11}$$

where the functions $\hat{H}^{\rm orb}_{\rm eff}$, $g^{\rm eff}_S$, and $g^{\rm eff}_{S_*}$ are given by specific ν-deformations of their counterparts in Eq. (B.1). In shaping all of them, a crucial step is to extend the definition of r_c to the comparable-mass case. Ref. [143] proved that the leading spin-spin effects can be incorporated by simply replacing the spin parameter $\hat{a}$ in Eq. (B.3) with its effective analogue

$$\hat{a}_0 \equiv \hat{a}_1 + \hat{a}_2 = \hat{a} + \hat{a}_*, \tag{B.12}$$

where $\hat{a}_{1,2} \equiv \left|\mathbf{S}_{1,2}\right| / (c m_{1,2} G M)$ and in the last equality we used

$$\frac{\mathbf{S}_1}{m_1} + \frac{\mathbf{S}_2}{m_2} = \frac{\mathbf{S} + \mathbf{S}_*}{M}, \tag{B.13}$$

as implied by Eq. (B.10). Furthermore, in order to also include next-to-leading order spin-spin effects, as it is currently done in `TEOBResumS`, we have to extend the redefinition of r_c to

$$r_c^2 \equiv r^2 + \hat{a}_0^2 + \frac{2\hat{a}_0^2}{c^2 r} + \delta\hat{a}^2, \tag{B.14}$$

$$\delta\hat{a}^2 \equiv \frac{1}{c^2 r}\left[\frac{5}{4}\sqrt{1-4\nu}(\hat{a}_1 - \hat{a}_2)\hat{a}_0 - \left(\frac{5}{4} + \frac{\nu}{2}\right)\hat{a}_0^2 + \left(\frac{1}{2} + 2\nu\right)\hat{a}_1\hat{a}_2\right], \tag{B.15}$$

We are now ready to specify the expressions of the three Hamiltonian functions appearing in Eq. (B.11). As regards $\hat{H}^{\rm orb}_{\rm eff}$, given its test-particle reduction (B.2) and its form (2.90) in the non-spinning case, we write

$$\hat{H}^{\rm orb}_{\rm eff} = c^2\sqrt{\frac{p_{r_*}^2}{c^2} + A(u, u_c)\left(1 + p_\varphi^2 u_c^2 c^2 + \frac{Q(u_c, p_{r_*})}{c^2}\right)} \tag{B.16}$$

where, in analogy with $u \equiv 1/(c^2 r)$, we also used $u_c \equiv 1/(c^2 r_c)$. Here, generalizing the test-particle result of Eq. (B.6), we consider

$$A(u, u_c) = P_5^1[A_{\leq 5\mathrm{PN}}]\hat{A}(u, u_c), \tag{B.17}$$

where $P_5^1[A_{\leq 5\mathrm{PN}}]$ is the 5PN resummed prescription used for the potential A in the non-spinning case, with the replacement $u \to u_c$, whereas $\hat{A}(u, u_c)$ is the correcting factor (B.8), simply rewritten in terms of u and u_c. By the same logic, considering Eq. (B.5), the potential D that defines the radial momentum $p_{r_*} = A/D^{1/2}\, p_r$ is given by

$$D(u, u_c) = \frac{u_c^2}{u^2} D_{\mathrm{orb}}(u_c), \tag{B.18}$$

with

$$D_{\mathrm{orb}}(u_c) = P_3^0[D_{\leq 3\mathrm{PN}}](u_c) = \frac{1}{1 + 6\nu u_c^2 - 2(3\nu - 26)\nu u_c^3}, \tag{B.19}$$

as in Eq. (2.60). Lastly we have

$$Q(u_c, p_{r_*}) = \frac{u_c^2}{c^2}\left[2(4 - 3\nu)\nu p_{r_*}^4\right], \tag{B.20}$$

again using u_c in place of u in the corresponding non-spinning expression.

On the spin-orbit side of the effective Hamiltonian, the two gyrogravitomagnetic functions $(g_S^{\mathrm{eff}}, g_{S_*}^{\mathrm{eff}})$ are incorporated in the factorized form

$$g_S^{\mathrm{eff}} = g_S^{\mathrm{eff},0} \hat{g}_S^{\mathrm{eff}}, \qquad g_{S_*}^{\mathrm{eff}} = g_{S_*}^{\mathrm{eff},0} \hat{g}_{S_*}^{\mathrm{eff}}, \tag{B.21}$$

where the Newtonian contributions

$$g_S^{\mathrm{eff},0} = 2c^6 u u_c^2, \qquad g_{S_*}^{\mathrm{eff},0} = \frac{3}{2} c^6 u_c^3, \tag{B.22}$$

are factored out in front of the PN residuals $\hat{g}_S^{\mathrm{eff}} = 1 + \mathcal{O}(1/c^2)$ and $\hat{g}_{S_*}^{\mathrm{eff}} = 1 + \mathcal{O}(1/c^2)$. These are explicitly obtained by resumming their 2PN expansions [270, 271], written in terms of just u_c and p_{r_*}, using Padé of the type P_n^0. Moreover: (i) the function $\hat{g}_{S_*}^{\mathrm{eff}}$ is hybridized with $\nu = 0$ terms up to 4PN, specifically taken from the simplified case of a spinning test-particle in circular motion around a Schwarzschild black hole; (ii) both $\hat{g}_S^{\mathrm{eff}}$ and $\hat{g}_{S_*}^{\mathrm{eff}}$ are flexed with the 3PN term $\nu u_c^3 c_3$, where c_3 is a ν-dependent tunable parameter that is fixed by fits to NR data, similarly to what is done for the parameter $a_{6,\mathrm{c}}$ in $A_{\leq 5\mathrm{PN}}$, which we already mentioned at the end of Sec. 2.1.4. For the resulting explicit expression of $\hat{g}_S^{\mathrm{eff}}$ and $\hat{g}_{S_*}^{\mathrm{eff}}$ used in `TEOBResumS`, see Eqs. (42)-(56) of Ref. [148].

B.2 Spin effects in insplunge waveform and radiation reaction force

In this section we collect and discuss the modifications, with respect to the insplunge quasi-circular waveform and the corresponding radiation reaction force, that allow `TEOBResumS` to faithfully capture spin-induced modulations in the GW signals.

At the level of the insplunge waveform, the first obvious difference with respect to its non-spinning counterpart of Sec. 2.2 is that the staring PN results for the spherical mode $h_{\ell m}$, used as input in the factorization procedure, are now to be taken in their full spin-dependent form, computed by enforcing that their source is a spinning compact binary. Correspondingly, each $h_{\ell m}$ is found to be separable in the sum

$$h_{\ell m} = h^{\rm orb}_{\ell m} + h^{\rm S}_{\ell m}, \tag{B.23}$$

between an orbital, spin-independent part $h^{\rm orb}_{\ell m}$ and the collection of all the spin-dependent terms $h^{\rm S}_{\ell m}$. Coming to the factorization procedure, the differences with respect to Sec. 2.2 are the following.

(i) In the Newtonian prefactor (2.101) and in effective source (2.105), the radius r_ω, which also enters the azimuthal velocity v_φ, is generalized to

$$r_{\omega_c} = \left[\frac{(r_c^3\psi_c)^{-1/2} + \left(g_S^{\rm eff}\hat{a} + g_{S_*}^{\rm eff}\hat{a}_*\right)/c}{\hat{H}_{\rm EOB}}\right]^{-2/3}_{p_{r_*}=0} \tag{B.24}$$

with the spin-flexed version ψ_c of the function ψ in Eq. (2.104) that is given by

$$\psi_c \equiv -\frac{2}{A(u_c)'}\left(u_c' + \frac{g_S^{\rm eff}{}'\hat{a} + g_{S_*}^{\rm eff}{}'\hat{a}_*}{c^6 u_c A(u_c)}\sqrt{\frac{A(u_c)}{c^2 p_\varphi^2} + A(u_c)u_c^2}\right), \tag{B.25}$$

where the prime denotes derivatives with respect to r.

(ii) By way of the separation (B.23), the residual PN amplitude $f_{\ell m}$ of Eq. (2.109) is itself decomposed in an orbital and a spinning part,

$$f_{\ell m} = f^{\rm orb}_{\ell m} + f^{S}_{\ell m}, \tag{B.26}$$

where $f^{\rm orb}_{\ell m}$ is exactly the residual PN amplitude factor considered in the non-spinning sector of the model. When m is even, the prescription laid down in Refs. [272, 273] and adopted in `TEOBResumS` provides for a factorization of $\rho_{\ell m} = (f_{\ell m})^{1/\ell}$ that is given by

$$\rho_{\ell m} = \rho^{\rm orb}_{\ell m}\hat{\rho}^{\rm S}_{\ell m}, \qquad \hat{\rho}^{\rm S}_{\ell m} \equiv T_{\rm PN}\left[1 + \frac{\rho^{\rm S}_{\ell m}}{\rho^{\rm orb}_{\ell m}}\right]. \tag{B.27}$$

Then, while $\rho^{\rm orb}_{\ell m}$ is treated precisely as reported below Eq. (2.111), the factor $\hat{\rho}^{\rm S}_{\ell m}$ is resummed according to the "iResum" paradigm [272], i.e. by replacing it with its inverse Taylor representation

$$\bar{\rho}^{\rm S}_{\ell m} \equiv \left(T_{\rm PN}\left[1/\hat{\rho}^{\rm S}_{\ell m}\right]\right)^{-1}. \tag{B.28}$$

When m is odd, the direct application of this procedure leads to formal singularities in the equal mass case, consequence of the proportionality of the odd-m Newtonian factor to $\delta m \equiv (m_1-m_2)/M = \sqrt{1-4\nu}$, which indeed vanishes for $\nu \to 1/4$. The solution proposed in Ref. [148, 272] is therefore to *defactorize* the quantity δm from the Newtonian factor, multiply it to $f_{\ell m}$, and consider the replacement

$$\delta m f_{\ell m} \to (\rho^{\rm orb}_{\ell m})^{\ell} \hat{f}^{\rm S}_{\ell m}, \qquad \hat{f}^{\rm S}_{\ell m} \equiv T_{\rm PN}\left[\delta m + \frac{\delta m f^{\rm S}_{\ell m}}{(\rho^{\rm orb}_{\ell m})^{\ell}}\right]. \tag{B.29}$$

In the resulting factor $\hat{f}^{\rm S}_{\ell m}$ we can always single out two distinct parts, one that is proportional to δm and one that is not, the latter corresponding to the set of terms that would diverge for $\nu \to 4$ without the factor δm in front. The prescription of Ref. [272] consists in separately resumming these two components with the same inverse Taylor representation (B.28) used for $\hat{\rho}^{\rm S}_{\ell m}$.

For a more detailed account of the various spin factors included in `TEOBResumS`, up to $\ell = 4$, see Sec. IVB of Ref. [273]. We finally mention that the PN waveform information for arbitrary ν that is ultimately collected in the spin factors discussed above is hybridized, similarly to the non-spinning case, with high-PN $\nu = 0$ results relative to a spinning test-mass around a Kerr black hole; see Sec. VB of [273] for more details on this.

Lastly, the radiation reaction force incorporates spin effects via the factorized spinning insplunge waveform we just discussed, following the same factorization prescription (2.121)-(2.124) adopted in the non-spinning sector of the model, modulo the simple difference that r_ω in Eq. (2.121) is replaced by its spin-dependent generalization r_{ω_c}, given in Eq. (B.24).

Appendix C

Long analytical expressions

We list here the explicit expressions of different useful quantities that would be cumbersome to insert in the main text.

C.1 2PN noncircular factors for the subdominant modes ($m \neq 0$)

In this Appendix we list the 2PN noncircular relativistic factors, that result from the factorization prescription of Sec. 3.2.2, for all the subdominant $m \neq 0$ modes up to $\ell = m = 4$,[1] before any resummation is performed. Note that the contributions that are not explicitly written are equal to 1 (or to 0, in the case of $\delta^{\text{inst-nc}}_{\ell m}$).

Tail noncircular factors

$$\hat{h}^{\text{tail-nc}}_{21} = 1 - \frac{\pi}{11520c^3}\Bigg[6ip_{r_*}u\bigg(3029 + 6035p_\varphi^2 u - 10870p_\varphi^4 u^2 + 8350p_\varphi^6 u^3 - 3215p_\varphi^8 u^4 + 511p_\varphi^{10}u^5\bigg) - \frac{15p_{r_*}^2}{p_\varphi}\bigg(635 - 1388p_\varphi^2 u + 666p_\varphi^4 u^2 - 92p_\varphi^6 u^3 - 13p_\varphi^8 u^4\bigg) + 20ip_{r_*}^3\bigg(619 - 981p_\varphi^2 u + 573p_\varphi^4 u^2 - 115p_\varphi^6 u^3\bigg) + \frac{15p_{r_*}^4}{p_\varphi u}\bigg(183 - 82p_\varphi^2 u - 17p_\varphi^4 u^2\bigg)\Bigg]. \tag{C.1}$$

$$\hat{h}^{\text{tail-nc}}_{31} = 1 - \frac{\pi}{1920c^3 p_\varphi^2\left(7 - 6p_\varphi^2 u\right)^2}\Bigg[ip_{r_*}\bigg(88130 - 107366p_\varphi^2 u$$

[1] For $\ell > 4$, at 2PN accuracy, all the modes present at most just their leading Newtonian contribution, which implies $\hat{h}_{\ell m} = 1$, i.e. no PN correcting factors.

$$
\begin{aligned}
&+ 89843p_\varphi^4u^2 - 388835p_\varphi^6u^3 + 588840p_\varphi^8u^4 - 397460p_\varphi^{10}u^5 + 139731p_\varphi^{12}u^6 \\
&- 20563p_\varphi^{14}u^7\Big) + \frac{p_{r_*}^2}{2p_\varphi u\big(7-6p_\varphi^2u\big)}\Big(2115120 - 3821769p_\varphi^2u + 915328p_\varphi^4u^2 \\
&- 2431548p_\varphi^6u^3 + 9399380p_\varphi^8u^4 - 10528645p_\varphi^{10}u^5 + 5655444p_\varphi^{12}u^6 \\
&- 1592318p_\varphi^{14}u^7 + 186288p_\varphi^{16}u^8\Big) - \frac{ip_{r_*}^3}{3p_\varphi^2u^2\big(7-6p_\varphi^2u\big)^2}\Big(38072160 \\
&- 92454747p_\varphi^2u + 79749569p_\varphi^4u^2 - 137703015p_\varphi^6u^3 + 356358768p_\varphi^8u^4 \\
&- 482607515p_\varphi^{10}u^5 + 363100527p_\varphi^{12}u^6 - 161234979p_\varphi^{14}u^7 + 40408200p_\varphi^{16}u^8 \\
&- 4441608p_\varphi^{18}u^9\Big) - \frac{p_{r_*}^4}{2p_\varphi^3u^3\big(7-6p_\varphi^2u\big)^3}\Big(304577280 - 928941216p_\varphi^2u \\
&+ 1082387695p_\varphi^4u^2 - 1365588354p_\varphi^6u^3 + 3139841017p_\varphi^8u^4 \\
&- 4991336104p_\varphi^{10}u^5 + 4638849326p_\varphi^{12}u^6 - 2632737900p_\varphi^{14}u^7 \\
&+ 916090404p_\varphi^{16}u^8 - 181221912p_\varphi^{18}u^9 + 15589584p_\varphi^{20}u^{10}\Big)\Big].
\end{aligned}
\tag{C.2}
$$

$$
\begin{aligned}
\hat{h}_{33}^{\text{tail-nc}} = 1 &- \frac{\pi}{3840c^3p_\varphi^2\big(2p_\varphi^2u+7\big)^2}\Big[ip_{r_*}\Big(47630 + 134366p_\varphi^2u + 721737p_\varphi^4u^2 \\
&- 429865p_\varphi^6u^3 + 308120p_\varphi^8u^4 - 107220p_\varphi^{10}u^5 + 16769p_\varphi^{12}u^6 - 337p_\varphi^{14}u^7\Big) \\
&+ \frac{p_{r_*}^2}{2p_\varphi u\big(2p_\varphi^2u+7\big)}\Big(381040 + 1407963p_\varphi^2u - 2751544p_\varphi^4u^2 + 8146332p_\varphi^6u^3 \\
&- 5435500p_\varphi^8u^4 + 3011095p_\varphi^{10}u^5 - 1073428p_\varphi^{12}u^6 + 170074p_\varphi^{14}u^7 \\
&+ 14688p_\varphi^{16}u^8\Big) - \frac{ip_{r_*}^3}{p_\varphi^2u^2\big(2p_\varphi^2u+7\big)^2}\Big(762080 + 3125521p_\varphi^2u + 5675333p_\varphi^4u^2 \\
&- 28858731p_\varphi^6u^3 + 28110216p_\varphi^8u^4 - 14716055p_\varphi^{10}u^5 + 7128059p_\varphi^{12}u^6 \\
&- 2725303p_\varphi^{14}u^7 + 281976p_\varphi^{16}u^8 + 41864p_\varphi^{18}u^9\Big) \\
&- \frac{p_{r_*}^4}{2p_\varphi^3u^3\big(2p_\varphi^2u+7\big)^3}\Big(6096640 + 27480928p_\varphi^2u + 92901791p_\varphi^4u^2 + 57821954p_\varphi^6u^3 \\
&- 472378615p_\varphi^8u^4 + 376035640p_\varphi^{10}u^5 - 164962538p_\varphi^{12}u^6 + 71523844p_\varphi^{14}u^7 \\
&- 24385644p_\varphi^{16}u^8 + 1291400p_\varphi^{18}u^9 + 320720p_\varphi^{20}u^{10}\Big)\Big].
\end{aligned}
\tag{C.3}
$$

Instantaneous noncircular factors

$$f_{21}^{\text{inst-nc}} = 1 + \frac{1}{c^2} p_{r_*}^2 \left(\frac{9}{14} + \frac{5\nu}{7} \right), \tag{C.4}$$

$$\delta_{21}^{\text{inst-nc}} = \frac{1}{c^2} p_{r_*} p_\varphi \left(\frac{1}{14} + \frac{6\nu}{7} \right). \tag{C.5}$$

$$\begin{aligned} f_{31}^{\text{inst-nc}} = 1 + \frac{1}{c^2} \Bigg\{ & \frac{p_{r_*}^2}{p_\varphi^2 u \big(-7 + 6 p_\varphi^2 u \big)^3} \Bigg[(-1076 + 1168\nu) + p_\varphi^2 u \Bigg(\frac{4783}{2} \\ & - 4242\nu \Bigg) + p_\varphi^4 u^2 (-1520 + 4834\nu) + p_\varphi^6 u^3 (6 - 2136\nu) + p_\varphi^8 u^4 (180 + 288\nu) \Bigg] \\ & + \frac{p_{r_*}^4}{p_\varphi^4 u^3 \big(-7 + 6 p_\varphi^2 u \big)^5} \Bigg[(154944 - 168192\nu) + p_\varphi^2 u (-569222 + 740344\nu) \\ & + p_\varphi^4 u^2 (840044 - 1241680\nu) + p_\varphi^6 u^3 (-622914 + 1014636\nu) \\ & + p_\varphi^8 u^4 (232812 - 408168\nu) + p_\varphi^{10} u^5 (-35208 + 65232\nu) \Bigg] \Bigg\}, \end{aligned} \tag{C.6}$$

$$\begin{aligned} \delta_{31}^{\text{inst-nc}} = \frac{1}{c^2} \Bigg\{ & \frac{p_{r_*}}{p_\varphi \big(7 - 6 p_\varphi^2 u \big)^2} \Bigg[\Bigg(\frac{269}{3} - \frac{292\nu}{3} \Bigg) + p_\varphi^2 u (-146 + 222\nu) \\ & + p_\varphi^4 u^2 (61 - 110\nu) \Bigg] + \frac{p_{r_*}^3}{p_\varphi^3 u^2 \big(7 - 6 p_\varphi^2 u \big)^4} \Bigg[(-12912 + 14016\nu) \\ & + p_\varphi^2 u (39410 - 52984\nu) + p_\varphi^4 u^2 (-45043 + 69758\nu) + p_\varphi^6 u^3 (22704 - 39288\nu) \\ & + p_\varphi^8 u^4 (-4248 + 8064\nu) \Bigg] \Bigg\}. \end{aligned} \tag{C.7}$$

$$\begin{aligned} f_{32}^{\text{inst-nc}} = 1 + \frac{1}{c^2} \Bigg\{ & \frac{p_{r_*}^2}{p_\varphi^2 u (-1 + 3\nu)} \Bigg[\Bigg(-\frac{187}{2880} + \frac{223\nu}{576} - \frac{265\nu^2}{576} \Bigg) \\ & + p_\varphi^2 u \Bigg(-\frac{221}{192} + \frac{547\nu}{192} + \frac{227\nu^2}{192} \Bigg) \Bigg] + \frac{p_{r_*}^4}{p_\varphi^4 u^3 (-1 + 3\nu)} \Bigg[\Bigg(\frac{187}{46080} \\ & - \frac{223\nu}{9216} + \frac{265\nu^2}{9216} \Bigg) + p_\varphi^2 u \Bigg(\frac{61}{3072} - \frac{323\nu}{3072} + \frac{317\nu^2}{3072} \Bigg) \Bigg] \Bigg\}, \end{aligned} \tag{C.8}$$

$$\begin{aligned} \delta_{32}^{\text{inst-nc}} = \frac{1}{c^2} \Bigg\{ & \frac{p_{r_*}}{p_\varphi (-1 + 3\nu)} \Bigg[\Bigg(-\frac{187}{720} + \frac{223\nu}{144} - \frac{265\nu^2}{144} \Bigg) + p_\varphi^2 u \Bigg(-\frac{433}{240} \\ & + \frac{355\nu}{48} - \frac{157\nu^2}{48} \Bigg) \Bigg] + \frac{p_{r_*}^3}{p_\varphi^3 u^2 (-1 + 3\nu)} \Bigg[\Bigg(\frac{187}{11520} - \frac{223\nu}{2304} + \frac{265\nu^2}{2304} \Bigg) \end{aligned}$$

$$+ p_\varphi^2 u\left(\frac{61}{768} - \frac{323\nu}{768} + \frac{317\nu^2}{768}\right)\Bigg]\Bigg\}. \tag{C.9}$$

$$f_{33}^{\text{inst-nc}} = 1 + \frac{1}{c^2}\Bigg\{\frac{p_{r_*}^2}{p_\varphi^2 u\big(7 + 2p_\varphi^2 u\big)^3}\Bigg[\left(\frac{1076}{9} - \frac{1168\nu}{9}\right) + p_\varphi^2 u\left(\frac{9161}{18} + \frac{2626\nu}{9}\right) + p_\varphi^4 u^2\left(\frac{1292}{3} - \frac{214\nu}{3}\right) + p_\varphi^6 u^3\left(\frac{1430}{3} - \frac{424\nu}{3}\right) + p_\varphi^8 u^4\left(\frac{20}{3} + \frac{32\nu}{3}\right)\Bigg] + \frac{p_{r_*}^4}{p_\varphi^4 u^3\big(7 + 2p_\varphi^2 u\big)^5}\Bigg[\left(-\frac{17216}{9} + \frac{18688\nu}{9}\right) + p_\varphi^2 u\left(-\frac{55034}{9} + \frac{52744\nu}{9}\right) + p_\varphi^4 u^2\left(-\frac{23140}{3} + \frac{23984\nu}{3}\right) + p_\varphi^6 u^3\left(\frac{11510}{3} - \frac{44260\nu}{3}\right) + p_\varphi^8 u^4\left(\frac{163540}{9} - \frac{57560\nu}{9}\right) + p_\varphi^{10} u^5\left(-\frac{11912}{3} + \frac{7888\nu}{3}\right)\Bigg]\Bigg\}, \tag{C.10}$$

$$\delta_{33}^{\text{inst-nc}} = \frac{1}{c^2}\Bigg\{\frac{p_{r_*}}{p_\varphi\big(7 + 2p_\varphi^2 u\big)^2}\Bigg[\left(\frac{269}{9} - \frac{292\nu}{9}\right) + p_\varphi^2 u\left(\frac{970}{9} - \frac{1142\nu}{9}\right) + p_\varphi^4 u^2\left(\frac{313}{3} - \frac{182\nu}{3}\right)\Bigg] + \frac{p_{r_*}^3}{p_\varphi^3 u^2\big(7 + 2p_\varphi^2 u\big)^4}\Bigg[\left(-\frac{4304}{9} + \frac{4672\nu}{9}\right) + p_\varphi^2 u\left(-\frac{12010}{9} + \frac{11288\nu}{9}\right) + p_\varphi^4 u^2(431 - 1318\nu) + p_\varphi^6 u^3\left(\frac{5456}{3} + \frac{968\nu}{3}\right) + p_\varphi^8 u^4(-1336 + 864\nu)\Bigg]\Bigg\}. \tag{C.11}$$

$$f_{42}^{\text{inst-nc}} = 1 + \frac{1}{c^2}\Bigg\{\frac{p_{r_*}^2}{\big(-7 - 3p_\varphi^2 u + 6p_\varphi^4 u^2\big)^3(-1 + 3\nu)}\Bigg[\left(-\frac{5495}{11} + \frac{78435\nu}{22} - \frac{123711\nu^2}{22}\right) + p_\varphi^2 u\left(\frac{22794}{55} - \frac{95055\nu}{22} + \frac{237351\nu^2}{22}\right) + p_\varphi^4 u^2\left(\frac{2308683}{220} - \frac{778917\nu}{22} + \frac{83871\nu^2}{22}\right) + p_\varphi^6 u^3\left(-\frac{4346379}{220} + \frac{1713879\nu}{22} - \frac{991377\nu^2}{22}\right) + p_\varphi^8 u^4\left(\frac{692577}{55} - \frac{603477\nu}{11} + \frac{491211\nu^2}{11}\right) + p_\varphi^{10} u^5\left(-\frac{127386}{55} + \frac{136890\nu}{11} - \frac{160650\nu^2}{11}\right) + p_\varphi^{12} u^6\left(-\frac{2484}{11} + \frac{2916\nu}{11} + \frac{11340\nu^2}{11}\right)\Bigg] + \frac{p_{r_*}^4}{u\big(-7 - 3p_\varphi^2 u + 6p_\varphi^4 u^2\big)^5(-1 + 3\nu)}\Bigg[\left(-\frac{997983}{11}\right.$$

$$+\frac{4635792\nu}{11}-\frac{4635792\nu^2}{11}\Big)+p_\varphi^2u\Big(\frac{43866123}{55}-\frac{47651520\nu}{11}$$
$$+\frac{63443142\nu^2}{11}\Big)+p_\varphi^4u^2\Big(\frac{35844849}{22}-\frac{16122492\nu}{11}-\frac{135164952\nu^2}{11}\Big)$$
$$+p_\varphi^6u^3\Big(-\frac{525077109}{44}+\frac{441545616\nu}{11}-\frac{53867457\nu^2}{11}\Big)$$
$$+p_\varphi^8u^4\Big(\frac{4684992993}{220}-\frac{914171508\nu}{11}+\frac{489089961\nu^2}{11}\Big)$$
$$+p_\varphi^{10}u^5\Big(-\frac{2041998687}{110}+\frac{865358424\nu}{11}-\frac{634963050\nu^2}{11}\Big)$$
$$+p_\varphi^{12}u^6\Big(\frac{96254487}{11}-\frac{433938060\nu}{11}+\frac{377733780\nu^2}{11}\Big)$$
$$+p_\varphi^{14}u^7\Big(-\frac{23603562}{11}+\frac{112003560\nu}{11}-\frac{109437480\nu^2}{11}\Big)$$
$$+p_\varphi^{16}u^8\Big(\frac{1077948}{5}-1069200\nu+1139184\nu^2\Big)\Big]\Big\}, \tag{C.12}$$

$$\delta_{42}^{\text{inst-nc}}=\frac{1}{c^2}\Big\{\frac{p_{r_*}p_\varphi u}{\left(7+3p_\varphi^2u-6p_\varphi^4u^2\right)^2(-1+3\nu)}\Big[\Big(-\frac{5513}{55}+\frac{5854\nu}{11}$$
$$-\frac{7548\nu^2}{11}\Big)+p_\varphi^2u\Big(-\frac{86061}{220}+\frac{13686\nu}{11}+\frac{273\nu^2}{11}\Big)+p_\varphi^4u^2\Big(\frac{139401}{220}$$
$$-\frac{29826\nu}{11}+\frac{22599\nu^2}{11}\Big)+p_\varphi^6u^3\Big(-\frac{2556}{11}+\frac{12186\nu}{11}-\frac{11988\nu^2}{11}\Big)\Big]$$
$$+\frac{p_{r_*}^3p_\varphi}{\left(7+3p_\varphi^2u-6p_\varphi^4u^2\right)^4(-1+3\nu)}\Big[\Big(-\frac{3434319}{110}+\frac{1677774\nu}{11}-\frac{1868580\nu^2}{11}\Big)$$
$$+p_\varphi^2u\Big(-\frac{1623252}{55}-\frac{321240\nu}{11}+\frac{4439970\nu^2}{11}\Big)+p_\varphi^4u^2\Big(\frac{80592003}{220}$$
$$-\frac{13474980\nu}{11}+\frac{1467963\nu^2}{11}\Big)+p_\varphi^6u^3\Big(-\frac{138830193}{220}+\frac{27487404\nu}{11}$$
$$-\frac{15732441\nu^2}{11}\Big)+p_\varphi^8u^4\Big(\frac{26404461}{55}-\frac{22944114\nu}{11}+\frac{18134496\nu^2}{11}\Big)$$
$$+p_\varphi^{10}u^5\Big(-\frac{9559404}{55}+\frac{8902440\nu}{11}-\frac{8355960\nu^2}{11}\Big)+p_\varphi^{12}u^6\Big(\frac{1342332}{55}$$
$$-\frac{1324512\nu}{11}+\frac{1395792\nu^2}{11}\Big)\Big]\Big\}. \tag{C.13}$$

$$f_{44}^{\text{inst-nc}}=1+\frac{1}{c^2}\Big\{\frac{p_{r_*}^2}{\left(7+51p_\varphi^2u+6p_\varphi^4u^2\right)^3(-1+3\nu)}\Big[\Big(\frac{5495}{11}-\frac{78435\nu}{22}$$

$$
\begin{aligned}
&+\frac{123711\nu^2}{22}\Big)+p_\varphi^2 u\Big(\frac{210159}{55}-\frac{667917\nu}{22}+\frac{914625\nu^2}{22}\Big)\\
&+p_\varphi^4 u^2\Big(-\frac{9429801}{55}+\frac{12229341\nu}{22}-\frac{2912121\nu^2}{22}\Big)\\
&+p_\varphi^6 u^3\Big(-\frac{19606626}{55}+\frac{22336029\nu}{22}+\frac{2602071\nu^2}{22}\Big)\\
&+p_\varphi^8 u^4\Big(-\frac{7261839}{55}+\frac{4772385\nu}{11}-\frac{1459053\nu^2}{11}\Big)\\
&+p_\varphi^{10} u^5\Big(-\frac{564948}{11}+\frac{1931958\nu}{11}-\frac{475470\nu^2}{11}\Big)\\
&+p_\varphi^{12} u^6\Big(-\frac{2484}{11}+\frac{2916\nu}{11}+\frac{11340\nu^2}{11}\Big)\Big]\\
&+\frac{p_{r_*}^4}{u\big(7+51p_\varphi^2 u+6p_\varphi^4 u^2\big)^5(-1+3\nu)}\Big[\Big(\frac{997983}{11}-\frac{4635792\nu}{11}\\
&+\frac{4635792\nu^2}{11}\Big)+p_\varphi^2 u\Big(-\frac{144030369}{110}+\frac{92715672\nu}{11}-\frac{152428248\nu^2}{11}\Big)\\
&+p_\varphi^4 u^2\Big(-\frac{737730837}{11}+\frac{3011803560\nu}{11}-\frac{2051555040\nu^2}{11}\Big)\\
&+p_\varphi^6 u^3\Big(-\frac{2431571553}{55}+\frac{1633697784\nu}{11}-\frac{187083648\nu^2}{11}\Big)\\
&+p_\varphi^8 u^4\Big(\frac{486563193}{5}-405446040\nu+297670464\nu^2\Big)\\
&+p_\varphi^{10} u^5\Big(\frac{3125458143}{110}-\frac{956714976\nu}{11}-\frac{188690472\nu^2}{11}\Big)\\
&+p_\varphi^{12} u^6\Big(-\frac{3895064577}{55}+\frac{3530464704\nu}{11}-\frac{3326475600\nu^2}{11}\Big)\\
&+p_\varphi^{14} u^7\Big(-\frac{673781166}{11}+\frac{2335443840\nu}{11}-\frac{497702880\nu^2}{11}\Big)\\
&+p_\varphi^{16} u^8\Big(\frac{305560836}{55}-\frac{229080960\nu}{11}+\frac{102316608\nu^2}{11}\Big)\Big]\Big\},
\end{aligned}
\tag{C.14}
$$

$$
\begin{aligned}
\delta_{44}^{\text{inst-nc}}=&-\frac{1}{c^2}\Big\{\frac{p_{r_*}p_\varphi u}{\big(7+51p_\varphi^2 u+6p_\varphi^4 u^2\big)^2(-1+3\nu)}\Big[\Big(\frac{11026}{55}-\frac{11708\nu}{11}\\
&+\frac{15096\nu^2}{11}\Big)+p_\varphi^2 u\Big(\frac{555681}{110}-\frac{233274\nu}{11}+\frac{175788\nu^2}{11}\Big)+p_\varphi^4 u^2\Big(\frac{939051}{110}\\
&-\frac{377406\nu}{11}+\frac{241380\nu^2}{11}\Big)+p_\varphi^6 u^3\Big(\frac{172872}{55}-\frac{126540\nu}{11}+\frac{47736\nu^2}{11}\Big)\Big]
\end{aligned}
$$

$$+\frac{p_{r_*}^3 p_\varphi}{\left(7+51p_\varphi^2 u+6p_\varphi^4 u^2\right)^4(-1+3\nu)}\Bigg[\left(\frac{3434319}{55}-\frac{3355548\nu}{11}+\frac{3737160\nu^2}{11}\right)$$
$$+p_\varphi^2 u\left(\frac{68284914}{55}-\frac{53840352\nu}{11}+\frac{31634784\nu^2}{11}\right)+p_\varphi^4 u^2\left(-\frac{69674769}{55}\right.$$
$$\left.+\frac{66841884\nu}{11}-\frac{71727336\nu^2}{11}\right)+p_\varphi^6 u^3\left(-\frac{221951034}{55}+\frac{179751888\nu}{11}\right.$$
$$\left.-\frac{118566720\nu^2}{11}\right)+p_\varphi^8 u^4\left(\frac{64377018}{55}-\frac{49429008\nu}{11}+\frac{25417152\nu^2}{11}\right)$$
$$+p_\varphi^{10} u^5\left(\frac{74535768}{55}-\frac{42300576\nu}{11}-\frac{20036160\nu^2}{11}\right)$$
$$\left.+p_\varphi^{12} u^6\left(-\frac{29497608}{55}+\frac{22006080\nu}{11}-\frac{9517824\nu^2}{11}\right)\right]\Bigg\}. \tag{C.15}$$

C.2 2PN-accurate subdominant multipoles of $\hat{\mathcal{F}}_\varphi$ ($m \neq 0$)

In Eq. (3.81) of the main text we showed the expression for the Taylor-expanded multipole $F_{22}^{\rm 2PN}$ of the angular radiation-reaction force, which enters the factorization procedure described in Sec. 3.5.2. Here we list for completeness all the other multipoles, $F_{\ell m}^{\rm 2PN}$, that are relevant at 2PN accuracy. Mind that, similarly to Eq. (3.81), we write each $F_{\ell m}^{\rm 2PN}$ without the overall c^{-5} factor. Our results read

$$F_{21}^{\rm 2PN}=-\frac{1}{c^2}p_\varphi^3 u^6\frac{1-4\nu}{9}-\frac{1}{c^4}\Bigg\{p_\varphi^3 u^7\left[\frac{5}{126}+\frac{13\nu}{63}-\frac{92\nu^2}{63}\right.$$
$$\left.+p_\varphi^2 u\left(-\frac{85}{126}+\frac{335\nu}{126}+\frac{10\nu^2}{63}\right)\right]\Bigg\}, \tag{C.16}$$

$$F_{31}^{\rm 2PN}=-\frac{1}{c^2}p_\varphi u^3(1-4\nu)\left[u^2\left(\frac{1}{24}-\frac{149p_\varphi^2 u}{2016}+\frac{11p_\varphi^4 u^2}{336}\right)+p_{r_*}^2 u\left(\frac{1}{336}\right.\right.$$
$$\left.\left.+\frac{p_\varphi^2 u}{48}\right)-\frac{p_{r_*}^4}{84}\right]+\frac{1}{c^4}p_\varphi u^4(1-4\nu)\Bigg\{u^2\left[\frac{2479}{6048}-\frac{31\nu}{189}+p_\varphi^2 u\left(-\frac{863}{1008}\right.\right.$$
$$\left.+\frac{559\nu}{2016}\right)+p_\varphi^4 u^2\left(\frac{445}{1344}-\frac{347\nu}{4032}\right)+p_\varphi^6 u^3\left(\frac{47}{504}-\frac{55\nu}{2016}\right)\Bigg]-p_{r_*}^2 u\left[\frac{73}{336}\right.$$
$$\left.-\frac{31\nu}{168}+p_\varphi^2 u\left(-\frac{3779}{4032}+\frac{775\nu}{1344}\right)+p_\varphi^4 u^2\left(\frac{51}{224}-\frac{3\nu}{14}\right)\right]$$
$$\left.+p_{r_*}^4\left[\frac{59}{672}-\frac{13\nu}{672}+p_\varphi^2 u\left(-\frac{83}{224}+\frac{51\nu}{224}\right)\right]\right\}, \tag{C.17}$$

$$F_{32}^{\rm 2PN}=-\frac{1}{c^4}p_\varphi^3 u^6(1-3\nu)^2\left[\frac{5}{126}u\left(1+7p_\varphi^2 u\right)-\frac{5}{252}p_{r_*}^2\right], \tag{C.18}$$

$$F_{33}^{\rm 2PN} = -\frac{1}{c^2}p_\varphi u^3(1-4\nu)\Bigg[u^2\left(\frac{5}{8}+\frac{845p_\varphi^2 u}{224}+\frac{115p_\varphi^4u^2}{112}\right)+p_{r_*}^2u\left(\frac{5}{112}-\frac{205p_\varphi^2u}{112}\right)-\frac{5}{28}p_{r_*}^4\Bigg]+\frac{1}{c^4}p_\varphi u^4(1-4\nu)\Bigg\{u^2\Bigg[\frac{12395}{2016}-\frac{155\nu}{63}+p_\varphi^2u\left(\frac{45175}{1008}-\frac{5065\nu}{288}\right)+p_\varphi^4u^2\left(\frac{66385}{4032}-\frac{37445\nu}{4032}\right)+p_\varphi^6u^3\left(\frac{265}{168}-\frac{335\nu}{672}\right)\Bigg]-p_{r_*}^2u\left[\frac{365}{112}-\frac{155\nu}{56}+p_\varphi^2u\left(\frac{68195}{4032}-\frac{81685\nu}{4032}\right)+p_\varphi^4u^2\left(\frac{985}{224}-\frac{545\nu}{56}\right)\right]+p_{r_*}^4\left[\frac{295}{224}-\frac{65\nu}{224}+p_\varphi^2u\left(-\frac{545}{96}-\frac{3065\nu}{672}\right)\right]\Bigg\}, \tag{C.19}$$

$$F_{42}^{\rm 2PN} = -\frac{1}{c^4}p_\varphi u^4(1-3\nu)^2\Bigg[u^2\left(\frac{205}{4536}-\frac{5p_\varphi^2u}{294}-\frac{575p_\varphi^4u^2}{10584}+\frac{55p_\varphi^6u^3}{1764}\right)-p_{r_*}^2u\left(\frac{25}{588}-\frac{865p_\varphi^2u}{10584}\right)+p_{r_*}^4\left(\frac{10}{441}-\frac{65p_\varphi^2u}{1764}\right)\Bigg], \tag{C.20}$$

$$F_{44}^{\rm 2PN} = -\frac{1}{c^4}p_\varphi u^4(1-3\nu)^2\Bigg[u^2\left(\frac{205}{648}+\frac{125p_\varphi^2u}{42}+\frac{1115p_\varphi^4u^2}{216}+\frac{145p_\varphi^6u^3}{252}\right)-p_{r_*}^2u\left(\frac{25}{84}+\frac{1705p_\varphi^2u}{1512}+\frac{95p_\varphi^4u^2}{42}\right)+p_{r_*}^4\left(\frac{10}{63}-\frac{25p_\varphi^2u}{252}\right)\Bigg]. \tag{C.21}$$

Notice that, at the 2PN accuracy we are considering here, all the subleading $\hat{\mathcal{F}}_\varphi$ multipoles listed above are present just the instantaneous part. This is simply related to the fact that their hereditary effect contributions appear at higher orders than the 2PN.

C.3 2PN noncircular instantaneous factor with time derivatives ($\ell = m = 2$)

Here we provide the full expression of the noncircular instantaneous factor introduced and tested in Sec. 3.7. This results from Eq. (3.106) and reads

$$\hat{h}_{22}^{\rm nc_{inst}} = 1+\frac{1}{\ddot{r}u+\dot{r}^2u^2-4i\dot{r}u\Omega-2\Omega^2-i\dot{\Omega}}\Bigg\{\frac{1}{c^2}\Bigg[i\dot{p}_{r_*}\dot{p}_\varphi u\left(-\frac{10}{21}-\frac{4\nu}{7}\right)+i\dot{p}_{r_*}p_\varphi\dot{r}u^2\left(-\frac{10}{21}-\frac{4\nu}{7}\right)+ip_{r_*}\dot{p}_\varphi\dot{r}u^2\left(-\frac{10}{21}-\frac{4\nu}{7}\right)+i\ddot{p}_{r_*}p_\varphi u\left(-\frac{5}{21}-\frac{2\nu}{7}\right)+ip_{r_*}\ddot{p}_\varphi u\left(-\frac{5}{21}-\frac{2\nu}{7}\right)+ip_{r_*}p_\varphi\ddot{r}u^2\left(-\frac{5}{21}-\frac{2\nu}{7}\right)+\dot{r}^2u^3\left(\frac{19}{7}-\frac{\nu}{7}\right)+\ddot{r}u^2\left(\frac{19}{14}-\frac{\nu}{14}\right)+p_\varphi\ddot{p}_\varphi u^2\left(\frac{1}{6}+\frac{\nu}{2}\right)+\dot{p}_\varphi^2u^2\left(\frac{1}{6}+\frac{\nu}{2}\right)+p_{r_*}^2\ddot{r}u\left(\frac{1}{7}+\frac{15\nu}{14}\right)+p_{r_*}^2\dot{r}^2u^2\left(\frac{1}{7}+\frac{15\nu}{14}\right)+p_{r_*}\ddot{p}_{r_*}\left(\frac{9}{14}+\frac{15\nu}{14}\right)$$

$$
\begin{aligned}
&+ \dot{p}_{r_*}^2\left(\frac{9}{14}+\frac{15\nu}{14}\right) + p_{r_*}\dot{p}_{r_*}\dot{r}u\left(\frac{18}{7}+\frac{30\nu}{7}\right) + p_\varphi^2\ddot{r}u^3\left(-\frac{1}{6}-\frac{\nu}{2}\right)\\
&+ p_\varphi^2\dot{r}^2u^4\left(-\frac{1}{6}-\frac{\nu}{2}\right) + ip_{r_*}\dot{p}_{r_*}\left(-\frac{18}{7}-\frac{30\nu}{7}\right)\Omega + ip_{r_*}^2\dot{r}u\left(-\frac{4}{7}-\frac{30\nu}{7}\right)\Omega\\
&+ ip_\varphi\dot{p}_\varphi u^2\left(-\frac{2}{3}-2\nu\right)\Omega + \dot{p}_{r_*}p_\varphi u\left(-\frac{20}{21}-\frac{8\nu}{7}\right)\Omega + p_{r_*}\dot{p}_\varphi u\left(-\frac{20}{21}\right.\\
&\left.-\frac{8\nu}{7}\right)\Omega + p_{r_*}p_\varphi\dot{r}u^2\left(-\frac{20}{21}-\frac{8\nu}{7}\right)\Omega + i\dot{r}u^2\left(-\frac{38}{7}+\frac{2\nu}{7}\right)\Omega\\
&+ ip_\varphi^2\dot{r}u^3\left(\frac{2}{3}+2\nu\right)\Omega + p_{r_*}^2\left(-\frac{2}{7}-\frac{15\nu}{7}\right)\Omega^2 + ip_{r_*}p_\varphi u\left(\frac{20}{21}+\frac{8\nu}{7}\right)\Omega^2\\
&+ ip_{r_*}^2\left(-\frac{1}{7}-\frac{15\nu}{14}\right)\dot{\Omega} + p_{r_*}p_\varphi u\left(-\frac{10}{21}-\frac{4\nu}{7}\right)\dot{\Omega}\Big]\\
&+ \frac{1}{c^4}\Big[i\ddot{p}_{r_*}p_\varphi^3u^3\left(\frac{10}{63}-\frac{2\nu}{21}\right) + p_{r_*}\dot{p}_{r_*}p_\varphi^2\dot{r}u^3\left(-\frac{3}{7}-2\nu-\frac{15\nu^2}{7}\right)\\
&+ p_\varphi^2\dot{p}_\varphi^2u^4\left(\frac{2}{63}-\frac{41\nu}{28}-\frac{41\nu^2}{21}\right) + p_\varphi\dot{p}_\varphi\dot{r}u^4\left(\frac{1703}{378}+\frac{1903\nu}{189}-\frac{31\nu^2}{27}\right)\\
&+ p_{r_*}\dot{p}_{r_*}p_\varphi\dot{p}_\varphi u^2\left(-\frac{25}{21}+\frac{\nu}{21}-\nu^2\right) + ip_{r_*}p_\varphi\dot{p}_\varphi^2u^3\left(\frac{5}{7}-\frac{11\nu}{7}-\frac{6\nu^2}{7}\right)\\
&+ p_\varphi^3\ddot{p}_\varphi u^4\left(-\frac{1}{126}-\frac{151\nu}{252}-\frac{103\nu^2}{126}\right) + p_{r_*}\ddot{p}_{r_*}p_\varphi^2u^2\left(-\frac{17}{42}-\frac{41\nu}{84}\right.\\
&\left.-\frac{11\nu^2}{14}\right) + \dot{p}_{r_*}^2p_\varphi^2u^2\left(-\frac{17}{42}-\frac{41\nu}{84}-\frac{11\nu^2}{14}\right) + p_\varphi^2\ddot{r}u^4\left(\frac{1361}{504}\right.\\
&\left.+\frac{1399\nu}{252}-\frac{95\nu^2}{126}\right) + ip_{r_*}\dot{p}_{r_*}^2p_\varphi u\left(\frac{5}{21}-\frac{43\nu}{21}-\frac{2\nu^2}{3}\right)\\
&+ ip_{r_*}^2\dot{p}_{r_*}\dot{p}_\varphi u\left(\frac{10}{21}-\frac{37\nu}{21}-\frac{2\nu^2}{3}\right) + ip_{r_*}^2\dot{p}_{r_*}p_\varphi\dot{r}u^2\left(\frac{10}{21}-\frac{37\nu}{21}-\frac{2\nu^2}{3}\right)\\
&+ i\dot{p}_{r_*}p_\varphi^2\dot{p}_\varphi u^3\left(\frac{50}{63}-\frac{26\nu}{21}-\frac{4\nu^2}{7}\right) + p_{r_*}^2p_\varphi^2\ddot{r}u^3\left(\frac{10}{21}-\frac{\nu}{4}-\frac{15\nu^2}{28}\right)\\
&+ p_{r_*}^2p_\varphi^2\dot{r}^2u^4\left(\frac{10}{21}-\frac{\nu}{4}-\frac{15\nu^2}{28}\right) + \ddot{r}u^3\left(\frac{5959}{1764}-\frac{2239\nu}{882}-\frac{223\nu^2}{441}\right)\\
&+ \dot{r}^2u^4\left(\frac{12457}{1764}-\frac{2581\nu}{882}-\frac{437\nu^2}{882}\right) + ip_{r_*}^2\ddot{p}_{r_*}p_\varphi u\left(\frac{5}{21}-\frac{37\nu}{42}-\frac{\nu^2}{3}\right)\\
&+ p_\varphi^4\dot{r}^2u^6\left(\frac{1}{21}-\frac{67\nu}{252}-\frac{20\nu^2}{63}\right) + ip_{r_*}p_\varphi^2\ddot{p}_\varphi u^3\left(\frac{25}{63}-\frac{13\nu}{21}-\frac{2\nu^2}{7}\right)\\
&+ ip_{r_*}p_\varphi^3\dot{r}^2u^5\left(\frac{5}{21}-\frac{11\nu}{21}-\frac{2\nu^2}{7}\right) + p_{r_*}^2p_\varphi\ddot{p}_\varphi u^2\left(-\frac{8}{21}-\frac{5\nu}{21}-\frac{\nu^2}{4}\right)\\
&+ p_{r_*}^2\dot{p}_\varphi^2u^2\left(-\frac{8}{21}-\frac{5\nu}{21}-\frac{\nu^2}{4}\right) + p_{r_*}^3\dot{p}_{r_*}\dot{r}u\left(-\frac{52}{21}+\frac{20\nu}{21}-\frac{5\nu^2}{21}\right)
\end{aligned}
$$

$$
+ ip_{r_*}^3\dot{p}_\varphi\dot{r}u^2\left(\frac{20}{63}-\frac{25\nu}{63}-\frac{2\nu^2}{9}\right)+p_{r_*}^2\dot{p}_{r_*}^2\left(-\frac{17}{14}+\frac{25\nu}{14}-\frac{5\nu^2}{28}\right)
+ p_{r_*}^2\dot{r}^2u^3\left(-\frac{30}{49}+\frac{283\nu}{98}-\frac{15\nu^2}{98}\right)+i\dot{p}_{r_*}\dot{p}_\varphi u^2\left(-\frac{10301}{2646}-\frac{6904\nu}{1323}
-\frac{200\nu^2}{1323}\right)+ip_{r_*}^3\ddot{p}_\varphi u\left(\frac{10}{63}-\frac{25\nu}{126}-\frac{\nu^2}{9}\right)+ip_{r_*}^3p_\varphi\ddot{r}u^2\left(\frac{10}{63}-\frac{25\nu}{126}-\frac{\nu^2}{9}\right)
+ i\ddot{p}_{r_*}p_\varphi u^2\left(-\frac{10301}{5292}-\frac{3452\nu}{1323}-\frac{100\nu^2}{1323}\right)+ip_{r_*}\ddot{p}_\varphi u^2\left(-\frac{10301}{5292}
-\frac{3452\nu}{1323}-\frac{100\nu^2}{1323}\right)+p_{r_*}^3\ddot{p}_{r_*}\left(-\frac{13}{21}+\frac{5\nu}{21}-\frac{5\nu^2}{84}\right)+p_{r_*}^4\ddot{r}u\left(-\frac{2}{21}
-\frac{25\nu}{168}-\frac{5\nu^2}{168}\right)+p_{r_*}^4\dot{r}^2u^2\left(-\frac{2}{21}-\frac{25\nu}{168}-\frac{5\nu^2}{168}\right)+p_{r_*}^2\ddot{r}u^2\left(\frac{985}{1764}
+\frac{1417\nu}{441}+\frac{59\nu^2}{1764}\right)+ip_{r_*}p_\varphi\ddot{r}u^3\left(-\frac{95}{147}-\frac{109\nu}{147}+\frac{2\nu^2}{49}\right)+
i\dot{p}_{r_*}p_\varphi\dot{r}u^3\left(-\frac{190}{147}-\frac{218\nu}{147}+\frac{4\nu^2}{49}\right)+ip_{r_*}\dot{p}_\varphi\dot{r}u^3\left(-\frac{190}{147}-\frac{218\nu}{147}+\frac{4\nu^2}{49}\right)
+ p_{r_*}\dot{p}_{r_*}\dot{r}u^2\left(\frac{3946}{441}+\frac{5605\nu}{441}+\frac{59\nu^2}{441}\right)+p_\varphi^2\dot{r}^2u^5\left(-\frac{19}{21}-\frac{8\nu}{3}+\frac{\nu^2}{7}\right)
+ p_{r_*}\ddot{p}_{r_*}u\left(\frac{2407}{882}+\frac{3121\nu}{882}+\frac{97\nu^2}{441}\right)+\dot{p}_{r_*}^2u\left(\frac{2407}{882}+\frac{3121\nu}{882}+\frac{97\nu^2}{441}\right)
+ ip_{r_*}p_\varphi^3\ddot{r}u^4\left(-\frac{5}{63}+\frac{3\nu}{7}+\frac{2\nu^2}{7}\right)+p_\varphi\ddot{p}_\varphi u^3\left(-\frac{1361}{756}-\frac{1399\nu}{378}+\frac{95\nu^2}{189}\right)
+ \dot{p}_\varphi^2u^3\left(-\frac{1361}{756}-\frac{1399\nu}{378}+\frac{95\nu^2}{189}\right)+i\dot{p}_{r_*}p_\varphi^3\dot{r}u^4\left(-\frac{10}{63}+\frac{6\nu}{7}+\frac{4\nu^2}{7}\right)
+ p_\varphi^4\ddot{r}u^5\left(\frac{1}{126}+\frac{151\nu}{252}+\frac{103\nu^2}{126}\right)+ip_{r_*}p_\varphi^2\dot{p}_\varphi\dot{r}u^4\left(-\frac{40}{63}+\frac{40\nu}{21}+\frac{8\nu^2}{7}\right)
+ p_\varphi^3\dot{p}_\varphi\dot{r}u^5\left(-\frac{5}{63}+\frac{109\nu}{63}+\frac{143\nu^2}{63}\right)+\dot{p}_{r_*}p_\varphi^3u^3\left(\frac{40}{63}-\frac{8\nu}{21}\right)\Omega
+ ip_\varphi^4\dot{r}u^5\left(-\frac{2}{63}-\frac{151\nu}{63}-\frac{206\nu^2}{63}\right)\Omega+ip_\varphi\dot{p}_\varphi u^3\left(\frac{1361}{189}+\frac{2798\nu}{189}
-\frac{380\nu^2}{189}\right)\Omega+p_{r_*}^2\dot{p}_{r_*}p_\varphi u\left(\frac{20}{21}-\frac{74\nu}{21}-\frac{4\nu^2}{3}\right)\Omega+p_{r_*}p_\varphi^2\dot{p}_\varphi u^3\left(\frac{100}{63}
-\frac{52\nu}{21}-\frac{8\nu^2}{7}\right)\Omega+ip_{r_*}\dot{p}_{r_*}u\left(-\frac{4814}{441}-\frac{6242\nu}{441}-\frac{388\nu^2}{441}\right)\Omega
+ p_{r_*}^3\dot{p}_\varphi u\left(\frac{40}{63}-\frac{50\nu}{63}-\frac{4\nu^2}{9}\right)\Omega+p_{r_*}^3p_\varphi\dot{r}u^2\left(\frac{40}{63}-\frac{50\nu}{63}-\frac{4\nu^2}{9}\right)\Omega
+ \dot{p}_{r_*}p_\varphi u^2\left(-\frac{10301}{1323}-\frac{13808\nu}{1323}-\frac{400\nu^2}{1323}\right)\Omega+p_{r_*}\dot{p}_\varphi u^2\left(-\frac{10301}{1323}\right.
$$

$$
\begin{aligned}
&- \frac{13808\nu}{1323} - \frac{400\nu^2}{1323}\Big)\Omega + ip_{r_*}^2 \dot{r} u^2 \Big(- \frac{985}{441} - \frac{5668\nu}{441} - \frac{59\nu^2}{441}\Big)\Omega + \\
&ip_{r_*}^4 \dot{r} u \Big(\frac{8}{21} + \frac{25\nu}{42} + \frac{5\nu^2}{42}\Big)\Omega + p_{r_*} p_\varphi \dot{r} u^3 \Big(- \frac{380}{147} - \frac{436\nu}{147} + \frac{8\nu^2}{49}\Big)\Omega \\
&+ ip_{r_*}^3 \dot{p}_{r_*} \Big(\frac{52}{21} - \frac{20\nu}{21} + \frac{5\nu^2}{21}\Big)\Omega + ip_{r_*}^2 p_\varphi \dot{p}_\varphi u^2 \Big(\frac{32}{21} + \frac{20\nu}{21} + \nu^2\Big)\Omega \\
&+ p_{r_*} p_\varphi^3 \dot{r} u^4 \Big(- \frac{20}{63} + \frac{12\nu}{7} + \frac{8\nu^2}{7}\Big)\Omega + i\dot{r} u^3 \Big(- \frac{5959}{441} + \frac{4478\nu}{441} \\
&+ \frac{892\nu^2}{441}\Big)\Omega + ip_{r_*}^2 p_\varphi^2 \dot{r} u^3 \Big(- \frac{40}{21} + \nu + \frac{15\nu^2}{7}\Big)\Omega + ip_\varphi^2 \dot{r} u^4 \Big(- \frac{1361}{126} \\
&- \frac{1399\nu}{63} + \frac{190\nu^2}{63}\Big)\Omega + ip_{r_*} \dot{p}_{r_*} p_\varphi^2 u^2 \Big(\frac{34}{21} + \frac{41\nu}{21} + \frac{22\nu^2}{7}\Big)\Omega \\
&+ ip_\varphi^3 \dot{p}_\varphi u^4 \Big(\frac{2}{63} + \frac{151\nu}{63} + \frac{206\nu^2}{63}\Big)\Omega + ip_{r_*} p_\varphi^3 u^3 \Big(- \frac{40}{63} + \frac{8\nu}{21}\Big)\Omega^2 \\
&+ p_{r_*}^2 u \Big(- \frac{1525}{441} - \frac{3121\nu}{441} - \frac{194\nu^2}{441}\Big)\Omega^2 + p_{r_*}^4 \Big(\frac{4}{21} + \frac{25\nu}{84} + \frac{5\nu^2}{84}\Big)\Omega^2 \\
&+ ip_{r_*} p_\varphi u^2 \Big(\frac{10301}{1323} + \frac{13808\nu}{1323} + \frac{400\nu^2}{1323}\Big)\Omega^2 + ip_{r_*}^3 p_\varphi u \Big(- \frac{40}{63} + \frac{50\nu}{63} \\
&+ \frac{4\nu^2}{9}\Big)\Omega^2 + p_{r_*}^2 p_\varphi^2 u^2 \Big(- \frac{4}{21} + \frac{41\nu}{42} + \frac{11\nu^2}{7}\Big)\Omega^2 + p_{r_*} p_\varphi^3 u^3 \Big(\frac{20}{63} - \frac{4\nu}{21}\Big)\dot{\Omega} \\
&+ p_{r_*}^3 p_\varphi u \Big(\frac{20}{63} - \frac{25\nu}{63} - \frac{2\nu^2}{9}\Big)\dot{\Omega} + ip_{r_*}^2 u \Big(- \frac{1525}{882} - \frac{3121\nu}{882} - \frac{97\nu^2}{441}\Big)\dot{\Omega} \\
&+ p_{r_*} p_\varphi u^2 \Big(- \frac{10301}{2646} - \frac{6904\nu}{1323} - \frac{200\nu^2}{1323}\Big)\dot{\Omega} + ip_{r_*}^4 \Big(\frac{2}{21} + \frac{25\nu}{168} + \frac{5\nu^2}{168}\Big)\dot{\Omega} \\
&+ ip_{r_*}^2 p_\varphi^2 u^2 \Big(- \frac{2}{21} + \frac{41\nu}{84} + \frac{11\nu^2}{14}\Big)\dot{\Omega}\Big]\Big\}.
\end{aligned}
\tag{C.22}
$$

Bibliography

[1] **Virgo, LIGO Scientific** Collaboration, B. P. Abbott *et. al.*, *Observation of Gravitational Waves from a Binary Black Hole Merger*, Phys. Rev. Lett. **116** (2016), no. 6 061102 [1602.03837].

[2] R.-G. Cai, Z. Cao, Z.-K. Guo, S.-J. Wang and T. Yang, *The Gravitational-Wave Physics*, Natl. Sci. Rev. **4** (2017), no. 5 687–706 [1703.00187].

[3] **LIGO Scientific** Collaboration, J. Aasi *et. al.*, *Advanced LIGO*, Class. Quant. Grav. **32** (2015) 074001 [1411.4547].

[4] **VIRGO** Collaboration, F. Acernese *et. al.*, *Advanced Virgo: a second-generation interferometric gravitational wave detector*, Class. Quant. Grav. **32** (2015), no. 2 024001 [1408.3978].

[5] **LIGO Scientific, Virgo** Collaboration, B. P. Abbott *et. al.*, *GWTC-1: A Gravitational-Wave Transient Catalog of Compact Binary Mergers Observed by LIGO and Virgo during the First and Second Observing Runs*, Phys. Rev. **X9** (2019), no. 3 031040 [1811.12907].

[6] **LIGO Scientific, Virgo** Collaboration, R. Abbott *et. al.*, *GWTC-2: Compact Binary Coalescences Observed by LIGO and Virgo During the First Half of the Third Observing Run*, Phys. Rev. X **11** (2021) 021053 [2010.14527].

[7] **LIGO Scientific, VIRGO, KAGRA** Collaboration, R. Abbott *et. al.*, *The population of merging compact binaries inferred using gravitational waves through GWTC-3*, 2111.03634.

[8] **LIGO Scientific, Virgo** Collaboration, R. Abbott *et. al.*, *GW190521: A Binary Black Hole Merger with a Total Mass of 150 M⊙*, Phys. Rev. Lett. **125** (2020), no. 10 101102 [2009.01075].

[9] **LIGO Scientific, Virgo** Collaboration, R. Abbott *et. al.*, *Properties and astrophysical implications of the 150 Msun binary black hole merger GW190521*, Astrophys. J. Lett. **900** (2020) L13 [2009.01190].

[10] **LIGO Scientific, Virgo** Collaboration, B. Abbott *et. al.*, *Binary Black Hole Population Properties Inferred from the First and Second Observing Runs of Advanced LIGO and Advanced Virgo*, Astrophys. J. Lett. **882** (2019), no. 2 L24 [1811.12940].

[11] **LIGO Scientific, Virgo** Collaboration, R. Abbott *et. al.*, *Population Properties of Compact Objects from the Second LIGO-Virgo Gravitational-Wave Transient Catalog*, Astrophys. J. Lett. **913** (2021), no. 1 L7 [2010.14533].

[12] B. F. Schutz, *Determining the Hubble Constant from Gravitational Wave Observations*, Nature **323** (1986) 310–311.

[13] **LIGO Scientific, VINROUGE, Las Cumbres Observatory, DLT40, Virgo, 1M2H, MASTER** Collaboration, B. P. Abbott *et. al.*, *A gravitational-wave standard siren measurement of the Hubble constant*, Nature (2017) [1710.05835].

[14] K. Hotokezaka, E. Nakar, O. Gottlieb, S. Nissanke, K. Masuda, G. Hallinan, K. P. Mooley and A. T. Deller, *A Hubble constant measurement from superluminal motion of the jet in GW170817*, Nature Astron. **3** (2019), no. 10 940–944 [1806.10596].

[15] **LIGO Scientific, Virgo** Collaboration, B. P. Abbott *et. al.*, *Tests of general relativity with GW150914*, Phys. Rev. Lett. **116** (2016), no. 22 221101 [1602.03841]. [Erratum: Phys. Rev. Lett.121,no.12,129902(2018)].

[16] **LIGO Scientific, Virgo** Collaboration, B. P. Abbott *et. al.*, *GW170817: Implications for the Stochastic Gravitational-Wave Background from Compact Binary Coalescences*, Phys. Rev. Lett. **120** (2018), no. 9 091101 [1710.05837].

[17] **LIGO Scientific, Virgo** Collaboration, B. P. Abbott *et. al.*, *GW170817: Observation of Gravitational Waves from a Binary Neutron Star Inspiral*, Phys. Rev. Lett. **119** (2017), no. 16 161101 [1710.05832].

[18] **Virgo, Fermi-GBM, INTEGRAL, LIGO Scientific** Collaboration, B. P. Abbott *et. al.*, *Gravitational Waves and Gamma-Rays from a Binary Neutron Star Merger: GW170817 and GRB 170817A*, Astrophys. J. **848** (2017), no. 2 L13 [1710.05834].

[19] E. Troja *et. al.*, *The X-ray counterpart to the gravitational wave event GW 170817*, Nature (2017) [1710.05433].

[20] V. Savchenko *et. al.*, *INTEGRAL Detection of the First Prompt Gamma-Ray Signal Coincident with the Gravitational-wave Event GW170817*, Astrophys. J. Lett. **848** (2017), no. 2 L15 [1710.05449].

[21] R. Margutti *et. al.*, *The Binary Neutron Star Event LIGO/Virgo GW170817 160 Days after Merger: Synchrotron Emission across the Electromagnetic Spectrum*, Astrophys. J. Lett. **856** (2018), no. 1 L18 [1801.03531].

[22] J. D. Lyman *et. al.*, *The optical afterglow of the short gamma-ray burst associated with GW170817*, Nat. Astron. **2** (2018), no. 9 751–754 [1801.02669].

[23] G. Ghirlanda, O. S. Salafia, Z. Paragi, M. Giroletti, J. Yang, B. Marcote, J. Blanchard, I. Agudo, T. An, M. G. Bernardini, R. Beswick, M. Branchesi, S. Campana, C. Casadio, E. Chassand e-Mottin, M. Colpi, S. Covino, P. D'Avanzo, V. D'Elia, S. Frey, M. Gawronski, G. Ghisellini, L. I. Gurvits, P. G. Jonker, H. J. van Langevelde, A. Melandri, J. Moldon, L. Nava, A. Perego, M. A. Perez-Torres, C. Reynolds, R. Salvaterra, G. Tagliaferri, T. Venturi, S. D. Vergani and M. Zhang, *Compact radio emission indicates a structured jet was produced by a binary neutron star merger*, Science **363** (Mar, 2019) 968–971 [1808.00469].

[24] M. Bailes *et. al.*, *Gravitational-wave physics and astronomy in the 2020s and 2030s*, Nature Rev. Phys. **3** (2021), no. 5 344–366.

[25] **VIRGO, KAGRA, LIGO Scientific** Collaboration, B. P. Abbott *et. al.*, *Prospects for Observing and Localizing Gravitational-Wave Transients with Advanced LIGO, Advanced Virgo and KAGRA*, Living Rev. Rel. **21** (2018) 3 [1304.0670]. [Living Rev. Rel.19,1(2016)].

[26] **LIGO Scientific** Collaboration, D. Shoemaker, *Gravitational wave astronomy with LIGO and similar detectors in the next decade*, 1904.03187.

[27] **KAGRA** Collaboration, T. Akutsu *et. al.*, *KAGRA: 2.5 Generation Interferometric Gravitational Wave Detector*, Nature Astron. **3** (2019), no. 1 35–40 [1811.08079].

[28] C. Unnikrishnan, *IndIGO and LIGO-India: Scope and plans for gravitational wave research and precision metrology in India*, Int.J.Mod.Phys. **D22** (2013) 1341010.

[29] M. Punturo, M. Abernathy, F. Acernese, B. Allen, N. Andersson *et. al.*, *The Einstein Telescope: A third-generation gravitational wave observatory*, Class.Quant.Grav. **27** (2010) 194002.

[30] **LIGO Scientific** Collaboration, B. P. Abbott *et. al.*, *Exploring the Sensitivity of Next Generation Gravitational Wave Detectors*, Class. Quant. Grav. **34** (2017), no. 4 044001 [1607.08697].

[31] **LISA** Collaboration, P. Amaro-Seoane *et. al.*, *Laser Interferometer Space Antenna*, 1702.00786.

[32] P. Amaro-Seoane, J. R. Gair, M. Freitag, M. Coleman Miller, I. Mandel, C. J. Cutler and S. Babak, *Astrophysics, detection and science applications of intermediate- and extreme mass-ratio inspirals*, Class. Quant. Grav. **24** (2007) R113–R169 [astro-ph/0703495].

[33] S. Babak, J. Gair, A. Sesana, E. Barausse, C. F. Sopuerta, C. P. L. Berry, E. Berti, P. Amaro-Seoane, A. Petiteau and A. Klein, *Science with the space-based interferometer LISA. V: Extreme mass-ratio inspirals*, Phys. Rev. D **95** (2017), no. 10 103012 [1703.09722].

[34] **TianQin** Collaboration, J. Luo *et. al.*, *TianQin: a space-borne gravitational wave detector*, Class. Quant. Grav. **33** (2016), no. 3 035010 [1512.02076].

[35] W.-R. Hu and Y.-L. Wu, *The Taiji Program in Space for gravitational wave physics and the nature of gravity*, Natl. Sci. Rev. **4** (2017), no. 5 685–686.

[36] S. Kawamura *et. al.*, *Current status of space gravitational wave antenna DECIGO and B-DECIGO*, PTEP **2021** (2021), no. 5 05A105 [2006.13545].

[37] P. A. Rosado, A. Sesana and J. Gair, *Expected properties of the first gravitational wave signal detected with pulsar timing arrays*, Mon. Not. Roy. Astron. Soc. **451** (2015), no. 3 2417–2433 [1503.04803].

[38] G. Hobbs, *The Parkes Pulsar Timing Array*, Class. Quant. Grav. **30** (2013) 224007 [1307.2629].

[39] M. Kramer and D. J. Champion, *The European Pulsar Timing Array and the Large European Array for Pulsars*, Class. Quant. Grav. **30** (2013) 224009.

[40] A. Brazier *et. al.*, *The NANOGrav Program for Gravitational Waves and Fundamental Physics*, 1908.05356.

[41] P. Tarafdar *et. al.*, *The Indian Pulsar Timing Array: First data release*, 2206.09289.

[42] G. Hobbs *et. al.*, *The international pulsar timing array project: using pulsars as a gravitational wave detector*, Class. Quant. Grav. **27** (2010) 084013 [0911.5206].

[43] S. R. Taylor, M. Vallisneri, J. A. Ellis, C. M. F. Mingarelli, T. J. W. Lazio and R. van Haasteren, *Are we there yet? Time to detection of nanohertz gravitational waves based on pulsar-timing array limits*, Astrophys. J. Lett. **819** (2016), no. 1 L6 [1511.05564].

[44] B. Haskell and K. Schwenzer, *Isolated Neutron Stars*. 2021. 2104.03137.

[45] E. Abdikamalov, G. Pagliaroli and D. Radice, *Gravitational Waves from Core-Collapse Supernovae*, 2010.04356.

[46] T. Papanikolaou, V. Vennin and D. Langlois, *Gravitational waves from a universe filled with primordial black holes*, JCAP **03** (2021) 053 [2010.11573].

[47] L. A. Wainstein and V. D. Zubakov, *Extraction of Signals from Noise*. 1970.

[48] **LIGO Scientific, Virgo** Collaboration, B. P. Abbott *et. al.*, *A guide to LIGO-Virgo detector noise and extraction of transient gravitational-wave signals*, 1908.11170.

[49] T. Bayes, Rev., *An essay toward solving a problem in the doctrine of chances*, Phil. Trans. Roy. Soc. Lond. **53** (1764) 370–418.

[50] M. Maggiore, *Gravitational Waves. Vol. 1: Theory and Experiments*. Oxford Master Series in Physics. Oxford University Press, 2007.

[51] **LIGO Scientific, VIRGO, KAGRA** Collaboration, R. Abbott *et. al.*, *GWTC-3: Compact Binary Coalescences Observed by LIGO and Virgo During the Second Part of the Third Observing Run*, 2111.03606.

[52] H. A. Lorentz and J. Droste, *The Motion of a System of Bodies under the Influence of their Mutual Attraction, According to Einstein's Theory*, pp. 330–355. Springer Netherlands, Dordrecht, 1937.

[53] A. Einstein, L. Infeld and B. Hoffmann, *The gravitational equations and the problem of motion*, Annals of Mathematics **39** (1938), no. 1 65–100.

[54] Y. Itoh, T. Futamase and H. Asada, *Equation of motion for relativistic compact binaries with the strong field point particle limit: Formulation, the first post-newtonian order, and multipole terms*, Phys. Rev. D **62** (Jul, 2000) 064002.

[55] Y. Itoh, T. Futamase and H. Asada, *Equation of motion for relativistic compact binaries with the strong field point particle limit: The second and half post-newtonian order*, Phys. Rev. D **63** (Feb, 2001) 064038.

[56] Y. Itoh and T. Futamase, *New derivation of a third post-newtonian equation of motion for relativistic compact binaries without ambiguity*, Phys. Rev. D **68** (Dec, 2003) 121501.

[57] Y. Itoh, *Equation of motion for relativistic compact binaries with the strong field point particle limit: Third post-newtonian order*, Phys. Rev. D **69** (Mar, 2004) 064018.

[58] Y. Itoh, *Third-and-a-half order post-newtonian equations of motion for relativistic compact binaries using the strong field point particle limit*, Phys. Rev. D **80** (Dec, 2009) 124003.

[59] L. Blanchet, G. Faye and B. Ponsot, *Gravitational field and equations of motion of compact binaries to* 5/2 *post-newtonian order*, Phys. Rev. D **58** (Oct, 1998) 124002.

[60] L. Blanchet and G. Faye, *Equations of motion of point particle binaries at the third postNewtonian order*, Phys. Lett. A **271** (2000) 58 [gr-qc/0004009].

[61] L. Blanchet and G. Faye, *Hadamard regularization*, J. Math. Phys. **41** (2000) 7675–7714 [gr-qc/0004008].

[62] L. Blanchet and G. Faye, *General relativistic dynamics of compact binaries at the third postNewtonian order*, Phys. Rev. D **63** (2001) 062005 [gr-qc/0007051].

[63] L. Blanchet and G. Faye, *Lorentzian regularization and the problem of point - like particles in general relativity*, J. Math. Phys. **42** (2001) 4391–4418 [gr-qc/0006100].

[64] V. C. de Andrade, L. Blanchet and G. Faye, *Third postNewtonian dynamics of compact binaries: Noetherian conserved quantities and equivalence between the harmonic coordinate and ADM Hamiltonian formalisms*, Class. Quant. Grav. **18** (2001) 753–778 [gr-qc/0011063].

[65] M. E. Pati and C. M. Will, *PostNewtonian gravitational radiation and equations of motion via direct integration of the relaxed Einstein equations. 2. Two-body equations of motion to second postNewtonian order, and radiation reaction to 3.5 postNewtonia order*, Phys. Rev. D **65** (2002) 104008 [gr-qc/0201001].

[66] L. Blanchet and B. R. Iyer, *Third postNewtonian dynamics of compact binaries: Equations of motion in the center-of-mass frame*, Class. Quant. Grav. **20** (2003) 755 [gr-qc/0209089].

[67] L. Blanchet, T. Damour and G. Esposito-Farese, *Dimensional regularization of the third postNewtonian dynamics of point particles in harmonic coordinates*, Phys. Rev. D **69** (2004) 124007 [gr-qc/0311052].

[68] T. Mitchell and C. M. Will, *Post-Newtonian gravitational radiation and equations of motion via direct integration of the relaxed Einstein equations. V. The Strong equivalence principle to second post-Newtonian order*, Phys. Rev. D **75** (2007) 124025 [0704.2243].

[69] P. Jaranowski and G. Schaefer, *Third postNewtonian higher order ADM Hamilton dynamics for two-body point mass systems*, Phys. Rev. **D57** (1998) 7274–7291 [gr-qc/9712075]. [Erratum: Phys. Rev.D63,029902(2001)].

[70] P. Jaranowski and G. Schaefer, *The Binary black hole problem at the third postNewtonian approximation in the orbital motion: Static part*, Phys. Rev. D **60** (1999) 124003 [gr-qc/9906092].

[71] P. Jaranowski and G. Schaefer, *The Binary black hole dynamics at the third postNewtonian order in the orbital motion*, Annalen Phys. **9** (2000) 378–383 [gr-qc/0003054].

[72] T. Damour, P. Jaranowski and G. Schaefer, *Poincare invariance in the ADM Hamiltonian approach to the general relativistic two-body problem*, Phys. Rev. D **62** (2000) 021501 [gr-qc/0003051]. [Erratum: Phys.Rev.D 63, 029903 (2001)].

[73] T. Damour, P. Jaranowski and G. Schaefer, *Dimensional regularization of the gravitational interaction of point masses*, Phys. Lett. B **513** (2001) 147–155 [gr-qc/0105038].

[74] P. Jaranowski and G. Schäfer, *Dimensional regularization of local singularities in the 4th post-Newtonian two-point-mass Hamiltonian*, Phys. Rev. D **87** (2013) 081503 [1303.3225].

[75] T. Damour, P. Jaranowski and G. Schäfer, *Nonlocal-in-time action for the fourth post-Newtonian conservative dynamics of two-body systems*, Phys. Rev. **D89** (2014), no. 6 064058 [1401.4548].

[76] W. D. Goldberger and I. Z. Rothstein, *An Effective field theory of gravity for extended objects*, Phys. Rev. D **73** (2006) 104029 [hep-th/0409156].

[77] W. D. Goldberger and I. Z. Rothstein, *Towers of Gravitational Theories*, Gen. Rel. Grav. **38** (2006) 1537–1546 [hep-th/0605238].

[78] W. D. Goldberger, *Les Houches lectures on effective field theories and gravitational radiation*, in *Les Houches Summer School - Session 86: Particle Physics and Cosmology: The Fabric of Spacetime*, 1, 2007. hep-ph/0701129.

[79] S. Foffa and R. Sturani, *Effective field theory calculation of conservative binary dynamics at third post-Newtonian order*, Phys. Rev. D **84** (2011) 044031 [1104.1122].

[80] S. Foffa and R. Sturani, *Tail terms in gravitational radiation reaction via effective field theory*, Phys. Rev. D **87** (2013), no. 4 044056 [1111.5488].

[81] S. Foffa and R. Sturani, *Dynamics of the gravitational two-body problem at fourth post-Newtonian order and at quadratic order in the Newton constant*, Phys. Rev. D **87** (2013), no. 6 064011 [1206.7087].

[82] S. Foffa and R. Sturani, *Effective field theory methods to model compact binaries*, Class. Quant. Grav. **31** (2014), no. 4 043001 [1309.3474].

[83] S. Foffa and R. Sturani, *Conservative dynamics of binary systems to fourth Post-Newtonian order in the EFT approach I: Regularized Lagrangian*, Phys. Rev. D **100** (2019), no. 2 024047 [1903.05113].

[84] S. Foffa, R. A. Porto, I. Rothstein and R. Sturani, *Conservative dynamics of binary systems to fourth Post-Newtonian order in the EFT approach II: Renormalized Lagrangian*, Phys. Rev. D **100** (2019), no. 2 024048 [1903.05118].

[85] S. Foffa, P. Mastrolia, R. Sturani, C. Sturm and W. J. Torres Bobadilla, *Static two-body potential at fifth post-Newtonian order*, Phys. Rev. Lett. **122** (2019), no. 24 241605 [1902.10571].

[86] J. Blümlein, A. Maier, P. Marquard and G. Schäfer, *Testing binary dynamics in gravity at the sixth post-Newtonian level*, Phys. Lett. B **807** (2020) 135496 [2003.07145].

[87] J. Blümlein, A. Maier, P. Marquard and G. Schäfer, *The fifth-order post-Newtonian Hamiltonian dynamics of two-body systems from an effective field theory approach*, Nucl. Phys. B **983** (2022) 115900 [2110.13822].

[88] B. Bertotti, *On gravitational motion*, Nuovo Cim. **4** (1956), no. 4 898–906.

[89] L. Bel, T. Damour, N. Deruelle, J. Ibanez and J. Martin, *Poincaré-invariant gravitational field and equations of motion of two*

pointlike objects: The postlinear approximation of general relativity, Gen. Rel. Grav. **13** (1981) 963–1004.

[90] Z. Bern, C. Cheung, R. Roiban, C.-H. Shen, M. P. Solon and M. Zeng, *Scattering Amplitudes and the Conservative Hamiltonian for Binary Systems at Third Post-Minkowskian Order*, Phys. Rev. Lett. **122** (2019), no. 20 201603 [1901.04424].

[91] C. Cheung and M. P. Solon, *Classical gravitational scattering at $\mathcal{O}(G^3)$ from Feynman diagrams*, JHEP **06** (2020) 144 [2003.08351].

[92] N. E. J. Bjerrum-Bohr, P. H. Damgaard, L. Planté and P. Vanhove, *The amplitude for classical gravitational scattering at third Post-Minkowskian order*, JHEP **08** (2021) 172 [2105.05218].

[93] Z. Bern, J. Parra-Martinez, R. Roiban, M. S. Ruf, C.-H. Shen, M. P. Solon and M. Zeng, *Scattering Amplitudes and Conservative Binary Dynamics at $\mathcal{O}(G^4)$*, Phys. Rev. Lett. **126** (2021), no. 17 171601 [2101.07254].

[94] C. Dlapa, G. Kälin, Z. Liu and R. A. Porto, *Dynamics of binary systems to fourth Post-Minkowskian order from the effective field theory approach*, Phys. Lett. B **831** (2022) 137203 [2106.08276].

[95] A. D. Fokker, *Ein invarianter variationssatz für die bewegung mehrerer elektrischer massenteilchen*, Zeitschrift für Physik **58** (May, 1929) 386–393.

[96] L. Bernard, L. Blanchet, A. Bohé, G. Faye and S. Marsat, *Fokker action of nonspinning compact binaries at the fourth post-Newtonian approximation*, Phys. Rev. D **93** (2016), no. 8 084037 [1512.02876].

[97] C. M. Will and A. G. Wiseman, *Gravitational radiation from compact binary systems: Gravitational wave forms and energy loss to second postNewtonian order*, Phys. Rev. D **54** (1996) 4813–4848 [gr-qc/9608012].

[98] C. M. Will, *Generation of postNewtonian gravitational radiation via direct integration of the relaxed Einstein equations*, Prog. Theor. Phys. Suppl. **136** (1999) 158–167 [gr-qc/9910057].

[99] M. E. Pati and C. M. Will, *PostNewtonian gravitational radiation and equations of motion via direct integration of the relaxed Einstein equations. 1. Foundations*, Phys. Rev. D **62** (2000) 124015 [gr-qc/0007087].

[100] L. Blanchet and T. Damour, *Radiative gravitational fields in general relativity I. general structure of the field outside the source*, Phil. Trans. Roy. Soc. Lond. A **320** (1986) 379–430.

[101] L. Blanchet, *Radiative gravitational fields in general relativity. 2. Asymptotic behaviour at future null infinity*, Proc. Roy. Soc. Lond. A **409** (1987) 383–399.

[102] L. Blanchet and T. Damour, *Tail transported temporal correlations in the dynamics of a gravitating system*, Phys. Rev. **D37** (1988) 1410.

[103] L. Blanchet, T. Damour and G. Schafer, *Postnewtonian hydrodynamics and postnewtonian gravitational wave generation for numerical relativity*, Mon. Not. Roy. Astron. Soc. **242** (1990) 289–305.

[104] L. Blanchet and T. Damour, *Postnewtonian generation of gravitational waves*, Annales Poincare Phys.Theor. **50** (1989) 377–408.

[105] L. Blanchet and T. Damour, *Hereditary effects in gravitational radiation*, Phys. Rev. **D46** (1992) 4304–4319.

[106] L. Blanchet, T. Damour, B. R. Iyer, C. M. Will and A. Wiseman, *Gravitational radiation damping of compact binary systems to second postNewtonian order*, Phys.Rev.Lett. **74** (1995) 3515–3518.

[107] L. Blanchet, *Quadrupole-quadrupole gravitational waves*, Class. Quant. Grav. **15** (1998) 89–111 [gr-qc/9710037].

[108] L. Blanchet, *On the multipole expansion of the gravitational field*, Class. Quant. Grav. **15** (1998) 1971–1999 [gr-qc/9801101].

[109] L. Blanchet, B. R. Iyer and B. Joguet, *Gravitational waves from inspiralling compact binaries: Energy flux to third postNewtonian order*, Phys. Rev. D **65** (2002) 064005 [gr-qc/0105098]. [Erratum: Phys.Rev.D 71, 129903 (2005)].

[110] L. Blanchet and B. R. Iyer, *Hadamard regularization of the third post-Newtonian gravitational wave generation of two point masses*, Phys. Rev. D **71** (2005) 024004 [gr-qc/0409094].

[111] L. Blanchet, G. Faye, B. R. Iyer and S. Sinha, *The third post-Newtonian gravitational wave polarisations and associated spherical harmonic modes for inspiralling compact binaries in quasi-circular orbits*, Class. Quant. Grav. **25** (2008) 165003 [0802.1249].

[112] L. Blanchet, *Gravitational Radiation from Post-Newtonian Sources and Inspiralling Compact Binaries*, Living Rev. Relativity **17** (2014) 2 [1310.1528].

[113] G. Faye, L. Blanchet and B. R. Iyer, *Non-linear multipole interactions and gravitational-wave octupole modes for inspiralling compact binaries to third-and-a-half post-Newtonian order*, Class. Quant. Grav. **32** (2015), no. 4 045016 [1409.3546].

[114] C. Cutler, E. Poisson, G. J. Sussman and L. S. Finn, *Gravitational radiation from a particle in circular orbit around a black hole. 2: Numerical results for the nonrotating case*, Phys. Rev. **D47** (1993) 1511–1518.

[115] P. R. Brady, J. D. E. Creighton and K. S. Thorne, *Computing the merger of black hole binaries: The IBBH problem*, Phys. Rev. D **58** (1998) 061501 [gr-qc/9804057].

[116] T. Damour, B. R. Iyer and B. S. Sathyaprakash, *Improved filters for gravitational waves from inspiralling compact binaries*, Phys. Rev. **D57** (1998) 885–907 [gr-qc/9708034].

[117] T. Regge and J. A. Wheeler, *Stability of a Schwarzschild singularity*, Phys. Rev. **108** (1957) 1063–1069.

[118] F. J. Zerilli, *Effective potential for even parity Regge-Wheeler gravitational perturbation equations*, Phys. Rev. Lett. **24** (1970) 737–738.

[119] S. A. Teukolsky, *Rotating black holes - separable wave equations for gravitational and electromagnetic perturbations*, Phys. Rev. Lett. **29** (1972) 1114–1118.

[120] S. A. Teukolsky, *Perturbations of a rotating black hole. 1. Fundamental equations for gravitational electromagnetic and neutrino field perturbations*, Astrophys. J. **185** (1973) 635–647.

[121] W. H. Press and S. A. Teukolsky, *Perturbations of a Rotating Black Hole. II. Dynamical Stability of the Kerr Metric*, Astrophys. J. **185** (1973) 649–674.

[122] S. Teukolsky and W. Press, *Perturbations of a rotating black hole. III - Interaction of the hole with gravitational and electromagnetic radiation*, Astrophys.J. **193** (1974) 443–461.

[123] Y. Mino, M. Sasaki, M. Shibata, H. Tagoshi and T. Tanaka, *Black hole perturbation: Chapter 1*, Prog.Theor.Phys.Suppl. **128** (1997) 1–121 [gr-qc/9712057].

[124] T. C. Quinn and R. M. Wald, *An Axiomatic approach to electromagnetic and gravitational radiation reaction of particles in curved space-time*, Phys.Rev. **D56** (1997) 3381–3394 [gr-qc/9610053].

[125] M. Sasaki and H. Tagoshi, *Analytic black hole perturbation approach to gravitational radiation*, Living Rev.Rel. **6** (2003) 6 [gr-qc/0306120].

[126] S. E. Gralla and R. M. Wald, *A Rigorous Derivation of Gravitational Self-force*, Class. Quant. Grav. **25** (2008) 205009 [0806.3293]. [Erratum: Class.Quant.Grav. 28, 159501 (2011)].

[127] L. Barack, *Gravitational self force in extreme mass-ratio inspirals*, Class.Quant.Grav. **26** (2009) 213001 [0908.1664].

[128] S. L. Detweiler, *Elementary development of the gravitational self-force*, Fundam. Theor. Phys. **162** (2011) 271–307 [0908.4363].

[129] E. Poisson, A. Pound and I. Vega, *The Motion of point particles in curved spacetime*, Living Rev.Rel. **14** (2011) 7 [1102.0529].

[130] L. Barack and A. Pound, *Self-force and radiation reaction in general relativity*, Rept. Prog. Phys. **82** (2019), no. 1 016904 [1805.10385].

[131] L. Barack, M. Colleoni, T. Damour, S. Isoyama and N. Sago, *Self-force effects on the marginally bound zoom-whirl orbit in Schwarzschild spacetime*, Phys. Rev. **D100** (2019), no. 12 124015 [1909.06103].

[132] S. D. Upton and A. Pound, *Second-order gravitational self-force in a highly regular gauge*, Phys. Rev. D **103** (2021), no. 12 124016 [2101.11409].

[133] F. Pretorius, *Evolution of binary black hole spacetimes*, Phys. Rev. Lett. **95** (2005) 121101 [gr-qc/0507014].

[134] M. Campanelli, C. O. Lousto, P. Marronetti and Y. Zlochower, *Accurate Evolutions of Orbiting Black-Hole Binaries Without Excision*, Phys. Rev. Lett. **96** (2006) 111101 [gr-qc/0511048].

[135] J. G. Baker, J. Centrella, D.-I. Choi, M. Koppitz and J. van Meter, *Gravitational wave extraction from an inspiraling configuration of merging black holes*, Phys. Rev. Lett. **96** (2006) 111102 [gr-qc/0511103].

[136] M. Boyle *et. al.*, *High-accuracy comparison of numerical relativity simulations with post-Newtonian expansions*, Phys. Rev. **D76** (2007) 124038 [0710.0158].

[137] P. Grandclement and J. Novak, *Spectral methods for numerical relativity*, Living Rev. Rel. **12** (2009) 1 [0706.2286].

[138] J. A. Faber and F. A. Rasio, *Binary Neutron Star Mergers*, Living Rev.Rel. **15** (2012) 8 [1204.3858].

[139] M. D. Duez and Y. Zlochower, *Numerical Relativity of Compact Binaries in the 21st Century*, Rept. Prog. Phys. **82** (2019), no. 1 016902 [1808.06011].

[140] A. Buonanno and T. Damour, *Effective one-body approach to general relativistic two-body dynamics*, Phys. Rev. **D59** (1999) 084006 [gr-qc/9811091].

[141] A. Buonanno and T. Damour, *Transition from inspiral to plunge in binary black hole coalescences*, Phys. Rev. **D62** (2000) 064015 [gr-qc/0001013].

[142] T. Damour, P. Jaranowski and G. Schaefer, *On the determination of the last stable orbit for circular general relativistic binaries at the third postNewtonian approximation*, Phys. Rev. **D62** (2000) 084011 [gr-qc/0005034].

[143] T. Damour, *Coalescence of two spinning black holes: An effective one-body approach*, Phys. Rev. **D64** (2001) 124013 [gr-qc/0103018].

[144] Y. Pan, A. Buonanno, M. Boyle, L. T. Buchman, L. E. Kidder *et. al.*, *Inspiral-merger-ringdown multipolar waveforms of nonspinning black-hole binaries using the effective-one-body formalism*, Phys.Rev. **D84** (2011) 124052 [1106.1021].

[145] A. Taracchini, Y. Pan, A. Buonanno, E. Barausse, M. Boyle *et. al.*, *Prototype effective-one-body model for nonprecessing spinning inspiral-merger-ringdown waveforms*, Phys.Rev. **D86** (2012) 024011 [1202.0790].

[146] Y. Pan, A. Buonanno, A. Taracchini, M. Boyle, L. E. Kidder *et. al.*, *Stability of nonspinning effective-one-body model in approximating two-body dynamics and gravitational-wave emission*, Phys.Rev. **D89** (2014) 061501 [1311.2565].

[147] T. Damour, A. Nagar and S. Bernuzzi, *Improved effective-one-body description of coalescing nonspinning black-hole binaries and its numerical-relativity completion*, Phys.Rev. **D87** (2013) 084035 [1212.4357].

[148] T. Damour and A. Nagar, *New effective-one-body description of coalescing nonprecessing spinning black-hole binaries*, Phys.Rev. **D90** (2014), no. 4 044018 [1406.6913].

[149] T. Damour and A. Nagar, *A new analytic representation of the ringdown waveform of coalescing spinning black hole binaries*, Phys.Rev. **D90** (2014) 024054 [1406.0401].

[150] A. Bohé *et. al.*, *Improved effective-one-body model of spinning, nonprecessing binary black holes for the era of gravitational-wave astrophysics with advanced detectors*, Phys. Rev. **D95** (2017), no. 4 044028 [1611.03703].

[151] A. Nagar, G. Riemenschneider and G. Pratten, *Impact of Numerical Relativity information on effective-one-body waveform models*, Phys. Rev. **D96** (2017), no. 8 084045 [1703.06814].

[152] R. Cotesta, A. Buonanno, A. Bohé, A. Taracchini, I. Hinder and S. Ossokine, *Enriching the Symphony of Gravitational Waves from Binary Black Holes by Tuning Higher Harmonics*, Phys. Rev. **D98** (2018), no. 8 084028 [1803.10701].

[153] A. Ramos-Buades, A. Buonanno, M. Khalil and S. Ossokine, *Effective-one-body multipolar waveforms for eccentric binary black holes with non-precessing spins*, 2112.06952.

[154] A. Nagar, G. Riemenschneider, G. Pratten, P. Rettegno and F. Messina, *Multipolar effective one body waveform model for spin-aligned black hole binaries*, Phys. Rev. D **102** (2020), no. 2 024077 [2001.09082].

[155] A. Nagar, A. Bonino and P. Rettegno, *Effective one-body multipolar waveform model for spin-aligned, quasicircular, eccentric, hyperbolic black hole binaries*, Phys. Rev. D **103** (2021), no. 10 104021 [2101.08624].

[156] G. Riemenschneider, P. Rettegno, M. Breschi, A. Albertini, R. Gamba, S. Bernuzzi and A. Nagar, *Assessment of consistent next-to-quasicircular corrections and postadiabatic approximation in effective-one-body multipolar waveforms for binary black hole coalescences*, Phys. Rev. D **104** (2021), no. 10 104045 [2104.07533].

[157] A. Nagar and P. Rettegno, *The next generation: Impact of high-order analytical information on effective one body waveform models for noncircularized, spin-aligned black hole binaries*, 2108.02043.

[158] A. Placidi, S. Albanesi, A. Nagar, M. Orselli, S. Bernuzzi and G. Grignani, *Exploiting Newton-factorized, 2PN-accurate, waveform multipoles in effective-one-body models for spin-aligned noncircularized binaries*, 2112.05448.

[159] S. Albanesi, A. Nagar, S. Bernuzzi, A. Placidi and M. Orselli, *Assessment of effective-one-body radiation reactions for generic planar orbits*, Phys. Rev. D **105** (2022), no. 10 104031 [2202.10063].

[160] S. Albanesi, A. Placidi, A. Nagar, M. Orselli and S. Bernuzzi, *New avenue for accurate analytical waveforms and fluxes for eccentric compact binaries*, Phys. Rev. D **105** (2022), no. 12 L121503 [2203.16286].

[161] L. Blanchet and T. Damour, *Radiative gravitational fields in general relativity. I. General structure of the field outside the source.*, Royal Society of London Proceedings Series A **320** (1986) 379–430.

[162] T. Damour and B. R. Iyer, *Multipole analysis for electromagnetism and linearized gravity with irreducible cartesian tensors*, Phys. Rev. **D43** (1991) 3259–3272.

[163] M. Maggiore and O. U. Press, *Gravitational Waves: Volume 1: Theory and Experiments*. Gravitational Waves. OUP Oxford, 2008.

[164] G. Faye, S. Marsat, L. Blanchet and B. R. Iyer, *The third and a half post-Newtonian gravitational wave quadrupole mode for quasi-circular inspiralling compact binaries*, Class. Quant. Grav. **29** (2012) 175004 [1204.1043].

[165] T. Damour, *Gravitational radiation and the motion of compact bodies*, in *Gravitational Radiation* (N. Deruelle and T. Piran, eds.), pp. 59–144, North-Holland, Amsterdam, 1983.

[166] T. Damour, *The problem of motion in Newtonian and Einsteinian gravity.*, pp. 128–198. 1987.

[167] F. Larrouturou, L. Blanchet, Q. Henry and G. Faye, *The quadrupole moment of compact binaries to the fourth post-Newtonian order: II. Dimensional regularization and renormalization*, Class. Quant. Grav. **39** (2022), no. 11 115008 [2110.02243].

[168] A. Einstein, *Über Gravitationswellen*, Sitzungsberichte der Königlich Preussischen Akademie der Wissenschaften (Jan., 1918) 154–167.

[169] V. Fock, *The Theory of Space, Time and Gravitation*.

[170] H. Bondi, M. G. J. van der Burg and A. W. K. Metzner, *Gravitational Waves in General Relativity. VII. Waves from Axi-Symmetric Isolated Systems*, Proceedings of the Royal Society of London Series A **269** (Aug., 1962) 21–52.

[171] R. K. Sachs, *Gravitational Waves in General Relativity. VIII. Waves in Asymptotically Flat Space-Time*, Proceedings of the Royal Society of London Series A **270** (Oct., 1962) 103–126.

[172] R. Penrose, *Asymptotic properties of fields and space-times*, Phys. Rev. Lett. **10** (1963) 66–68.

[173] E. T. Newman and T. W. J. Unti, *A Class of Null Flat-Space Coordinate Systems*, Journal of Mathematical Physics **4** (Dec., 1963) 1467–1469.

[174] K. S. Thorne, *Multipole Expansions of Gravitational Radiation*, Rev. Mod. Phys. **52** (1980) 299–339.

[175] R. Penrose, *Zero rest-mass fields including gravitation: Asymptotic behaviour*, Proceedings of the Royal Society of London. Series A, Mathematical and Physical Sciences **284** (1965), no. 1397 159–203.

[176] R. P. Geroch and G. T. Horowitz, *Asymptotically simple does not imply asymptotically Minkowskian*, Phys. Rev. Lett. **40** (1978) 203–206.

[177] L. Blanchet, G. Faye and F. Larrouturou, *The quadrupole moment of compact binaries to the fourth post-Newtonian order: from source to canonical moment*, Class. Quant. Grav. **39** (2022), no. 19 195003 [2204.11293].

[178] O. Poujade and L. Blanchet, *PostNewtonian approximation for isolated systems calculated by matched asymptotic expansions*, Phys. Rev. D **65** (2002) 124020 [gr-qc/0112057].

[179] L. Blanchet, G. Faye and S. Nissanke, *On the structure of the post-Newtonian expansion in general relativity*, Phys. Rev. D **72** (2005) 044024 [gr-qc/0503075].

[180] L. Blanchet, *Gravitational wave tails of tails*, Class. Quant. Grav. **15** (1998) 113–141 [gr-qc/9710038]. [Erratum: Class.Quant.Grav. 22, 3381 (2005)].

[181] D. Trestini, F. Larrouturou and L. Blanchet, *The Quadrupole Moment of Compact Binaries to the Fourth post-Newtonian Order: Relating the Harmonic and Radiative Metrics*, 2209.02719.

[182] L. E. Kidder, *Using Full Information When Computing Modes of Post-Newtonian Waveforms From Inspiralling Compact Binaries in Circular Orbit*, Phys. Rev. **D77** (2008) 044016 [0710.0614].

[183] T. Damour and A. Nagar, *The Effective One Body description of the Two-Body problem*, Fundam. Theor. Phys. **162** (2011) 211–252 [0906.1769].

[184] T. Damour, *The general relativistic two body problem*, 1312.3505.

[185] S. Akcay, R. Gamba and S. Bernuzzi, *A hybrid post-Newtonian – effective-one-body scheme for spin-precessing compact-binary waveforms*, Phys. Rev. D **103** (2021), no. 2 024014 [2005.05338].

[186] R. Gamba, S. Akçay, S. Bernuzzi and J. Williams, *Effective-one-body waveforms for precessing coalescing compact binaries with post-Newtonian Twist*, 2111.03675.

[187] S. Akcay, S. Bernuzzi, F. Messina, A. Nagar, N. Ortiz and P. Rettegno, *Effective-one-body multipolar waveform for tidally interacting binary neutron stars up to merger*, Phys. Rev. **D99** (2019), no. 4 044051 [1812.02744].

[188] A. Nagar, F. Messina, P. Rettegno, D. Bini, T. Damour, A. Geralico, S. Akcay and S. Bernuzzi, *Nonlinear-in-spin effects in effective-one-body waveform models of spin-aligned, inspiralling, neutron star binaries*, Phys. Rev. **D99** (2019) 044007 [1812.07923].

[189] T. Damour, P. Jaranowski and G. Schäfer, *Fourth post-Newtonian effective one-body dynamics*, Phys. Rev. **D91** (2015), no. 8 084024 [1502.07245].

[190] D. Bini, T. Damour and A. Geralico, *Novel approach to binary dynamics: application to the fifth post-Newtonian level*, Phys. Rev. Lett. **123** (2019), no. 23 231104 [1909.02375].

[191] D. Bini, T. Damour and A. Geralico, *Binary dynamics at the fifth and fifth-and-a-half post-Newtonian orders*, Phys. Rev. D **102** (2020), no. 2 024062 [2003.11891].

[192] D. Bini, T. Damour and A. Geralico, *Sixth post-Newtonian local-in-time dynamics of binary systems*, Phys. Rev. D **102** (2020), no. 2 024061 [2004.05407].

[193] D. Bini, T. Damour and A. Geralico, *Sixth post-Newtonian nonlocal-in-time dynamics of binary systems*, 2007.11239.

[194] T. Damour and N. Deruelle, *Radiation Reaction and Angular Momentum Loss in Small Angle Gravitational Scattering*, Phys. Lett. A **87** (1981) 81.

[195] T. Damour and G. Schäfer, *HIGHER ORDER RELATIVISTIC PERIASTRON ADVANCES AND BINARY PULSARS*, Nuovo Cim. **B101** (1988) 127.

[196] R. L. Arnowitt, S. Deser and C. W. Misner, *Gravitational-electromagnetic coupling and the classical self-energy problem*, Phys. Rev. **120** (1960) 313–320.

[197] T. Damour, *The Motion of Compact Bodies and Gravitational Radiation*, Fundam. Theor. Phys. **9** (1984) 89–106.

[198] D. Brouwer and G. M. Clemence, *Methods of celestial mechanics*. 1961.

[199] J. Blümlein, A. Maier and P. Marquard, *Five-Loop Static Contribution to the Gravitational Interaction Potential of Two Point Masses*, Phys. Lett. B **800** (2020) 135100 [1902.11180].

[200] D. Bini, T. Damour and A. Geralico, *Confirming and improving post-Newtonian and effective-one-body results from self-force computations along eccentric orbits around a Schwarzschild black hole*, Phys. Rev. D **93** (2016), no. 6 064023 [1511.04533].

[201] L. Barack and N. Sago, *Beyond the geodesic approximation: conservative effects of the gravitational self-force in eccentric orbits around a Schwarzschild black hole*, Phys.Rev. **D83** (2011) 084023 [1101.3331].

[202] T. Damour, *Classical and quantum scattering in post-Minkowskian gravity*, Phys. Rev. D **102** (2020), no. 2 024060 [1912.02139].

[203] A. Nagar, G. Pratten, G. Riemenschneider and R. Gamba, *A Multipolar Effective One Body Model for Non-Spinning Black Hole Binaries*, 1904.09550.

[204] P. C. Peters, *Gravitational Radiation and the Motion of Two Point Masses*, Phys. Rev. **136** (1964) B1224–B1232.

[205] D. Bini and T. Damour, *Gravitational radiation reaction along general orbits in the effective one-body formalism*, Phys.Rev. **D86** (2012) 124012 [1210.2834].

[206] A. Buonanno, Y. Chen and T. Damour, *Transition from inspiral to plunge in precessing binaries of spinning black holes*, Phys. Rev. **D74** (2006) 104005 [gr-qc/0508067].

[207] A. Buonanno, G. B. Cook and F. Pretorius, *Inspiral, merger and ring-down of equal-mass black-hole binaries*, Phys. Rev. D **75** (2007) 124018 [gr-qc/0610122].

[208] A. Nagar, T. Damour and A. Tartaglia, *Binary black hole merger in the extreme mass ratio limit*, Class. Quant. Grav. **24** (2007) S109–S124 [gr-qc/0612096].

[209] Y. Pan, A. Buonanno, J. G. Baker, J. Centrella, B. J. Kelly, S. T. McWilliams, F. Pretorius and J. R. van Meter, *A Data-analysis driven comparison of analytic and numerical coalescing binary waveforms: Nonspinning case*, Phys. Rev. D **77** (2008) 024014 [0704.1964].

[210] A. Buonanno, Y. Pan, J. G. Baker, J. Centrella, B. J. Kelly, S. T. McWilliams and J. R. van Meter, *Toward faithful templates for non-spinning binary black holes using the effective-one-body approach*, Phys. Rev. **D76** (2007) 104049 [0706.3732].

[211] T. Damour and A. Nagar, *Faithful Effective-One-Body waveforms of small-mass-ratio coalescing black-hole binaries*, Phys. Rev. **D76** (2007) 064028 [0705.2519].

[212] T. Damour and A. Nagar, *Comparing Effective-One-Body gravitational waveforms to accurate numerical data*, Phys. Rev. **D77** (2008) 024043 [0711.2628].

[213] T. Damour, B. R. Iyer and A. Nagar, *Improved resummation of post-Newtonian multipolar waveforms from circularized compact binaries*, Phys. Rev. **D79** (2009) 064004 [0811.2069].

[214] T. Damour and A. Gopakumar, *Gravitational recoil during binary black hole coalescence using the effective one body approach*, Phys. Rev. **D73** (2006) 124006 [gr-qc/0602117].

[215] S. Albanesi, A. Nagar and S. Bernuzzi, *Effective one-body model for extreme-mass-ratio spinning binaries on eccentric equatorial orbits: Testing radiation reaction and waveform*, Phys. Rev. D **104** (2021), no. 2 024067 [2104.10559].

[216] M. Davis, R. Ruffini, W. H. Press and R. H. Price, *Gravitational radiation from a particle falling radially into a schwarzschild black hole*, Phys. Rev. Lett. **27** (1971) 1466–1469.

[217] W. H. Press, *Long Wave Trains of Gravitational Waves from a Vibrating Black Hole*, Astrophys.J. **170** (1971) L105–L108.

[218] M. Davis, R. Ruffini and J. Tiomno, *Pulses of gravitational radiation of a particle falling radially into a schwarzschild black hole*, Phys. Rev. **D60** (1999) 124004 [gr-qc/9904059].

[219] R. H. Price and J. Pullin, *Colliding black holes: The Close limit*, Phys. Rev. Lett. **72** (1994) 3297–3300 [gr-qc/9402039].

[220] X. Jiménez-Forteza, D. Keitel, S. Husa, M. Hannam, S. Khan and M. Pürrer, *Hierarchical data-driven approach to fitting numerical relativity data for nonprecessing binary black holes with an application to final spin and radiated energy*, Phys. Rev. **D95** (2017), no. 6 064024 [1611.00332].

[221] E. Berti, V. Cardoso and C. M. Will, *On gravitational-wave spectroscopy of massive black holes with the space interferometer LISA*, Phys. Rev. **D73** (2006) 064030 [gr-qc/0512160].

[222] I. Hinder, B. Vaishnav, F. Herrmann, D. Shoemaker and P. Laguna, *Universality and final spin in eccentric binary black hole inspirals*, Phys. Rev. D **77** (2008) 081502 [0710.5167].

[223] J. Samsing, M. MacLeod and E. Ramirez-Ruiz, *The Formation of Eccentric Compact Binary Inspirals and the Role of Gravitational Wave Emission in Binary-Single Stellar Encounters*, Astrophys. J. **784** (2014) 71 [1308.2964].

[224] C. L. Rodriguez, S. Chatterjee and F. A. Rasio, *Binary Black Hole Mergers from Globular Clusters: Masses, Merger Rates, and the Impact of Stellar Evolution*, Phys. Rev. **D93** (2016), no. 8 084029 [1602.02444].

[225] K. Belczynski, D. E. Holz, T. Bulik and R. O'Shaughnessy, *The first gravitational-wave source from the isolated evolution of two 40-100 Msun stars*, Nature **534** (2016) 512 [1602.04531].

[226] J. H. VanLandingham, M. C. Miller, D. P. Hamilton and D. C. Richardson, *The Role of the Kozai–lidov Mechanism in Black Hole Binary Mergers in Galactic Centers*, Astrophys. J. **828** (2016), no. 2 77 [1604.04948].

[227] J. Samsing, *Eccentric Black Hole Mergers Forming in Globular Clusters*, Phys. Rev. **D97** (2018), no. 10 103014 [1711.07452].

[228] C. L. Rodriguez, P. Amaro-Seoane, S. Chatterjee and F. A. Rasio, *Post-Newtonian Dynamics in Dense Star Clusters: Highly-Eccentric, Highly-Spinning, and Repeated Binary Black Hole Mergers*, Phys. Rev. Lett. **120** (2018), no. 15 151101 [1712.04937].

[229] M. E. Lower, E. Thrane, P. D. Lasky and R. Smith, *Measuring eccentricity in binary black hole inspirals with gravitational waves*, Phys. Rev. D **98** (2018), no. 8 083028 [1806.05350].

[230] L. Gondán and B. Kocsis, *High eccentricities and high masses characterize gravitational-wave captures in galactic nuclei as seen by Earth-based detectors*, Mon. Not. Roy. Astron. Soc. **506** (2021), no. 2 1665–1696 [2011.02507].

[231] R. M. O'Leary, B. Kocsis and A. Loeb, *Gravitational waves from scattering of stellar-mass black holes in galactic nuclei*, Mon. Not. Roy. Astron. Soc. **395** (2009), no. 4 2127–2146 [0807.2638].

[232] F. Antonini, S. Toonen and A. S. Hamers, *Binary black hole mergers from field triples: properties, rates and the impact of stellar evolution*, Astrophys. J. **841** (2017), no. 2 77 [1703.06614].

[233] M. Favata, *Systematic parameter errors in inspiraling neutron star binaries*, Phys.Rev.Lett. **112** (2014) 101101 [1310.8288].

[234] M. Favata, C. Kim, K. G. Arun, J. Kim and H. W. Lee, *Constraining the orbital eccentricity of inspiralling compact binary systems with Advanced LIGO*, Phys. Rev. D **105** (2022), no. 2 023003 [2108.05861].

[235] P. Saini, M. Favata and K. G. Arun, *Systematic bias on parameterized tests of general relativity due to neglect of orbital eccentricity*, 2203.04634.

[236] S. A. Bhat, P. Saini, M. Favata and K. G. Arun, *Systematic bias on the inspiral-merger-ringdown consistency test due to neglect of orbital eccentricity*, 2207.13761.

[237] K. Breivik, C. L. Rodriguez, S. L. Larson, V. Kalogera and F. A. Rasio, *Distinguishing Between Formation Channels for Binary Black Holes with LISA*, Astrophys. J. Lett. **830** (2016), no. 1 L18 [1606.09558].

[238] V. Cardoso, C. F. B. Macedo and R. Vicente, *Eccentricity evolution of compact binaries and applications to gravitational-wave physics*, Phys. Rev. D **103** (2021), no. 2 023015 [2010.15151].

[239] I. Hinder, L. E. Kidder and H. P. Pfeiffer, *An eccentric binary black hole inspiral-merger-ringdown gravitational waveform model from numerical relativity and post-Newtonian theory*, 1709.02007.

[240] A. Ramos-Buades, S. Husa, G. Pratten, H. Estellés, C. Garc´ia-Quirós, M. Mateu-Lucena, M. Colleoni and R. Jaume, *First survey of spinning eccentric black hole mergers: Numerical relativity simulations, hybrid waveforms, and parameter estimation*, Phys. Rev. D **101** (2020), no. 8 083015 [1909.11011].

[241] E. A. Huerta *et. al.*, *Physics of eccentric binary black hole mergers: A numerical relativity perspective*, Phys. Rev. **D100** (2019), no. 6 064003 [1901.07038].

[242] A. Ramos-Buades, M. van de Meent, H. P. Pfeiffer, H. R. Rüter, M. A. Scheel, M. Boyle and L. E. Kidder, *Eccentric binary black holes: Comparing numerical relativity and small mass-ratio perturbation theory*, Phys. Rev. D **106** (2022), no. 12 124040 [2209.03390].

[243] K. G. Arun, L. Blanchet, B. R. Iyer and M. S. S. Qusailah, *Inspiralling compact binaries in quasi-elliptical orbits: The Complete 3PN energy flux*, Phys. Rev. D **77** (2008) 064035 [0711.0302].

[244] K. G. Arun, L. Blanchet, B. R. Iyer and M. S. S. Qusailah, *Tail effects in the 3PN gravitational wave energy flux of compact binaries in quasi-elliptical orbits*, Phys. Rev. D **77** (2008) 064034 [0711.0250].

[245] K. G. Arun, L. Blanchet, B. R. Iyer and S. Sinha, *Third post-Newtonian angular momentum flux and the secular evolution of orbital elements for inspiralling compact binaries in quasi-elliptical orbits*, Phys. Rev. D **80** (2009) 124018 [0908.3854].

[246] C. K. Mishra, K. G. Arun and B. R. Iyer, *Third post-Newtonian gravitational waveforms for compact binary systems in general orbits: Instantaneous terms*, Phys. Rev. **D91** (2015), no. 8 084040 [1501.07096].

[247] A. Klein, Y. Boetzel, A. Gopakumar, P. Jetzer and L. de Vittori, *Fourier domain gravitational waveforms for precessing eccentric binaries*, Phys. Rev. **D98** (2018), no. 10 104043 [1801.08542].

[248] Y. Boetzel, C. K. Mishra, G. Faye, A. Gopakumar and B. R. Iyer, *Gravitational-wave amplitudes for compact binaries in eccentric orbits at the third post-Newtonian order: Tail contributions and postadiabatic corrections*, Phys. Rev. D **100** (2019), no. 4 044018 [1904.11814].

[249] S. Tiwari, G. Achamveedu, M. Haney and P. Hemantakumar, *Ready-to-use Fourier domain templates for compact binaries inspiraling along moderately eccentric orbits*, Phys. Rev. **D99** (2019), no. 12 124008 [1905.07956].

[250] M. Ebersold, Y. Boetzel, G. Faye, C. K. Mishra, B. R. Iyer and P. Jetzer, *Gravitational-wave amplitudes for compact binaries in eccentric orbits at the third post-Newtonian order: Memory contributions*, Phys. Rev. D **100** (2019), no. 8 084043 [1906.06263].

[251] M. Khalil, A. Buonanno, J. Steinhoff and J. Vines, *Radiation-reaction force and multipolar waveforms for eccentric, spin-aligned binaries in the effective-one-body formalism*, Phys. Rev. D **104** (2021), no. 2 024046 [2104.11705].

[252] Z. Cao and W.-B. Han, *Waveform model for an eccentric binary black hole based on the effective-one-body-numerical-relativity formalism*, Phys. Rev. **D96** (2017), no. 4 044028 [1708.00166].

[253] T. Hinderer and S. Babak, *Foundations of an effective-one-body model for coalescing binaries on eccentric orbits*, Phys. Rev. **D96** (2017), no. 10 104048 [1707.08426].

[254] D. Chiaramello and A. Nagar, *Faithful analytical effective-one-body waveform model for spin-aligned, moderately eccentric, coalescing black hole binaries*, Phys. Rev. D **101** (2020), no. 10 101501 [2001.11736].

[255] A. Nagar, P. Rettegno, R. Gamba and S. Bernuzzi, *Effective-one-body waveforms from dynamical captures in black hole binaries*, Phys. Rev. D **103** (2021), no. 6 064013 [2009.12857].

[256] **LIGO Scientific, Virgo** Collaboration, R. Abbott *et. al.*, *GW190521: A Binary Black Hole Merger with a Total Mass of* $150M_{\odot}$, Phys. Rev. Lett. **125** (2020), no. 10 101102 [2009.01075].

[257] **LIGO Scientific, Virgo** Collaboration, R. Abbott *et. al.*, *Properties and Astrophysical Implications of the 150* $M_{\odot}$ *Binary Black Hole Merger GW190521*, Astrophys. J. Lett. **900** (2020), no. 1 L13 [2009.01190].

[258] R. Gamba, M. Breschi, G. Carullo, P. Rettegno, S. Albanesi, S. Bernuzzi and A. Nagar, *GW190521: A dynamical capture of two black holes*, Submitted to Nature Astronomy (June, 2021) [2106.05575].

[259] A. Ramos-Buades, A. Buonanno, M. Khalil and S. Ossokine, *Effective-one-body multipolar waveforms for eccentric binary black holes with non-precessing spins*, 2112.06952.

[260] A. Gopakumar and B. R. Iyer, *Second postNewtonian gravitational wave polarizations for compact binaries in elliptical orbits*, Phys. Rev. D **65** (2002) 084011 [gr-qc/0110100].

[261] R.-M. Memmesheimer, A. Gopakumar and G. Schaefer, *Third post-Newtonian accurate generalized quasi-Keplerian parametrization for compact binaries in eccentric orbits*, Phys. Rev. D **70** (2004) 104011 [gr-qc/0407049].

[262] R. W. O'Shaughnessy, *Transition from inspiral to plunge for eccentric equatorial Kerr orbits*, Phys. Rev. D **67** (2003) 044004 [gr-qc/0211023].

[263] L. C. Stein and N. Warburton, *Location of the last stable orbit in Kerr spacetime*, Phys. Rev. D **101** (2020), no. 6 064007 [1912.07609].

[264] E. Harms, S. Bernuzzi, A. Nagar and A. Zenginoglu, *A new gravitational wave generation algorithm for particle perturbations of the Kerr spacetime*, Class.Quant.Grav. **31** (2014) 245004 [1406.5983].

[265] A. Nagar and P. Rettegno, *Efficient effective one body time-domain gravitational waveforms*, Phys. Rev. **D99** (2019), no. 2 021501 [1805.03891].

[266] "Updated Advanced LIGO sensitivity design curve." https://dcc.ligo.org/LIGO-T1800044/public.

[267] "SXS Gravitational Waveform Database." https://data.black-holes.org/waveforms/index.html.

[268] T. Damour, P. Jaranowski and G. Schäfer, *Effective one body approach to the dynamics of two spinning black holes with next-to-leading order spin-orbit coupling*, Phys.Rev. **D78** (2008) 024009 [0803.0915].

[269] E. Barausse, E. Racine and A. Buonanno, *Hamiltonian of a spinning test-particle in curved spacetime*, Phys. Rev. D **80** (2009) 104025 [0907.4745]. [Erratum: Phys.Rev.D 85, 069904 (2012)].

[270] A. Nagar, *Effective one body Hamiltonian of two spinning black-holes with next-to-next-to-leading order spin-orbit coupling*, Phys.Rev. **D84** (2011) 084028 [1106.4349].

[271] E. Barausse and A. Buonanno, *Extending the effective-one-body Hamiltonian of black-hole binaries to include next-to-next-to-leading spin-orbit couplings*, Phys.Rev. **D84** (2011) 104027 [1107.2904].

[272] A. Nagar and A. Shah, *Factorization and resummation: A new paradigm to improve gravitational wave amplitudes*, Phys. Rev. **D94** (2016), no. 10 104017 [1606.00207].

[273] F. Messina, A. Maldarella and A. Nagar, *Factorization and resummation: A new paradigm to improve gravitational wave amplitudes. II: the higher multipolar modes*, Phys. Rev. **D97** (2018), no. 8 084016 [1801.02366].